Effect of Ballast Pockets on the Stability of Railway Embankments

Lan Luo

A Thesis

In

The Department

of

Building, Civil, and Environment Engineering

Presented in Partial Fulfillment of the Requirements

for the Degree of Master of Applied Science (Geotechnical Engineering) at

Concordia University

Montréal, Québec, Canada

March 2022

CONCORDIA UNIVERSITY

School of Graduate Studies

This is to certify that the thesis prepared

By: Lan Luo

Entitled: Effect of Ballast Pockets on the Stability of Railway Embankments

and submitted in partial fulfillment of the requirements for the degree of

Master of Applied Science (Geotechnical Engineering)

complies with regulations of the University and meets the accepted standards with respect to originality and quality.

Signed by the final Examining Committee:

_____ Chair

Dr. B. Li

_____ Examiner

Dr. E. Erkmen

_____ Examiner

Dr. B. Li

_____ Supervisor

Dr. A. M. Zsaki

Approved by _____

Dr. A. Bagchi Chair of Department

_____2022 _____

Dean *Dr. M. Debbabi*

Abstract

Effect of Ballast Pockets on the Stability of Railway Embankments

Lan Luo

The formation of ballast pockets results from excessive plastic deformation of clay subgrade, a common subgrade failure resulting from the repeated loading of the subgrade by passing trains. Ballast pockets reduce the stability of clay slopes under railway embankments, further affecting the safe traversal of freight trains on the track. Therefore, quantifying the impact of ballast pockets on slope stability is important for railway operation safety. This thesis uses two-dimensional models using the finite element shear strength reduction method to conduct a coupled deformation and pore fluid flow analysis for slope stability evaluation under undrained conditions. The control variable method is used to perform a series of parameter studies, including geometric characteristics of the slope, railway embankment and ballast pockets, and freight train speeds. For slopes with different parameters, maximum safe train speed information is presented with a minimum factor of safety of 1.3. The research results show that freight trains can traverse on tracks built on a lower slope of 3H:1V inclination and a 3 m railway embankment at a relatively higher maximum safe speed. Finally, this research identifies the maximum safe speed a train can use, through given the geometric parameters of the slope, railway embankment, and ballast pockets.

Acknowledgement

First and foremost, I would like to express my heartfelt thanks to my supervisor, Dr. Attila Michael Zsaki, for giving me this opportunity to conduct research and study. His professional guidance and consistent support helped me complete my research project.

In addition, I would also like to express my gratitude to my parents and friends, who have always firmly supported me, accompanied and encouraged me.

Finally, I would like to acknowledge the financial support provided by that was provided by Dr. Attila Michael Zsaki through GCS FRS fund to successfully complete my research.

Table of contents

List of tables

List of figures

List of symbols

A	=	bearing area of cross tie (mm^2)
$[B]$	=	strain-displacement matrix
c	=	cohesion (kPa)
D	=	wheel diameter (in.) or (mm)
$[D]$	=	stress-strain matrix
DF	=	distribution factor of axle load carried by a single tie (%)
E	=	Young's modulus (MPa)
E', ν'	=	effective elastic parameters (MPa)
e	=	void ratio
$F_{(n)}$	=	internal force in the spring caused by its current deformed state (kN)
FS	=	factor of safety
$\{F\}$	=	vector of all incremental element nodal forces (N)
He	=	railway embankment height (m)
Hs	=	natural slope height (m)
IF	=	impact factor (%)
K	=	stiffness of the spring (N/m)
K'	=	soil bulk modulus (MPa)
$[K_c]$	=	global fluid stiffness matrix
$[K_e]$	=	global elastic stiffness matrix
k	=	hydraulic conductivity (cm/s)
k_x	=	horizontal hydraulic conductivity (cm/s)
k_y	=	vertical hydraulic conductivity (cm/s)
$[k_c]$	=	element fluid stiffness matrix
$[k_e]$	=	element elastic stiffness matrix
L	=	influence length of an axle load or adjacent axle loads (km)
m	=	the ratio of the depth of water in ballast pockets to the ballast pockets' depth
n	=	step number

p	=	mean total stress (kPa)
P	=	applied load (kN) or (lbf)
P_{avg}	=	average ballast pressure (psi) or (MPa)
q_x, q_y	=	volumetric flow rates per unit area into and out o the element (m^3/s)
Q	=	plastic potential function
R_C	=	compressive strength (MPa)
R_F	=	rate of FS change (%)
R_T	=	tensile strength (MPa)
t	=	loading pulse duration (h)
U	=	displacement (m)
$\{U\}$	=	vector of all incremental element nodal displacements (m)
ΔU	=	displacement increment (m)
u	=	displacement in x direction (m)
u_w	=	excess pore stress (kPa)
V	=	train speed (km/h) or (mph)
ν	=	Poisson's ratio
w	=	displacement in y direction (m)
λ	=	a positive scalar of proportionality which is dependent on the state of stress and the load history
ϕ	=	friction angle (°)
$\varepsilon_x, \varepsilon_y, \gamma_{xy}$	=	strain components in the *xy* plane
γ_w	=	unit weight of water (kN/m^3)
σ	=	normal stress (kPa)
σ'	=	effective stress (kPa)
$\underline{\sigma}$	=	stress tensor (kN/m^2) or (kPa)
τ	=	shear strength (kPa)
$d\underline{\varepsilon^p}$	=	incremental plastic strain (m/m)

Chapter 1 Introduction

1.1 Background

Transportation is an essential part of a nation's economy and plays a vital role in developing the economy and society. As a country with multiple transportation modes, Canada's economic development is closely related to transportation (Transport Canada 2018). According to the 2011 transportation and the economy report (Transport Canada 2011), the transportation services sector contributed $53 billion to gross domestic product (GDP), which was 4.2% of Canada's total GDP. Truck transportation was an essential source of transportation benefits, with 31% of the sector's share of GDP. The economic benefits of rail transportation accounted for 11% of GDP, second to truck and air (Transport Canada 2011). Figure 1.1 shows the share of Canadian transportation GDP in 2011. The 'others' item in Figure 1.1 represents the output from the transportation support and scenic and sightseeing activities segments, including airport operations, operations of terminals and harbors, and arrangement of freight transportation services.

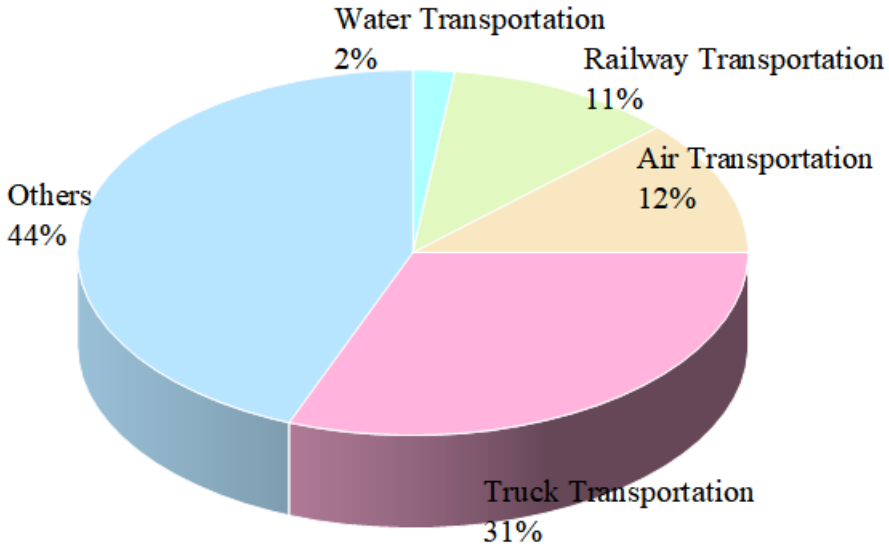

Fig. 1.1. Share of Canadian transportation GDP in 2011 (Transports Canada 2011).

As an essential mode of transportation, the railways are a large and well-developed system in Canada. According to Transport Canada (2018), there are 41,465 route-kilometers of track in Canada, as illustrated in Figure 1.2, of which 52.8% is owned by Canadian National (CN) and 30.7% (12,709 km) is owned by Canadian Pacific Railway (CP). The CN and CP companies are both freight railway companies. Railway transportation is divided into passenger transportation and freight transportation, and the main economic benefit of rail transportation comes from freight transportation. In 2006, freight transportation revenues accounted for $9.4 billion or 89.9% of the rail transportation industry's total operating revenues (Statistics Canada 2006).

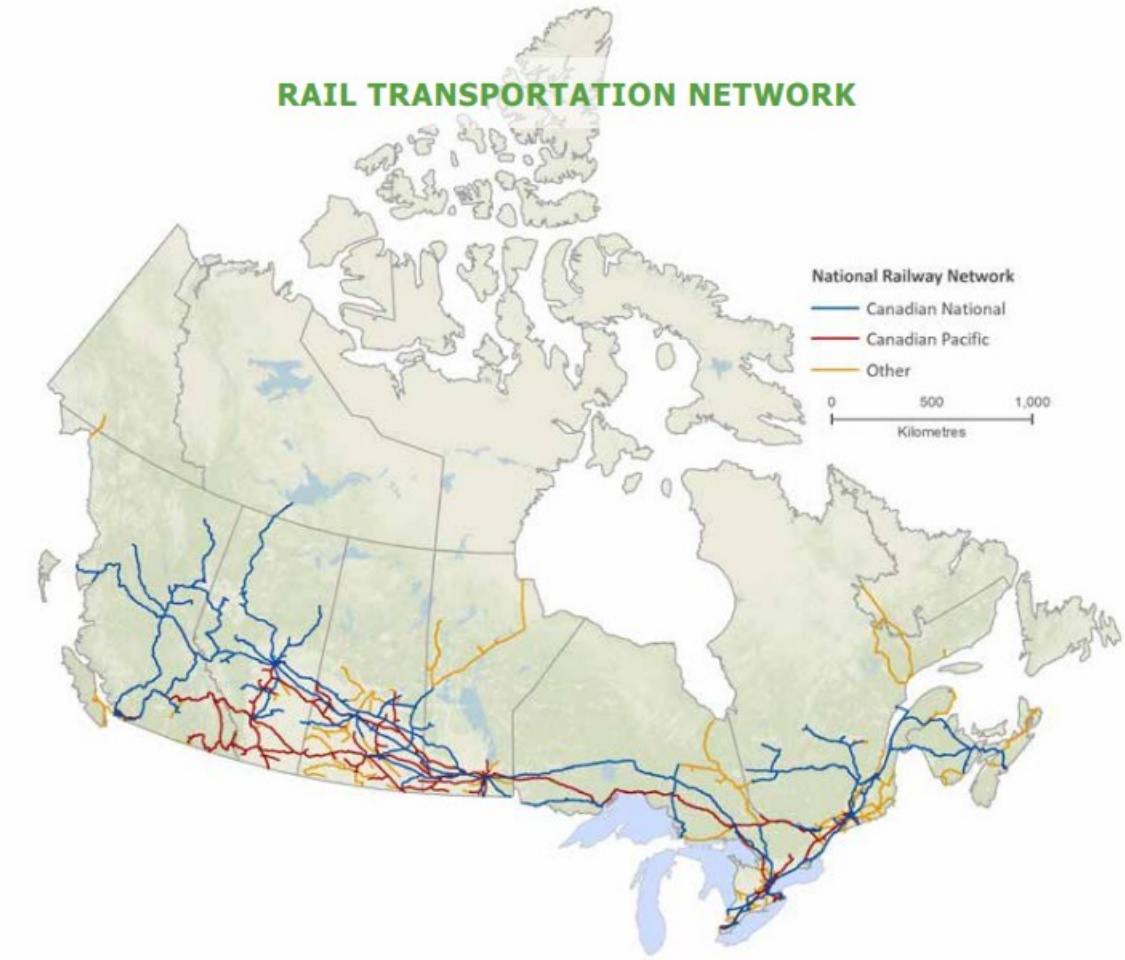

Fig. 1.2. The Canadian railway network in 2018 (Transport Canada 2018).

With the development of a railway system, freight railway transportation has become an important means of transporting heavy goods and containerized traffic over long distances. From 2000 to 2010 (except for 2009), over 300 million tonnes of goods were transported by railway each year (Transport Canada 2011). However, railway accidents occurred frequently.

In 2018, the number of rail accidents reported to the Transportation Safety Board of Canada (TSBC) was 1,172, as shown in Figure 1.3, and this figure increased 7% by 2017 (1091). Almost 30% of all trains involved in rail accidents were freight trains, 5% (68) were passenger trains and the remaining 65% comprised mainly single cars/cuts of cars, locomotives, and track units (TSBC 2018). The TSBC noted the severity of railway accidents and has analyzed accidents to determine their causes. Two freight railway accidents involving embankment or subgrade failure, which were investigated and reported by TSB, are discussed below.

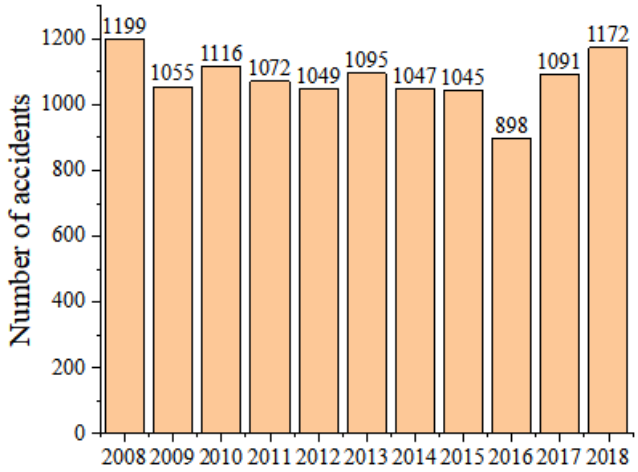

Fig. 1.3. Number of rail accidents, 2008 to 2018 (TSB 2018).

One derailment occurred on 31 May 1998 with CN freight train No. 981-31, traveling to Nelson, British Columbia, from Cranbrook, British Columbia. The train encountered a subgrade depression at Mile 59.1 near Creston, British Columbia. This accident caused three locomotives and eight gondola cars to derail, resulting in approximately 21,000 liters of diesel fuel and silver and lead concentrate (approximately 90 cubic meters) being released. The cause of the accident was saturation and failure of the subgrade fill, exacerbated by rainfall, inadequate performance of the drainage system and the high susceptibility of the subgrade fill material to water changes. Cycling loads generated by trains may have been another reason contributing to this accident (TSBC 1998).

The second accident occurred on 26 June 1999 with CP freight train No. 474-25, traveling from Winnipeg, Manitoba, to Thunder Bay, Ontario. The train encountered a subgrade depression at Mile 5.3 in the Keewatin subdivision near Keewatin, Ontario. Eight freight cars derailed and minor track and equipment were damaged, but no injuries were involved (TSBC 1999). According to the analysis report by TSBC (1999), the drainage system was blocked, which forced water from rainfall to flow between the north and south main tracks, causing the subgrade to be saturated. Similar to the previous accident, loads generated by train operation contributed to the failure of the embankment.

These two accidents occurred because of the embankment's flawed drainage system and the cycling loads imposed on the track. Since ballast pockets can cause the poor drainage of the track structure (Tzanakakis et al. 2013), ballast pockets are a potential cause of embankment failure and resulting derailments. Therefore, it is necessary to study the influence of ballast pockets on the stability of embankment slopes.

1.2 Research objectives and scope

When a depression develops in the top formation or subgrade below the tracks, ballast pockets can be created. Growth of these ballast pockets can trap water in depressions and saturate the soil under the rail, leading to embankment and subgrade failure and resulting in derailments (Tzanakakis et al. 2013). The derailment of trains threatens crews and passengers'

safety and causes severe economic losses. This research investigates the development of ballast pockets and their effect on embankment slope stability. In characterizing the railway embankment-subgrade systems, the following parameters are considered: slope geometry and material properties, characteristics of ballast pockets (geometry, position, material properties, and water level retained in ballast pockets), and moving freight train speeds. The factor of safety of the slope is used to serve as a measure to quantify the effect of ballast pockets. Based on the investigation results, guidelines are derived for the maximum allowable train speed for a given railway slope. The specific objectives are:

- Build two-dimensional finite element models of a railway embankment established on a clay slope with different slope ratios and existing ballast pockets under the rails;
- Apply the worst drainage conditions (undrained conditions) for coupled (groundwater flow and stress) analysis on slope stability and summarize its performance and critical trends;
- Investigate the effect of different train speeds on the stability of a railway embankment (with ballast pockets under the track);
- Evaluate the allowable maximum train speed for various characteristics of ballast pockets and geometric parameters.

The two-dimensional models developed in the analysis assumed an infinitely long tangent track section. This study does not include curved tracks and does not consider rainfall, wind, and other environmental changes.

1.3 Research methodology

The following research methodology was used:

a) Finite element method (FEM)-based simulation using Rocscience's RS2 software (RS2) (Rocscience Inc. 2021a)

   According to the literature review, essential model parameters governing the model's behavior can be identified (such as railway embankment dimensions, soil properties, slope inclination ratios, ballast pocket dimensions, loading generated by trains). A set of parametric studies was performed using RS2 after developing a basic model.

b) Parametric study

   A *control variable* method was used to investigate each principal model parameter separately. In this study, three sets of models were developed to conduct a comprehensive parametric study of the main parameters. The models included:

   i. Set I: Dry slope model

   ii. Set II: Slope model of existing ballast pockets under the track

   iii. Set III: Slope model of existing ballast pockets and moving train loads.

   The worst case of drainage-(undrained) condition in slope stability was used in the

models. The parametric study in those three sets of models comprises:

1. Different ballast pocket geometries and water levels retained in the ballast pockets
2. Variation of slope geometry and subgrade with different dynamic loads caused by moving trains, including the effects of slope height, subgrade height, and slope inclination.

c) Data analysis

According to the parametric study results for different conditions, the principles of slope stability under different conditions can be better understood if examined from plots of data. We developed a chart of maximum safe train speed with different ballast pocket characteristics.

The primary method we used in analysis was the finite element shear strength reduction (SSRFEM) method, which was used to calculate the effect of ballast pockets on slope stability. The FEM coupled with deformation and pore fluid flow, was adopted to evaluate the stability due to fluid flow within a slope.

1.4 Thesis outline

This thesis is presented in five chapters. In the first chapter, the state of transportation in Canada and the importance of railway transportation are presented. Two examples of freight train derailments are given to analyze the potential causes of train accidents. Soil saturation, which is the principle of ballast pockets, can cause embankment failure, and dynamic loads generated by heavy freight trains can lead to the instability of the embankment and subgrade. The research objectives and scope are introduced, followed by a description of the methodology used in this project.

Chapter 2 presents a literature review, beginning with a general background of ballast pockets and a method to analyze saturated soil behavior in a slope. The railway track structure, loads generated by a moving train on the railway track, and load transfer mechanism are introduced, which help the computation of train loads on the railway embankment. Next, relevant major parameters determining the success of models are given, followed by the introduction of methods used for analyzing slope stability in geomechanics. By comparing these methods, the most suitable method for this research was selected. Finally, constitutive models for soils are introduced.

Chapter 3 outlines the development of numerical models. Moreover, RS2 is verified as an effective tool that can model both ballast pockets and dynamic loadings generated by moving trains.

Chapter 4 conducts parametric analyses for three sets of models with different settings discussed in Chapter 3 (water level settings, ballast pockets settings, and load settings), and summarizes the influence of relevant parameters of ballast pockets on slope stability. The chapter includes a detailed discussion of the impact of train loads on the models.

Chapter 5 presents conclusions, limitations, and recommendations for future studies.

Chapter 2 Literature review

2.0 Introduction

Investigating the implication of ballast pockets on the stability of railway embankments has been addressed to some extent in previous research literature. However, the present study's main purpose is to relate the effects of ballast pockets with dynamic loading caused by moving trains, which has not been previously considered. This chapter first introduces the background of the research. It establishes the foundation for the next two chapters, determining model parameters and generation and analysis of models. This chapter consists of five sections. Section 2.1 describes the formation of ballast pockets, their influence on slopes, and the behavior of saturated soils. Section 2.2 introduces the composition of the railway track and load transfer mechanism from freight cars to rails to ties, from ties to ballast, subballast, and finally, subgrade. The method for calculating loads due to passing trains on the railway track foundation is outlined. Section 2.3 presents the method of identifying parameters that determine a representative model and establishes these parameters' credible ranges. Section 2.4 introduces current practice methods that can be used for solving the slope stability problem and gives reasons for selecting the FEM as the optimal method for this study. Based on previous related research, SSRFEM method was an effective method for analyzing slope stability. Finally, Section 2.5 introduces typical soil constitutive models for FEM analysis.

2.1 Ballast pockets formation and flow through saturated porous medium

This section introduces the formation of ballast pockets and their influence on a railway embankment slope. The principle of fluid flow through the soil is discussed, as these two topics are closely related.

2.1.1 Formation of ballast pockets

The formation of ballast pockets results from excessive plastic deformation of fine-grained soil subgrade, a common subgrade failure resulting from the repeated loading of the subgrade by passing trains (Li et al. 2016). Once there is moisture at the boundary of the ballast and the fine-grained material of the embankment, loads on the embankment can lead to the intermixing of soil with water and then the separation of the two through the dynamic action exerted by passing wheels. This process can result in the formation of a slurry. This slurry can migrate upwards and foul the ballast by reducing its drainage properties. Simultaneously, ballast particles can be forced downwards into the plastic slurry under the influence of gravity and train loading. After repeated action over a long time, ballast pockets form (Hay 1982). Figure 2.1 presents the cross and longitudinal section of ballast pockets.

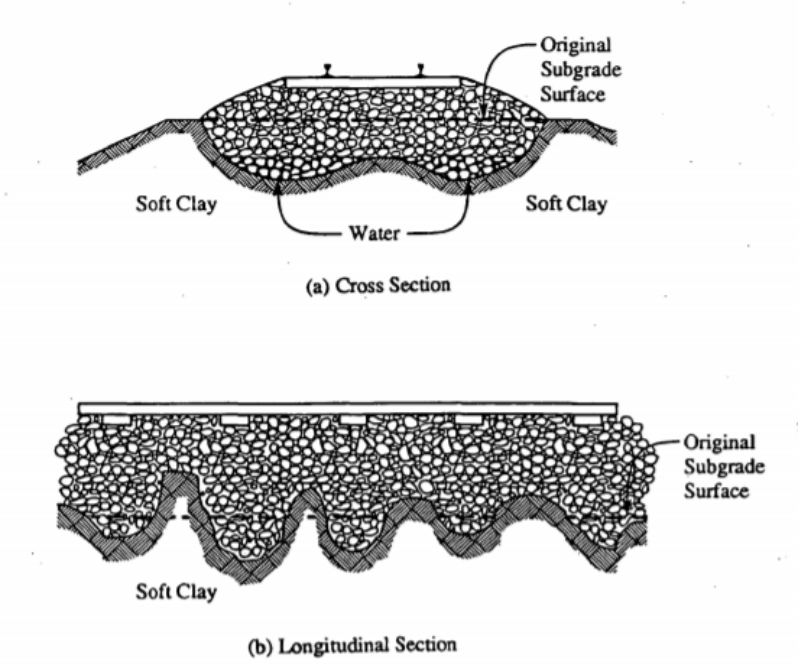

Fig. 2.1. Typical ballast pockets (Li and Selig 1995).

Ballast pockets can be formed in two positions. Figure 2.2(a) shows a common condition with ballast pockets formed under the center of cross ties. Due to the gradual movement and plastic deformation of the clay roadbed, the ballast pocket can also be moved to one side of the track, resulting in a "bathtub" effect, as illustrated in Figure 2.2(b) (Li et al. 2016).

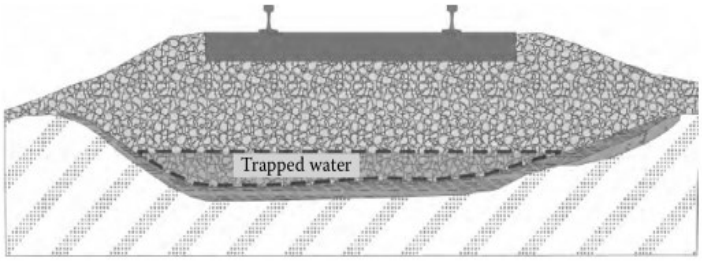

(a) Ballast pockets under the center of cross ties;

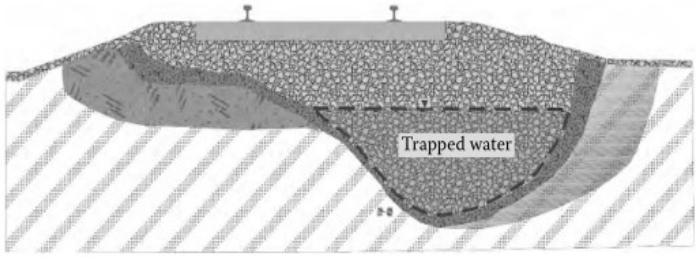

(b) Ballast pockets under one side of cross ties.

Fig. 2.2. Different positions of ballast pockets (Li et al. 2016).

Formation of ballast pockets is often accompanied by depression of the embankment under a

track, so the embankment with the ballast pockets can sink to a certain depth. Therefore, the excessive plastic deformation of the ballast pockets can damage the embankment's surface and have a more significant impact at a depth below the embankment (Li et al. 2016).

2.1.2 Development of ballast pockets on slopes

Ballast pockets can weaken the drainage capacity of the ballast. Ballast pockets are often referred to as water pockets because they are always full of water in the depression they create (Li et al. 2016). Since the water cannot be discharged from under the track and railway embankment, the surrounding soil becomes soft and eventually reaches a saturated state, resulting in considerable loss of its strength (Indraratna et al. 2011). As the process progresses, the water and weak soil combine, causing the ballast pockets to produce embankment slope failure (Li et al. 2016). This process of slope instability, caused by ballast pockets, is shown in Figure 2.3.

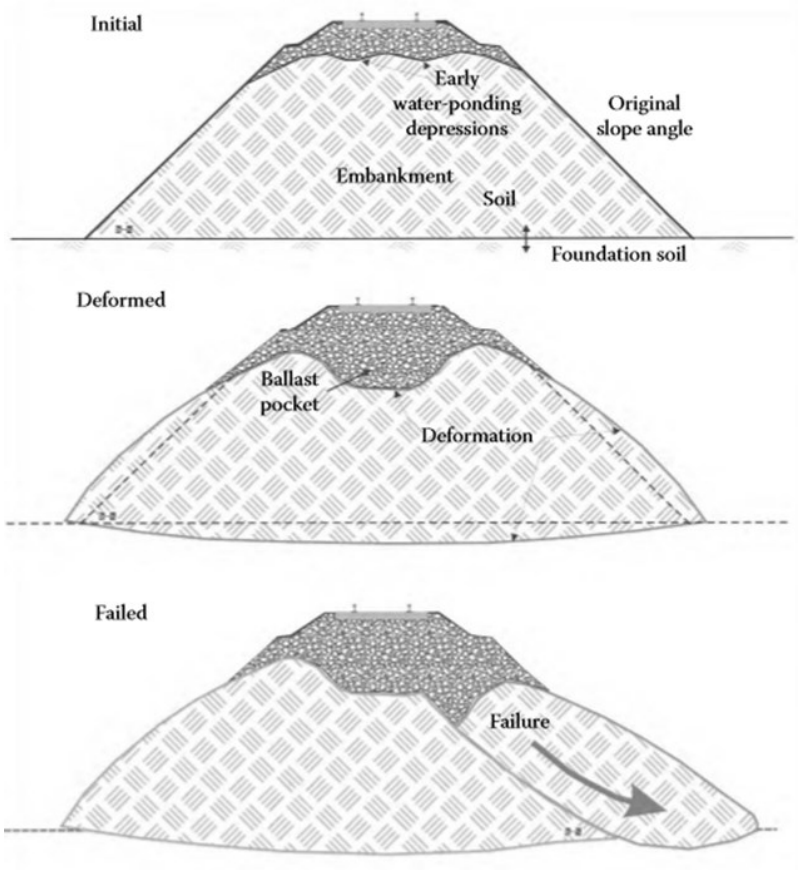

Fig. 2.3. Ballast pocket induced slope instability (Li et al. 2016).

Figure 2.3 presents a ballast pocket existing under the center of cross ties, and then a slope failure caused by the ballast pocket under one side of the track, as described in Figure 2.4 (a). Comparing the two slope failures in Figure 2.4, it can be inferred that the slope failure caused by the ballast pocket connects the geometry of the ballast pocket and the water level remaining in ballast pockets, which is the crucial point for analysis in this thesis.

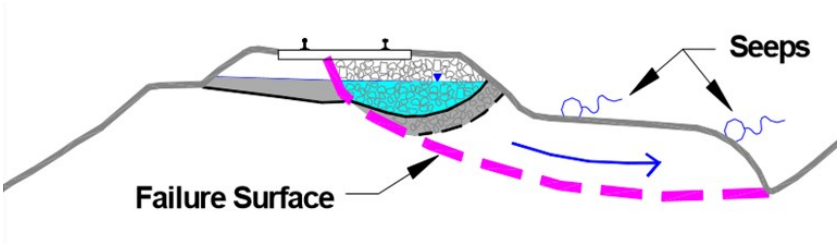

(a) Shallow shear failure;

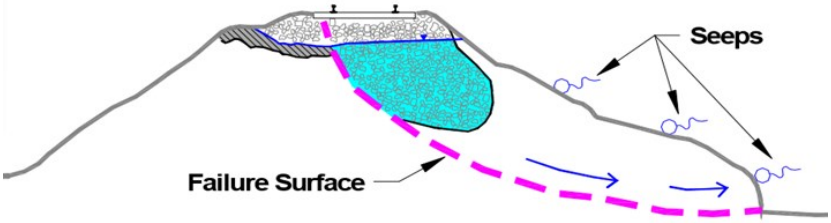

(b) Deeper shear failure.

Fig. 2.4. Ballast pockets associated with common subgrade failure modes (Australian Rail Track Corporation 2015).

2.1.3 Behavior of saturated soils – coupled consideration of deformation and pore fluid flow

Water retained in ballast pockets is a significant factor impacting soil behavior, since water can saturate the soil and reduce its shear strength. The behavior of a (saturated) porous soil structural system under dynamic or static loading should be defined by considering the coupling between flow and deformation. The behavior of the mixture of soil and water can be affected by many factors, such as the solid particle (soil skeleton) deformation, the relative motion of particles and water, the pore water movement, and deformation (Desai and Zaman 2013).

Biot (1941) has investigated elastic materials' behavior, from which the formulation for coupled, solid-fluid behavior was developed. In Biot's theory, several basic properties of the soil are assumed: 1) isotropy of the material, 2) reversibility of stress-strain relations under final equilibrium conditions, 3) linearity of stress-strain relations, 4) minor strains, 5) the incompressibility of water, 6) possible air bubbles in the water, 7) the water obeys Darcy's law when flowing through the porous skeleton (Biot 1941).

The soil skeleton is regarded as a porous elastic solid, and the laminar pore fluid is coupled to the solid under conditions of equilibrium and continuity. Biot's governing equation is (Smith et al. 2013):

$$\frac{K\prime}{w}\left[k_x\frac{\partial^2 u_w}{\partial x^2}+k_y\frac{\partial^2 u_w}{\partial y^2}+k_z\frac{\partial^2 u_w}{\partial z^2}\right]=\frac{\partial u_w}{\partial t}-\frac{\partial p}{\partial t} \tag{2.1}$$

Where K' is the soil bulk modulus and p is the mean total stress.

For two-dimensional equilibrium without body forces, the gradient of effective stress is augmented by the gradients of fluid pressure u_w which results in the following equations (Smith et al. 2013).

$$\frac{\partial \sigma_x'}{\partial x} + \frac{\partial \tau_{xy}}{\partial y} + \frac{\partial u_w}{\partial y} = 0 \tag{2.2a}$$

$$\frac{\partial \tau_{xy}}{\partial x} + \frac{\partial \sigma_y'}{\partial y} + \frac{\partial u_w}{\partial y} = 0 \tag{2.2b}$$

Where $\sigma_x' = \sigma_x - u_w$ and $\sigma_y' = \sigma_y - u_w$ are 'effective' stresses.

The constitutive law for the solid in plane strain is (Smith et al. 2013):

$$\begin{Bmatrix} \sigma_x' \\ \sigma_y' \\ \tau_{xy} \end{Bmatrix} = \frac{E'(1-\nu')}{(1+\nu')(1-2\nu')} \begin{bmatrix} 1 & \frac{\nu'}{1-\nu'} & 0 \\ \frac{\nu'}{1-\nu'} & 1 & 0 \\ 0 & 0 & \frac{1-2\nu'}{2(1-\nu')} \end{bmatrix} \begin{Bmatrix} \varepsilon_x \\ \varepsilon_y \\ \gamma_{xy} \end{Bmatrix} \tag{2.3}$$

Where E' and ν' are effective elastic parameters (elastic modulus and Poisson's ratio).

The solid- strain-displacement equations are given by (Smith et al. 2013):

$$\begin{Bmatrix} \varepsilon_x \\ \varepsilon_y \\ \gamma_{xy} \end{Bmatrix} = \begin{bmatrix} \frac{\partial}{\partial x} & 0 \\ 0 & \frac{\partial}{\partial y} \\ \frac{\partial}{\partial y} & \frac{\partial}{\partial x} \end{bmatrix} \begin{Bmatrix} u \\ w \end{Bmatrix} \tag{2.4}$$

Where ε_x, ε_y and γ_{xy} are strain components in the xy plane, u and w are displacements in the x- and y- directions.

Under plane strain conditions, according to the usual operational sequence of the formulation of displacement method, the stress terms in Equation 2.2 can be expressed in terms of displacements (Griffiths 1994).

$$\frac{E'(1-\nu')}{(1+\nu')(1-2\nu')}\left[\frac{\partial^2 u}{\partial x^2} + \frac{(1-2\nu')}{2(1-\nu')}\frac{\partial^2 u}{\partial y^2} + \frac{1}{2(1-\nu')}\frac{\partial^2 w}{\partial x\,\partial y}\right] + \frac{\partial u_w}{\partial x} = 0 \tag{2.5a}$$

$$\frac{E'(1-\nu')}{(1+\nu')(1-2\nu')}\left[\frac{1}{2(1-\nu')}\frac{\partial^2 u}{\partial x\,\partial y} + \frac{\partial^2 w}{\partial y^2} + \frac{(1-2\nu')}{2(1-\nu')}\frac{\partial^2 w}{\partial x^2}\right] + \frac{\partial u_w}{\partial y} = 0 \tag{2.5b}$$

Similarly, the constitutive law for the fluid in plane strain is (Smith et al. 2013):

$$\begin{Bmatrix} q_x \\ q_y \end{Bmatrix} = \frac{1}{\gamma_w} \begin{bmatrix} k_x & 0 \\ 0 & k_y \end{bmatrix} \begin{Bmatrix} \frac{\partial u_w}{\partial x} \\ \frac{\partial u_w}{\partial y} \end{Bmatrix} \tag{2.6}$$

Where q_x and q_y are the volumetric flow rates per unit area into and out of the element, k_x is the material permeability in the x-direction, k_y is the material permeability in the y-direction, and r_w is the unit weight of water.

According to the 2D continuity considerations, the rate of the net flow must be equal to the rate of change of volume of the soil element (Smith et al. 2013), thus

$$\frac{\partial \mathrm{q_x}}{\partial \mathrm{x}} + \frac{\partial \mathrm{q_y}}{\partial \mathrm{y}} = -\frac{d}{dt}\left(\frac{\partial u}{\partial x} + \frac{\partial w}{\partial y}\right) \tag{2.7}$$

Where t represents time.

Combined with Equation (2.6), thus

$$\frac{d}{dt}\left(\frac{\partial u}{\partial x} + \frac{\partial w}{\partial y}\right) + \frac{k_x}{r_w}\frac{\partial^2 u_w}{\partial x^2} + \frac{k_y}{r_w}\frac{\partial^2 u_w}{\partial y^2} = 0 \tag{2.8}$$

The coupled Biot formulations for 2D poroelastic material can, therefore, be represented by Equations 2.5 and 2.8. The displacements and excess pore pressure at spatial location (x, y) at any time t can be estimated according to a solution to these equations (Smith et al. 2013).

For coupled problems involving a mixture of solid and fluid (water), the FEM is a good choice of solution method, and is introduced in detail in Section 2.4.

According to Desai and Zaman (2013), for Biot's formulation, there are two types of nodal unknowns, displacements. Figure 2.5 shows a schematic of a typical FEM discretization.

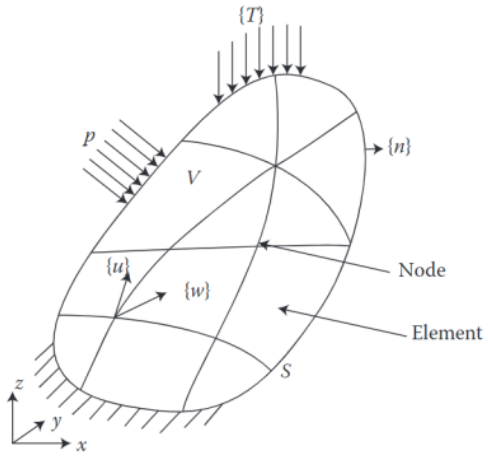

Fig. 2.5. Finite element discretization coupling Biot's theory (Desai and Zaman 2013).

2.2 Analysis of moving loads on the railway embankment

Understanding and quantifying the loading on the railway track foundation and the mechanism by which loads are transferred from the wheel-rail interface to the track foundation are critical to the design and repair of the railway track and subgrade. The load characteristics of railway tracks used for heavy freight traffic may vary considerably from high-speed passenger railway tracks (Li et al. 2016). This chapter begins by introducing the railway track structure and then presents the load transfer mechanism.

2.2.1 Railway track structure

The railway track is built to ensure that trains can pass safely and smoothly while transporting

passengers and cargo. The railway track is divided into two main types: ballasted track and slab track, as portrayed in Figure 2.6 (Kouroussis et al. 2015). Compared to the slab track, the ballasted track needs less initial investment and is easier to lay. Simultaneously, the structure of a ballasted track can provide better drainage (Esveld 2001). Since analyzing the influence of ballast pockets on embankment slopes is the chief aim of this study, a ballasted track is selected, which is commonly used in Canada and the United States.

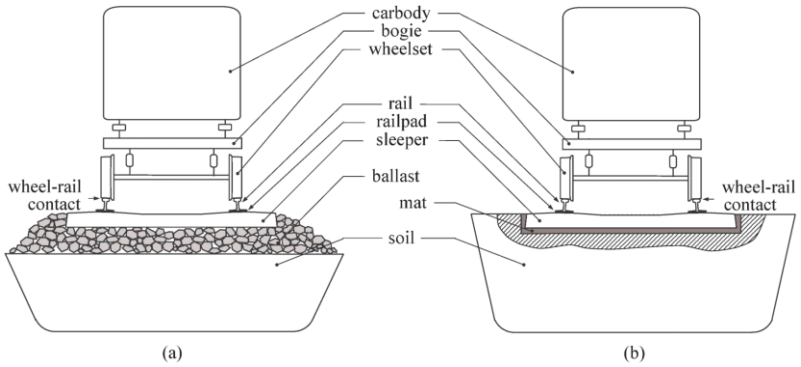

Fig. 2.6. Main components of a track (longitudinal view): (a) Ballasted track; (b) Slab track (Kouroussis et al. 2015).

Figure 2.6(a) shows the composition of a ballasted track. It consists of two parts: superstructure and substructure. The main load-supporting elements are included in the superstructure, such as the rail, tie (sleeper), and fastening system. The substructure includes structures related to the geotechnical system such as ballast, subballast, and subgrade (formation) (Li et al. 2016). Superstructure and substructure are equally significant for passenger safety and comfort and the quality of ride for passenger and freight trains (Remennikov and Kaewunruen 2008).

The following is a brief description of the substructure layers (as shown in Figure 2.7) in which the ballast pockets can be produced. The ballast layer is primarily composed of crushed stone and has three main functions. The first function is to distribute the load from the sleepers evenly to the subgrade; the second is to act as a spring to absorb the shock of dynamic loads; the third is to allow the rail system to maintain a good drainage state by discharging the moisture and water out of the track system. The subballast is a transition layer separating the upper layer of large particles and the lower layer of fine particles. Subballast can buffer loads passing from the ballast layer before reaching the subgrade and help drain out water retained in the subgrade. The subgrade (formation) is the bottom of the entire substructure. Its most important role is to support the entire track and keep the track structure stable (Tzanakakis et al. 2013). The substructure plays a vital role in track drainage and load distribution.

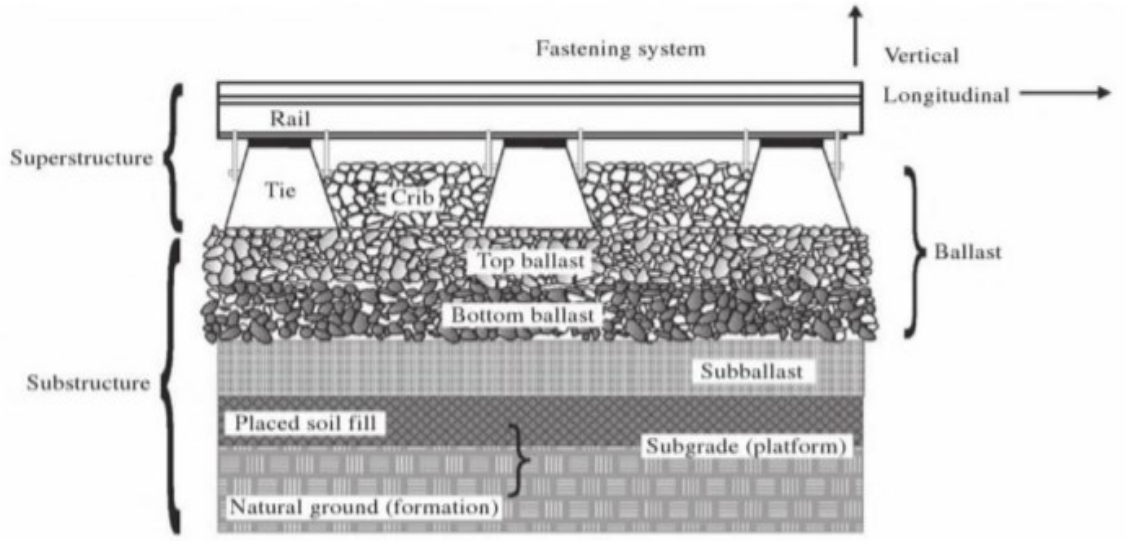

Fig. 2.7. Simplified components of a typical ballasted track (Alemu 2011).

2.2.2 Moving loads on the railway track foundation

Stresses and strains in the track foundation are generated by transferring three types of loads (static, cyclic, and dynamic) to the track and subgrade. The stress states of the three elements in the track foundation under moving wheels are shown in Figure 2.8, which presents only the vertical and longitudinal stresses (Li et al. 2016).

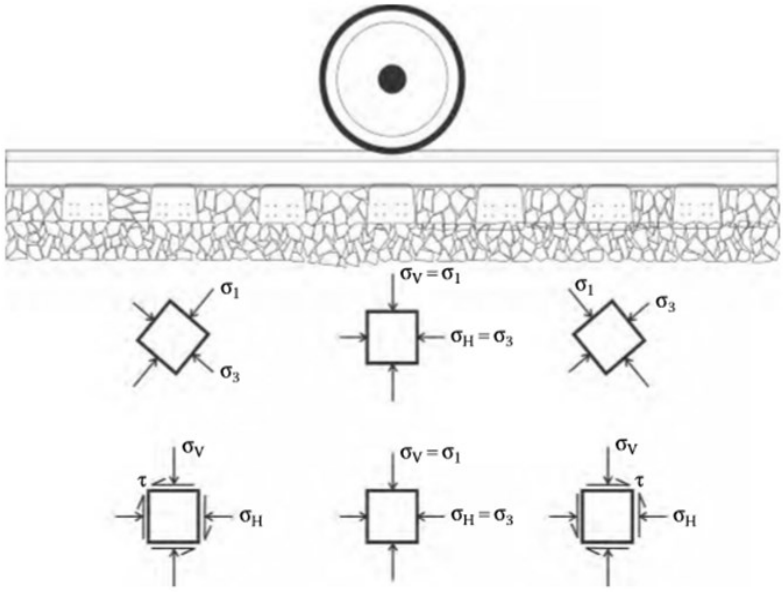

Fig. 2.8. Stress in track foundation (Li et al. 2016).

When the shear stress is zero, the normal stress is considered the primary stress. For elements directly under the wheel load, the vertical and lateral normal stresses are called principal stresses. In Figure 2.8, the larger stress of the principal stresses is represented by σ_1, and the minor principal stress is represented by σ_3 (Li et al. 2016).

Subsequently, three types of loads that transfer to the track foundation are introduced.

a) Static loads exerted on the track foundation consist of the train's weight (i.e., the live load) and the weight of track and subgrade (i.e., the dead load). Live loads are considered the significant component of static loads, but when designing and analyzing the slope stability of track built on a high subgrade or embankment, dead loads also need significant consideration. Stress distributions with depth due to the live loads and dead loads are different. The stress generated by the live load decreases as the depth of the track and subgrade increases, while the stress caused by the dead load increases with increasing depth (Li et al. 2016).

b) Moving loads generated by a train traveling on a track create loading pulses quickly and repeatedly applied to the track and subgrade. Due to the characteristics of loading pulses, the effects of cyclic loads on a track and subgrade differ from sustained static loads. The changes in loading rate affect the subgrade soil properties, so it is essential to identify the duration of a transient loading pulse, which is primarily influenced by the operating speed of a train and the depth of consideration. Thus, the loading pulse duration can be calculated according to Equation 2.9 (Li et al. 2016).

$$t = \frac{L}{V} \tag{2.9}$$

Where t = the loading pulse duration (h), V = the speed of the train (km/h), L = the influence length (km) of an axle load or adjacent axle loads for a given depth of ballast or subgrade.

Indraratna et al. (2010) have investigated the behavior of ballast under many cycles through large-scale cyclic triaxial tests. The results show that permanent deformation and degradation of ballast increase with the frequency of loading and number of cycles at frequencies ranging from 10 to 40 Hz. Particle breakage is mainly due to the tensile stress developed during cyclic loading and is located mainly toward the movement of ballast particles.

c) For dynamic wheel loads, if the duration of loads is short, the vehicle suspension has little or no effect. If the loads are long, the response of a vehicle suspension considerably affects the forces involved. No matter how long the dynamic load is, the magnitude of load applied on the track under train operations and the static wheel load magnitude are different. Augmenting the static wheel load by a dynamic, impact load factor is a standard method for selecting a design dynamic wheel load (Li et al. 2016).

2.2.3 Load transfer mechanism

The vehicle-rail contact determines the magnitude of wheel-rail interaction forces. According to the frequency components spectrum, when force components are at a high frequency, they dissipate quickly after being transferred from the wheel-rail interface. Static or dynamic wheel loads with lower frequencies continue to be transmitted to the underlying substructure layer, and the coverage area continuously increases with the increasing depth, as shown in Figure 2.9 (a) (Li et al. 2016). In Figure 2.9(a), Selig and Waters (1994) have assumed the

distribution of vertical stress to be uniform in the substructure. Figure 2.9 (b) illustrates a modified spread model.

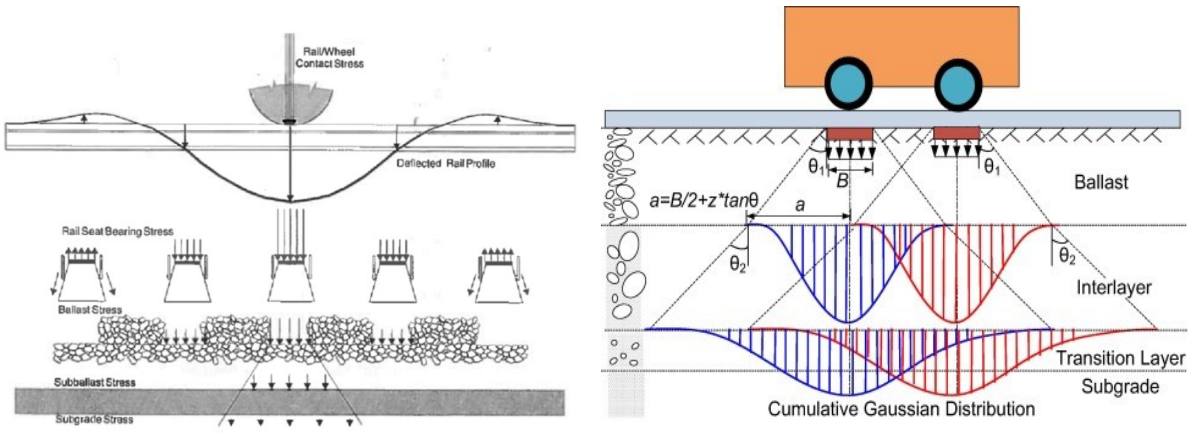

(a) (b)

Fig. 2.9. (a) Load spread model (Selig and Waters 1994), and (b) modified load spread model (Zhang et al. 2016).

AREMA (2012) confirms that tie-to-ballast pressures are not uniformly distributed across or along the bottom of a tie. AREMA recommends impact factors can calculate the average pressure at the bottom of the tie, as shown in Equation 2.10.

$$P_{avg} = \frac{2P*\frac{DF}{100}*(1+\frac{IF}{100})}{A} \tag{2.10}$$

In Equation 2.5, P represents the *wheel load* in pounds-force (lbf), IF, which equals $33V/100D$, represents the *impact factor* intended to estimate the dynamic forces due to wheel irregularities, V represents the known *velocity* in miles-per-hour (mph), D represents the nominal *wheel diameter* in inches (in), DF represents the *distribution factor* in percent (%), and A represents the *contact area* of the crosstie.

AREMA estimates the distribution factor in Equation 2.10, varies by relationships of varying degrees of track modulus, crosstie type, and crosstie spacing. Figure 2.10 presents one such conventional relationship cited in the AREMA standards that provides the distribution factor needs for Equation 2.10.

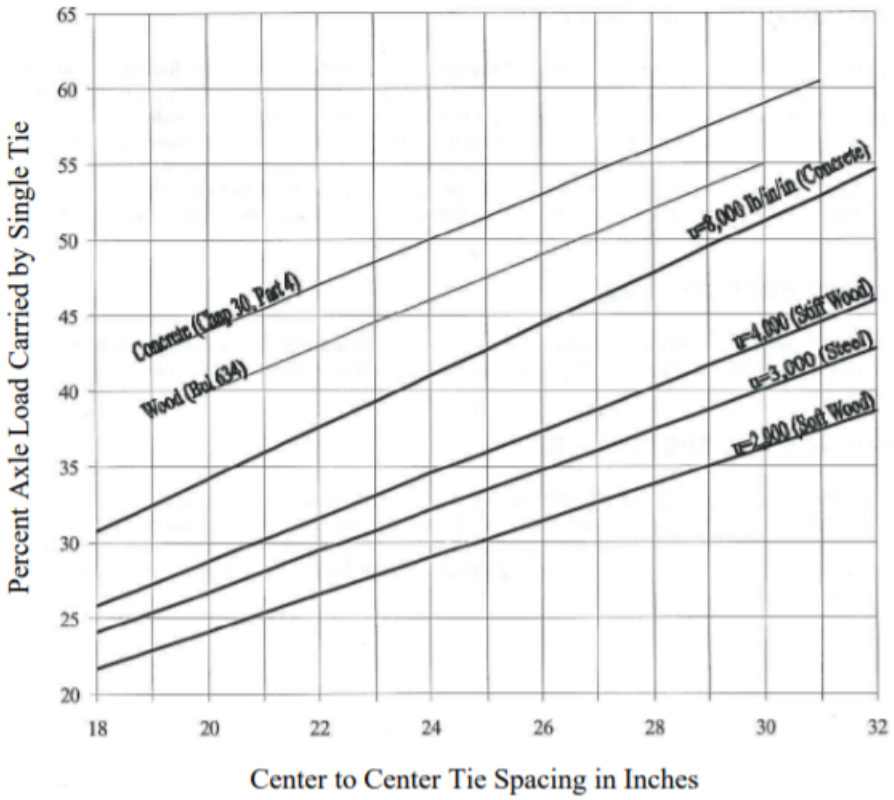

Fig. 2.10. AREMA's estimated distribution of loads (AREMA 2018).

AREMA (2018) presents various methods for determining the area, A, used in Equation 2.8. In Chapter 16 of the AREMA manual, the crosstie's bearing area is defined as two-thirds of the crosstie footprint (as shown in Figure 2.11), which is developed for the new construction of the track. In Chapter 30, the crosstie's bearing area appears to be the entire footprint of the crosstie, which is more suitable for the existing track.

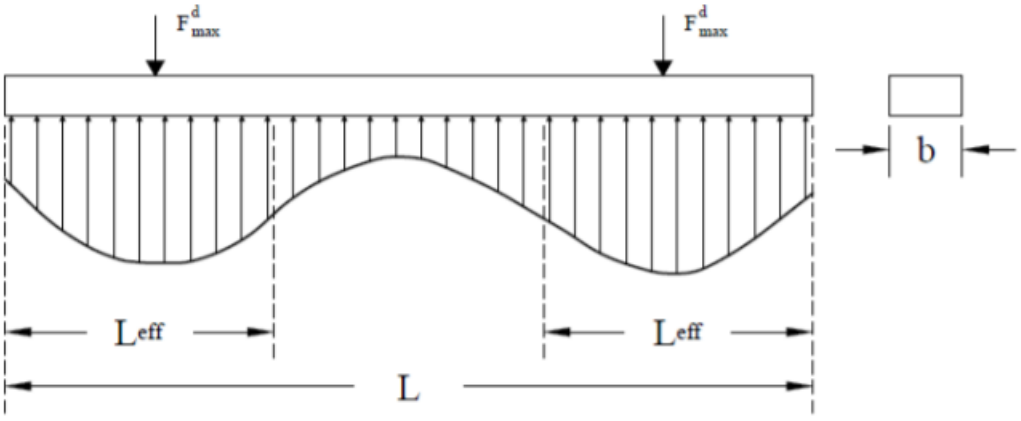

Fig. 2.11. Two-Thirds assumed crosstie footprint (Watts 2018).

2.3 Key parameters of the model

It is essential to identify critical parameters and credible ranges of these parameters, which are the primary goal of this section. This study's model consists of four main components: the freight trains, the rail system, the foundation, and the ballast pockets. Therefore, the main parameters considered include freight train size, the magnitude of moving loads, the dimension of the railway embankments, slope inclination ratios, and soil and material characteristics.

2.3.1 Parameters for describing freight trains

Trains (or rolling stock) usually comprise two types of vehicles: 1) a locomotive or a powered car that ensures the regular operation of the train; 2) passenger coaches carrying passengers or freight cars and wagons carrying goods (Tzanakakis et al. 2013). Figure 2.12 shows typical freight cars used in North America (AREMA 2012). For freight cars in North America, the most commonly used wheel diameters are 840mm and 920 mm, and the latter accounts for a more significant proportion in the design of current and future freight cars (Stephen and Uhlig 2013).

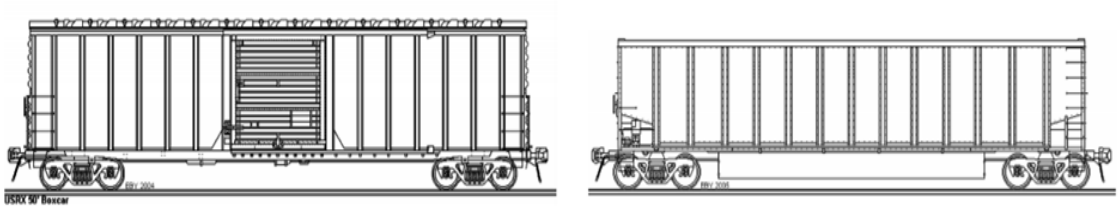

Fig. 2.12. Typical freight cars used in North America (AREMA 2012).

The number of axles per vehicle or car can define vehicles, and rail track forces can then be investigated (Tzanakakis et al. 2013). Table 2.1 introduces the static axle loading of various types of rolling stock.

Table 2.1. Static axle loading of various types of rolling stocks (Esveld 2001)

Train types	Number of axles	Axle loads under services	
		Empty loads (kN)	Fully loaded (kN)
Trams	4	50	70
Light-rail	4	80	100
Passenger coach	4	100	120
Passenger motor coach	4	150	170
Locomotives	4 or 6	215	n/a
Freight wagon	2	120	225
Heavy haul (U.S.A, Australia)	4	120	250-350

Reasonable operating speeds are another important parameter of freight trains. Based on the following table, the maximum allowable operating speed for freight trains is 120 km/h.

Table 2.2. Maximum speeds for different railway lines (Esveld 2001)

Type of railway lines	Freight trains	Passenger trains
Branch lines	30-40 km/h	/
Secondary lines	60-80 km/h	80-120 km/h
Main lines	100-120 km/h	160-200 km/h
High speed lines	/	250-300 km/h

According to the parameter values of freight trains in North America in Table 2.1 and 2.2, the freight train is a train with four axles per car and 36,000 lbs (160 kN) for each axle (loaded) in this study. Freight train speed cannot exceed 120 km/h on a main line.

2.3.2 Parameters for railway track structure

The railway track comprises a superstructure and a substructure. This section introduces the railway track structure parameters by separately describing the parameters of the superstructure and substructure.

a) Superstructure

Figure 2.13 shows the track's superstructure elements, and in this section, the track gauge, the sleeper dimensions, sleeper spacing, and properties of their materials are introduced.

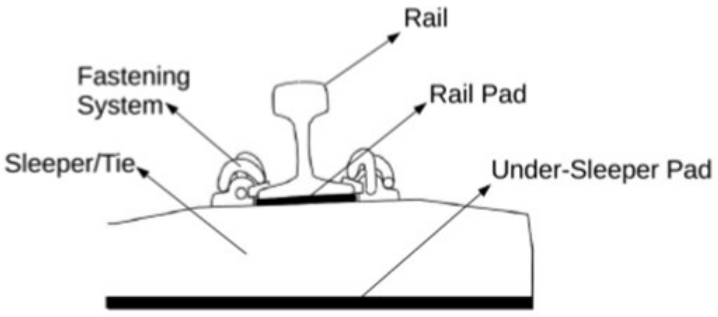

Fig. 2.13. Scheme of track's superstructure elements (Dahlberg 2003).

The distance between the rails' inner sides is defined as the track gauge established at 14 mm below the top of the rail (Profillidis 2014). Table 2.3 shows primary railway track gauges used around the world. Standard track gauge is defined as 1,435 mm by AREMA (1996). Based on Table 2.3, the standard track gauge in Figure 2.14 is used widely by many countries and regions, such as North America and China.

Table 2.3. Principal railway track gauges (Puffert 2002)

Gauge		Major countries and regions	Proportion of world total (percent)
English (ft.-in.)	Metric (mm.)		
2'6"	762	China*, India*	1.7
3'0"	914	Colombia, Guatemala, Ireland*	0.6
3'3.37"	1000	Chile*, Spain*, India*, Brazil*…	8.8
3'6"	1067	Australia*, Japan*, New Zealand…	9.0
4'8.5"	1435	Europe*, North America, China*…	58.2
5'0"	1524	Finland, Mongolia, Former USSR	12.8
5'3"	1600	Australia*, Brazil*, Ireland*	1.2
5'6"	1676	Chile*, India*, Pakistan*…	7.0

Notes: * means countries or regions use more than one gauge. Percentages add to less than 100 due to additional, rare gauges.

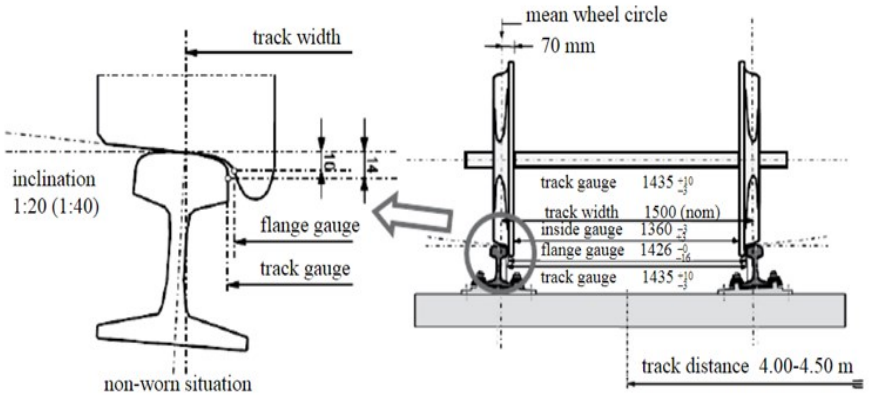

Fig. 2.14. A standard gauge track (Shevtsov 2008).

Based on sleepers' materials, sleepers (or cross ties) are divided into timber sleepers and concrete sleepers. In most parts of Europe, Japan and certain African countries, concrete sleepers can meet more than half of the annual sleeper needs. However, in the United States, Canada, and some other countries, fewer concrete sleepers are being used than in the previously mentioned countries, due to the abundance of forestry products. The geometric and material properties of sleepers used in North America are introduced in Table 2.4 and Table 2.5.

Table 2.4. Sleeper geometric properties (Selig and Waters 1994)

Variable	Units	Wood	Concrete
Spacing	in. (mm)	19.5 (495)	24 (610)
Length	ft. (m)	8.5 (2.59)	8.5 (2.6)
Width	in. (mm)	9.0 (229)	10.8 (274)
Cross-sectional area	In^2. (mm^2)	63.0 (40600)	86.6 (55900)
Weight	lb. (N)	250 (1110)	850 (3780)

Table 2.5. Sleeper material properties (Profillidis 2014)

Material	Modulus of elasticity (MPa)	Poisson's ratio	Tensile strength R_T (MPa)	Compressive strength R_C (MPa)
Reinforced-concrete sleeper	2.94×10^4	0.25	2.94	29.42
Prestressed-concrete sleeper	4.90×10^4	0.25	5.88	8.83
Tropical timber sleeper	2.45×10^4	0.25	9.81	98.07
Rail (steel)	2.06×10^5	0.25	686.47	588.40

An analysis of Table 2.5 shows that the tensile and compressive strengths of timber sleepers are higher than that of concrete sleepers. The timber sleeper can be assumed to be a better material.

In North American practice, the parameters of track superstructure selected for this study are 1,435 mm rail gauge, and the timber sleeper which is 229 mm in width, 2,590 mm in length, and 495 mm in spacing, center to center.

b) Substructure

The typical sectional track substructure is shown in Figure 2.15. The ballast thickness design, measured from the lower side of the sleeper, should create an even load on the subgrade (Esveld 2001). The ballast layer thickness can determine the ballast confining pressure (Indraratna et al. 2009) and influence the ballast settlement in a railway caused by long-term traffic loading. The track needs confining pressure and lateral strength, provided by the ballast shoulder width and side slope (Sadeghi et al. 2016). In Table 2.6, geometric parameters of ballast layer are given.

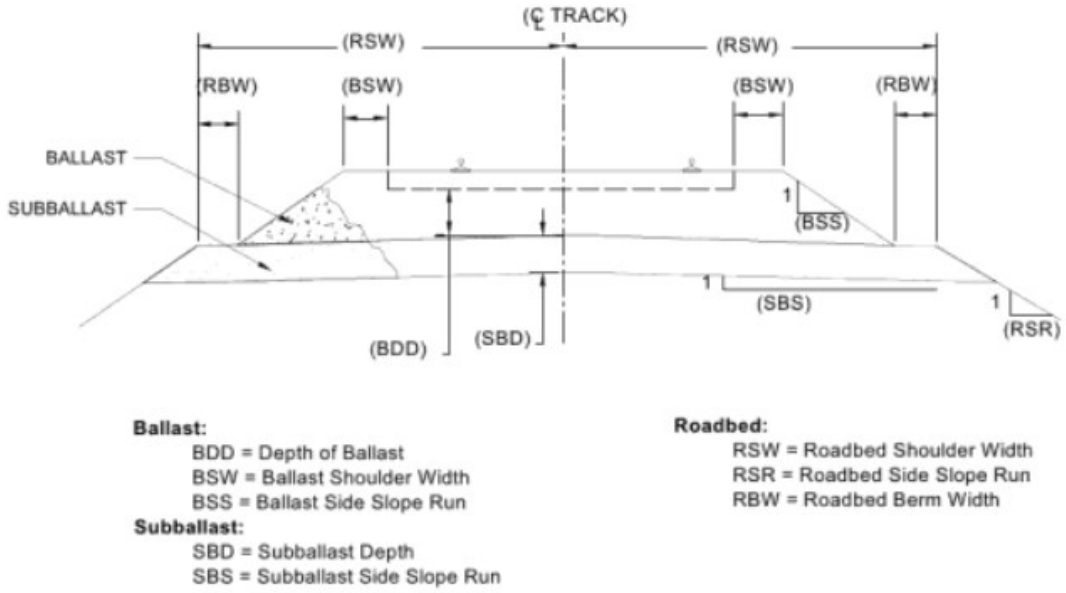

Fig. 2.15. Typical section track substructure (AREMA 2000).

Table 2.6. Geometric parameters of ballast layer (AREMA 2012)

Requirements	USA
Ballast Depth underside of sleeper to the top of the finished formation	>12 in (304 mm)** Main line
Ballast shoulder width	>12 in (304 mm) (CWR) Main line
Side Slope of the ballast shoulder	Height: horizontal: 1:2

Noted: **The measurement is made under the line rail in tangent track, or under inside rail in curved track, and is made with respect to the top of the sub-ballast at the center line.

For the mainline, the ballast layer thickness and the ballast shoulder width should be larger than 12 inches (304 mm) (AREMA 2012). The subballast layer thickness is usually approximately 6 inches (152mm) (Middleton et al. 2007). The subballast section's width depends on the width of the roadbed, since the subballast should extend the entire width of the embankment, capping the top surface. The top of the subballast section should project at least 24 inches (608 mm) beyond the ballast slope's toe because the end slope of the subballast is usually the same as the slope of the lower subgrade (TRB 2012).

The thickness of the subgrade is usually over 2,000 mm and filled with natural soil or fill material (Egeli and Usun 2012).

Strong and uniform-grade, angular geomaterials are selected as ballast materials to support the train load (Indraratna et al. 2011). The subballast layer is the coarse aggregate with a grain size of 0-31.5 mm. Values of the mechanical characteristics of track substructure materials are shown in Table 2.7. Ballast pockets could be generated in the subgrade made of soft clay, as shown in Figure 2.2.1, so the properties of the subgrade in Table 2.7 are soft clay subgrade characteristics. Table 2.8 shows the range of Young's moduli of clay subgrade.

Table 2.7. Values of the mechanical characteristics of railway substructure materials (Profillidis 2014; Li et al. 2016; Allan 2012)

Material	Density (kN/m^3)	Modulus of elasticity (MPa)	Poisson's ratio v	Cohesion c (kPa)	Friction angle ϕ (°)
Ballast	17.3	127.49	0.2	0	45
Subballast	18.8	196.13	0.3	0	35
Subgrade	18.0	20.00	0.3	10	30

Table 2.8. Range of Young's moduli of clay subgrade (Ejezie 2014)

Type of soil		Young's modulus, E (MPa)
Clay	Very soft	2-5
	Soft	5-25
	Medium	15-50

In track design and maintenance, drainage of the track is a crucial factor that needs to be considered. Values of hydraulic conductivity for different kinds of soil are summarized in

Table 2.9.

Table 2.9. Hydraulic conductivity for common soil types (Budhu 2008)

Soil type	k (cm/s)	Description	Drainage
Clean gravel	>1.0	High	Very good
Clean sands, clean sand and gravel mixtures	1.0 to 10^{-3}	Medium	Good
Fine sands, silts, mixtures comprising sands, silts, and clays	10^{-3} to 10^{-5}	Low	Poor
Silt, silt clay	10^{-5} to 10^{-7}	Very low	Poor
Homogeneous clays	$<10^{-7}$	Practically impervious	Very poor

A slope of 3H:1V or 2H:1V is commonly used in embankments. (Some railroads with coarse rock fill use 1H:1V or 5H:4V slope.) The two common slopes are considered in this study. The inclination of a ballast slope may differ from that of a subballast and subgrade slope, as shown in Table 2.10.

Table 2.10. Values of slope inclination (Xu 2019)

Name	Horizontal: Vertical	
Ballast slope	2:1	2:1
Subballast and subgrade slope	2:1	3:1

2.3.3 Properties of fouled ballast

Ballast pockets are full of fouled ballasts and dirty subballasts (AREMA 2012), and the properties of fouled ballasts are introduced below. Table 2.11 introduces the dry unit weight range and responding void volume of ballast under different conditions.

Table 2.11. Unit weight/void volume relationships of ballast (Li et al. 2016)

Ballast condition	Unit weight		Void volume
	(lb/ft^3)	(kN/m^3)	(%)
Loose	95	14.9	41
Compact	110	17.3	35
Moderately fouled	125	19.6	26
Heavily fouled	135	21.2	20

By conducting large-scale triaxial tests on ballast, Indraratna et al. (1998), have reported that coarser particles have smaller Poisson's ratio and smaller deformation modulus. The v = 0.4 can be considered a typical Poisson's ratio for fouled ballast (Selig and Waters 1994). Table 2.12 shows measured ballast elastic moduli. Wet fouled ballast has lower elastic modulus than clean ballast and dry fouled ballast.

Table 2.12. Measured ballast elastic modulus (Stark et al. 2016)

Ballast condition	Modulus	
	(ksi)	(MPa)
Clean – dry and wet	30-40	200-275
Fouled – dry	50-55	340-380
Fouled – wet	20-25	135-170

Particles in both fresh and fouled ballast are noncohesive (Kumara and Hayano 2016). Table 2.13 summarizes the internal friction angles of clean ballast and wet fouled ballast. Tutumluer et al. (2008) have found that the clean ballast has the most significant friction angle compared with fouled ballast. The friction angle of fouled ballast decreases with increasing water content, which means dry fouled ballast has a larger friction angle than wet fouled ballast. Table 2.14 shows specific values of hydraulic conductivity for fouled ballast.

Table 2.13. Summary of ballast internal friction angles (Tutumluer et al. 2008)

Ballast condition	Fouling Index (%)	Friction angle (°)
Clean	0	45.0
	5	44.7
Wet	15	37.7
	25	34.5

Table 2.14. Hydraulic conductivity values for fouled ballast (Parsons 1990)

Fouling Category	Fouling Index	Hydraulic Conductivity k (mm/s)
Clean	<1	25-50
Moderately clean	1-9	2.5-25
Moderately fouled	10-19	1.5-2.5
Fouled	20-39	0.005-1.5
Highly fouled	>39	<0.005

2.3.4 Properties of foundation soil

The properties of soils include unit weight, cohesion, angle of internal friction, Poisson's ratio and Young's modulus. In Table 2.15, typical values of moist or saturated unit weight, cohesion and angle of internal friction under undrained or drained conditions are given.

Table 2.15. Typical values of unit weight, cohesion and internal friction angle for sand and clay soils (Saifi et al. 2015; Brzeziński et al. 2018; Xie et al. 2014; Sharma et al. 2009; Ortiz 1986; Chakeri and Ünver 2014; Bagińska 2016; Wei et al. 2018; Xiao and Zhang 2011; Zhang et al. 2005)

Type of soil	Unit weight (kN/m^3)	Cohesion (kPa)	Internal friction angle (°)	Poisson's ratio	Young's modulus (MPa)
Sand	18.0	0.0	30.0	0.3	30
Silty sand	19.5	2.0	31.1	0.2	60
Sandy slit	18.2	3.0	30.3	0.24	45
Silt	19.7	3.0	36.0	0.3-0.35	-
Sandy clay	18.2	31.5	10.0	0.3	21.1
Silty clay	18.0	8.0-14.0	20.5-30.0	0.3	<25
Clay	19.0	30.0	35.0	0.27	30
Organic clay	12.5	7.0	20.0	0.3	18

2.4 Slope stability analysis methods

The slope stability problem is a statically indeterminate one. Many methods are used to quantify slope stability, such as the limit equilibrium method and various numerical methods (Cheng and Lau 2008). In this chapter, the principles of two-dimensional (2D) slope stability methods are discussed.

2.4.1 Limit equilibrium method

Limit equilibrium methods (LEMs) are still the most popular approaches to analyzing slope stability due to their simplicity (Cheng and Lau 2008). Figure 2.16 illustrates slope stability analysis using LEM. Given a potential slip surface, its FS is calculated as the ratio of shear strength over actual shear stress when force or moment limit equilibrium conditions are satisfied (Duncan and Wright 2005). The slip surface is often divided into slices for computation. Limit equilibrium method includes a group of slice methods, such as simplified Bishop's method, Janbu's method, Spencer's method, and Morgenstern-Price method. These methods are widely used to calculate the FS_{LEM} of slope stability in geotechnical engineering practice, where FS_{LEM} denotes the minimum FS among all potential slip surfaces (Liu et al. 2019). Limit equilibrium method often generates many potential slip surfaces in advance (Duncan and Wright 2005) or uses optimization algorithms (Cheng and Lau 2008) to find the critical slip surface corresponding to FS_{LEM} (Liu et al. 2019).

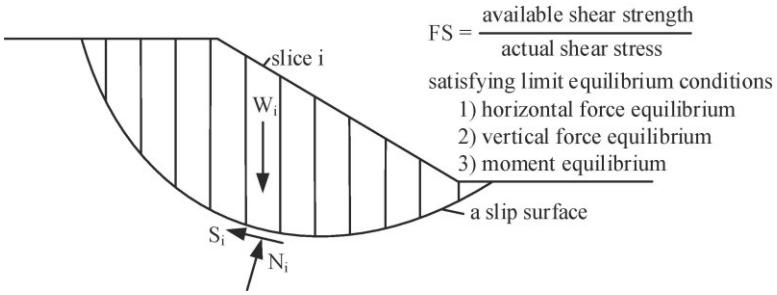

Fig. 2.16. Schematic illustration of slope stability analysis using LEM (Liu et al. 2019).

2.4.2 Numerical methods

Limit equilibrium method satisfies the evaluation of slope stability in geotechnical engineering, while advanced numerical methods can improve and supplement with LEM results. Limit equilibrium method is usually independent of the stress distribution within the slope, but sometimes it is necessary to evaluate the stresses, strains, and deformations inside a slope or an embankment, which can be solved by applying numerical methods (Chowdhury et al. 2010). The discrete element method (DEM), boundary element method (BEM), finite difference method (FDM), and FEM are introduced in this section. With the exception of DEM, which is a discontinuum method, the other three methods are continuum methods, treating the soil mass as a continuous material (Nikolić et al. 2016).

a. Discrete element method (DEM)

Cundall (1974) initially developed DEM, a numerical technique for studying the dynamic behavior of rock masses. As this technique has evolved, it has been widely used in various research applications in geotechnical engineering, such as creep of soils, and granular material flow (Ting et al. 1993).

In this technique, each particle in the soil mass is identified separately according to its physical properties (its geometry mass, moment of inertia and contact properties), as shown in Figure 2.17. Each particle (or discrete element) is considered to be geometrically deformed with deformable contacts (Ting et al. 1993).

Compared with FEM, the most commonly used and comprehensive numerical analysis method in soil mechanics, DEM, has many advantages. The distinct behavior of granular materials can be realistically simulated in DEM, and any dynamic change during the simulation can be observed. Discrete element method requires fewer parameters with precise physical meanings when defining the behavior of materials. However, it is challenging to form model geometry, which is one of the main disadvantages of DEM. Moreover, DEM requires excessive computational time, making it impractical to simulate large problems (Ardiç 2006).

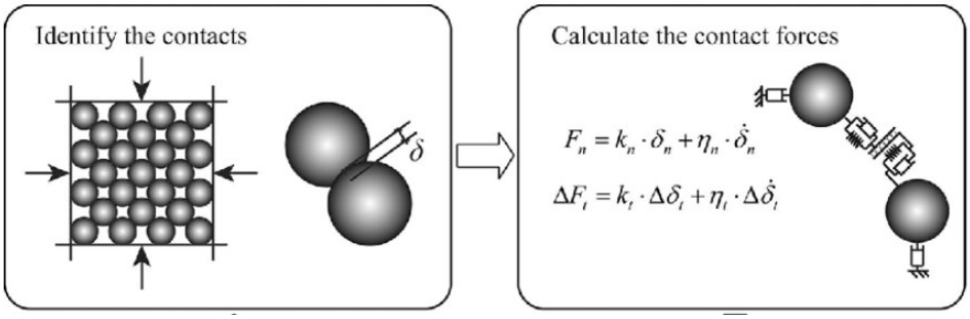

Fig. 2.17. Scheme of particle-particle contact in DEM (Liu et al. 2018).

b. Boundary element method (BEM)

Boundary element method is a numerical method for solving partial differential equations. The basic principle of BEM is to fit the boundary values into the integral equation using a

given boundary condition. Therefore, discretization is only required on the boundary where the number of boundary elements is limited, as shown in Figure 2.18. After finding the boundary solution, the integral equation can be used again to calculate the solution directly inside or outside the domain.

The main advantage of BEM is that the model size is reduced by one dimension, so for 2D BEM problems, the boundary element is a one-dimensional line that can be constant, linear or quadratic (Nikolić et al. 2016) However, the fundamental solution generating singular integrals can be complex or may even not be suitable for general anisotropic dynamic materials, which is an essential drawback of BEM (Hall and Oliveto 2004).

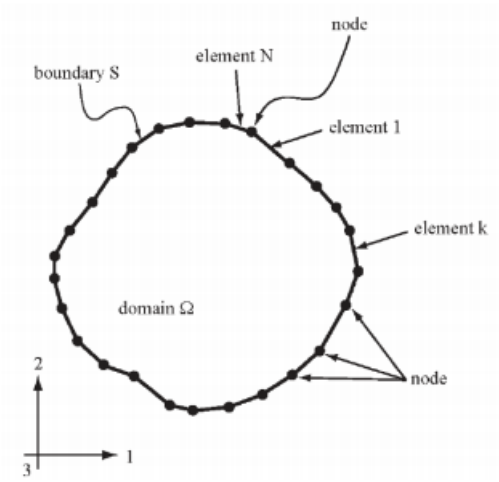

Fig. 2.18. Example of Discretization with Boundary Elements in 2D (Bobet 2010).

c. Finite difference method (FDM)

Finite difference method is perhaps the oldest numerical technique used for solving partial differential equations, which are given initial values or boundary values (Desai and Christian 1977). The method's general principle is in using the finite differences defined over a specific interval in the coordinate directions to replace the partial derivatives in the governing equations. A domain needs to be divided into a grid of nodes, among which the finite differences are defined. A regular grid, such as a rectangle, is used in the standard FDM, which is the most critical limitation of this method (Nikolić et al. 2016). Figure 2.19 shows a finite difference grid in 2D.

This method is suitable for incorporating nonlinear material behavior. Sufficiently small loading increments are involved in a step-by-step process, and the solution can be obtained when the process reaches the desired final state. The displacements at a grid point can be obtained after each loading step. Then, stresses are updated according to the material's nonlinear behavior, and another smaller loading increment is added to the original increments. The new increment begins with the previously incrementally updated stress field. Unlike other techniques that use implicit solution methods (such as FEMs), this is a forward-looking solution that does not require iteration (Bobet 2010). However, flexibility is the main disadvantage of FDM, since more regular solutions and triangulations are required in this method. There are difficulties in imposing boundary conditions (Mansour 2018).

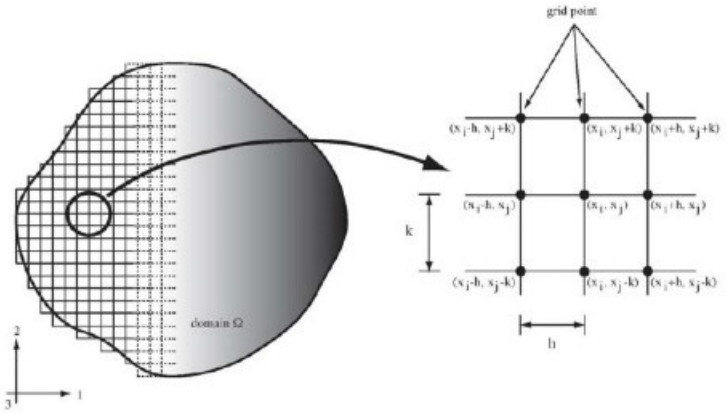

Fig. 2.19. Finite Difference Grid in 2D (Bobet 2010).

d. Finite element method (FEM)

Finite element method, is a numerical method used to find approximate solutions to differential equations' boundary value problems (Nikolić et al. 2016). It originated in the early 1960s (Clough 1960) and was rapidly developed in the late 1970s and early 1980s (Zienkiewicz 1977; Bathe 1982). The general principle behind the FEM is to divide the domain of the problem into smaller sub-domains called finite elements, perform the local approximation within each finite element, implement the finite element assembly and find the solution of the global systems of equation (Nikolić et al. 2016).

Desai and Christian (1977) have divided this method into six steps:

1. Discretization: Divide the domain into smaller finite elements including the nodes on the element boundaries or within an element, as shown in Figure 2.20.

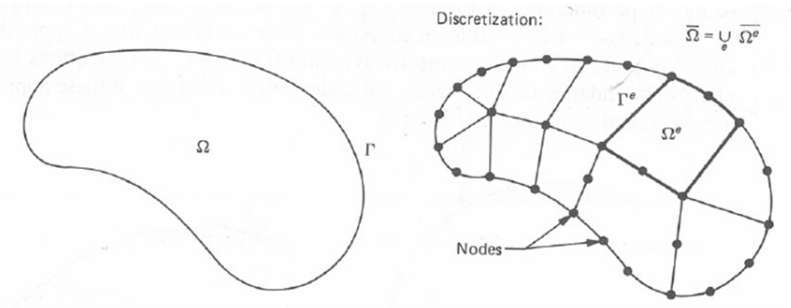

Fig. 2.20. 2D domain and 2D mesh for finite-element spatial discretization (after Hughes 1987).

2. Select an unknown quantity over each element, such as the displacement or stress, then determine the functions or models of this quantity (e.g.displacement functions, interpolation functions, etc.), based on which the following computation is done.

   As usual in a displacement method, σ and ε are eliminated so that the final coupled variables are u, v and excess pore pressure u_w. Discretizing results in the following equations (Smith et al. 2013):

$$u = [N]\{u\} = \sum N_i u \tag{2.11a}$$

$$v = [N]\{v\} = \sum N_i v \tag{2.11b}$$

$$u_w = [N]\{u_w\} = \sum N_i u_w \tag{2.11c}$$

The approximating functions N_i are called shape functions or interpolation functions. Usually they are derived using polynomials (Smith et al. 2013).

3. Derive equations for determining finite element properties. The relationship between the nodal displacements and nodal forces is called element stiffness characteristics.

   The equations in Biot's theory (see Equations 2.2 and 2.8) lead to the following equilibrium and continuity equations (Smith et al. 2013):

$$[k_e]\{u\} + [C]\{u_w\} = \{f\} \tag{2.12}$$

$$[C]^T\{\frac{du}{dt}\} - [k_c]\{u_w\} = \{0\} \tag{2.13}$$

   Where, for a three-noded element

$$u = \begin{Bmatrix} u_1 \\ v_1 \\ u_2 \\ v_2 \\ u_3 \\ v_3 \end{Bmatrix} \tag{2.14}$$

$$u_w = \begin{Bmatrix} u_{w1} \\ u_{w2} \\ u_{w3} \end{Bmatrix} \tag{2.15}$$

   Additionally, $[k_e]$ and $[k_c]$ are the element elastic and fluid stiffness matrices, and {f} is the element external loading vector. [C] is a rectangular coupling matrix.

   For finite elements in the context of plan plasticity, the element elastic stiffness matrix has the form (Smith et al. 2013)

$$[k_e] = \iint [B]^T [D][B] dxdy \tag{2.16}$$

   Where $[B]$ and $[D]$ are the strain-displacement and stress-strain metrics, respectively.

   A fluid element has a fluid stiffness matrix defined as (Smith et al. 2013)

$$[k_c] = \iint [T]^T [K][T] dxdy \tag{2.17}$$

Where the property matrix $[K]$ is analogous to the stress- strain matrix $[D]$ in solid mechanics, and the matrix $[T]$ is similar to $[B]$.

4. Establish global equations based on properties of elements. Each element stiffness matrix is to be placed in the global stiffness matrix appropriately.

$$[K_e]\{U\} + [C]\{u_w\} = \{F\} \tag{2.18}$$

$$[C]^T\{\frac{dU}{dt}\} - [K_c]\{u_w\} = \{0\} \tag{2.19}$$

Where $[K_e]$ and $[K_c]$ are the global elastic and fluid stiffness matrices, {U} is the vector of all incremental element nodal displacements and {F} is the global external loading vector.

5. Modify the system's stiffness relationship, the global relation, by limiting the geometric boundary conditions. Vanishing of slopes can be seen as natural boundary conditions.

6. Calculate nodal displacements as the primary quantity of the global relation. Then, the secondary quantities such as stresses and strains can be calculated from the primary quantity.

Nikolić et al. (2016) have summarized the advantages of FEM. All the listed advantages of FEM position this technology as the most widely used numerical method in soil and rock mechanics (Nikolić et al. 2016).

1. FEM can represent heterogeneous materials such as soils or rocks, in which the unique material properties can be assigned to different finite elements.

2. The meshes in FEM can be structured and irregular.

3. FEM can represent various nonlinear and inelastic types of material behavior.

4. FEM is a suitable tool for representing geometric nonlinearities, contact mechanisms, fluid-structure interaction, connecting the scales from nano and microscale to large and macro scales, and so on.

2.4.3 Shear strength reduction – based slope stability analysis using FEM

The FEM is widely used to analyze slope stability, and SSRFEM is one of the most popular techniques for FEM slope analysis (Griffiths and Lane 1999). The SSR principle can be simplified as using a factor of safety to systematically reduce the shear strength of the material and calculate the FEM model of the slope until deformations are too large to accept or solutions to FEM do not converge (Hammah et al. 2005).

In the SSRFEM, elastoplastic strength for slope materials is assumed, and the material shear strengths are gradually reduced until collapse occurs. For a Mohr-Coulomb material, shear strength reduced by a safety factor F can be determined based on the following equation (Rocscience Inc. 2004).

$$\frac{\tau}{F} = \frac{c'}{F} + \frac{\sigma tan\phi'}{F} \tag{2.20}$$

This equation can be simplified as

$$\frac{\tau}{F} = c^* + tan\phi^* \tag{2.21}$$

In this case,

$$c^* = \frac{c'}{F};\ \phi^* = arctan(\frac{tan\phi'}{F}) \tag{2.22}$$

Where τ = the shear strength, σ = the normal stress, c' and ϕ' are the shear strength parameters. c^* and ϕ^* are reduced Mohr-Coulomb shear strength parameters, and these values can be input into the FE model and used in the analysis.

For Mohr-Coulomb materials, the procedures for searching for the critical safety factor value, F, which brings the previously stable slope to the verge of failure, are (Rocscience Inc. 2004):

Step 1: Develop a slope FE model, using the deformation and strength properties established for the slope materials. Compute the model and record the maximum total deformation on the slope.

Step 2: Gradually increase F's value while calculating the corresponding Mohr-Coulomb material parameters based on Equation 2.9. Enter new strength properties in the slope model and re-compute. Record the maximum total deformation of the slope.

Step 3: Repeat Step 2, systematically incrementing F, until the FE model does not converge to a solution, which means before the slope fails, the material strength should be reduced continually. The slope safety factor *F* is the critical F value just beyond which collapse occurs. (If a slope is unstable initially, F values in Steps 2 and 3 must be reduced until the FE model converges to a solution.)

Compared with traditional LEM, the SSRFEM offers many significant advantages (Rocscience Inc. 2004):

1. In SSRFEM technology, there is no need to assume the failure mechanisms in advance (the type, shape, and location of failure surfaces), since this technology can establish the critical failure mechanism automatically.
2. This technology can eliminate assumptions about the inclinations and locations of inter-slice forces.
3. This technique can model construction procedures and sequences (i.e., loading paths).
4. Compared with LEM, it can be easily applied to three-dimensional slope modeling.

2.4.4 Convergence criteria

The criterion used to judge the slope instability can be divided into three categories (Dai et al. 2017):

a. The convergence criterion. The nonconvergence of finite element numerical iteration is regarded as a sign of slope instability (Luan et al. 2003).

b. The plastic region criterion. The formation of a continuous breakthrough area is a sign of slope instability (Zhang 1998).

c. The characteristic point displacement criterion. The appearance of displacement mutation points of the characteristic parts is taken as a sign of slope destruction (Zheng et al. 2002).

In the SSRFEM, the convergence criterion is always used to judge slope instability (Gupta 2012). The principle of this criterion used in RS2 is described below.

Based on SSR theory, the shear slope failure occurs when the FE calculation is non-convergent due to the reduction of strength parameters (Shao et al. 2012). Using the case of a single force applied to a nonlinear spring, it is simpler to explain the solution process of FE and the convergence definition. Furthermore, there is a relationship between the applied load and displacement, as follows (Rocscience Inc. 2018):

$$KU = P \tag{2.23}$$

Where $K = K(U)$ is the non-linear stiffness of the spring, which is a function of displacement. Figure 2.21 shows the nonlinear response of the spring to the loads.

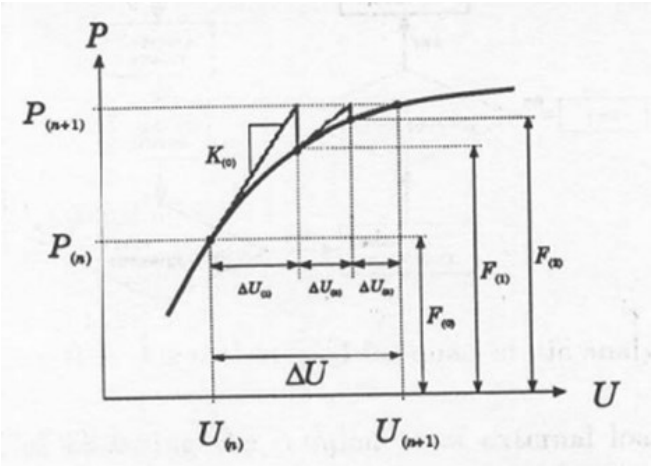

Fig. 2.21. The non-linear response of the spring to the loads (Rocscience Inc. 2018).

In combining with Figure 2.21 and assuming the application of load step $P_{(n)}$ to the spring, the displacement $U_{(n)}$ is obtained. Then the spring response (the displacement increment ΔU illustrated in Figure 2.20) with application of load step $P_{(n+1)}$ needs to be determined. Before applying the new load, the resisting (internal) force $F_{(0)}$ in the spring caused by its current deformed state is in equilibrium with the applied (external) load $P_{(n)}$ (Rocscience Inc. 2018).

First, the tangent stiffness, $K_{(0)}$, at the original of the curve, can be used throughout all iterations for the new load. The current displacement increment can be obtained based on Equation 2.24 (Rocscience Inc. 2018).

$$\Delta U_{(1)} = K_{(0)}^{-1}(P_{(n+1)} - F_{(0)}) \tag{2.24}$$

And the solution can be updated.

$$U_{(n+1)} = U_{(n)} + \Delta U_{(1)} \tag{2.25}$$

Then, the internal force $F_{(1)}$ can be calculated based on the current displacement state. It can be seen that the current force error or load imbalance $P_{(n+1)} - F_{(1)}$ is large, and the aim of the iterations is to reduce the load imbalance to a very small number (Rocscience Inc. 2018).

In the next iteration, starting at the more accurate displacement $U_{(n+1)}$ and applying the same load step $P_{(n+1)}$, a new displacement increment $\Delta U_{(2)}$ smaller than the previous increment $\Delta U_{(1)}$is obtained. Repeating the procedures described above, an updated internal force $F_{(2)}$ is calculated, which is closer to the corresponding applied load $P_{(n+2)}$ (Rocscience Inc. 2018).

After continued iterations, the load imbalance should reduce, displacement increments $\Delta U_{(i)}$ should approach zero, and updates of $U_{(n+1)}$ should gradually approach the real solution. The criteria used to stop the continued iterations are shown below (Rocscience Inc. 2018):

- Absolute Energy Criterion:

$$\frac{\Delta U_{(i)}^{T}(P_{(n)} - F_{(i)})}{\Delta U_{(0)}^{T}(P_{(n)} - F_0)} < \textit{(specified energy tolerance)} \tag{2.26}$$

- Absolute Force Criterion:

$$\frac{(P_{(n)} - F_{(i)})}{(P_{(n)})} < \textit{(specified tolerance)} \tag{2.27}$$

The program needs to satisfy two criteria at the same time in order to stop iterations.

2.4.5 Determination of factor of safety (FS)

A particular FS is challenging to specify because it is related to many factors where the slope is located, such as the geological conditions, the population density, environmental conditions, and so on (Budhu 2008).

FS <1.0 indicates that the slope is unstable and failure is about to occur. FS> 1.0 indicates that the slope is stable, and FS over 1.0 is a measure of the reserve force used to resist movement. The typical value of acceptable FS slope stability is 1.3-1.5. Human-made slopes (embankment filling and foundation pit excavation) are usually designed with a slope ratio that mimics the natural slope, and the slope has an F.S. of at least slightly greater than 1 (FS > 1.0). Therefore, with proper consideration of design and construction (such as drainage, compaction, and elimination of weak areas), a FS 1.3-1.5 is usually acceptable (Li et al. 2016). In this study, the minimum FS is adopted as 1.3 to ensure the adequate performance of slopes.

2.5 Constitutive models for soils

Various constitutive models have been proposed to describe soil behavior and have been applied in FE modeling for geotechnical engineering application (Ti et al. 2009). This section introduces the principles of the elastic soil model (Hooke's model), (modified) cam-clay model, and elastic-plastic soil model (Mohr-Coulomb model).

2.5.1 Elastic soil model (Hooke's model)

A linear elastic model is based upon Hooke's law. Hooke's law for two-dimensional stress is (Punmia et al. 2005)

$$\begin{Bmatrix} \varepsilon_x \\ \varepsilon_y \\ \gamma_{xy} \end{Bmatrix} = \frac{1}{E}\begin{bmatrix} 1 & -\nu & 0 \\ -\nu & 1 & 0 \\ 0 & 0 & 2(1+\nu) \end{bmatrix}\begin{Bmatrix} \sigma_x \\ \sigma_y \\ \tau_{xy} \end{Bmatrix} \tag{2.28}$$

where ε, σ are the strains, normal stresses in the X and Y directions, respectively, γ, τ are the shear strain, shear stress in the XY plane, respectively, E is the elastic modulus, and ν is Poisson's ratio.

Hook's model is a linear elastic model, but the behavior of soil is highly nonlinear and irreversible, so this model is unable to capture the soil's essential characteristics (Wani and Showkat 2018).

2.5.2 (Modified) Cam-clay model

Modified cam-clay (MCC) model is an elastic-plastic, strain-hardening model in which hardening plasticity is used to model the nonlinear behavior. The model's basis is Critical State (Ti et al. 2009). In critical state mechanics, the state of a soil sample is characterized by three parameters, mean stress p', deviatoric stress q, and specific volume ν (Wani and Showkat 2018).

Where,

$$p' = \frac{\sigma_1^{'} + \sigma_2^{'} + \sigma_3^{'}}{3} \tag{2.29}$$

$$q = \frac{1}{\sqrt{2}}\sqrt{(\sigma_1^{'} - \sigma_2^{'})^2 + (\sigma_2^{'} - \sigma_3^{'})^2 + (\sigma_1^{'} - \sigma_3^{'})^2} \tag{2.30}$$

The value of specific volume ν equals to $1 + e$, where e is the void ratio of soil (Wani and Showkat 2018).

Following are the components of critical state theory.

(a) Virgin consolidation line

Based on the assumptions of this model, when soft soil samples are slowly compressed under isotropic stress conditions and perfectly drained conditions, the relationship between specific volume ν and mean stress p can be represented using a straight line known as normal compression line (NCL) or virgin compression line and a set of straight swelling lines. (see Figure 2.22) (Wani and Showkat 2018).

The equation of the virgin consolidation line is (Rocscience Inc. 2021b)

$$v = N - \lambda lnp' \tag{2.31}$$

The swelling line is give as (Rocscience Inc. 2021b)

$$v = v_s - \kappa lnp' \tag{2.32}$$

The values of λ, N, κ are the characteristic properties of a soil, λ is the slope of NCL on $v - lnp'$ plane, while κ is the slope of swelling line, N is the specific volume of NCL at unit pressure.

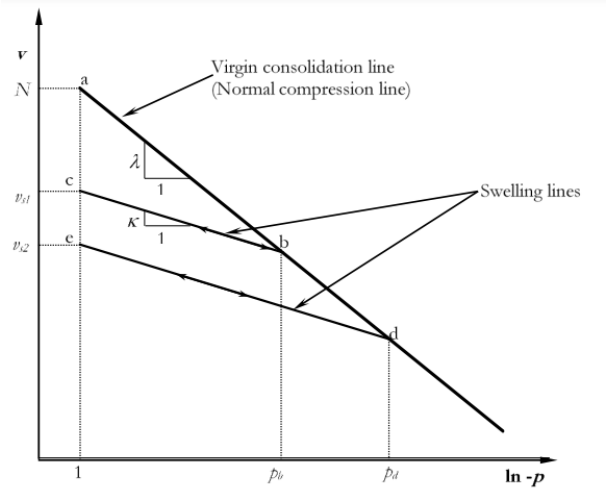

Fig. 2.22. Typical behavior of clays in consolidation test (Rocscience Inc. 2021b).

The hardening behavior of the MCC model is formulated based on the virgin consolidation line, whereas the swelling line is used to calculate the elastic properties (Rocscience Inc. 2021b).

(b) The critical state line

The critical state line (CSL) can describe the critical state where the soil deforms under constant stress without any change in volume (see Figure 2.23). As seen in Figure 2.23, the CSL is parallel to the virgin consolidation line in $v - lnp$ space (Wani and Showkat 2018).

At critical state (Wani and Showkat 2018),

$$v = \Gamma - \lambda lnp' \tag{2.33}$$

Where, the parameter Γ is the specific volume of the swelling line at unit pressure.

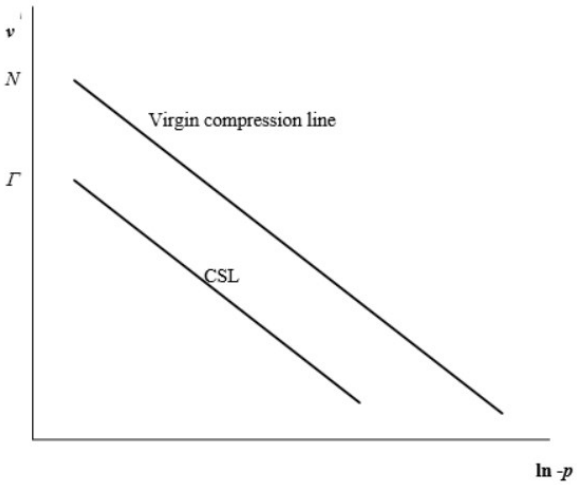

Fig. 2.23. Typical critical state line and virgin compression line of clays (Rocscience Inc. 2021b).

(c) Yield functions

The yield function for MCC model is (Wani and Showkat 2018)

$$\frac{q^2}{p'^2} + M^2\left(1 - \frac{p_0'}{p'}\right) = 0 \tag{2.34}$$

In $p - q$ plane, the MCC yield surface plots as an elliptical curve (Figure 2.24). The size of the yield surface is controlled by the parameter p_0' (known as the yield stress or pre-consolidation pressure). M is the slope of CSL in $p - q$ plane. A key feature of the CSL is that it intersects the yield curve at the point where it reaches a maximum (Wani and Showkat 2018).

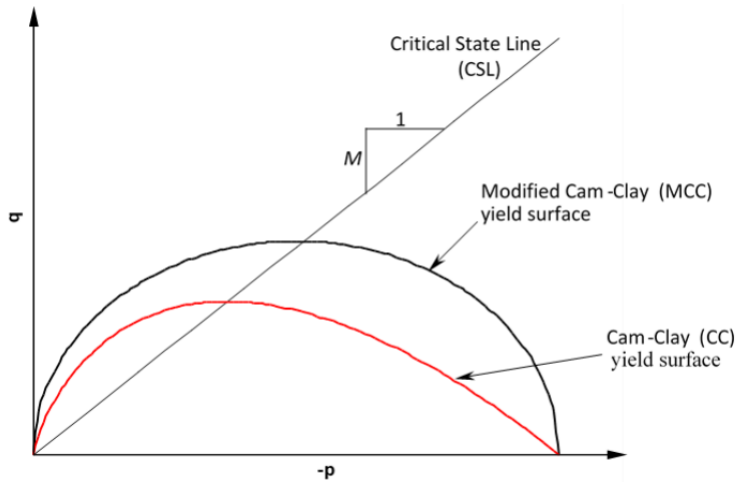

Fig. 2.24. Yield surface of the Modified Cam Clay models in $p - q$ plane (Rocscience Inc. 2021b).

In the case of primary, undrained, deviatoric loading of soft soils, the model predicts more realistic, undrained shear strength than the Mohr-Coulomb model. However, due to its inability to predict observed softening and dilatancy of dense sands and the undrained response of very loose sands, the critical state has been less successful in modeling granular materials. This model is more suitable for describing deformation rather than failure, especially for normally consolidated soft soils (Ti et al. 2009).

2.5.3 Elastic-plastic soil model (Mohr-Coulomb model)

The Mohr-Coulomb model is an elastic plastic model that is commonly used to model soil behavior. Under the general stress state, the stress-strain of the model changes linearly within the elastic range, with two defining parameters (Young's modulus and Poisson's ratio) from Hooke's law. The failure criterion is defined by two parameters (friction angle and cohesion), and there is a parameter used to describe the flow rule (dilatancy angle, which is caused by using the nonassociated flow rule, which is modeling a real irreversible change in volume because of shearing) (Ti et al. 2009).

The classical elastic-plastic model has four ingredients to be characterized (Bertram and Gluge 2013):

(a) An elastic law, which demonstrates the elastic behavior of the material before yielding. In this research, Hooke's law is used to model the elastic deformation, as shown in Section 2.5.1.

(b) A yield function (Figure 2.25), used to indicate whether the material is plastically yielding. It can be written as (Kempfert and Gebreselassie 2006):

$$F(\underline{\sigma}) = 0 \qquad \textit{Yield} \tag{2.35}$$

$$F(\underline{\sigma}) < 0 \qquad \textit{Elastic State} \tag{2.36}$$

Where F is the yield function, $\underline{\sigma}$ is stress tensor.

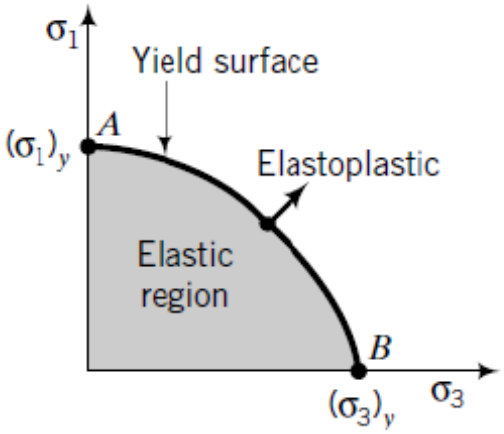

Fig. 2.25. Yield surface (Punmia et al. 2005).

In 1773, through observation of actual soil, Coulomb found that soil failure is often related to its surface rupture. He described his failure criterion for this surface (Davis and Selvadurai 2002):

$$\tau = c + \sigma tan\phi \tag{2.37}$$

Where τ = shear stress at failure, c = effective cohesion, $\emptyset$ = effective friction angle.

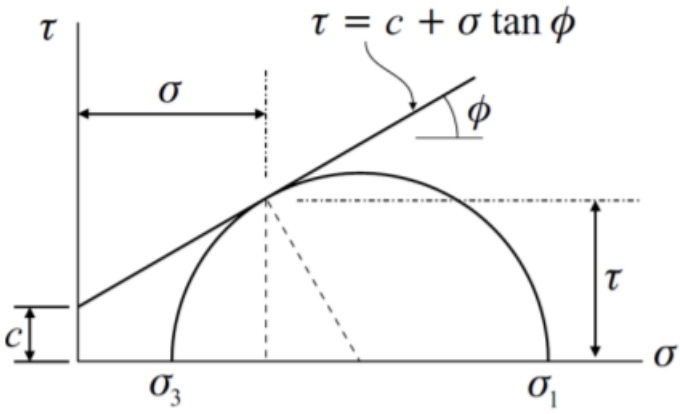

Fig. 2.26. The Coulomb failure criterion (Davis and Selvadurai 2002).

Assuming the maximum principal stress and minimum principal stress are used to express the Mohr-Coulomb criterion, the shearing stress and normal stress on the plane where material failure occurs are (Davis and Selvadurai 2002):

$$\tau = \frac{1}{2}(\sigma_1 - \sigma_3)cos\phi \tag{2.38}$$

$$\sigma = \frac{1}{2}(\sigma_1 + \sigma_3) - \frac{1}{2}(\sigma_1 - \sigma_3)sin\phi \tag{2.39}$$

Combining with Equation (2.30), Mohr-Coulomb failure criterion can be adopted as the yield function corresponding to the convention of principal stresses:

$$F = \frac{1}{2}\sigma_1(1 - sin\phi) - \frac{1}{2}\sigma_3(1 + sin\phi) - ccos\phi = 0 \tag{2.40}$$

It is noted that the intermediate principal stress σ_2 cannot influence F.

(c) A hardening function, used to signal the manner in which the yield function changes due to plastic straining $h = h(\varepsilon^p)$, in which case the yield function (Equation 2.31) can be written as (Kempfert and Gebreselassie 2006):

$$\mathrm{F}(\underline{\sigma}, h) = 0 \tag{2.41}$$

Where h is the hardening parameter.

For a 'perfectly plastic' material, on yield, even if the stress no longer changes, the plastic strain can also increase indefinitely without external restrictions. Figure 2.27 illustrates the stress-strain response in simple tension for this material. The liner elastic response can be seen before the stress reaches the yield value, after which the strain still accumulates, but the stress no longer changes. The flat response characterizes perfect plasticity (Davis and Selvadurai 2002).

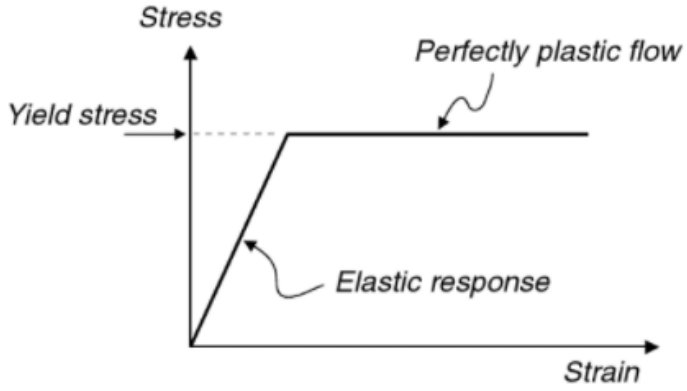

Fig. 2.27. Stress-strain response for a perfectly plastic material (Davis and Selvadurai 2002).

In contrast to perfect plasticity, for a 'work hardening' material, the yield surface may change after initial yielding has occurred. The yield surface changes are usually related to the amount of plastic strain or the accumulated plastic work. Figure 2.28 shows the response of this kind of material to simple tension. Stress and strain are always a one-to-one relationship (Davis and Selvadurai 2002).

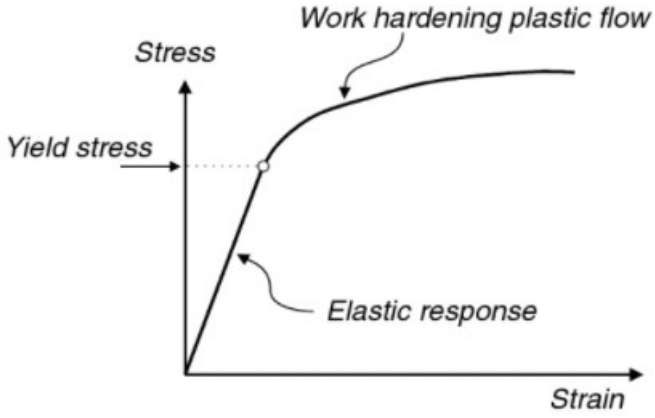

Fig. 2.28. Stress-strain response for a work hardening plastic material (Davis and Selvadurai 2002).

(d) A flow rule determining the direction of plastic straining and can be written as (Kempfert and Gebreselassie 2006):

$$d\underline{\varepsilon^p} = d\lambda \frac{\partial Q}{\partial \underline{\sigma}} \tag{2.42}$$

Where $d\underline{\varepsilon^p}$ is the incremental plastic strain, Q is a plastic potential function, λ is a positive scalar of proportionality which is dependent on the state of stress and the load history. Figure 2.29 shows the yield surface, the potential function, and the flow rule.

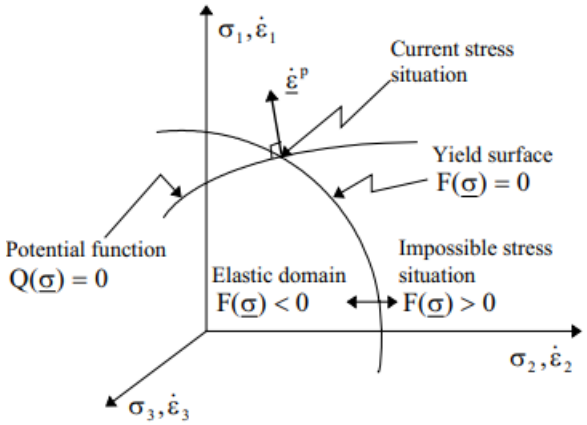

Fig. 2.29. Schematic representations of the yield surface, the potential function, and the flow rule (Kempfert and Gebreselassie 2006).

When performing a slope stability analysis using SSRFEM, the factored shear strength can be calculated by applying the Strength Reduction Factor the shear strength defined in Equation (2.37) (Rocscience Inc. 2021c)

$$\frac{\tau}{SRF} = \frac{c - \sigma_n tan\varphi}{SRF} \tag{2.43}$$

The factored Mohr Coulomb properties after the application of SRF are (Rocscience Inc. 2021c)

$$c_{SRF} = \frac{c}{SRF}, \quad \varphi_{SRF} = atan(\frac{tan\varphi}{SRF}) \tag{2.44}$$

Combined with the Shear Strength Reduction (SSR) method, this model can evaluate safety factors equivalent to those calculated by the limit equilibrium method, and in some cases better predict failure modes and safety factors. It can also calculate load displacements in simulations including geological materials such as gravel, sand and rock (Rocscience Inc. 2021c).

Chapter 3 Development of the slope stability numerical model

3.0 Introduction

This section describes the generation of numerical models based on the literature review. Analysis results were compared with the literature-reported cases to verify RS2's suitability for further simulation work. The behavior of rails and sleepers was not considered in this study because studying their behavior is not the aim of this research. Train loads on the sleeper's contact surface and ballast of all models were manually calculated and then applied to the model. Section 3.1 describes the creation of each part of the model, such as external train loads, the track's superstructure, the substructure of the track, natural slope, and water conditions. Section 3.2 validates a case similar to the model in this research, which shows that RS2 can successfully analyze the slope stability under these conditions.

3.1 Process of building the simulation model

In this part, the generation process of a typical model is introduced step-by-step. First, a selection is made of appropriate track superstructure parameters, followed by a calculation of external loads applied to the tie-ballast contact surface; subsequently, all the dimensions of the track substructure are determined. After confirming the natural slope's dimension, applied load and water conditions, the model is complete. In this process, the assignment of material properties, the setting of boundary conditions and the generation of mesh elements should be considered.

3.1.1 Geometry of track and load condition

The track should be designed according to the external loads on the tie-ballast contact surface, which depends on the arrangement of heavy-haul freight trains. In the practical case, the number of axles of rolling stock in a heavy-haul freight train in North America is four (Esveld 2001), and the load for each axle is 36,000 lbs (160kN) (AREMA 2013). The diameter of typical freight car wheels is 0.914 m (36 inches) (Stephen and Uhlig 2013). The track's dimensions based on the literature review are listed in Table 3.1 (Selig and Waters 1994).

Table 3.1. Sleeper geometric properties (Selig and Waters 1994)

Parameter	Unit	Value
Gauge	m	1.435
Spacing	mm	495
Length	m	2.59
Width	mm	229
Cross-sectional area	mm^2	40600

Typical freight cars used in North America (AREMA 2012) are supported by two trucks with two axles per truck, as shown in Figure 3.1. The distance between two trucks of a car is much larger than that between each truck's axles in the side-view longitudinal section. Since the work is concentrated on the front-view transverse section, to simplify the calculation, two-wheel loads per truck can be simplified as one, which counts the result of loads on two adjacent axles.

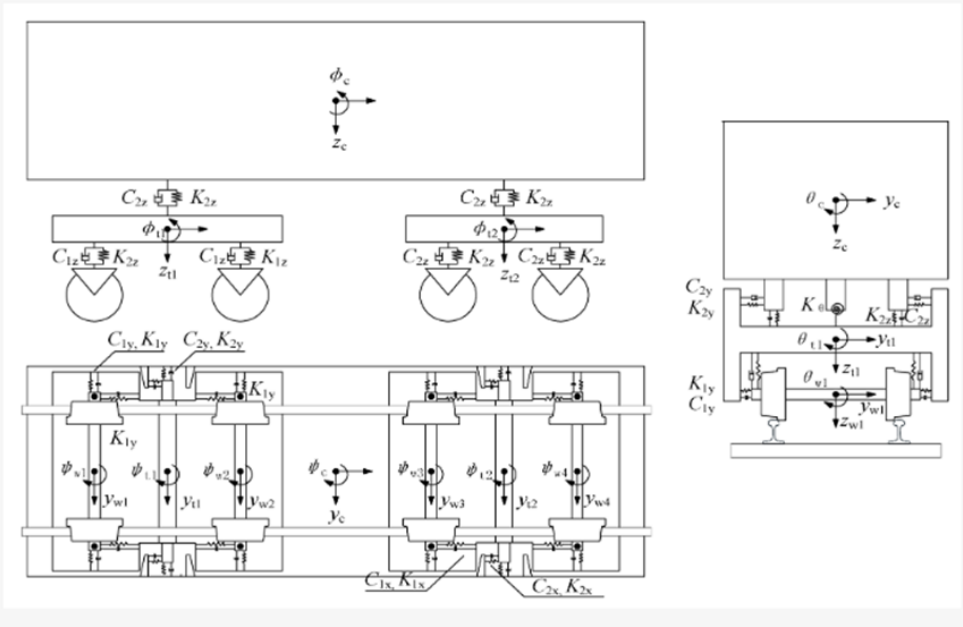

Fig. 3.1. Vehicle-track system dynamic model (Zhou et al. 2020).

In this study, the following assumptions were made to specify the load conditions, which should be studied carefully for obtaining external forces:

1. Trains traversing the superelevation curve at different speeds change the distribution of lateral and vertical forces acting on each track (Federal Railroad Administration 2019). To eliminate the influence of curve driving on the load distribution in this study, it is assumed that the train travels on a tangent track without considering the curve of the track.
2. From Section 2.2.2, augmenting the static wheel load by an impact load factor, one can obtain a dynamic wheel load. According to the equation recommended by AREMA (2012), the dynamic load factor is related to the train's speed. To simplify the calculation, the speed of the train is assumed to be constant.
3. Throughout the research process, the train runs smoothly and at a constant speed.
4. The influence of external conditions such as weather and temperature are not considered in the research.

Load transmissions from wheel-rail interface downward across tracks were presented in Section 2.2.3, and the approach to calculating the pressure at the sleeper and ballast contact according to the applied force, was introduced. Figure 3.2 shows the main steps in the calculation process.

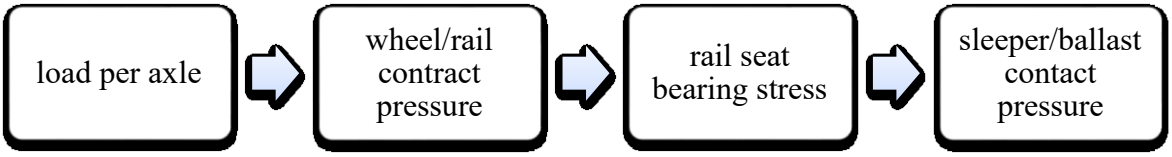

Fig. 3.2. Calculation process of load transmission.

According to Equation 2.8 in Section 2.2.3, different train speeds correspond to different load factors. Thus, assuming different speeds of trains, one can obtain corresponding load factors and the average pressure at the bottom of the tie, as shown in Table 3.2.

Table 3.2. Average pressure at the bottom of the tie for different train speeds

Train speed	mph	0	25	50	75
	km/h	0	40	80	120
Impact factor	/	0	0.2292	0.4583	0.6875
Impact factor in percent	%	0	22.92	45.83	68.75
Average ballast pressure at tie face	kPa	210.42	258.65	307.15	355.08

Note: A = the length of the crosstie * the width of the crosstie = 593110 mm^2 = 0.59311 m^2.

According to Figure 2.10, DF corresponding to a wooden tie with a spacing of 495mm is about 39 in percent.

3.1.2 Geometry of the entire numerical model

After determining the ballast pressure at the tie face, an embankment model could be built based on the dimensions of each part of the embankment given in Section 2.3.2. The embankment structure consists of sleepers, ballast, subballast, and subgrade, and all dimensions of the model are shown in Figure 3.3. The ballast shoulder and roadbed shoulder width are set to 0.35 m and 0.65 m because they cannot be less than 304 mm and 608 mm (AREMA 2012; TRB 2012). The sleepers with a height of 0.2 m were supported by a 0.3m layer of ballast, a 0.2 m layer of subballast, and finally a 0.3 m layer of subgrade (Connolly et al. 2014). The inclinations of the side slopes of ballast, subballast, and subgrade are used as 2H:1V (two horizontal to one vertical). It should be noted that the sleeper is not established in the model since the train loads are transferred to the average ballast pressure (uniform load) at the tie's bottom.

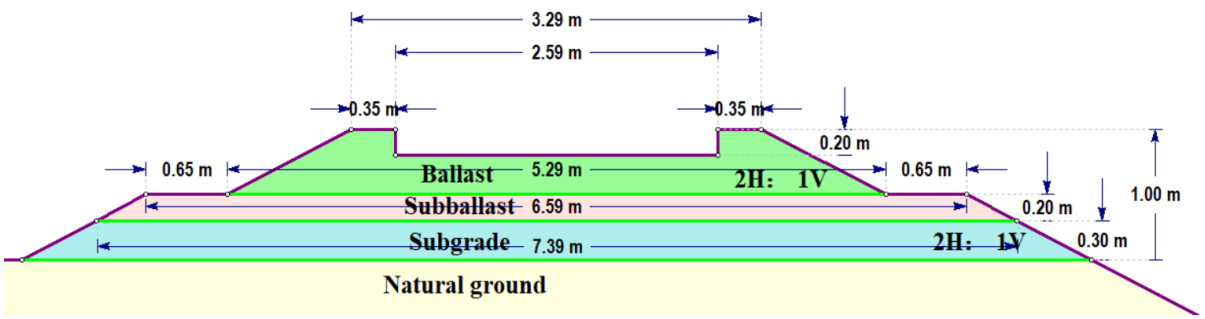

Fig. 3.3. Typical cross-section of a railway embankment structure with dimensions.

The embankment height in this study ranges from 1 m to 3 m (rounded in whole numbers) by changing the subgrade height. The natural ground slope height ranges from 1 m to 5 m (rounded in whole numbers). The subgrade slope is regarded as another variable, with values of 3H:1V or 2H:1V. The train's speed running on the track can affect the tie-ballast interface load, so the train speed is one variable.

In the research, there are some models with ballast pockets. Based on Section 2.1.1, once the moisture and fine-grained subgrade soil intermixes and forms the slurry, it migrates upwards and fouls the ballast. At the same time, the ballast is forced downwards into the slurry under the influence of the train loading. Finally, ballast pockets form and sink into the subgrade (Li et al. 2016). Figure 3.4 shows a perpendicular section of a railway embankment with ballast pockets. It indicates that the fouled ballast can take away a part of the clean subballast in the process of downward migration, make it contaminated, and they eventually form ballast pockets together. The rest of the subballast is not affected. Ballast pockets contain fouled ballast and dirty subballast (AREMA 2012), but the subballast occupies a small proportion of materials of the model, so the characteristics of the fouled ballast are used to represent the characteristics of the material in the ballast pockets.

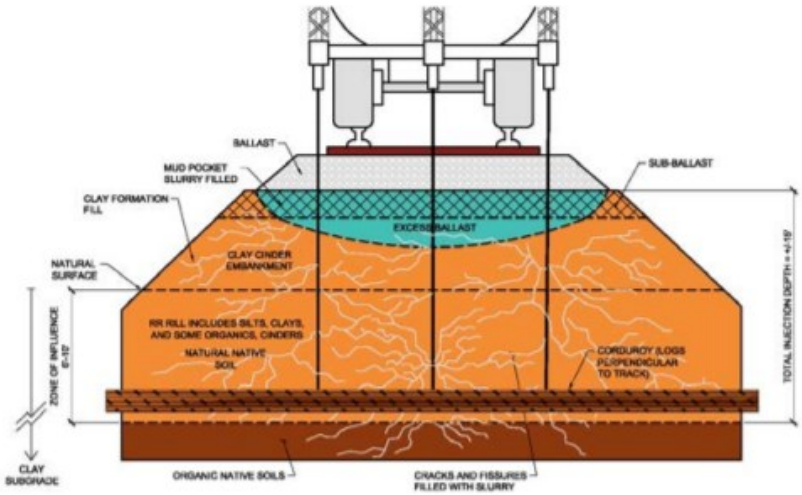

Fig. 3.4. Perpendicular section of a railway embankment with ballast pockets (Hill and Colwell 2018).

Figure 3.5 shows the models with ballast pockets under the center of the tie and one side of the tie. The width and the depth of ballast pockets and the water level retained in the ballast pockets are all variables considered in the research. The dimensions of models in Figure 3.5 (a) and (b) are the same, except that the ballast pocket positions are different. The left vertex of the upper boundary of the ballast pockets in Figure 3.4 (b) (the vertex in the red box in the figure) is located directly below the center of the tie. The depth of ballast pockets is defined as the depth of the ballast sinking into the subgrade, denoted by p in Figure 3.5. The width of ballast pockets is defined as the width of the bottom of ballast pockets, represented by w in Figure 3.5.

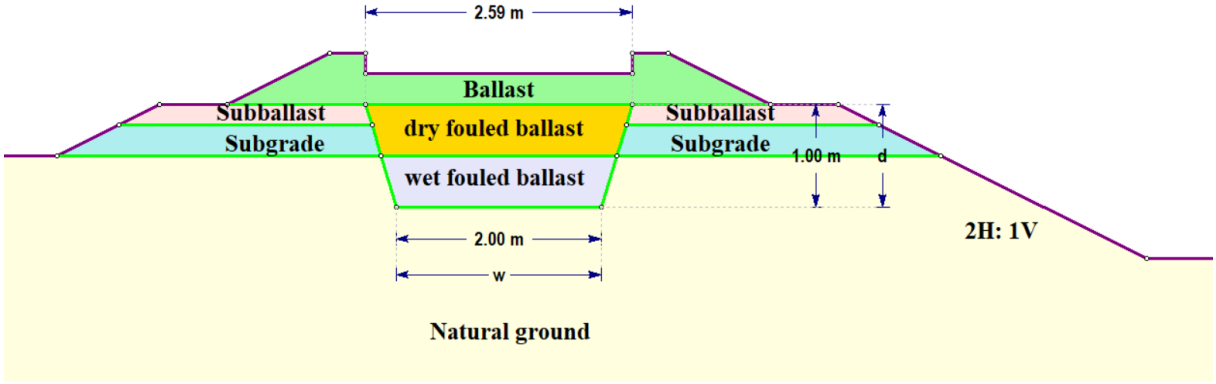

(a) Ballast pockets under the center of the track

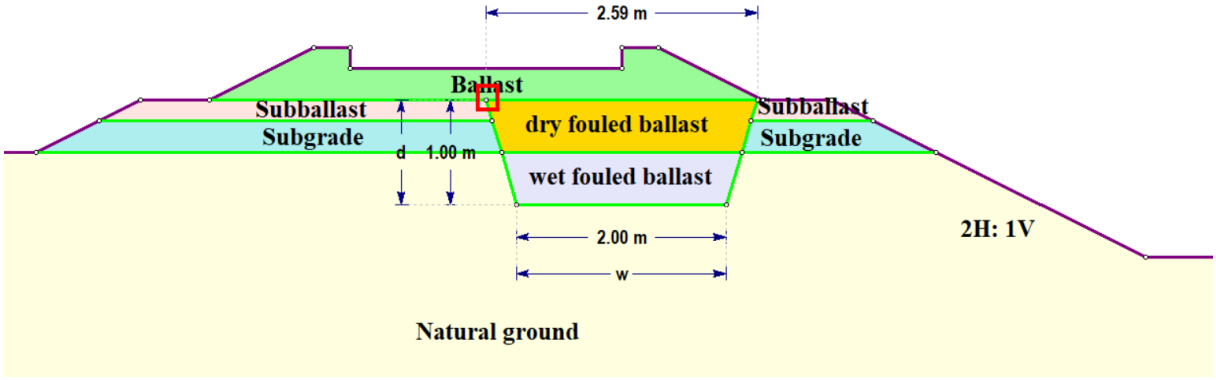

(b) Ballast pockets under one side of the track

Fig. 3.5. Typical cross-section of a railway embankment with ballast pockets.

Kovačević et al. (2019) has used ground penetrating radar (GPR) technology to survey the railway embankment with ballast pockets in Croatia, and the measured ballast depth was 1.0 m. The typical ballast depth on the Croatian network is 0.5 m (Kovačević et al. 2019), which means that the depth of the ballast pockets is 0.5 m. Li and Wilk (2021) and Basye and Wilk (2020) have observed ballast pockets with depths of 3 ft (0.9 m) and 5 ft (1.5 m), respectively, using GPR. Therefore, the value of p is set to 0.5 m, 1.0 m or 1.5 m. However, there is currently no research on the width of ballast pockets. Considering the model's external dimensions in this study, it was necessary to ensure the sizes of ballast pockets fit the various locations in the model. The value of w is, therefore, set to 1.0 m, 1.5 m or 2 m. The upper boundary width of ballast pockets was set to be the same as the width of the tie (2.59 m).

The natural ground dimensions under the railway embankment should be dictated by avoiding stress reflections at the model boundaries. The dimensions of the natural ground foundation and the embankment dimensions, as shown in Figure 3.6, have the following relationship:

The natural ground's right-side height is set at approximately three times the sum height of railway embankment and slope, which is expressed in Equation 3.1.

$$f \approx 3(e + d) \tag{3.1}$$

On the left side, the exposed natural ground length (a) is at least equal to the embankment's bottom width (b) (Equation 3.2). The length of the exposed natural ground on the right side (c) is at least greater than 1.5 times the length value of b (Equation 3.3).

$$a \geq b \tag{3.2}$$

$$c \geq 1.5b \tag{3.3}$$

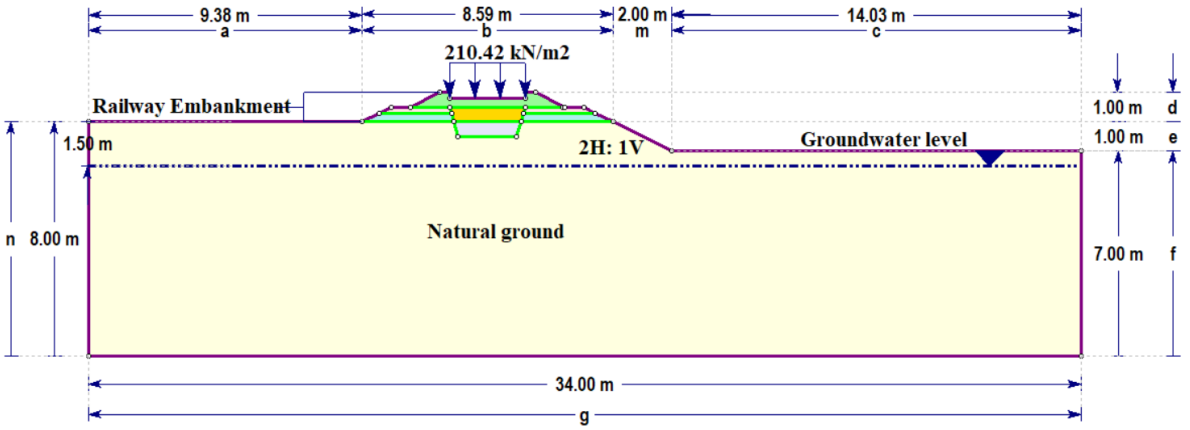

Fig. 3.6. Cross section of the numerical model with dimensions.

The measurement results of Yu and Hsi (2005) and Wu et al. (2019) were referenced when setting the water level in the foundation. Yu and Hsi (2005) have observed that the groundwater level in a particular area in Singapore was 1-1.5 m below the surface, and Wu et al. (2019) have observed that the groundwater in a specific area in China was 0.9-1.5 m below the surface. Therefore, the water level is set at 1.5 m below the bottom of the railway embankment, as shown in Figure 3.6, which means the embankment and slope are not submerged.

3.1.3 Material properties

The soil type of each embankment's layer was introduced in Section 2.3. A ballast layer made from crushed stone is essential to maintain a good drainage state. The subballast is a transition layer made of broadly graded coarse aggregate (gravel and sand). Soft clay is the material of the subgrade, in which ballast pockets can be formed. Ahn (2019) has found that sensitive subsoils under the railway embankment are silt clays, so silty clays are chosen as the natural ground soil in this research. Table 3.3 summarizes properties of the railway embankment and foundation soil. All soil layers are modelled as elastic-plastic materials, with a failure criterion based on Mohr-Coulomb.

Table 3.3. Material properties of the railway embankment and foundation soil

Name	Unit weight	Porosity	Cohesion	Friction angle	Poisson's ratio	Young's modulus	Permeability
	kN/m^3	\	kPa	°	\	MPa	cm/s
Ballast	17	0.5	0	45	0.2	127.49	1.0×10^{-1}
Subballast	19	0.5	0	35	0.3	196.13	1.0×10^{-3}
Subgrade	18	0.3	10	30	0.3	25.00	1.0×10^{-5}
Natural ground	18	0.3	12	22	0.3	18.00	1.0×10^{-6}
Dry, fouled ballast	21	0.3	0	40	0.4	160.00	1.0×10^{-2}
Wet, fouled ballast	23	0.3	0	30	0.4	80.00	1.0×10^{-3}

3.1.4 Mesh convergence study

After defining all boundaries, the finite element mesh can be created. The mesh generation procedure comprises two general steps: discretization of boundaries, followed by meshing of the domain. A 6-noded (quadratic interpolation order with mid-side nodes) triangle was chosen as the models' finite element mesh type. Using elements with mid-side nodes significantly increases the size of the matrixes used in solving the problem. The mesh type is uniform. However, the boundary discretization and element densities of the embankment structure and the potential sliding area (the area within the dotted frame) are manually increased, as shown in Figure 3.7, to concentrate elements where they are needed the most.

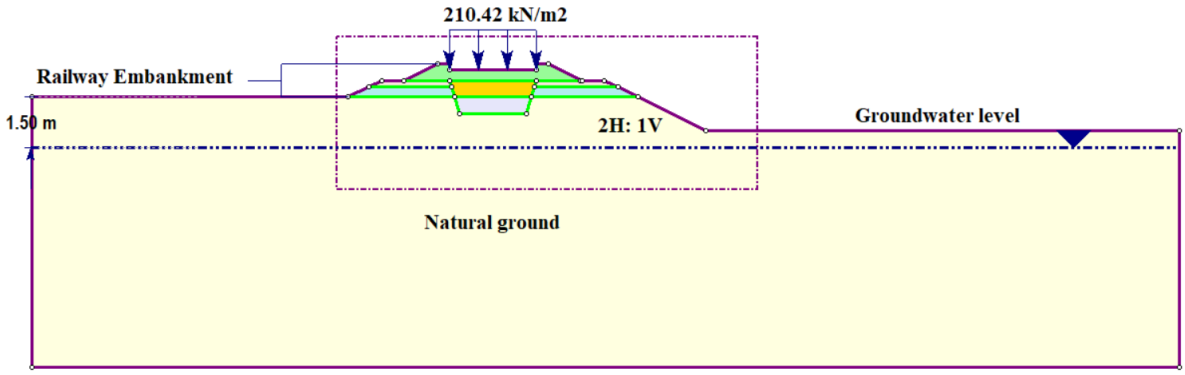

Fig. 3.7. Rectangular area of the numerical model with higher boundary discretization and element densities.

The process of mesh convergence involves increasing the number of elements (reducing the size of the element) and analyzing the effect of the process on the solution's accuracy. The mesh convergence determines how many elements are needed to ensure that the analysis results are not affected by changing the element number. As the number of elements increases, the solution can become more accurate. The higher the accuracy, the larger the simulation can become in terms of the data stored and processed, which enables a longer running time. Thus, mesh convergence studies are often used to obtain the optimal balance between accuracy and runtime.

In this study, the element number used to discretize the numerical model shown in Figure 3.7 was initially approximately 500, and the number was increased to approximately 16,000, with

the step increase of $2^n * N$ (N =500, and n =0, 1, 2…). Numerical models with 260 elements and 755 elements were also studied to more clearly observe the FS value change. The corresponding FS and computation time with a different number of mesh elements are summarized in Table 3.4. Based on Table 3.4, the value of the critical FS of this model is 1.21. With this value, the differences in FS can be calculated by applying Equation 3.4.

$$FS\ error = \frac{FS-1.21}{1.21} \tag{3.4}$$

Table 3.4. The FS and computation time corresponding to a different number of mesh elements of the numerical model

Number of elements	FS	FS error	Computation time (min)
260	1.45	19.83%	2.42
476	1.29	6.61%	3.65
755	1.25	3.31%	4.92
992	1.23	1.65%	5.87
2054	1.22	0.83%	10.25
4014	1.21	0.00%	18.00
8084	1.21	0.00%	30.24
15963	1.21	0.00%	52.21

Figure 3.8 shows that the mesh convergence occurs at 4,014 mesh elements, where the FS difference curve reaches 0%. The mesh element number adopted in this numerical model is 4,014.

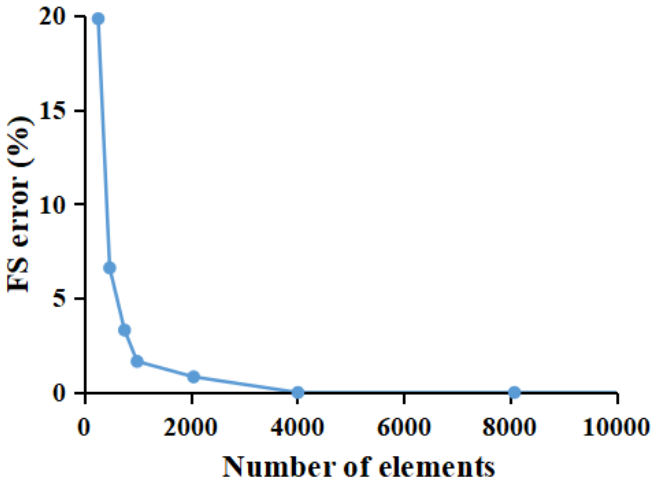

Fig. 3.8. Critical mesh elements for the numerical model.

3.1.5 Boundary conditions

Figure 3.9 shows the complete model available for calculation. Boundaries are set at the bottom, left, and right sides of the numerical model. There are restraints in the X and Y directions at the bottom of the model (fixed boundary condition), including the corners, while the vertical sides only have restraints in the X direction, allowing gravity to act in the Y direction. The boundary conditions remain unchanged throughout the simulation.

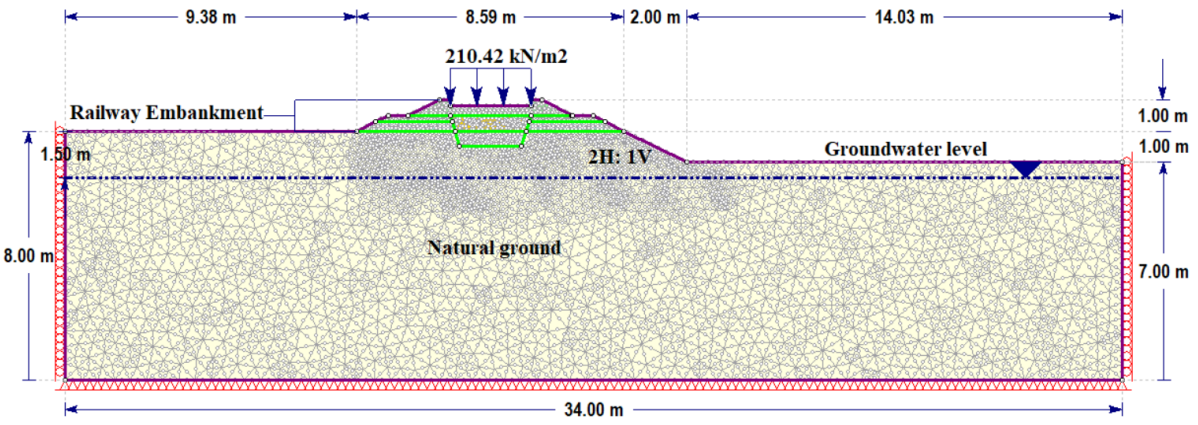

Fig. 3.9. Cross section of a complete model.

3.2 Verification

Before commencing the analysis of embankment models, RS2's results needs to be verified. Two examples of slopes are selected from the literature and analyzed using RS2. Subsequently, a comparison is made between the results found in the literature and obtained by RS2. The selected reference used LEM, FEM, and SSRFEM to study slope stability. In this section, simulation results obtained by RS2 and results found in the literature are attached for comparison.

3.2.1 Model description

The model in Case I is a layered slope taken from Arai and Tagyo (1985). In this model, a layer of low resistance is interposed between two layers of higher strength. Greco (1996) has analyzed this model using LEM, while Nakamura et al. (2008) have studied it using SSRFEM. Case II's model is taken from Griffiths and Lane (1999), representing a homogeneous and isotropic earth dam on a foundation. Griffiths and Lane (1999) have used FEM to study the slope's stability, while SSRFEM was used by Huang and Jia (2009) to analyze the same model. The models are shown in Figure 3.10, and Table 3.5 lists the material properties of each model.

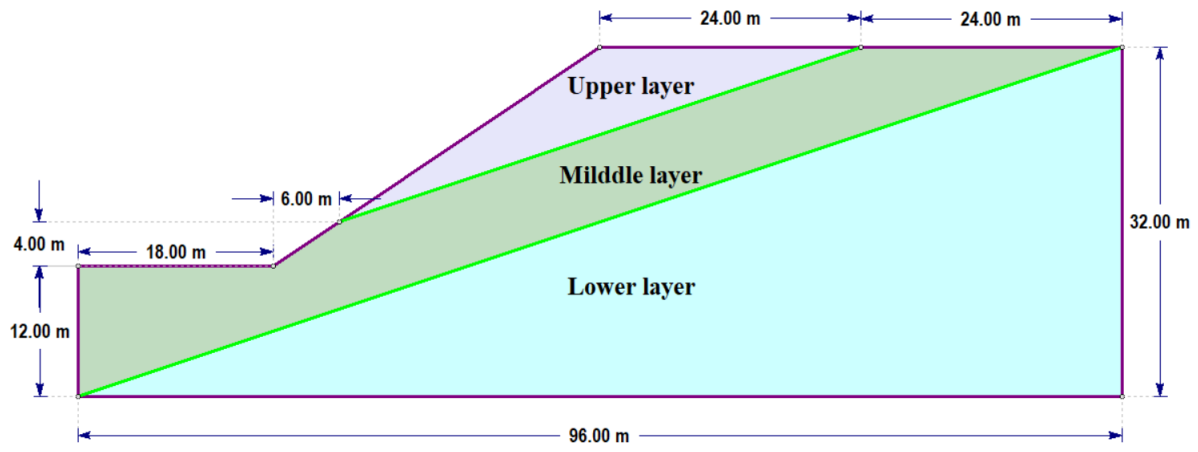

Fig. 3.10. (a) Geometry of Case I model for verification (Arai and Tagyo 1985);

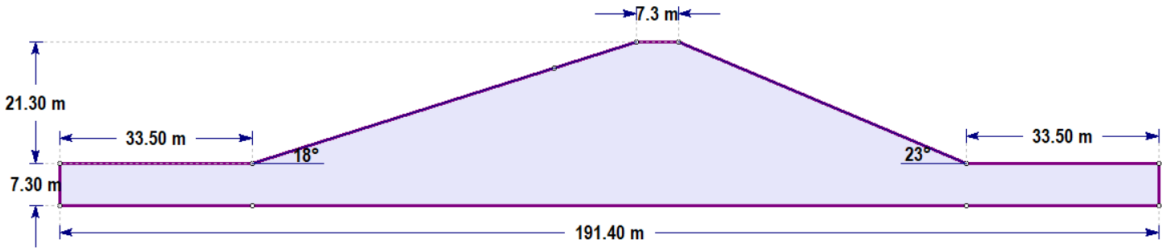

Fig. 3.10. (b) Geometry of Case II model for verification (Griffiths and Lane 1999).

Table 3.5. Material properties of models for verification

Cases	Layer	Unit weight (kN/m^3)	Possion's ratio	Cohesion (kN/m^2)	Friction angle (°)	Young's modulus (kPa)
Case I	Upper layer	18.82	0.3	29.4	12	$1*10^5$
	Middle layer	18.82	0.3	9.8	5	$1*10^5$
	Lower layer	18.82	0.3	294.0	40	$1*10^5$
Case II	Earth dam and foundation soil	18.20	0.3	13.8	37	$1*10^5$

3.2.2 Results and discussion

The model computation results reported in the references and obtained by RS2 are shown as follows. Figures 3.11 and 3.12 reveal each model's failure mechanism using different methods, and the values of the corresponding safety factors are listed in Table 3.6.

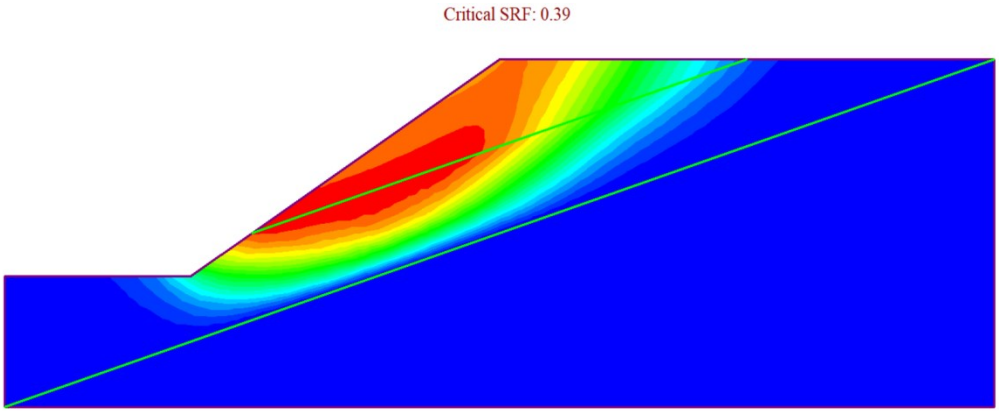

Fig. 3.11. (a) Result of Case I model obtained from RS2;

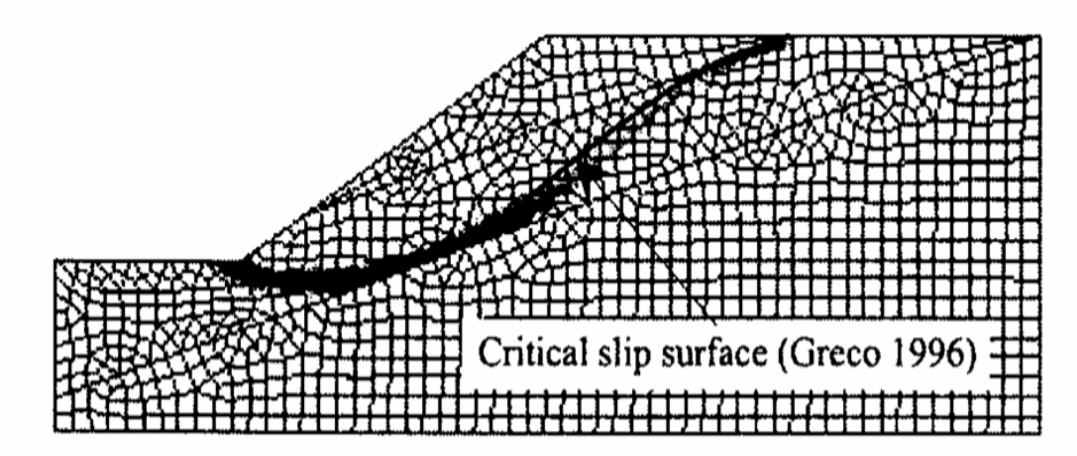

Fig. 3.11. (b) Results of Case I models captured in the work of Greco (1996) (LEM) and Nakamura et al. (2008) (SSRFEM)

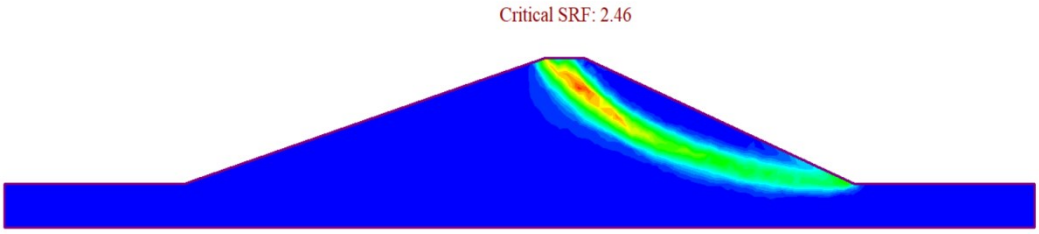

(a) Result of Case II model obtained from RS2;

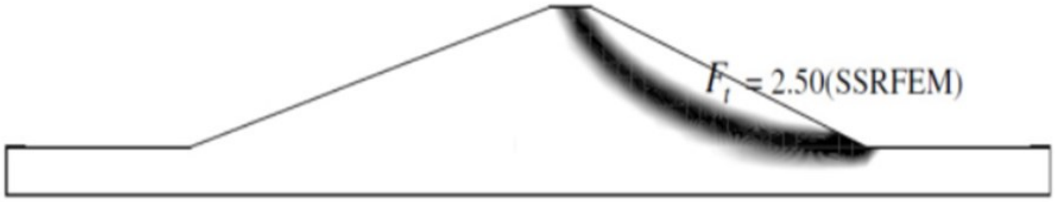

(b) Result of Case II model captured in the work of Huang and Jia (2009);

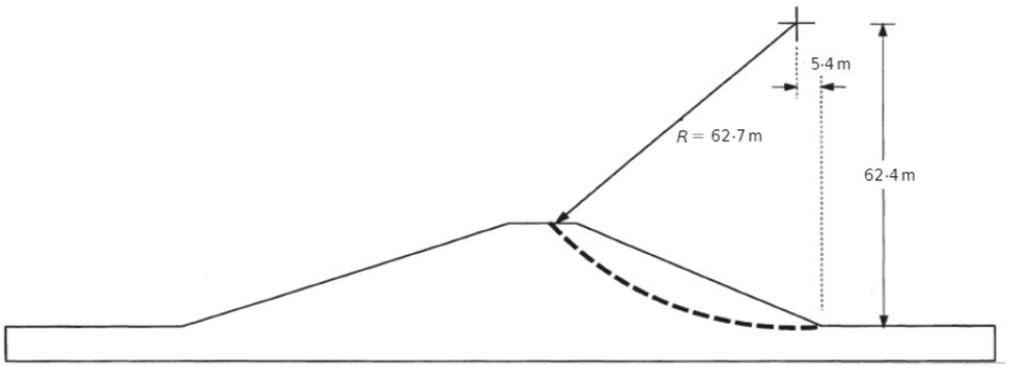

(c) Result of Case II model captured in the work of Griffiths and Lane (1999)

Fig. 3.12. Comparison of failure mechanism for Case II.

Table 3.6. Comparison of safety factor values obtained by different methods for each case

Cases	FS		
	RS2	Reference	
	SSRFEM	LEM	SSRFEM
Case I	0.39	0.388	0.417
Case II	2.46	2.40	2.50

Combining the observations from Figure 3.11 and 3.12 and Table 3.6, it can be seen that for each model, the critical SRF obtained by RS2 is quite close to the safety factor obtained by various methods in the literature, and the failure mechanism in each case is consistent. Therefore, the simulation result of RS2 using SSRFEM is reliable, which means RS2 can be used in this study.

Chapter 4 Analysis of ballast pockets and discussion of simulation results

4.0 Introduction

This research uses RS2 FEM software to study three different simulation models. These models involve three different scenarios: a) dry slopes (no groundwater flow) (Set I) b) existing ballast pockets under the track (Set II) c) both existing ballast pockets under the track and a moving freight train (Set III). Groundwater flows in models in Sets II and III. The control variable method was used to study model parameters. This chapter includes four sections. Section 4.1 introduces the three key sets of models. Section 4.2 conducts parameter studies on Set I and Set II models. Given the complexity of Set III models, their results are discussed separately in Section 4.3, including the relationship between the slope geometry and ballast pockets information and maximum safe train speeds. Finally, Section 4.4 summarizes the conclusions.

4.1 Three sets of models

The three sets of models study the influence of ballast pockets and freight train operations on slope stability. Set I models are the most basic, describing dry slopes without trains on the track. This set serves as the benchmark since it represents the safest conditions. Set II models are studied, adding the existence of ballast pockets and groundwater. Set III models add the operation of moving freight trains based on Set II models. The following three aspects were involved when interpreting the model: a) grouping for parameter study, b) describing simulation results c) discussing the results of the safety factor. The pore water pressure distribution and element yielding distribution of models in different sets are also involved and analyzed.

4.1.1 Set I – dry slope models

The dry slope model represents the slope with no phreatic surface, no groundwater accumulated in the ballast pocket, and no train loads. As shown in Figure 4.1, three parameters are involved in this scenario: railway embankment height, natural slope height, and slope ratio. Figure 4.1 summarizes all the combinations of critical values (from top to bottom) for the dry slope parametric study. Each combination represents a case (model). A total of 30 models are studied in this section. To better analyze the simulation results, based on the above three parameters, all combinations are divided into two groups, including six subgroups with 30 cases in Table 4.1.

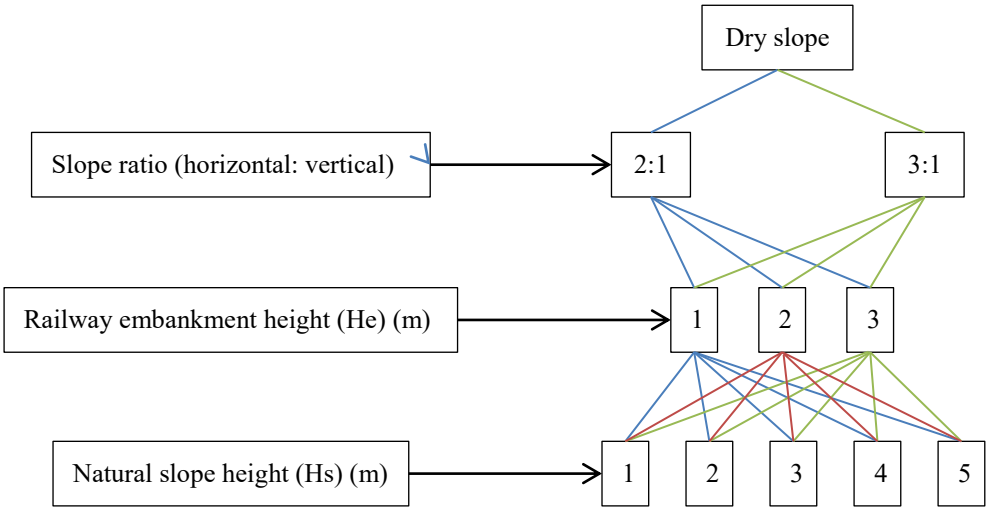

Fig. 4.1. Diagram of various cases in Set I – dry slope model.

Table 4.1. Grouping for cases in Set I – dry slope model

Groups	Slope ratio	Subgroup	He (m)	Hs (m)
Group 1	2:1	Subgroup 1	1	1-5
		Subgroup 2	2	1-5
		Subgroup 3	3	1-5
Group 2	3:1	Subgroup 4	1	1-5
		Subgroup 5	2	1-5
		Subgroup 6	3	1-5

As one parameter, the slope ratio has two values, 3H:1V and 2H:1V (horizontal: vertical). The height of the railway embankment (He) is set to 1, 2 or 3 m. The natural slope height (Hs) ranges from 1 to 5 m (rounded in whole numbers). Other dimensions of the model have been determined in Section 3.1 and remain unchanged during the analysis. Figure 4.2 shows a series of models. The models in Figures 4.2(b)-(d) differ only by one parameter from the model in Figure 4.2(a); the rest remain constant. The model in Figure 4.2(a) has a slope ratio of 3H:1V; the railway embankment height and the natural slope height are set to 1 m. The model in Figure 4.2(b) has a different slope ratio from the previous model, 2H:1V. The model in Figure 4.2(c) is obtained by increasing the railway embankment height to 3 m. In Figure 4.2(d), the natural slope height is 5 m.

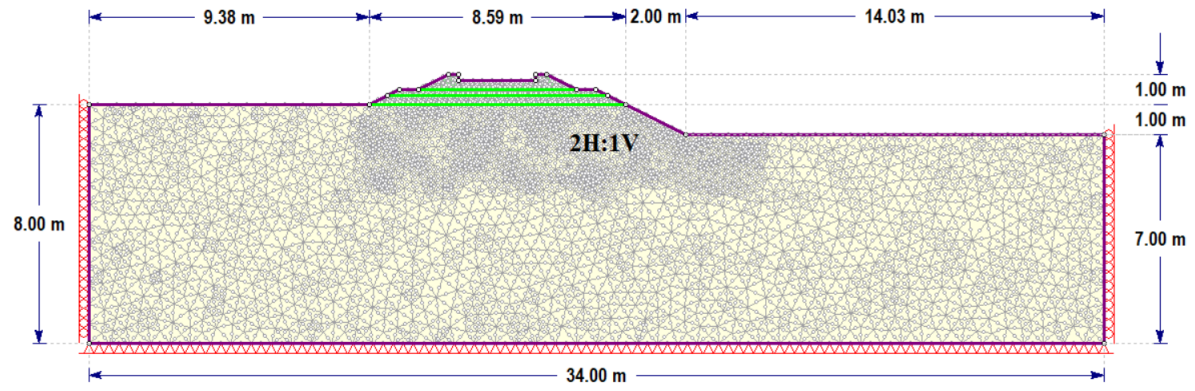

Fig. 4.2. (a) Set I model geometry: slope ratio = 2H:1V, He = 1 m, Hs = 1 m;

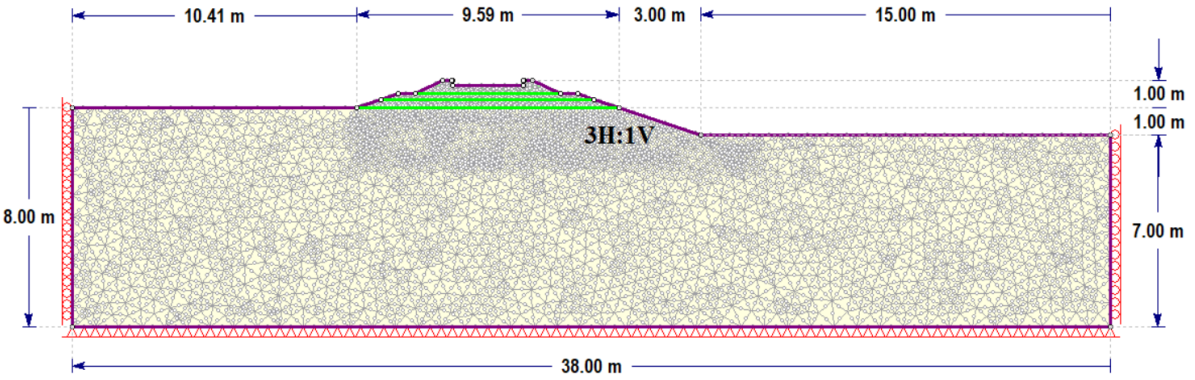

Fig. 4.2. (b) Set I model geometry: slope ratio = 3H:1V, He = 1 m, Hs = 1 m;

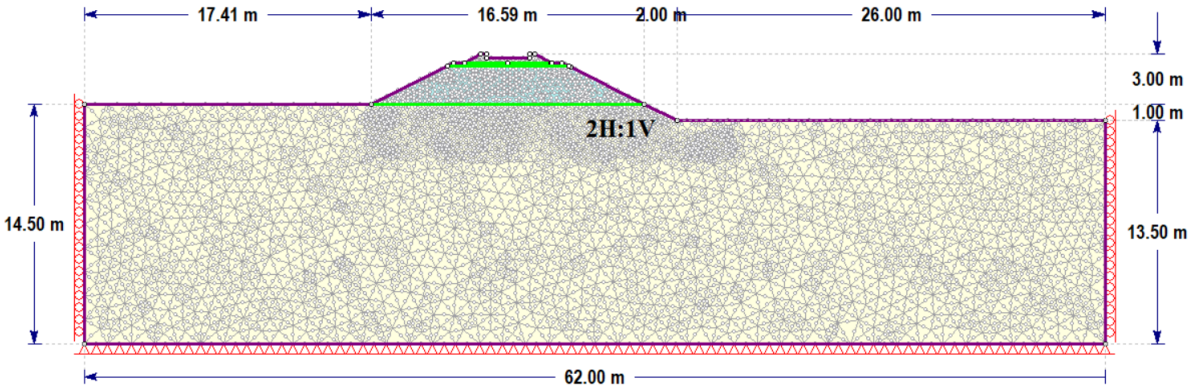

Fig. 4.2. (c) Set I model geometry: slope ratio = 2H:1V, He = 3 m, Hs = 1 m;

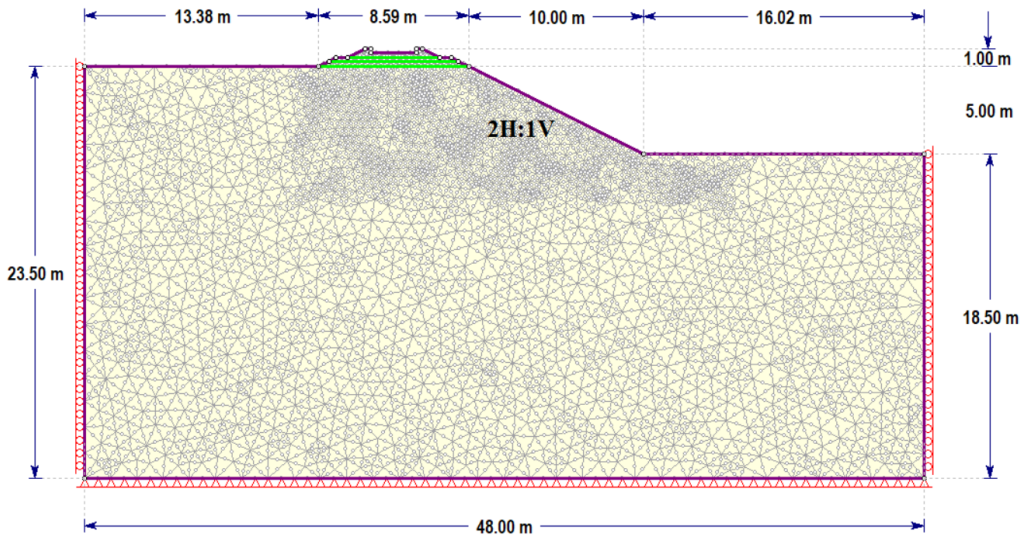

Fig. 4.2. (d) Set I model geometry: slope ratio = 2H:1V, He = 1 m, Hs = 5 m, (continued).

Figure 4.3 shows the corresponding simulation results of models shown in Figure 4.2, from which the maximum shear strain contours and critical SRF values of models can be seen. The model in Figure 4.3(b) (slope = 3H:1V, He = 1 m, Hs = 1 m) has the highest critical SRF value of 9.20. In contrast, the model in Figure 4.3(d) (slope = 2H:1V, He = 1 m, Hs = 5 m) has the lowest critical SRF value of 6.45. These simulation results demonstrate that making the slope relatively flat can increase a slope's stability. In addition, the failure type of dry models in Figure 4.3 is slope failure because the failure surface is a circular slip surface, emanating from the left embankment slope and day-lighting beyond the right embankment slope.

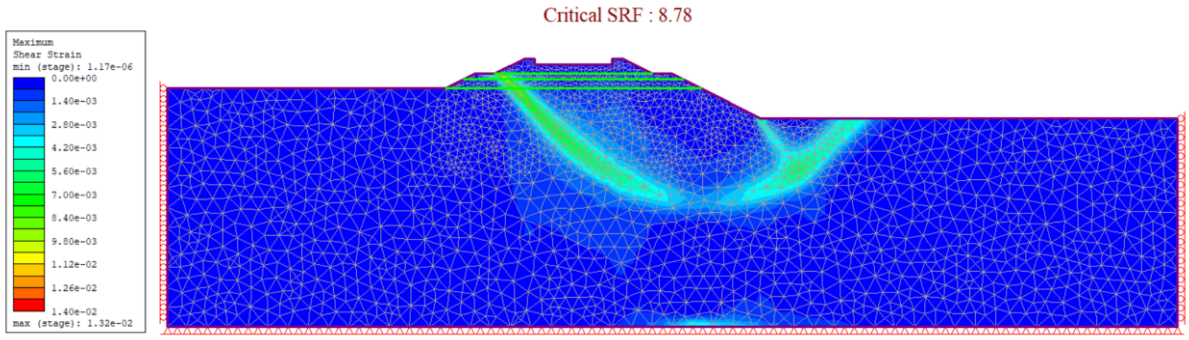

Fig. 4.3. (a) Simulation result for the Set I model: slope ratio = 2H:1V, He = 1 m, Hs = 1 m;

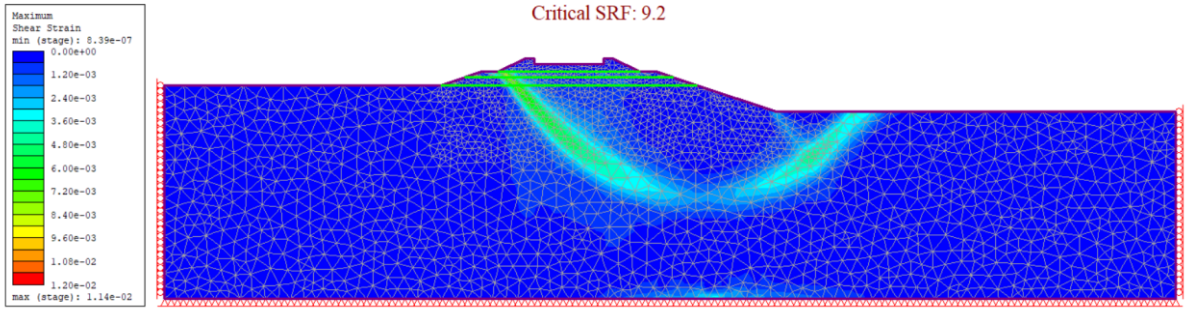

Fig. 4.3. (b) Simulation result for the Set I model: slope ratio = 3H:1V, He = 1 m, Hs = 1 m;

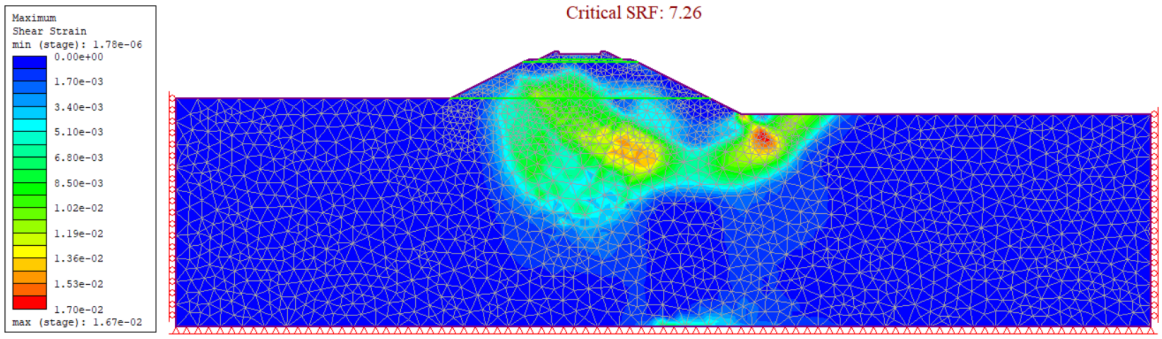

Fig. 4.3. (c) Simulation result for the Set I model: slope ratio = 2H:1V, He = 3 m, Hs = 1 m, (continued);

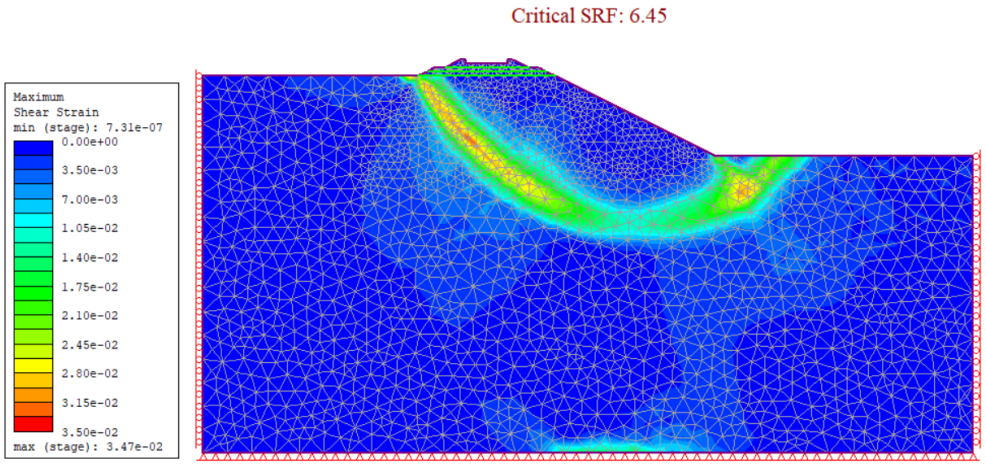

Fig. 4.3. (d) Simulation result for the Set I model: slope ratio = 2H:1V, He = 1 m, Hs = 5 m, (continued).

Table 4.2. FS results of all cases in Set I

Groups	Subgroups	FS				
		Natural slope height (Hs) (m)				
		1	2	3	4	5
Group 1	Subgroup 1	8.78	7.82	7.39	6.73	6.45
	Subgroup 2	8.07	7.23	6.74	6.43	6.11
	Subgroup 3	7.26	6.63	6.34	6.13	5.72
Group 2	Subgroup 4	9.20	8.31	7.92	7.54	6.95
	Subgroup 5	8.54	7.73	7.25	6.93	6.61
	Subgroup 6	7.73	7.11	6.82	6.51	6.20

4.1.2 Set II – models with existing ballast pockets

In Set II, in addition to the three factors (slope ratio, railway embankment height, and natural slope height) discussed in the previous dry slope model (Set I), dimensions and location of ballast pockets, and the height of water retained in ballast pockets are included. In Section 3.1.2, these parameters (except for the water height in the ballast pockets) have already been introduced. Ballast pockets exist respectively under the center of the tie or under one side of the tie. In this study, when ballast pockets are located under one side of the tie, ballast pockets are set under the right side of the tie because the ballast pockets towards the open slope are

assumed to be more detrimental in reducing slope stability. The ballast pockets' width is set to 1.0 m, 1.5 m, or 2.0 m, and their depth is set to 0.5 m, 1.0 m, or 1.5 m. In the parametric study, it is assumed that there is a numerical relationship between the water height in ballast pockets and the ballast pockets' depth, as shown in Equation 4.1.

$$m = \frac{the\ water\ height\ in\ ballast\ pockets}{the\ depth\ of\ ballast\ pockets} \tag{4.1}$$

The value of m is set to 1/2 or 1.

m = 1/2 means that materials in the lower half of ballast pockets are submerged in water.

m = 1 means that all materials in ballast pockets are submerged in water.

Similar to Figure 4.1, Figure 4.4 summarizes all combinations of seven parameters studied in these models with ballast pockets. Therefore, 1,080 different cases are investigated in Set II. Table I-1 in Appendix I lists all these cases, with four groups and 18 subgroups. It is generally believed that cohesive soil under undrained conditions has the lowest FS value compared with fully drained and partially drained conditions, so that all models are calculated in undrained condition.

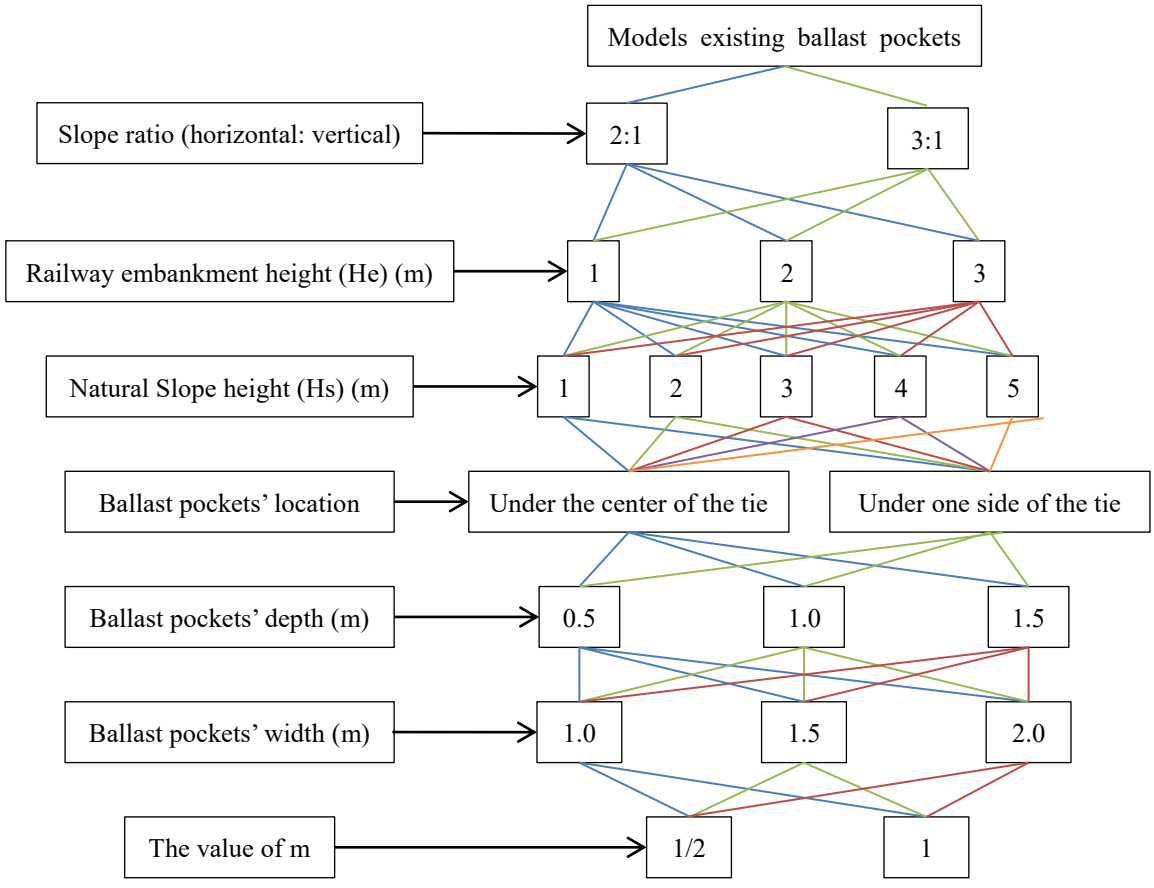

Fig. 4.4. Diagram of various cases in Set II-models existing ballast pockets.

Compared to models in Set I, Set II models add groundwater and ballast pockets. In order to show the influence of ballast pockets, Set I models with groundwater are analyzed. All

combinations are divided into two groups, including six subgroups with 30 cases.

To ensure that the natural slope is not submerged, the groundwater level of the model on the left side is 1.5 m below the bottom of the railway embankment, as described in section 3.1.2. The groundwater height of the exposed natural ground on the right side is equal to the height of the exposed ground on the right side. The models with a slope height of 1 m are an exception. Their groundwater levels are -1.5m below the bottom of the railway embankment, and there is no need to consider the left or right side of the model. The FS results of Set I models only adding groundwater are shown in Table 4.3. Figures 4.5(a)-(d) show the corresponding simulation results of models in Figures 4.2(a)-(d), after adding groundwater to them.

Table 4.3. FS results of Set I models adding groundwater

Groups	Series	FS				
		Natural slope height (Hs) (m)				
		1	2	3	4	5
Group 3	Series1	3.96	2.85	2.36	2.04	1.86
	Series 2	2.98	2.39	2.12	1.92	1.76
	Series 3	2.50	2.14	1.96	1.82	1.70
Group 4	Series 4	4.36	3.15	2.63	2.32	2.09
	Series 5	3.30	2.68	2.40	2.20	2.04
	Series 6	2.81	2.43	2.26	2.10	1.98

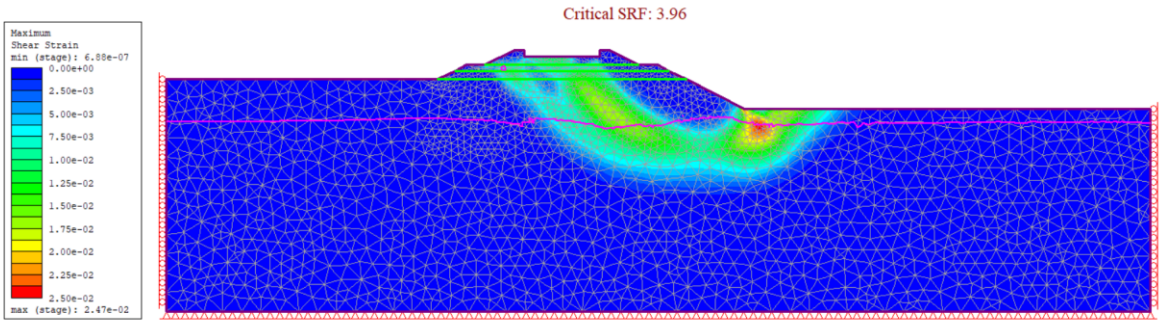

Fig. 4.5. (a) Simulation result for the Set I model adding groundwater: slope ratio = 2H:1V, He = 1 m, Hs = 1 m;

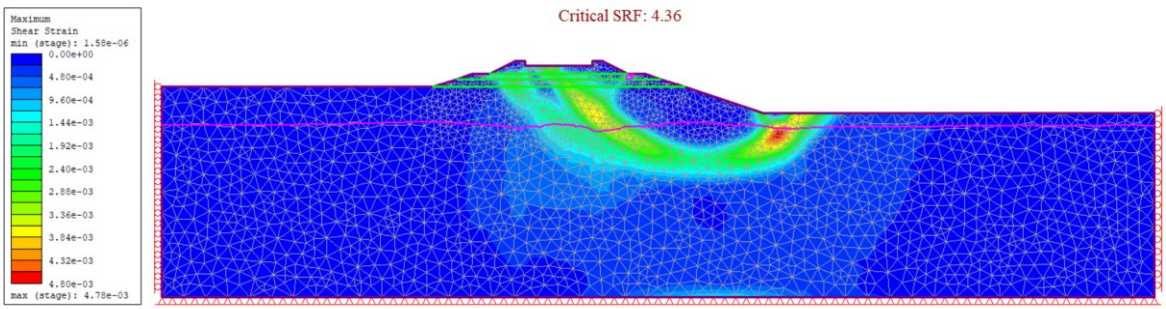

Fig. 4.5. (b) Simulation result for the Set I model adding groundwater: slope ratio = 3H:1V, He = 1 m, Hs = 1 m;

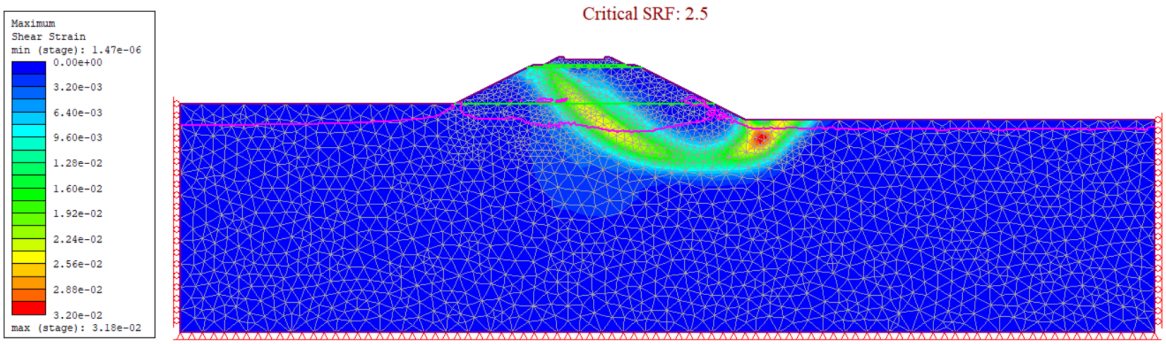

Fig. 4.5. (c) Simulation result for the Set I model adding groundwater: slope ratio = 2H:1V, He = 3 m, Hs = 1 m, (continued);

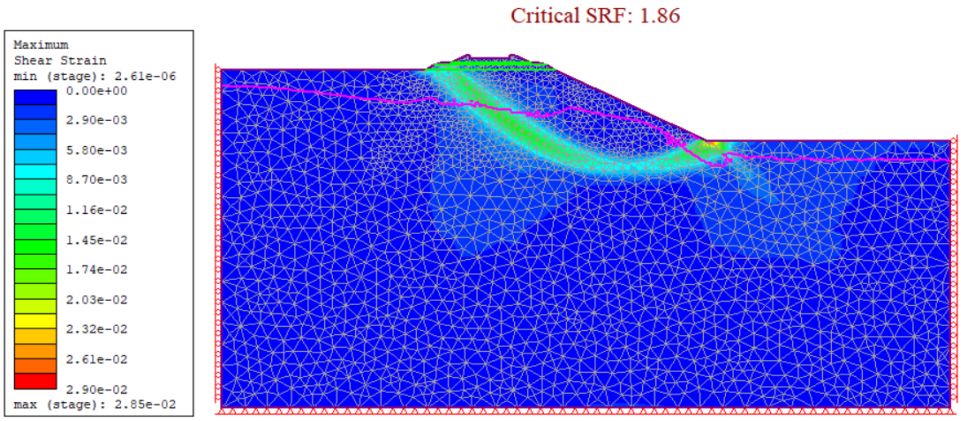

Fig. 4.5. (d) Simulation result for the Set I model adding groundwater: slope ratio = 2H:1V, He = 1 m, Hs =5 m, (continued).

Next, ballast pockets under the center of the tie with a depth of 1.5 m, a width of 2 m, and an m value of 1/2 are added onto the Group 3 and 4 models, generating models in Subgroup 29 and 47 (see Table I-1 in Appendix I). The FS results of these models are shown in Table 4.4. Figures 4.6 (a)-(d), shows the simulation results of models in Figures 4.2(a)-(d), adding groundwater and ballast pockets (i.e. Set II models). In order to verify that ballast pockets can reduce slope stability, the FS results of models in Subgroup 29 and 47 were compared with the results of Set I models, which only add groundwater (as shown in Table 4.3). The comparison result is shown in Table 4.5. The rate of FS change in Table 4.5 reflects the influence of the ballast pockets on the model. It is obtained by dividing the amount of FS change caused by the ballast pockets by the FS value of the model only with groundwater.

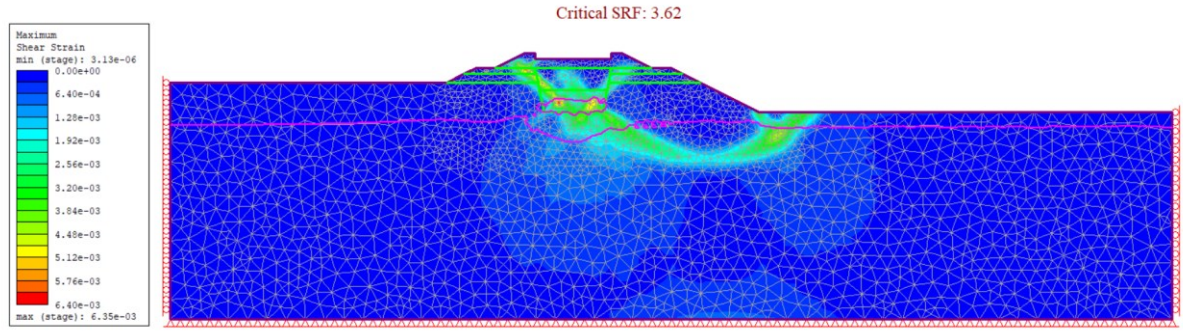

(a) Simulation result for the model: slope ratio= 2H:1V, He = 1 m, Hs = 1 m;

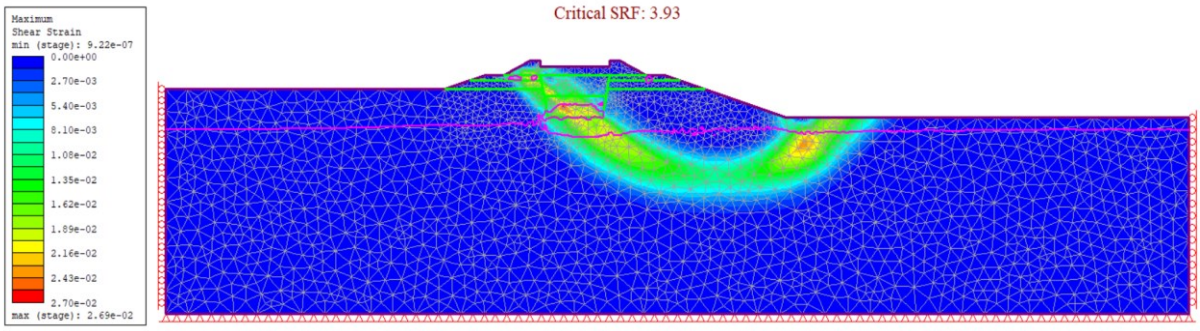

(b) Simulation result for the model: slope ratio= 3H:1V, He = 1 m, Hs = 1 m;

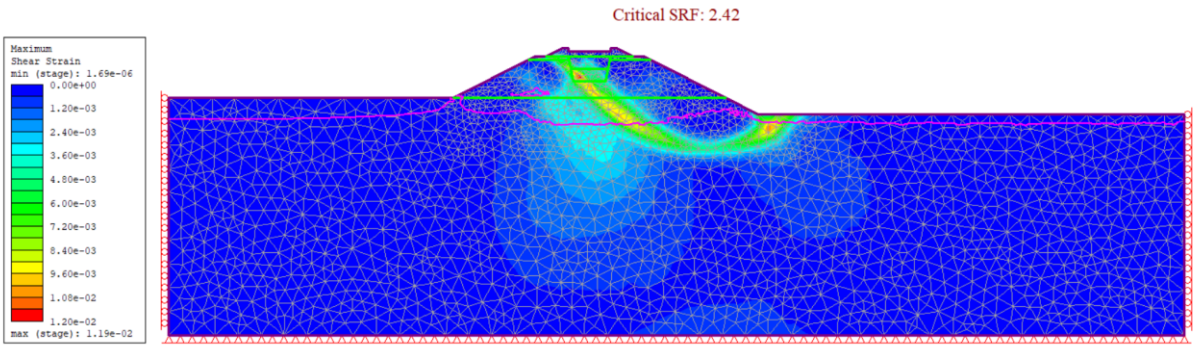

(c) Simulation result for the model: slope ratio = 2H:1V, He = 3 m, Hs = 1 m;

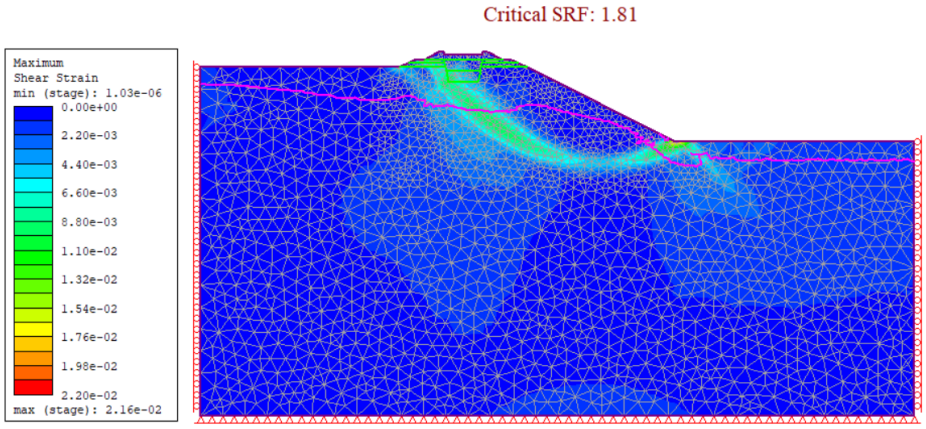

(d) Simulation result for the model: slope ratio = 2H:1V, He = 1 m, Hs = 5 m.

Fig. 4.6. Simulation results for Set I models adding groundwater and ballast pockets.

Table 4.4. FS results of part of Set II models

Groups	Subgroups	Series	Railway embankment Height (He) (m)	FS				
				Natural slope height (Hs) (m)				
				1	2	3	4	5
Group 5	Subgroup 23	Series 7	1	3.62	2.67	2.26	1.98	1.81
		Series 8	2	2.82	2.31	2.07	1.89	1.74
		Series 9	3	2.42	2.10	1.94	1.80	1.69
Group 6	Subgroup 41	Series 10	1	3.93	2.97	2.56	2.27	2.05
		Series 11	2	3.15	2.61	2.36	2.17	2.02
		Series 12	3	2.74	2.39	2.23	2.08	1.97

Table 4.5. Comparison between models adding groundwater and models adding groundwater and ballast pockets

Groups	Series	FS				
		Natural slope height (Hs) (m)				
		1	2	3	4	5
Group 3	Series 1	3.96	2.85	2.36	2.04	1.86
Group 5	Series 7	3.62	2.67	2.26	1.98	1.81
Rate of FS change (%)		**-8.6**	**-6.3**	**-4.2**	**-2.9**	**-2.7**
Group 3	Series 2	2.98	2.39	2.12	1.92	1.76
Group 5	Series 8	2.82	2.31	2.07	1.89	1.74
Rate of FS change (%)		**-5.4**	**-3.3**	**-2.4**	**-1.6**	**-1.1**
Group 3	Series 3	2.50	2.14	1.96	1.82	1.70
Group 5	Series 9	2.42	2.10	1.94	1.80	1.69
Rate of FS change (%)		**-3.2**	**-1.9**	**-1.0**	**-1.1**	**-0.6**
Group 3	Series 4	4.36	3.15	2.63	2.32	2.09
Group 6	Series 10	3.93	2.97	2.56	2.27	2.05
Rate of FS change (%)		**-9.9**	**-5.7**	**-2.3**	**-2.6**	**-2.0**
Group 3	Series 5	3.30	2.68	2.40	2.20	2.04
Group 6	Series 11	3.15	2.61	2.36	2.17	2.02
Rate of FS change (%)		**-4.5**	**-2.6**	**-1.7**	**-1.4**	**-1.0**
Group 3	Series 6	2.81	2.43	2.26	2.10	1.98
Group 6	Series 12	2.74	2.39	2.23	2.08	1.97
Rate of FS change (%)		**-2.6**	**-1.6**	**-1.3**	**-1.0**	**-0.5**

From Table 4.5, it can be seen that ballast pockets can reduce slope stability. Next, the control variable method is used to study ballast pocket parameters on the slope stability one by one.

Figures 4.7(a)-(e) show a series of models with ballast pockets. The models in Figures 4.7(b)-(e) differ only by one parameter from the model in Figure 4.7(a), and the rest remain constant. These models' external boundaries are the same as those of Set I's corresponding model (slope ratio = 3H:1V, He =3 m, Hs =1 m). To better show the parameter changes of ballast pockets, the embankment and slope parts are mainly intercepted. The corresponding

critical SRF and maximum shear strain profile results obtained by these models through simulation are shown in Figure 4.8.

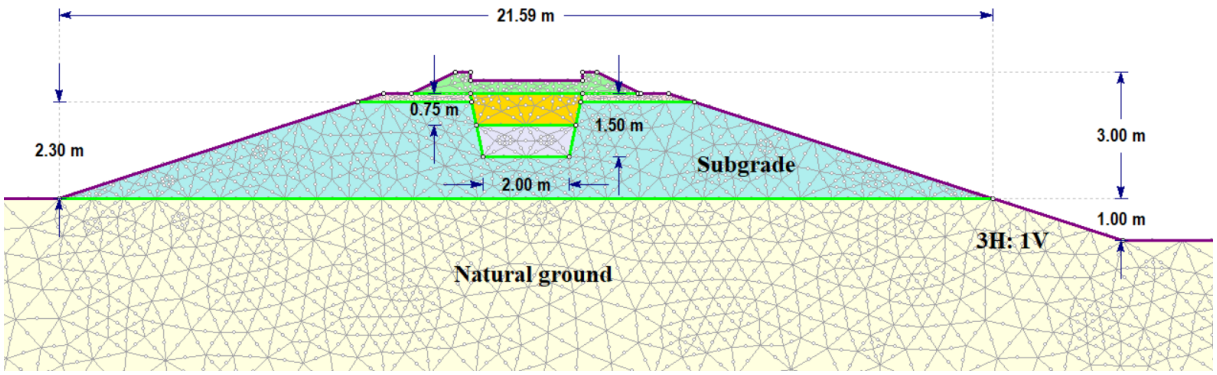

Fig. 4.7. (a) Ballast pocket geometry and position: depth = 1.5 m, width = 2.0 m, the value of m = 1/2, under the center of the tie;

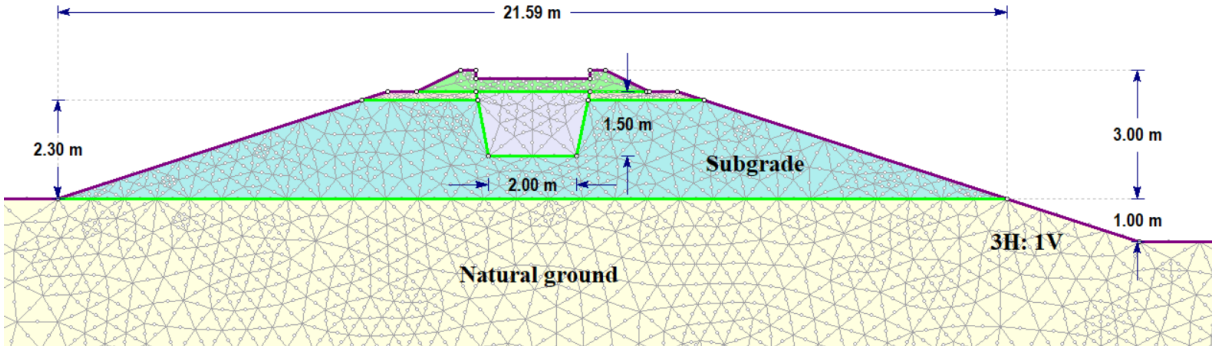

Fig. 4.7. (b) Ballast pocket geometry and position: depth =1.5 m, width = 2.0 m, the value of m = 1.0, under the center of the tie;

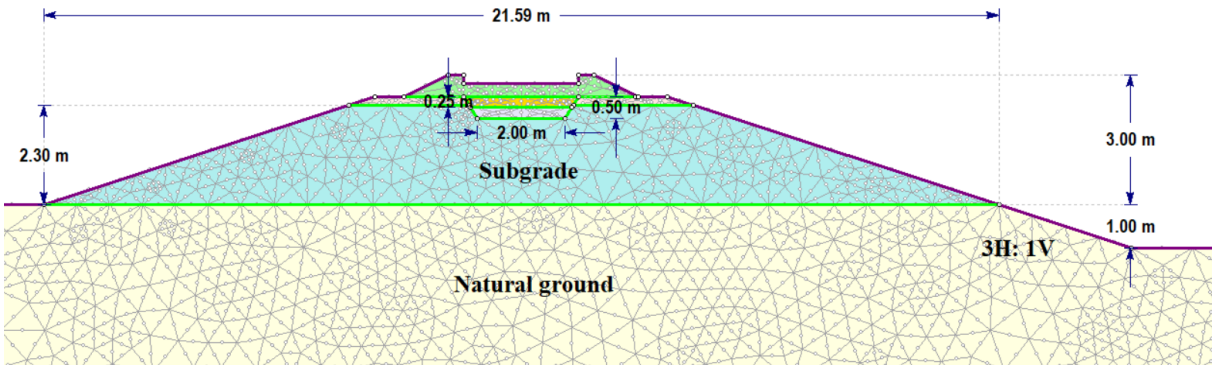

Fig. 4.7. (c) Ballast pocket geometry and position: depth = 0.5 m, width = 2.0 m, the value of m = 1/2, under the center of the tie;

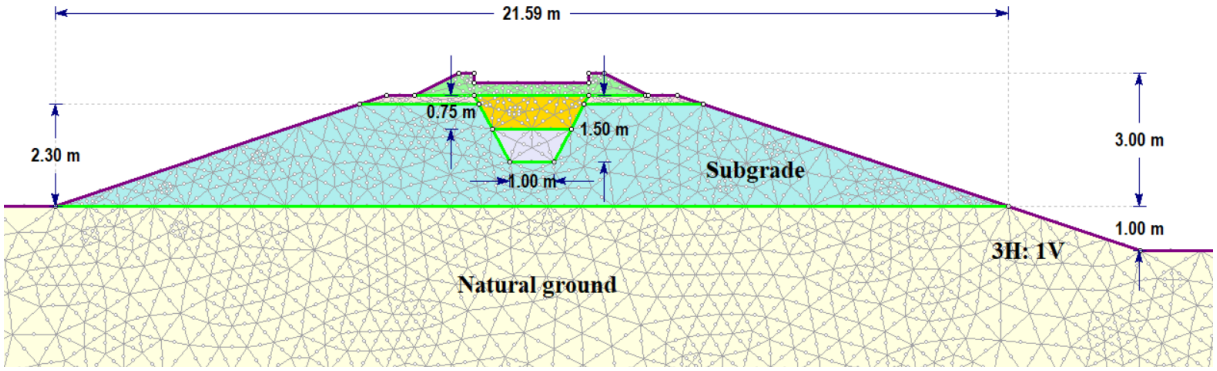

Fig. 4.7. (d) Ballast pocket geometry and position: depth = 1.5 m, width = 1.0 m, the value of m = 1/2, under the center of the tie, (continued);

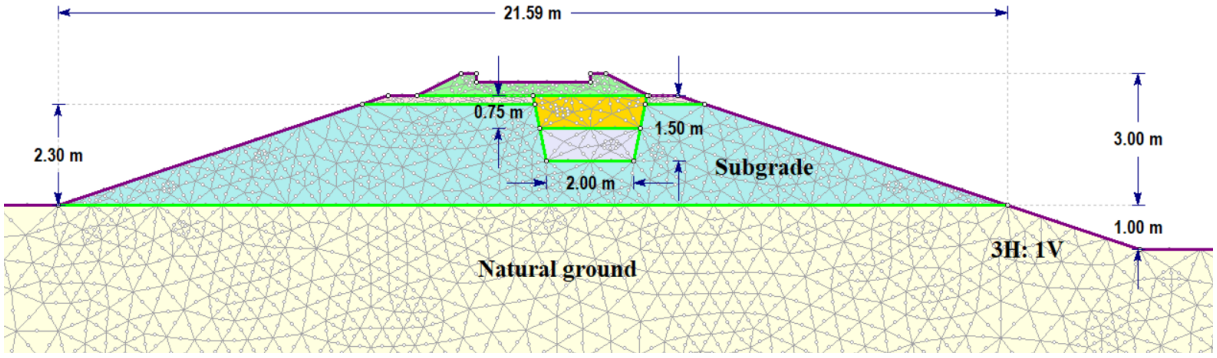

Fig. 4.7. (e) Ballast pocket geometry and position: depth = 1.5 m, width = 2.0 m, the value of m = 1/2, under one side of the tie, (continued).

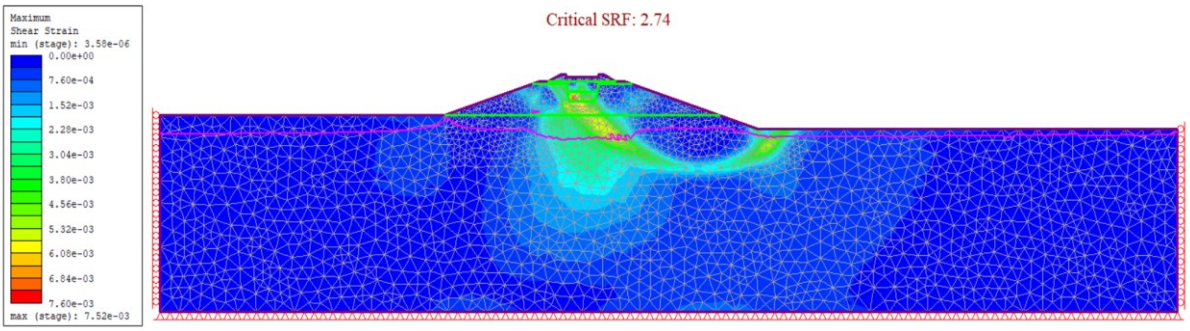

Fig. 4.8. (a) Maximum shear strain contour for the selected model with ballast pockets. Ballast pocket geometry and position: depth = 1.5 m, width = 2.0 m, the value of m = 1/2, under the center of the tie;

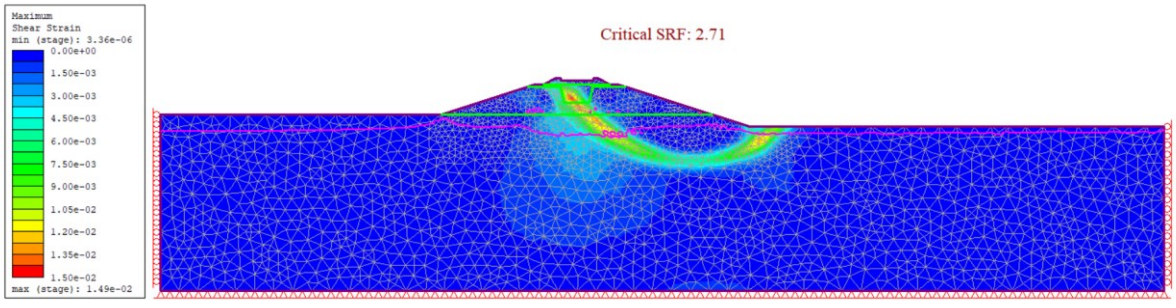

Fig. 4.8. (b) Maximum shear strain contour for the selected model with ballast pockets. Ballast pocket geometry and position: depth = 1.5m, width = 2.0 m, the value of m = 1, under the center of the tie;

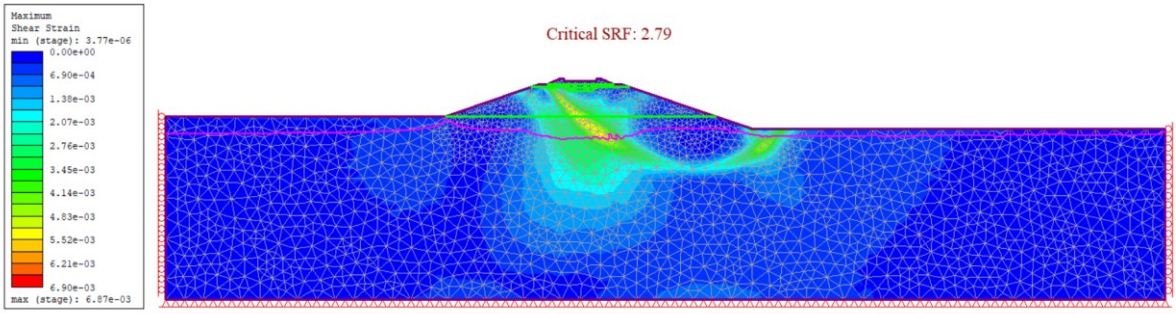

Fig. 4.8. (c) Maximum shear strain contour for the selected model with ballast pockets. Ballast pocket geometry and position: depth = 0.5 m, width = 2.0 m, the value of m = 1/2, under the center of the tie, (continued);

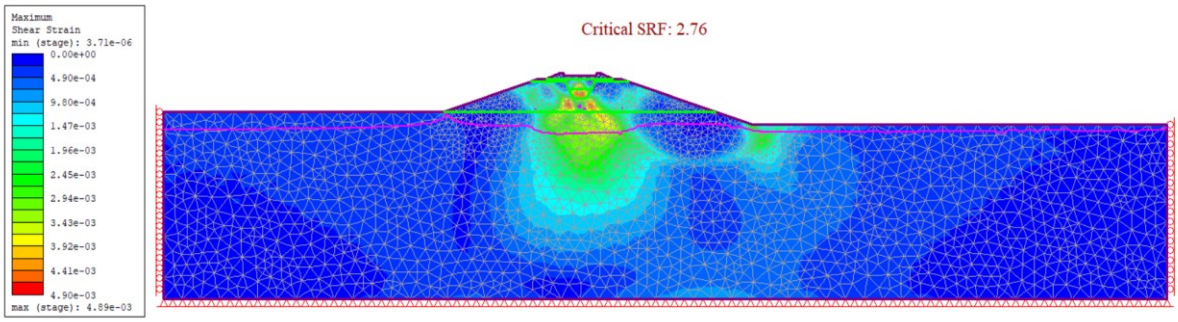

Fig. 4.8. (d) Maximum shear strain contour for the selected model with ballast pockets. Ballast pocket geometry and position: depth = 1.5 m, width = 1.0 m, the value of m = 1/2, under the center of the tie, (continued);

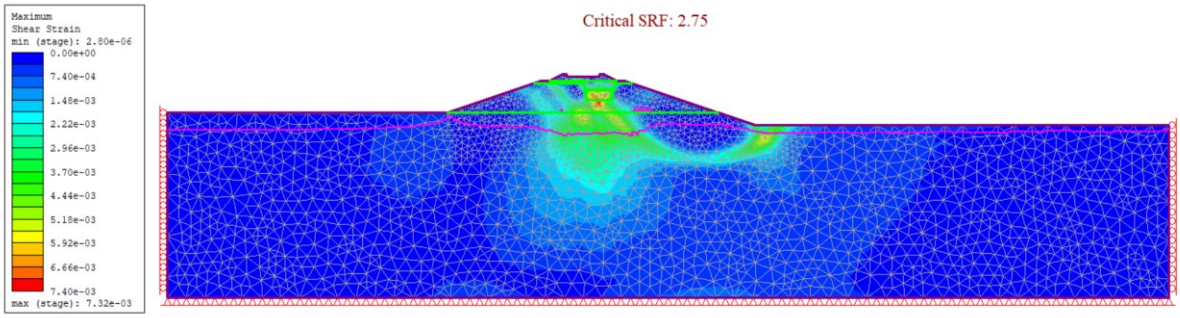

Fig. 4.8. (e) Maximum shear strain contour for the selected model with ballast pockets. Ballast pocket geometry and position: depth = 1.5 m, width = 2.0 m, the value of m = 1/2, under one side of the tie, (continued).

It can be seen from Figure 4.8 that the maximum shear strain of the model often appears at ballast pockets, which can reflect that the ballast pockets harm the slope stability. In addition, the failure type of models existing ballast pockets in Figure 4.8 is slope failure. The shape and location of the failure surfaces were different to those found from Set I, signifying a failure signifying a failure emanating from the left embankment slope and experiencing ballast pockets. The FS results of all cases in Set II are shown in Table II-1 in Appendix II. The influence of ballast pockets parameters on models are studied in Section 4.2.2.

4.1.3 Set III – modeling existing ballast pockets and freight train loads

The models in Set III add freight train loads to the models in Set II. Similar to Figure 4.1 and Figure 4.4, Figure 4.9 summarizes all combinations of the eight key parameters studied in the

models with existing ballast pockets and freight train loads conditions, for a total of 4,320 cases. This part aims to search for the maximum safe train speed in the range of 0 km/h (0 mph) to 120 km/h (75 mph). Table I-2 in Appendix I lists all combined cases, with four groups, consisting of 18 subgroups.

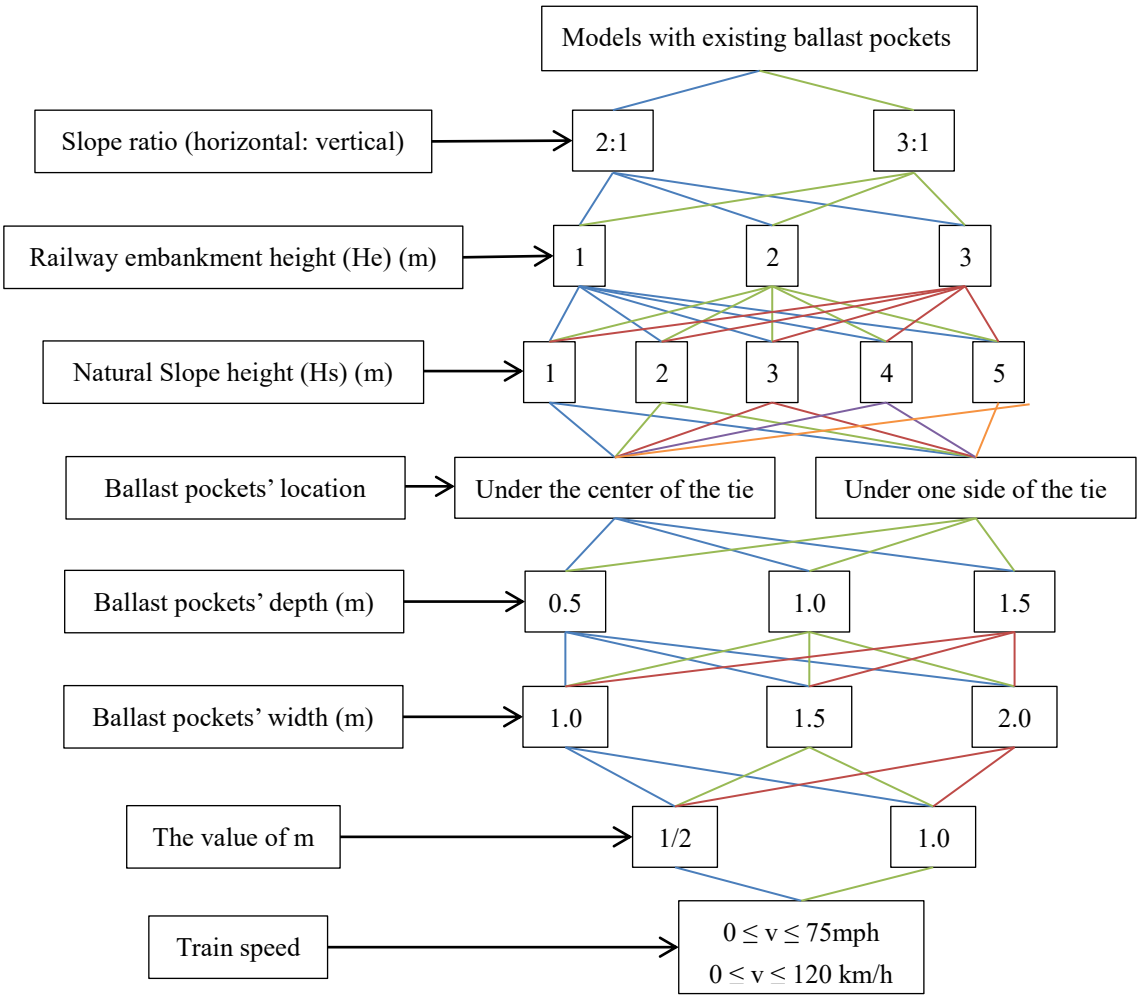

Fig. 4.9. Diagram of various cases in Set III-models existing ballast pockets and freight train loads conditions.

The maximum safe train speed of the applied train load can be obtained through the following calculation process shown in Figure 4.10. All train speeds mentioned in this process are calculated based on the train load applied to the sleeper's bottom. The train's initial speed is set to 0 km/h (0 mph) and increases by 8 km/h (5 mph) in each step to search for slope failures. According to Section 2.4.6, *slope failure* is defined as the value of FS less than 1.3. The inability to fully apply the load in the FEM model is also considered a failure condition. When a failure was detected, the speed was reduced by 8 km/h (5 mph). If the reduced speed is less than 120 km/h (75 mph), this speed is the maximum safe train speed; otherwise, if it is greater than or equal to 120 km/h, 120 km/h is regarded as the maximum safe train speed. Under particular circumstances, even a train stopped on the tracks (speed of 0 km/h) can damage the slope. In this case, it can be considered that no maximum speed is attained.

To more directly reflect the influence of ballast pockets and train loads on the models' FS value, models with ballast pockets shown in Figures 4.8 (a)-(e) were selected as examples. Figures 4.11 (a)-(e) show the maximum shear strain profile of the selected models with a

stationary train.

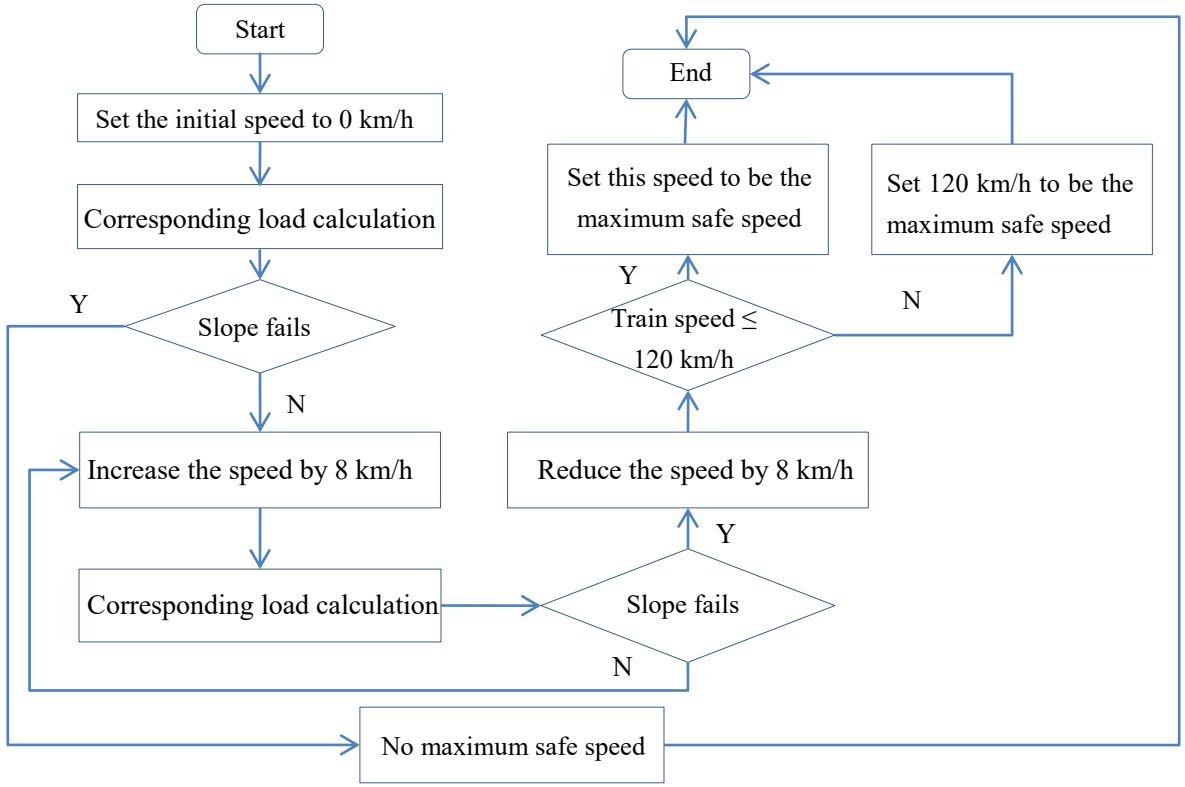

Fig. 4.10. Flowchart for calculating the maximum safe freight train speed.

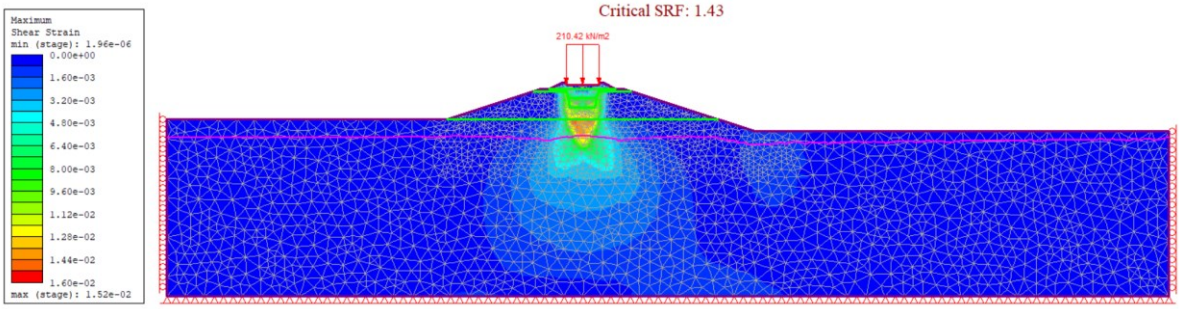

Fig. 4.11. (a) Maximum shear strain contour for the selected model with ballast pockets and a stationary train. Ballast pocket geometry and position: depth = 1.5m, width = 2.0 m, the value of m = 1/2, under the center of the tie;

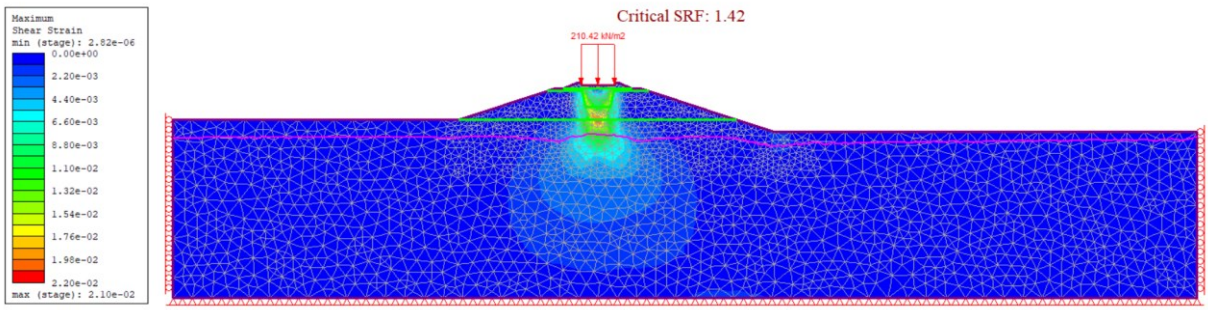

Fig. 4.11. (b) Maximum shear strain contour for the selected model with ballast pockets and a stationary train. Ballast pocket geometry and position: depth = 1.5m, width = 2.0 m, the value of m = 1, under the center of the tie;

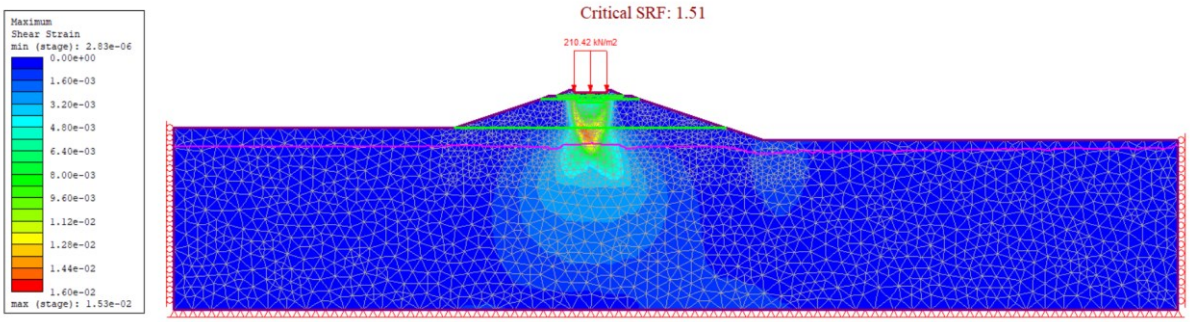

Fig. 4.11. (c) Maximum shear strain contour for the selected model with ballast pockets and a stationary train. Ballast pocket geometry and position: depth = 0.5 m, width = 2.0 m, the value of m = 1/2, under the center of the tie, (continued);

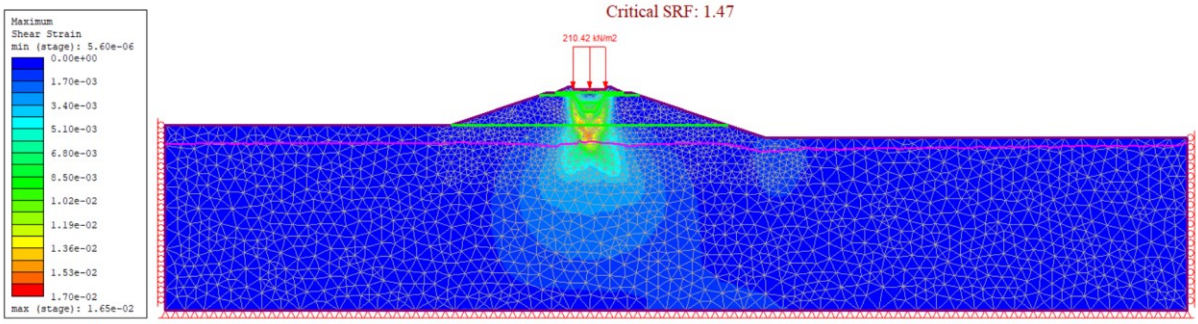

Fig. 4.11. (d) Maximum shear strain contour for the selected model with ballast pockets and a stationary train. Ballast pocket geometry and position: depth = 1.5 m, width = 1.0 m, the value of m = 1/2, under the center of the tie, (continued);

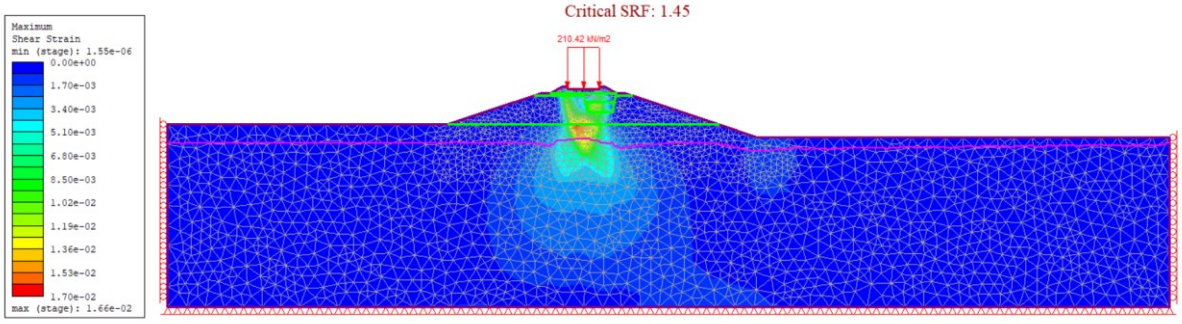

Fig. 4.11. (e) Maximum shear strain contour for the selected model with ballast pockets and a stationary train. Ballast pocket geometry and position: depth = 1.5 m, width = 2.0 m, the value of m = 1/2, under one side of the tie, (continued).

By comparing FS results in Figures 4.8 and 4.11, the application of external train loads on models can reduce slope stability. In addition, based on the failure surface of models in Figure 4.11, it can be referred that the failure type of models existing ballast pockets and a train load is bearing capacity failure, which is different from the models in Sets I and II. In addition, the left starting point of the failure surface in Fig.15 is away from the left embankment slope. For the sake of brevity, all FS results of Set III models with a stationary train on railway embankments are summarized in Table II-2 in Appendix II.

The resulting FS value of some cases is less than 1.3. Freight trains cannot stop or pass the track, and there is no acceptable safe train speed in this model. Table II-3 in Appendix II lists each Set III case's maximum safe train speed (in mph and km/h). If the top safe train speed is equal to 0 km/h, the track allows freight trains to remain stationary. If the maximum safe train speed is more than 0 km/h, the freight train with a rate not exceeding the maximum safe speed can carefully move on the track. The corresponding FS results of cases with the maximum train speed are shown in Table II-4 in Appendix II. Section 4.3 further discusses the maximum safe train speeds and FS results.

4.1.4 Distribution of pore water pressure of models in three sets

Before, the settings of models in different sets and the simulation results regarding to the FS values and maximum shear strain are shown. This section mainly analyzes the distribution of pore water pressure of models in different sets. The models in Figure 4.12 (a)-(c) have a slope ratio of 2H:1V, and their embankment height and slope height are 3m and 1m, respectively. And the specific settings of models in these figures are introduced in Section 4.1.1-4.1.3.

Figure 4.12 (a) shows that Set I models are dry models without pore water pressure. As shown in Figure 4.12 (b)-(c), models in Sets II and III under undrained conditions exist positive and negative pore pressure. The pore water pressure is positive (downwards) when soil is fully saturated (below the groundwater table). Some parts of soil above water level generate negative pore water pressure upward due to the capillary rise and get saturated. The absolute value of negative pore pressure decreases with the increasing depth; conversely, the positive pore pressure absolute value increases with the depth increase. Besides, the embankment part of Set III models is enlarged (see Figure 4.12 (c)). Figure 4.12 (c) shows that the pore pressure value at the sleeper/ballast interface in Set III models is high due to the train load.

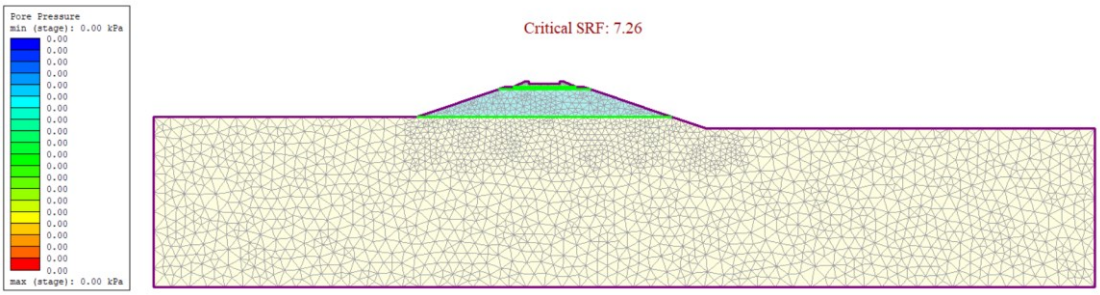

Fig. 4.12. (a) The distribution of pore water pressure of Set I model;

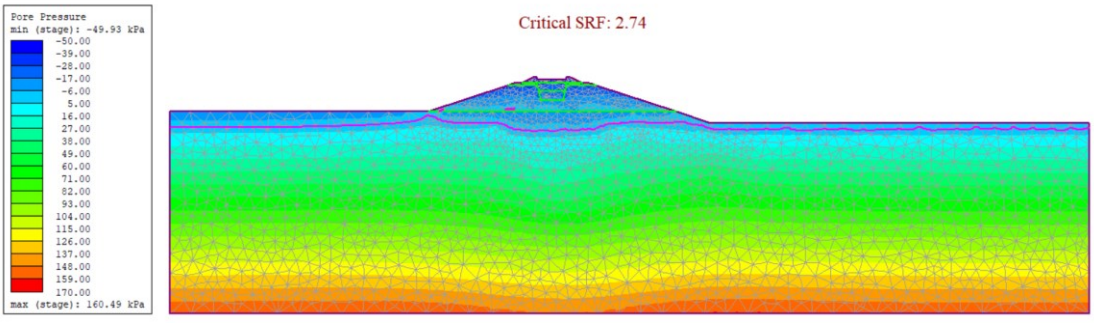

Fig. 4.12. (b) The distribution of pore water pressure of Set II models with ballast pockets: Ballast pocket geometry and position: depth = 1.5 m, width = 2.0 m, the value of m = 1/2, under the center of the tie;

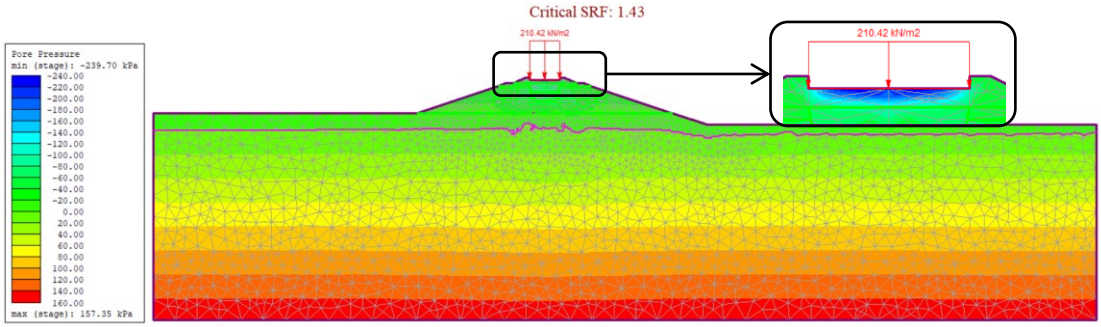

Fig. 4.12. (c) The distribution of pore water pressure of Set III models with ballast pockets and the train load: Ballast pocket geometry and position: depth = 1.5 m, width = 2.0 m, the value of m = 1/2, under the center of the tie, (continued).

4.1.5 Distribution of element yielding of models in three sets

This section mainly introduces the yielded element distribution of models in different sets. Figure 4.13 (a)-(c) show the element yielding distribution of models shown in Figure 4.12 (a)-(c). In these figures, the elements represented by "x" yield in shear, and the elements described by "o" yield in tension.

The Set I model shown in Figure 4.13 (a) only have elements yielding in shear. The yielded elements are mainly distributed in the slope failure area (including the embankment and the particular area below the embankment and slope). The models in Sets II and III shown in Figure 4.13 (b) and (c) have elements yielding in shear and tension. For the model in Set II (see Figure 4.13 (b)), elements yielding in shear are mainly distributed in the slope failure area, and elements yielding in tension are concentrated at the subgrade and the boundary of the exposed natural ground on the right side. Besides, elements yielding in tension almost all yield in shear. The model in Set III shown in Figure 4.13 (c) has elements yielding in shear at the area below the sleeper reaching a certain depth and elements yielding in tension at the embankment and the boundary of the exposed natural ground on the right side. Elements yielding in shear at the embankment also yield in tension.

Comparing the models shown in Figure 4.13 (a)-(c), increasing the ballast pockets and train load on the models, in turn, leads to a significant reduction in the area of yielded elements, and the overall contours of the yielded elements in the models in Set I and Set II are similar and completely different from that in Set III models. And the number of elements yielding in tensor in Set II models is more than that in Set III models, particularly at the boundary of the exposed natural ground on the right side.

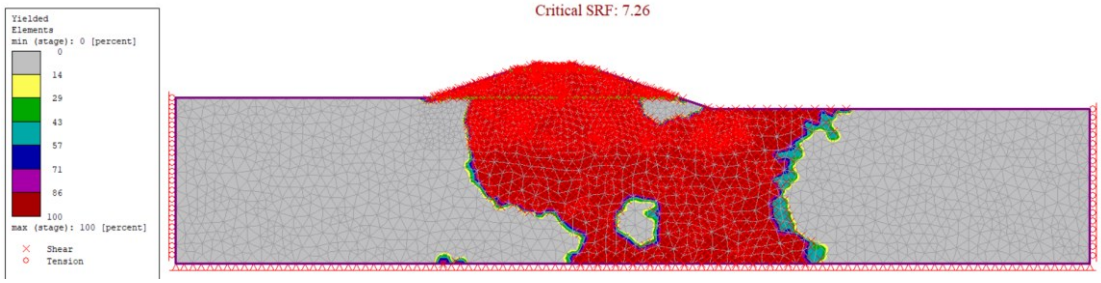

Fig. 4.13. (a) The distribution of element yielding of Set I model;

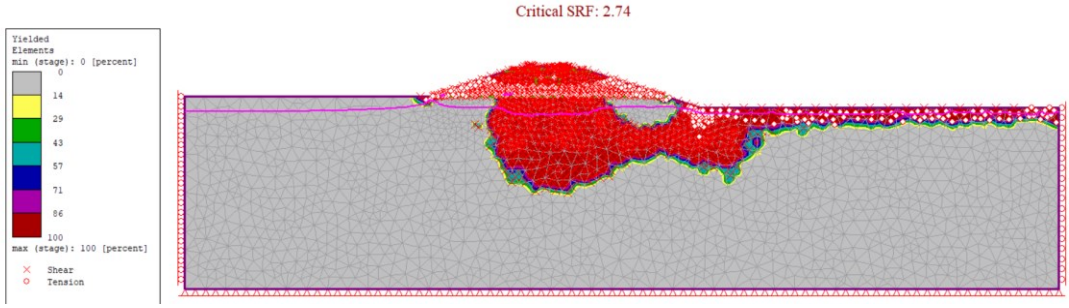

Fig. 4.13. (b) The distribution of element yielding of Set II models with ballast pockets: Ballast pocket geometry and position: depth = 1.5 m, width = 2.0 m, the value of m = 1/2, under the center of the tie, (continued);

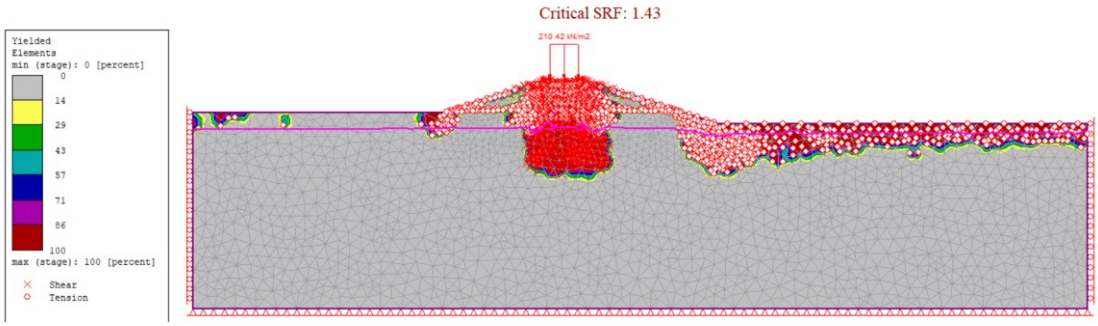

Fig. 4.13. (c) The distribution of element yielding of Set III models with ballast pockets and the train load: Ballast pocket geometry and position: depth = 1.5 m, width = 2.0 m, the value of m = 1/2, under the center of the tie, (continued).

4.2 Discussion of models in Sets I and II

This section discusses the simulation results of three sets of models presented in Section 4.1. Set I models investigated the parameters of the natural slope height, railway embankment height, and slope ratio. The parameters of ballast pockets were studied in the models of Set II. To better show how FS interacts with each parameter, a set of graphs showing the development trends of FS are provided.

4.2.1 Comparison of simulation results for models in Set I

The geometric parameters of Set I models (natural slope height, railway subgrade height, slope ratio) have been introduced in Figure 4.1. Next, the influence of these parameters on slope stability is analyzed one by one.

Figure 4.14 shows FS results versus natural slope heights in a range of 1 m to 5 m with three railway embankment heights. It can be seen from Figure 4.14 that the increase of natural slope height and railway embankment height can considerably reduce slope stability. The relatively flat slope helps to stabilize the slope. Figure 4.14 uses abbreviations to represent each subgroup. For example, SG.1 represents Subgroup 1. This abbreviation is used to represent subgroups in each subsequent figure.

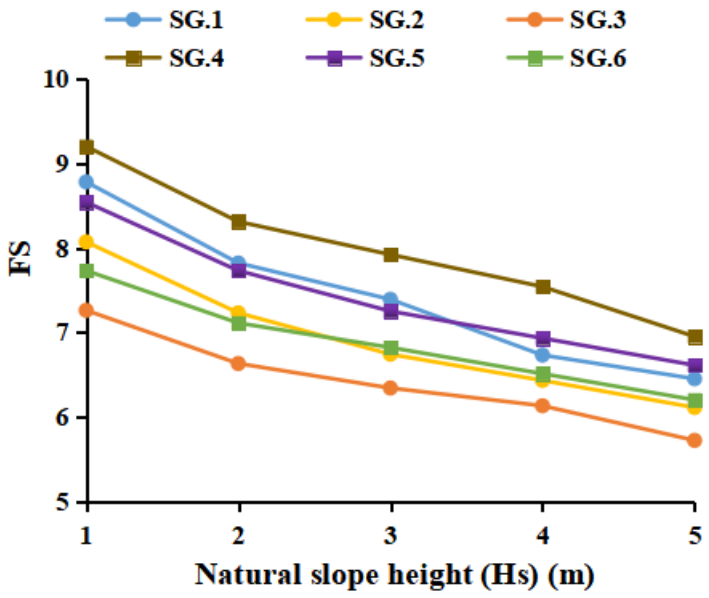

Fig. 4.14. FS results of Set I models versus the natural slope height.

The changes in the FS results of models with different natural slope height in the same subgroup is evaluated by Equation 4.2, as shown below:

$$R_F = \frac{FS_{m,b} - FS_{m,a}}{FS_{m,a}} \tag{4.2}$$

Where m is the subgroup number (m = 1, 2, 3, 4, 5, 6), and a and b is the natural slope height (a = 1, b = 1, 2, 3, 4, 5). The meaning of $FS_{m,b}$ is the FS value of the model with a b m natural slope height in Subgroup m, similar, the mean of $FS_{m,a}$ is the FS value of the model with a 1 m natural slope height in Subgroup m. R_F means is the rate of FS change from the model with an a natural slope height in Subgroup m to the model with an 1m natural slope height in Subgroup m.

Table 4.6 shows the FS change rate caused by the natural slope height increase, and the FS rate of change versus natural slope height is visualized in Figure 4.15. It can be seen from Figure 4.15 that all the lines have an upward trend as the natural slope height increases, which means that the more the natural slope height increases, the more significant the decrease in the FS value of models. In addition, it can be seen that as the railway embankment height increases or the slope becomes gentler, the decrease in the FS value caused by the increase in the natural slope height becomes smaller.

Table 4.6. Rate of FS change of Set I models caused by the natural slope height increase

Groups	Subgroups	FS				
		Natural slope height (Hs) (m)				
		1	2	3	4	5
Group 1	Subgroup 1	8.78	7.82	7.39	6.73	6.45
Rate of FS change (%)		**0.00**	**-10.93**	**-15.83**	**-23.35**	**-26.54**
Group 1	Subgroup 2	8.07	7.23	6.74	6.43	6.11
Rate of FS change (%)		**0.00**	**-10.41**	**-16.48**	**-20.32**	**-24.29**
Group 1	Subgroup 3	7.26	6.63	6.34	6.13	5.72
Rate of FS change (%)		**0.00**	**-8.68**	**-12.67**	**-15.56**	**-21.21**
Group 2	Subgroup 4	9.20	8.31	7.92	7.54	6.95
Rate of FS change (%)		**0.00**	**-9.67**	**-13.91**	**-18.04**	**-24.46**
Group 2	Subgroup 5	8.54	7.73	7.25	6.93	6.61
Rate of FS change (%)		**0.00**	**-9.48**	**-15.11**	**-18.85**	**-22.60**
Group 2	Subgroup 6	7.73	7.11	6.82	6.51	6.20
Rate of FS change (%)		**0.00**	**-8.02**	**-11.77**	**-15.78**	**-19.79**

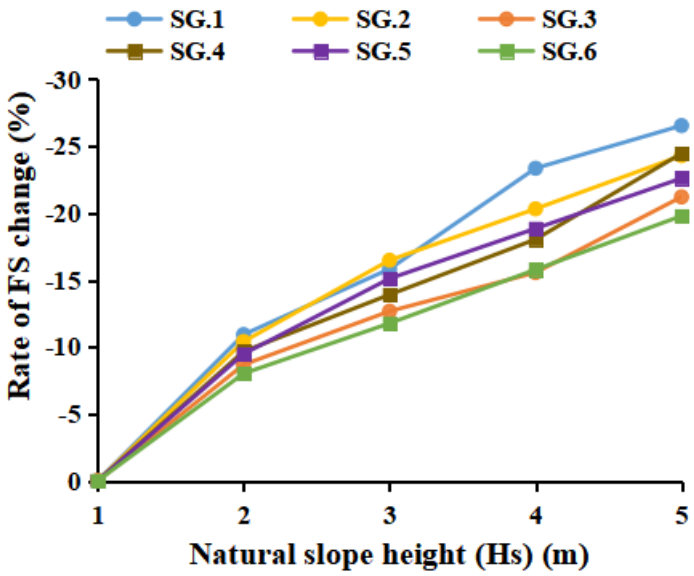

Fig. 4.15. Relationship between the rate of FS change of Set I models caused by increasing the natural slope height and the natural slope height.

Similarly, the changes in the FS results of each subgroup (SG.) in Group 1 and Group 2 is evaluated by Equation 4.3, as shown below:

$$R_F = \frac{FS_{n,a} - FS_{m,a}}{FS_{m,a}} \tag{4.3}$$

Where m and n are the subgroup number (m = 1, 4, n = 2, 3, 5, 6), and a is the natural slope height (a = 1, 2, 3, 4, 5). The mean of $FS_{n,a}$ is the FS value of the model with an a m natural slope height in Subgroup n. Similarly, the mean of $FS_{m,a}$ is the FS value of the model with an a m natural slope height in Subgroup m. R_F means the rate of FS changes from the model with an a m natural slope height in Subgroup m to the model with an n m natural slope height in Subgroup n.

Table 4.7 summarizes the FS change rate between subgroups versus natural slope heights in a range of 1 m to 5 m with three railway embankment heights. It is necessary to note that all FS change rate results are obtained by comparing with the subgroup with a 1 m railway embankment height in the same group. Models' FS change rate caused by the railway embankment height increase versus natural slope height is plotted in Figure 4.16.

It can be concluded from Figure 4.14 that as the railway embankment height increases, the FS value of models decreases. The absolute values of the FS change rate of models with a natural slope height of 4 m and a slope ratio of 3H:1V have achieved overtake. However, the absolute values of the FS rate of change of models with a slope ratio of 2H:1V are more significant, which means the stability of models with a slope ratio of 2H:1V is more affected by the increase in railway embankment height. With the increase of natural slope height, the curves in Figure 4.16 show a downward trend, except for the gray line representing the comparison results of Subgroups 4 and 5. The impact of the increase in the railway embankment height on models can reduce with the increase in the natural slope height.

Table 4.7. Rate of FS change of Set I models caused by the railway embankment height increase

Groups	Subgroups	FS				
		Natural slope height (Hs) (m)				
		1	2	3	4	5
Group 1	Subgroup 1	8.78	7.82	7.39	6.73	6.45
	Subgroup 2	8.07	7.23	6.74	6.43	6.11
Rate of FS change (%)		**-8.09**	**-7.54**	**-8.80**	**-4.46**	**-5.27**
Group 1	Subgroup 3	7.26	6.63	6.34	6.13	5.72
Rate of FS change (%)		**-17.31**	**-15.22**	**-14.21**	**-8.92**	**-11.32**
Group 2	Subgroup 4	9.20	8.31	7.92	7.54	6.95
	Subgroup 5	8.54	7.73	7.25	6.93	6.61
Rate of FS change (%)		**-7.17**	**-6.98**	**-8.46**	**-8.09**	**-4.89**
Group 2	Subgroup 6	7.73	7.11	6.82	6.51	6.20
Rate of FS change (%)		**-15.98**	**-14.44**	**-13.89**	**-13.40**	**-10.79**

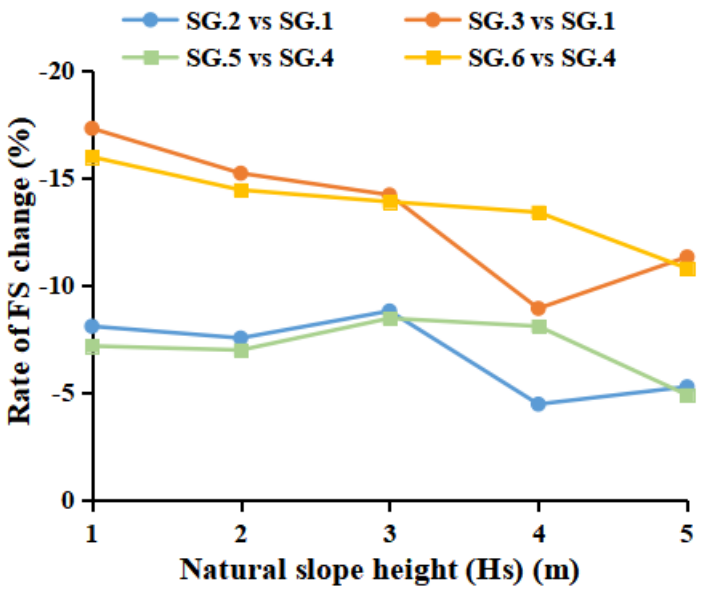

Fig. 4.16. Relationship between the rate of FS change of Set I models caused by increasing the railway embankment height and the natural slope height..

Table 4.8 concludes the rate of FS change caused by the slope ratio of models from 2H:1V to 3H:1V. It is obtained by dividing the amount of FS change caused by slope ratio change by the FS value of the model with a slope ratio of 2H:1V. Figure 4.17 shows the correlation of FS rate of change with slope heights more intuitively. Except for models with a natural slope height of 4 m, the change in slope ratio leads to a greater FS rate of change for models with higher railway embankment height or natural slope height. The smaller the height of the railway embankment of the model with a natural slope height of 4 m, the greater the rate of change of FS.

Table 4.8. Rate of FS change of Set I models caused by making the slope flat

Groups	Subgroups	Railway embankment height (He) (m)	Rate of FS change (%)				
			Natural slope height (Hs) (m)				
			1	2	3	4	5
Group 2 vs Group 1	SG.4 vs SG.1	1	4.8	6.3	7.2	12.0	7.8
	SG.5 vs SG.2	2	5.8	6.9	7.6	7.8	8.2
	SG.6 vs SG.3	3	6.5	7.3	7.6	6.2	8.4

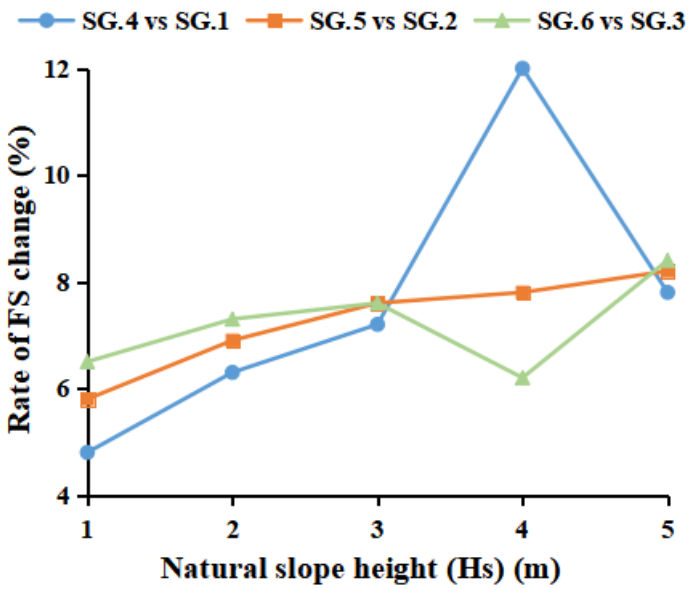

Fig. 4.17. Relationship between the rate of FS change of Set I models caused by making the slope flat and the natural slope height.

4.2.2 Comparison of simulation results for models in Set II

Set II models focused on the influence of ballast pocket-related parameters (the depth, width, position of ballast pockets, and the water level in the ballast pockets). Before analyzing the influence of these parameters on the FS value of the model, the other three parameters are analyzed (natural slope height, railway embankment height and slope ratio), which are involved in Set II models and studied in Set I models.

Figure 4.18 shows FS results of models in Subgroup 7 (2H:1V) and Subgroup 25 (3H:1V) versus natural slope heights in a range of 1 m to 5 m with three railway embankment heights. Models in Subgroup 7 and 25 have the same ballast pocket-related parameters.

Figure 4.18 shows that increasing the height of the railway embankment reduces the FS value and increasing the natural slope height can also cause slope instability. However, the stability of the entire structure can be increased by making the slope flatter. The influence of these three parameters on the slope stability is the same as the conclusion obtained by the Set I model study.

Similar to the analysis of Set I models, the values of the FS change rate caused by the three parameters versus the natural slope height are plotted, respectively, as shown in Figures 4.19.

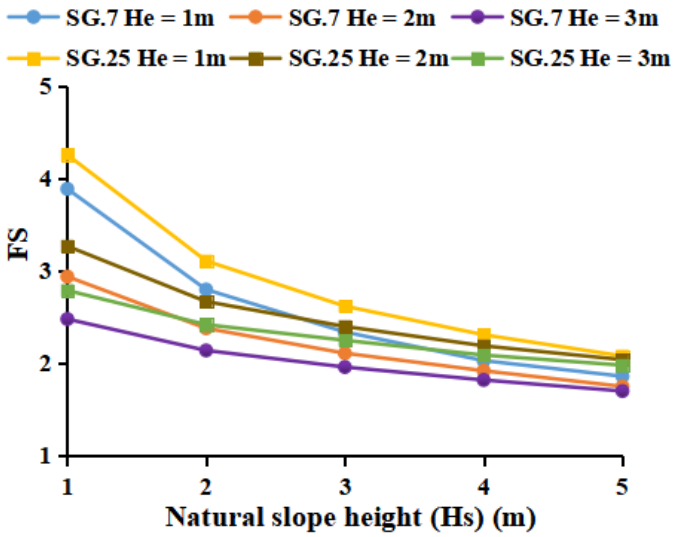

Fig. 4.18. FS results of models in Subgroup 7 (2H:1V) and Subgroup 25 (3H:1V) versus the natural slope heights.

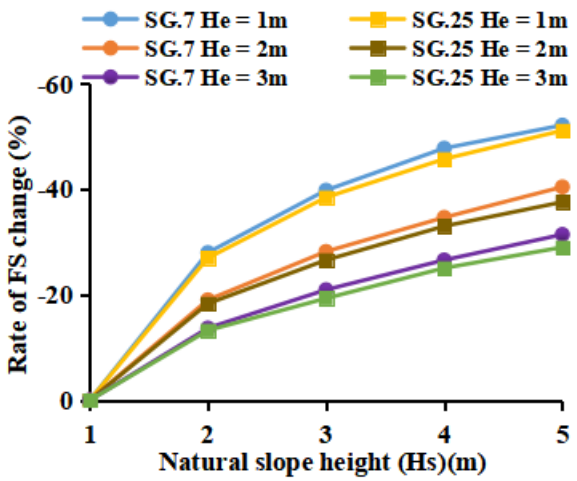

(a) Rate of FS change caused by the natural slope height increase

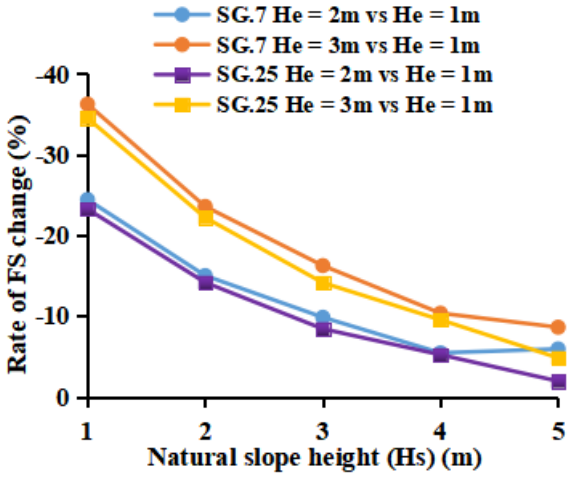

(b) Rate of FS change caused by the railway embankment height increase

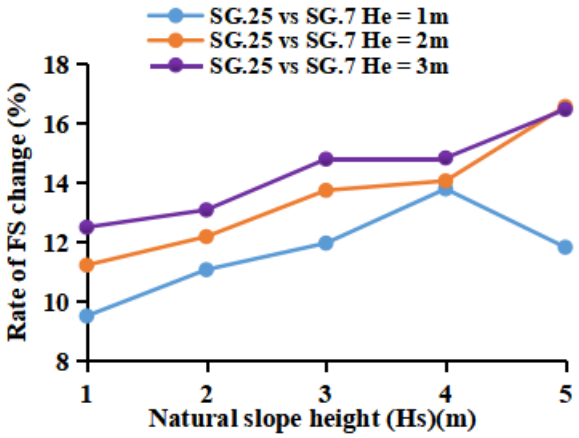

(c) Rate of FS change caused by making the slope flat

Fig. 4.19. Relationship between the rate of FS change of models in Subgroups 7 and 25 caused by three basic parameter variations and the natural slope height.

The curves in Figures 4.19 (a) and (c) show an upward trend with the increase of natural slope height, while curves in Figure 4.19 (b) show a downward trend. Figure 4.19 shows that with the increase of natural slope height, the decrease of FS value caused by the increase of railway embankment height becomes smaller. Conversely, with the increase of railway embankment height, the degree of the decrease in FS values of models is reduced by the increase of natural slope height. Compared with models with a slope ratio of 3H:1V, FS values of models with 2H:1V are more affected by the increase in railway embankment height and natural slope height.

The ballast pocket-related parameters are next analyzed, one by one.

(a) Influence of the depth of ballast pockets

FS values of models in Subgroups 7, 13 and 19 in Group 5 and Subgroups 25, 31 and 37 in Group 6 are listed in Table 4.9. Models in the first three subgroups have a slope ratio of 2H:1V and models in the last three subgroups have a slope ratio of 3H:1V. All models mentioned in these six subgroups have one different ballast pocket-related parameter, the depth of ballast pockets. Note, the ballast pockets in these models are under the center of the tie. The depth of ballast pockets in Subgroup 7 and 25, Subgroup 13 and 31, Subgroup 19 and 37 is 0.5 m, 1.0 m, and 1.5 m, respectively. FS values of the first subgroup in each group act as a reference to calculate the rate of FS change. The rates of FS change caused by the increase in the ballast pockets' depth are summarized in Table 4.9.

From Table 4.9, it can be seen that increasing the depth of ballast pockets can reduce slope stability, since all the FS change rate values in Table 4.9 are not greater than zero, and as the ballast pockets' depth increases, the absolute values of the rate of FS change keep increasing. Values of the FS change rate of Groups 5 and 6 versus the natural slope height are plotted in Figures 4.20 (a) and (b), respectively.

Table 4.9. Rate of FS change of models in Groups 5 and 6 caused by increasing the depth of ballast pockets (ballast pockets under the center of the tie)

Groups	Subgroups	Railway embankment height (He) (m)	Rate of FS change (%)				
			Natural slope height (Hs) (m)				
			1	2	3	4	5
Group 5	Subgroup 7	1	3.89	2.80	2.34	2.03	1.86
	Subgroup 13	1	3.77	2.74	2.30	2.01	1.84
Rate of FS change (%)			**-3.08**	**-2.14**	**-1.71**	**-0.99**	**-1.08**
Group 5	Subgroup 7	2	2.94	2.38	2.11	1.92	1.75
	Subgroup 13	2	2.88	2.35	2.10	1.91	1.75
Rate of FS change (%)			**-2.04**	**-1.26**	**-0.47**	**-0.52**	**0**
Group 5	Subgroup 7	3	2.48	2.14	1.96	1.82	1.70
	Subgroup 13	3	2.47	2.13	1.95	1.81	1.70
Rate of FS change (%)			**-0.40**	**-0.47**	**-0.51**	**-0.55**	**0**

Table 4.9. Rate of FS change of models in Groups 5 and 6 caused by increasing the depth of ballast pockets (ballast pockets under the center of the tie) – Continued

Groups	Subgroups	Railway embankment height (He) (m)	FS				
			Natural slope height (Hs) (m)				
			1	2	3	4	5
Group 5	Subgroup 19	1	3.64	2.68	2.27	1.99	1.84
Rate of FS change (%)			**-6.43**	**-4.29**	**-2.99**	**-1.97**	**-1.08**
Group 5	Subgroup 19	2	2.83	2.32	2.08	1.90	1.74
Rate of FS change (%)			**-3.74**	**-2.52**	**-1.42**	**-1.04**	**-0.57**
Group 5	Subgroup 19	3	2.45	2.12	1.95	1.81	1.69
Rate of FS change (%)			**-1.21**	**-0.93**	**-0.51**	**-0.55**	**-0.59**
Group 6	Subgroup 25	1	4.26	3.11	2.62	2.31	2.08
	Subgroup 31	1	4.10	3.05	2.60	2.29	2.07
Rate of FS change (%)			**-3.76**	**-1.93**	**-0.76**	**-0.87**	**-0.48**
Group 6	Subgroup 25	2	3.27	2.67	2.40	2.19	2.04
	Subgroup 31	2	3.22	2.65	2.38	2.19	2.03
Rate of FS change (%)			**-1.53**	**-0.75**	**-0.83**	**0**	**-0.49**
Group6	Subgroup 25	3	2.78	2.42	2.25	2.09	1.98
	Subgroup 31	3	2.76	2.41	2.24	2.09	1.97
Rate of FS change (%)			**-0.72**	**-0.41**	**-0.44**	**0**	**-0.51**
Group 6	Subgroup 37	1	3.99	2.99	2.57	2.29	2.06
Rate of FS change (%)			**-6.34**	**-3.86**	**-1.91**	**-0.87**	**-0.96**
Group 6	Subgroup 37	2	3.17	2.61	2.37	2.18	2.03
Rate of FS change (%)			**-3.06**	**-2.25**	**-1.25**	**-0.46**	**-0.49**
Group 6	Subgroup 37	3	2.76	2.40	2.24	2.08	1.97
Rate of FS change (%)			**-0.72**	**-0.83**	**-0.44**	**-0.48**	**-0.51**

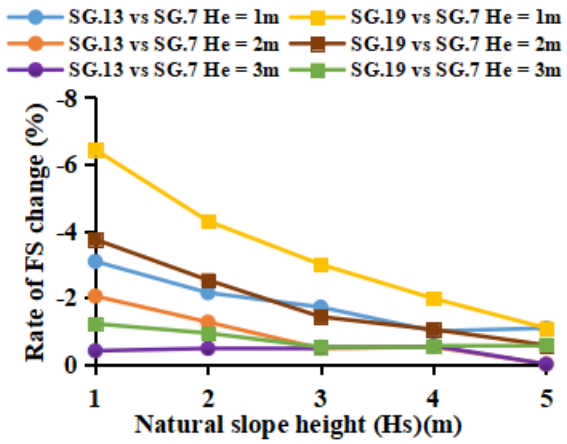

(a) Comparison results of subgroups in Group 5

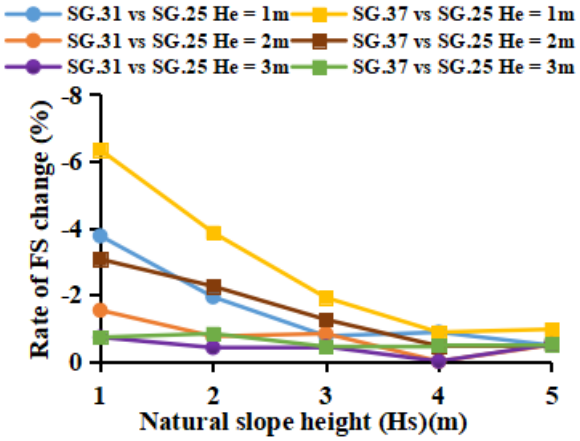

(b) Comparison results of subgroups in Group 6

Fig. 4.20. Relationship between the rate of FS change of models in Groups 5 and 6 caused by increasing the depth of ballast pockets and the natural slope height (ballast pockets under the center of the tie).

The curves in Figure 4.20 representing the comparison results of models with a railway embankment height of 1 m or 2 m show a clear downward trend, indicating that as the natural slope height increases, the change of FS value by the increase in the ballast pockets' depth becomes smaller. Otherwise, the curves representing the comparison results of models with a railway embankment height of 3 m are relatively gentle. Although there are some variations in the results, the difference between overall values is not significant.

In addition, it can be seen from Figure 4.20 that as the railway embankment height decreases, slope stability is more affected by the increase of ballast pockets' depth. Comparing Figures 4.20(a) and (b), it can be concluded that the increase of ballast pocket depth has a more significant impact on models with a slope ratio of 2H:1V.

The positions of ballast pockets in the analyzed models above are all below the center of the tie. To verify the influence of the ballast pockets' depth on the FS value of the model when ballast pockets are located below one side of the tie, Subgroups 43, 49, and 55 in Group 7 and Subgroups 61, 67, and 73 in Group 8 are selected. Models in these six subgroups and the models in Groups 5 and 6 analyzed above are only different in the position of the ballast pockets, and other parameters are the same. Models in Subgroups 43, 49, and 55 have a slope ratio of 2H:1V and models in Subgroups 61, 67, and 73 have a slope ratio of 3H:1V. The depth of ballast pockets in Subgroup 43 and Subgroup 61, Subgroup 49 and Subgroups 67, 55, and 73 is 0.5 m, 1.0 m, and 1.5 m, respectively. Values of the FS change rate of Groups 7 and 8 versus the natural slope height are plotted in Figures 4.21 (a) and (b), respectively.

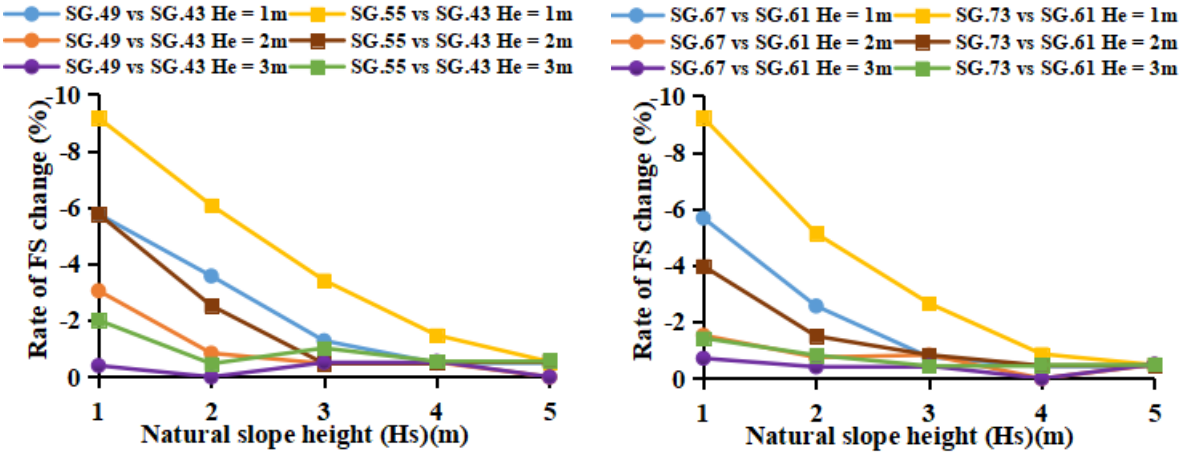

(a) Comparison results of subgroups in Group 7

(b) Comparison results of subgroups in Group 8

Fig. 4.21. Relationship between the rate of FS change of models in Groups 7 and 8 caused by increasing the depth of ballast pockets and the natural slope height (ballast pockets under one side of the tie).

Similar to curves in Figure 4.20, the trends in Figure 4.21 representing the comparison results of models with a railway embankment height of 3 m are relatively flat. The other curves in Figure 4.20 have a significant decrease with the increase in natural slope height. Models with ballast pockets under the center of the tie and with ballast pockets under one side of the tie are affected similarly by the increase in depth of the ballast pockets. Comprehensive analysis of Groups 5-8, models with ballast pockets under one side of the center and a railway embankment height of 1m are most affected by the increase in ballast pockets' depth, while

the impact of the increase in the ballast pockets' depth on models with ballast pockets under one side of the center and a railway embankment height of 3m is minimal.

(b) Influence of the width of ballast pockets

Similar to analyzing the influence of the ballast pockets' depth on the slope stability, models with ballast pockets located below the center of the tie are analyzed first. Table 4.10 presents FS values of models in Subgroups 7, 9, and 11 in Group 5 and Subgroups 25, 27, and 29 in Group 6. The ballast pockets' width of models in Subgroups 7 and 25, Subgroups 9 and 27，Subgroups 11 and 29 are 1.0 m, 1.5 m or 2. 0m, respectively. Subgroup 7, 9, and 11 models have a slope ratio of 2H:1V. Applying the slope ratio of 3H:1V to these models, Subgroups 25, 27, and 29 are formed. Table 4.10 also shows the comparison results of the models of each two groups of subgroups in the same group. Models with 1.0 m width ballast pockets in the first subgroup in each group are used as a reference for comparison. The absolute values of the rate of FS change in Table 4.10 do not exceed 0.5%, and many are even equal to 0, which shows that increasing the ballast pockets' width has little effect on slope stability.

Table 4.10. Rate of FS change of models in Groups 5 and 6 caused by increasing the width of ballast pockets (ballast pockets under the center of the tie)

Groups	Subgroups	Railway embankment height (He) (m)	FS				
			Natural slope height (Hs) (m)				
			1	2	3	4	5
Group 5	Subgroup 7	1	3.89	2.80	2.34	2.03	1.86
	Subgroup 9	1	3.88	2.79	2.33	2.03	1.86
Rate of FS change (%)			**-0.26**	**-0.36**	**-0.43**	**0**	**0**
Group 5	Subgroup 7	2	2.94	2.38	2.11	1.92	1.75
	Subgroup 9	2	2.94	2.37	2.11	1.91	1.75
Rate of FS change (%)			**0**	**-0.42**	**0**	**-0.52**	**0**
Group 5	Subgroup 7	3	2.48	2.14	1.96	1.82	1.70
	Subgroup 9	3	2.48	2.13	1.96	1.81	1.70
Rate of FS change (%)			**0**	**-0.47**	**0**	**-0.55**	**0**
Group 5	Subgroup 11	1	3.88	2.79	2.33	2.03	1.86
Rate of FS change (%)			**-0.26**	**-0.36**	**-0.43**	**0**	**0**
Group 5	Subgroup 11	2	2.94	2.37	2.11	1.91	1.75
Rate of FS change (%)			**0**	**-0.42**	**0**	**-0.52**	**0**
Group 5	Subgroup 11	3	2.48	2.13	1.96	1.81	1.70
Rate of FS change (%)			**0**	**-0.47**	**0**	**-0.55**	**0**
Group 6	Subgroup 25	1	4.26	3.11	2.62	2.31	2.08
	Subgroup 27	1	4.25	3.10	2.61	2.30	2.08
Rate of FS change (%)			**-0.23**	**-0.32**	**-0.38**	**-0.43**	**0**
Group 6	Subgroup 25	2	3.27	2.67	2.40	2.19	2.04
	Subgroup 27	2	3.26	2.66	2.39	2.19	2.04
Rate of FS change (%)			**-0.31**	**-0.37**	**-0.42**	**0**	**0**

Table 4.10. Rate of FS change of models in Groups 5 and 6 caused by increasing the width of ballast pockets (ballast pockets under the center of the tie) – Continued

Groups	Subgroups	Railway embankment height (He) (m)	FS				
			Natural slope height (Hs) (m)				
			1	2	3	4	5
Group6	Subgroup 25	3	2.79	2.42	2.25	2.09	1.98
	Subgroup 27	3	2.79	2.42	2.25	2.09	1.98
Rate of FS change (%)			**0**	**0**	**0**	**0**	**0**
Group 6	Subgroup 29	1	4.24	3.10	2.61	2.30	2.08
Rate of FS change (%)			**-0.47**	**-0.32**	**-0.38**	**-0.43**	**0**
Group 6	Subgroup 29	2	3.25	2.66	2.39	2.19	2.04
Rate of FS change (%)			**-0.61**	**-0.37**	**-0.42**	**0**	**0**
Group 6	Subgroup 29	3	2.79	2.42	2.25	2.09	1.98
Rate of FS change (%)			**0**	**0**	**0**	**0**	**0**

By keeping the parameters of the above models unchanged with the exception of the ballast pockets' position, if the ballast pockets are formed under one side of the tie, Subgroups 43, 45 and 47 in Group 7 and Subgroups 61, 63 and 65 in Group 8 are formed. The same method is used to analyze these subgroups and compute the FS change rate caused by the increase of ballast pockets' width. The comparison results are summarized in Table 4.11.

Table 4.11. Rate of FS change of models in Groups 7 and 8 caused by increasing the width of ballast pockets (ballast pockets under one side of the tie)

Groups	Subgroup	Railway embankment height (He) (m)	Rate of FS change (%)				
			Natural slope height (Hs) (m)				
			1	2	3	4	5
Group 7	SG.45 vs SG.43	1	-0.26	-0.36	0	0	0
		2	-0.68	-0.42	0	0	0
		3	0	0	0	0	0
	SG.47 vs SG.43	1	-0.52	-0.71	0	0	0
		2	-1.02	-0.42	0	0	0
		3	0	0	0	0	0
Group 8	SG.63 vs SG.61	1	-0.71	0	0	0	0
		2	-0.31	0	-0.42	0	0
		3	0	-0.41	0	0	0
	SG.65 vs SG.61	1	-0.95	-0.32	0	0	0
		2	-0.31	-0.37	-0.42	0	0
		3	-0.36	-0.41	0	0	-0.51

From Table 4.11, it can be seen that the absolute values of the rate of FS change due to the increase of ballast pockets' width are small, which is consistent with the comparison results shown in Table 4.10. The increase in the width of ballast pockets does not significantly affect

the slope stability.

(c) Influence of the water level in ballast pockets

Models with ballast pockets under the center of the tie are studied first. FS results and FS change rate of models caused by the rise in the water level of ballast pockets in Subgroups 7 and 8, Subgroups 13 and 14, Subgroups 19 and 20 are summarized in Table 4.12. The slope ratio of models in these subgroups is 2H:1V. Two subgroups are a combination; only the water level in ballast pockets is different between them. Successively, the depth of ballast pockets in these three combinations is 0.5 m, 1.0 m and 1.5 m.

It can be seen from Table 4.12 that the values of the rate of FS change are not greater than zero, which means the increase of the water level in ballast pockets can reduce the FS value of the model. Figure 4.22 visualizes the rate of FS change summarized in Table 4.12 versus natural slope heights in the range of 1 m to 5 m.

Table 4.12. Rate of FS change of models in Group 5 caused by increasing in the water level in ballast pockets (ballast pockets under the center of the tie)

Group	Subgroup	Railway embankment height (He) (m)	FS				
			Natural slope height (Hs) (m)				
			1	2	3	4	5
Group 5	Subgroup 7	1	3.89	2.80	2.34	2.03	1.86
	Subgroup 8	1	3.85	2.78	2.32	2.03	1.85
Rate of FS change (%)			**-1.03**	**-0.71**	**-0.85**	**0**	**-0.54**
Group 5	Subgroup 7	2	2.94	2.38	2.11	1.92	1.75
	Subgroup 8	2	2.91	2.37	2.11	1.91	1.75
Rate of FS change (%)			**-1.02**	**-0.42**	**0**	**-0.52**	**0**
Group 5	Subgroup 7	3	2.48	2.14	1.96	1.82	1.70
	Subgroup 8	3	2.48	2.13	1.96	1.81	1.70
Rate of FS change (%)			**0**	**-0.47**	**0**	**-0.55**	**0**
Group 5	Subgroup 13	1	3.77	2.74	2.30	2.01	1.84
	Subgroup 14	1	3.69	2.70	2.27	1.99	1.83
Rate of FS change (%)			**-2.12**	**-1.46**	**-1.30**	**-1.00**	**-0.54**
Group 5	Subgroup 13	2	2.88	2.35	2.10	1.91	1.75
	Subgroup 14	2	2.83	2.32	2.09	1.90	1.74
Rate of FS change (%)			**-1.74**	**-1.28**	**-0.48**	**-0.52**	**-0.57**
Group 5	Subgroup 13	3	2.47	2.13	1.95	1.81	1.70
	Subgroup 14	3	2.45	2.12	1.95	1.81	1.69
Rate of FS change (%)			**--0.81**	**-0.47**	**0**	**0**	**-0.59**
Group 5	Subgroup 19	1	3.64	2.68	2.27	1.99	1.84
	Subgroup 20	1	3.54	2.62	2.23	1.96	1.82
Rate of FS change (%)			**-2.75**	**-2.24**	**-1.76**	**-1.51**	**-1.09**

Table 4.12. Rate of FS change of models in Group 5 caused by increasing in the water level in ballast pockets (ballast pockets under the center of the tie) – Continued

Groups	Subgroups	Railway embankment height (He) (m)	FS				
			Natural slope height (Hs) (m)				
			1	2	3	4	5
Group 5	Subgroup 19	2	2.83	2.32	2.08	1.90	1.74
	Subgroup 20	2	2.75	2.27	2.05	1.88	1.73
Rate of FS change (%)			**-2.83**	**-2.16**	**-1.44**	**-1.05**	**-0.57**
Group 5	Subgroup 19	3	2.45	2.12	1.95	1.81	1.69
	Subgroup 20	3	2.40	2.09	1.94	1.80	1.69
Rate of FS change (%)			**-2.04**	**-1.42**	**-0.51**	**-0.55**	**0**

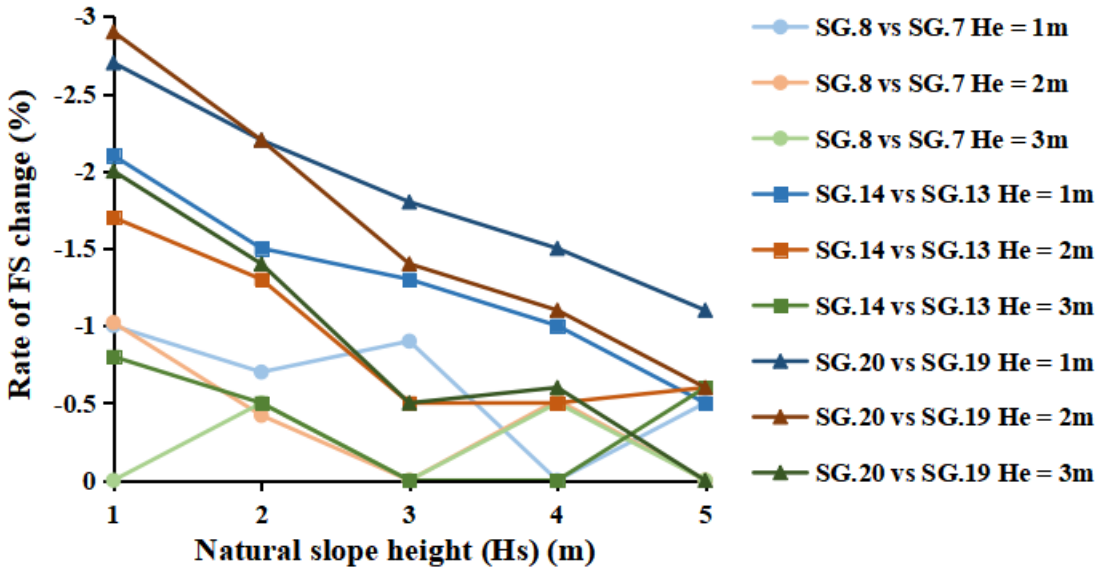

Fig. 4.22. Relationship between the rate of FS change of models in Group 5 caused by increasing in the water level in ballast pockets and the natural slope height (ballast pockets under the center of the tie).

Although curves in Figure 4.22 have variations, they show a downward trend as the natural slope height increases. The curves representing the comparison results of Subgroups 19 and 20 decrease more noticeably with the increase of slope height, indicating that the increase of ballast pockets depth can enhance the influence of the rise in the water level of ballast pockets on the slope stability. In addition, it can be seen that reducing the railway embankment height can also enhance the impact of the rise in the water level of ballast pockets on the FS value.

Applying a slope ratio of 3H:1V on the above comparison models can form Subgroups 25, 26, 31, 32, 37, and 38 in Group 6. In addition, Group 7 and 8 models, in which ballast pockets are under one side of the tie, are also compared. These subgroups are compared in the same way. The values of the rate of FS change of these subgroups versus the natural slope height are plotted in Figures 4.23 (a)-(c).

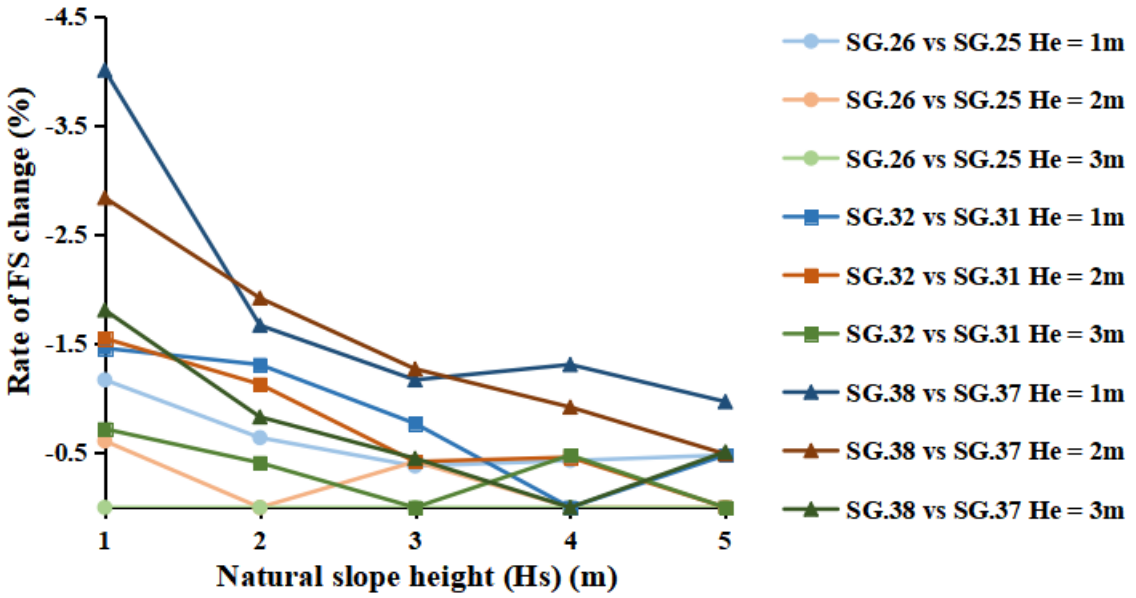

Fig. 4.23. (a) Relationship between the rate of FS change of models in Group 6 caused by increasing in the water level in ballast pockets and the natural slope height (ballast pockets under the center of the tie);

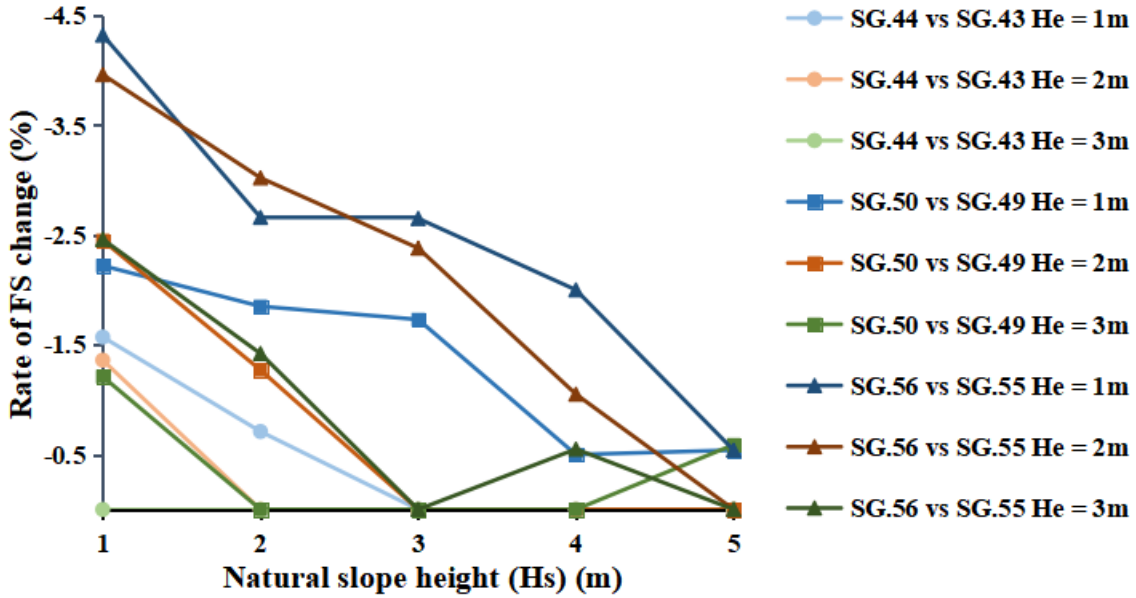

Fig. 4.23. (b) Relationship between the rate of FS change of models in Group 7 caused by increasing in the water level in ballast pockets and the natural slope height (ballast pockets under one side of the tie);

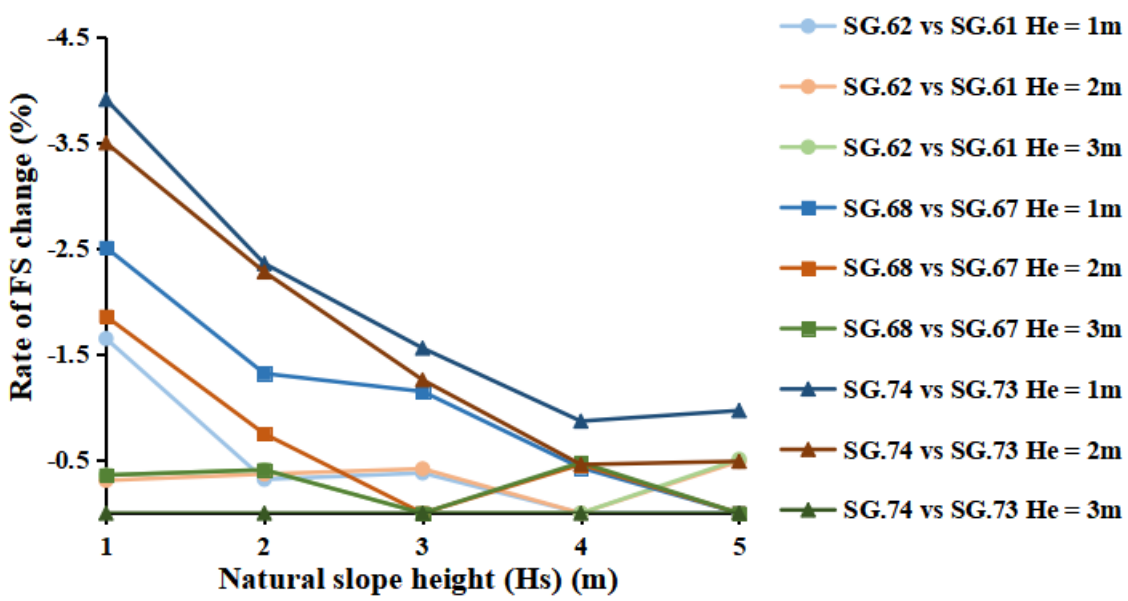

Fig. 4.23. (c) Relationship between the rate of FS change of models in Group 8 caused by increasing in the water level in ballast pockets and the natural slope height (ballast pockets under one side of the tie), (continued).

Like the curves in Figure 4.22, most of the curves in Figure 4.23 show a downward trend as the natural slope height increases. However, the trends of curves representing the comparison results of the railway embankment height of 3m are relatively flat, although they fluctuate with the increase of the natural slope height. It can be seen in Figure 4.23 that as the railway embankment height and natural slope height increase, the influence of the widening of the ballast pockets on the slope stability gradually decreases. With the deepening of ballast pockets, the widening of ballast pockets escalates the influence of slope stability. Overall, the value ranges of the corresponding curves of the curves in Figures 4.22 and 4.23 are similar, which shows that the slope ratio and ballast pockets' position have little effect on the influence of ballast pockets' width on models.

(d) The influence of the position of ballast pockets

Ballast pockets studied in this research thesis have two positions: under the center of a tie and under one side of a tie. Twelve subgroups are selected to verify the influence of different positions of ballast pockets; models with slope ratios of 2H:1V and 3H:1V are both included. Since it was found in the previous analysis that the change of the ballast pockets' width has little effect on the FS value, three subgroups with different depths of ballast pockets in each group are selected to compare the effect of the ballast pockets' position. The ballast pockets' depth of the models in the three subgroups of each group is 0.5 m, 1.0 m or 1.5 m, respectively. The comparison results of the rate of FS change caused by different ballast pockets' positions are summarized and shown in Table 4.13. The rate of FS change is obtained according to Equation 4.4.

$$R_F = \frac{FS_2 - FS_1}{FS_1} \tag{4.4}$$

FS_1 is the FS value of the model where ballast pockets are located under the center of the tie,

and FS_2 is the FS value obtained by keeping the other parameters unchanged and only existing ballast pockets to under one side of the tie.

Table 4.13. Rate of FS change of Set II models caused by the different ballast pockets' positions

Groups	Subgroup	Railway embankment height (He) (m)	FS				
			Natural slope height (Hs) (m)				
			1	2	3	4	5
		1	-1.78	0	0	0	0
	SG.43 vs SG.7	2	0.34	0	0	0	0
		3	0.40	-0.47	0	0	0
Group 7		1	-4.51	-1.46	0.43	0.50	0.54
vs	SG.49 vs SG.13	2	-0.69	0.43	0	0	0
Group 5		3	0.40	0	0	0	0
		1	-4.67	-1.87	-0.44	0.50	0.54
	SG.55 vs SG.19	2	-1.77	0	0.96	0.53	0
		3	-0.41	0	0	0	0
		1	-0.70	0.32	0.38	0	0
	SG.61 vs SG.25	2	0	0	0	0	0
		3	0.36	0.41	0	0	0
Group 8		1	-2.68	-0.33	0.38	0.44	0
vs	SG.67 vs SG.31	2	0	0	0	0	0
Group 6		3	0	0.41	0	0	0
		1	-3.76	-1.00	-0.39	0	0.49
	SG.73 vs SG.37	2	-0.95	-0.77	0.42	0	0
		3	0	0.42	0	0	0

It can be found in Table 4.13 that the models with a 1m railway embankment height and a 1m natural slope height have the most prominent rate of FS change caused by the different positions of ballast pockets. For these models, ballast pockets under one side of the tie are more likely to cause slope instability, and models with deeper ballast pockets are more harmful. The absolute values of the rate of FS change of other models are mostly less than 1%, which shows that the different ballast pocket positions have little effect on the FS value of these models. In addition, some of the FS rate of change values in Table 4.13 are greater than zero, and some are less than zero. There is no clear rule for these values.

To sum up, ballast pockets under the center of the tie are safer for models with a railway embankment height of 1 m and a natural slope height of 1 m. For most models, the different ballast pocket positions have no significant influence on the slope stability of the model.

4.3 Results discussion of Set III

Set III models are obtained by adding a freight train with different speeds to Set II models. Similar to the analysis of Set II models, the influence of slope geometry and ballast pockets

on Set III models are analyzed and shown in Section 4.3.1. The maximum freight train speed that Set II models can withstand is studied in Section 4.3.2.

4.3.1 Influence of slope geometry and ballast pockets for Set III models under a stationary train

Through the analysis of Set I and Set II models, it can be found that, except for the ballast pockets' width and position, the parameters listed below have a significant impact on the slope stability of the models. The influence of these parameters on Set III models is analyzed one by one:

(a) influence of slope ratio;

(b) influence of railway embankment height;

(c) influence of natural slope height;

(d) influence of depth of ballast pockets;

(e) influence of water level in ballast pockets.

(a) The influence of slope ratio

Subgroup 79 in Group 9 (2H:1V) and Subgroup 97 in Group 10 (3H:1V) are used to verify the influence of the slope ratio. The ballast pocket-related parameters of the models in these two subgroups are precisely the same. The comparison of FS results and FS change rate of models in these two subgroups are shown in Table 4.14. Models with a slope of 3H:1V are safer because the values of the FS change rate are positive. For models with a 5 m natural slope height and a 1 m embankment, when the slope ratio increases from 2H:1V to 3H:1V, the increase in FS results reaches a top value of 10.9%. Models with a 1m natural slope and 3m embankment have the minimum FS change rate among all models, which is 8.5%.

Table 4.14. Rate of FS change of models with a stationary train in Subgroups 79 and 97 caused by making the slope flat

Groups	Subgroups	Railway embankment height (He) (m)	FS				
			Natural slope height (Hs) (m)				
			1	2	3	4	5
Group 9	Subgroup 79	1	1.24	1.23	1.22	1.20	1.19
Group 10	Subgroup 97	1	1.36	1.35	1.34	1.32	1.32
Rate of FS change (%)			**9.68**	**9.77**	**9.84**	**10.0**	**10.92**
Group 9	Subgroup 79	2	1.30	1.29	1.28	1.27	1.25
Group 10	Subgroup 97	2	1.42	1.41	1.40	1.40	1.38
Rate of FS change (%)			**9.23**	**9.30**	**9.38**	**10.24**	**10.40**
Group 9	Subgroup 79	3	1.41	1.40	1.39	1.38	1.37
Group 10	Subgroup 97	3	1.53	1.52	1.51	1.50	1.49
Rate of FS change (%)			**8.51**	**8.57**	**8.63**	**8.70**	**8.76**

The values of the rate of FS change versus the natural slope height are plotted in Figure 4.24,

which can display the relationship of rate of FS change versus embankment height and natural slope height more intuitively. A higher natural slope and lower embankment lead to a higher FS change rate.

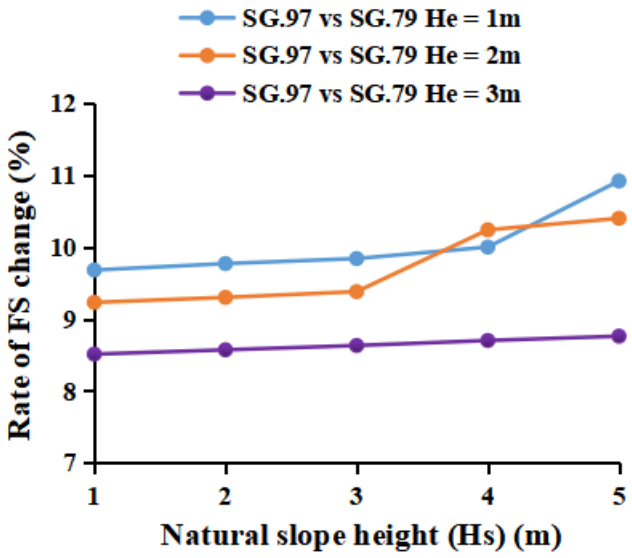

Fig. 4.24. Relationship between the rate of FS change of models in Subgroups 79 and 97 with a stationary train caused by making the slope flat and the natural slope height.

Subgroups 80 and 85 in Group 9 (2H:1V) and Subgroups 98 and 103 in Group 10 (3H:1V) are selected for comparison to verify whether models with different ballast pockets also meet the above rules. Subgroups 85 and 103 and Subgroups 80 and 98 are formed by changing the depth of ballast pockets and water level in the ballast pockets of the above two subgroups models, respectively. Tables 4.15 and 4.16 show the FS and FS change rate values of models in these subgroups, and the comparison results versus natural slope height are plotted in Figure 4.25 (a)-(b).

Table 4.15. Rate of FS change of models with a stationary train in Subgroups 80 and 98 caused by making the slope flat

Groups	Subgroups	Railway embankment height (He) (m)	FS				
			Natural slope height (Hs) (m)				
			1	2	3	4	5
Group 9	Subgroup 80	1	1.23	1.22	1.22	1.19	1.19
Group 10	Subgroup 98	1	1.35	1.34	1.34	1.32	1.32
Rate of FS change (%)			**9.76**	**9.84**	**9.84**	**10.92**	**10.92**
Group 9	Subgroup 80	2	1.29	1.28	1.28	1.27	1.25
Group 10	Subgroup 98	2	1.41	1.4	1.4	1.4	1.38
Rate of FS change (%)			**9.30**	**9.38**	**9.38**	**10.24**	**10.40**
Group 9	Subgroup 80	3	1.4	1.39	1.38	1.38	1.37
Group 10	Subgroup 98	3	1.52	1.51	1.5	1.5	1.49
Rate of FS change (%)			**8.57**	**8.63**	**8.70**	**8.70**	**8.76**

Table 4.16. Rate of FS change of models with a stationary train in Subgroups 85 and 103 caused by making the slope flat

Groups	Subgroups	Railway embankment height (He) (m)	FS				
			Natural slope height (Hs) (m)				
			1	2	3	4	5
Group 9	Subgroup 85	1	1.23	1.22	1.21	1.19	1.18
Group 10	Subgroup 103	1	1.34	1.33	1.32	1.32	1.32
Rate of FS change (%)			**8.94**	**9.02**	**9.09**	**10.92**	**11.86**
Group 9	Subgroup 85	2	1.29	1.28	1.27	1.25	1.24
Group 10	Subgroup 103	2	1.4	1.39	1.39	1.38	1.37
Rate of FS change (%)			**8.53**	**8.59**	**9.45**	**10.40**	**10.48**
Group 9	Subgroup 85	3	1.39	1.38	1.38	1.37	1.36
Group 10	Subgroup 103	3	1.51	1.50	1.49	1.48	1.48
Rate of FS change (%)			**8.63**	**8.70**	**7.97**	**8.03**	**8.82**

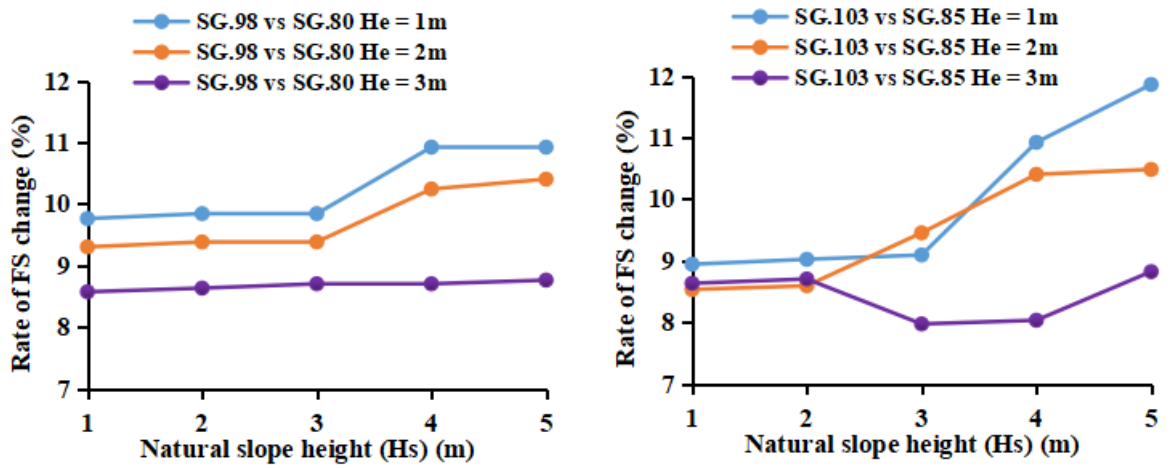

(a) Comparison results of Subgroups 80 and 98

(b) Comparison results of Subgroups 85 and 103

Fig. 4.25. Relationship between the rate of FS change of models in Subgroups 80, 85, 98 and 103 with a stationary train caused by making the slope flat and the natural slope height.

Figure 4.25 shows that all the values of the FS change rate are positive, so models with a 3H:1V slope are much safer. Although the curves in Figure 4.25 (b) have some crossovers, a higher natural slope and lower embankment lead to a higher FS change rate. This conclusion is the same as the previous conclusion obtained by comparing Subgroups 79 and 97, so it can be considered that this conclusion applies to models with different ballast pockets. In addition, a comparison of the values of the rate of FS change in Tables 4.14 and 4.15 due to slope ratio increase is insensitive to the ballast pocket's depth and water level, showing a negligible difference. It can be concluded, when conditions permit, that it is better to choose a slope with 3H:1V.

(b) The influence of railway embankment height

Subgroups 79, 80, 85 in Group 9 and Subgroups 97, 98 103 in Group 10 are selected to analyze the influence of the railway embankment height. These subgroups have been used to study the influence of the slope ratio and are also be used to study the effect of different natural slope heights. Table 4.17 compares models with a 2 m and 3 m embankment with models with a 1 m embankment. All the FS change rate values in Table 4.17 are positive, indicating that increasing the railway embankment height can enhance the slope stability.

Table 4.17. Rate of FS change of models with a stationary train in Groups 9 and 10 caused by increasing the railway embankment height

Groups	Subgroups	Railway embankment height (He) (m)	Rate of FS change (%)				
			Natural slope height (Hs) (m)				
			1	2	3	4	5
Group 9	Subgroup 79	He = 2m vs He = 1m	4.84	4.88	4.92	5.83	5.04
		He = 3m vs He = 1m	13.71	13.82	13.93	15.00	15.13
	Subgroup 80	He = 2m vs He = 1m	4.88	4.92	4.92	6.72	5.04
		He = 3m vs He = 1m	13.82	13.93	13.11	15.97	15.13
	Subgroup 85	He = 2m vs He = 1m	4.88	4.92	4.96	5.04	5.08
		He = 3m vs He = 1m	13.01	13.11	14.05	15.13	15.25
Group 10	Subgroup 97	He = 2m vs He = 1m	4.41	4.44	4.48	6.06	4.55
		He = 3m vs He = 1m	7.75	7.80	7.86	7.14	7.97
	Subgroup 98	He = 2m vs He = 1m	4.44	4.48	4.48	6.06	4.55
		He =3m vs He = 1m	7.80	7.86	7.14	7.14	7.97
	Subgroup 103	He = 2m vs He = 1m	4.48	4.51	5.30	4.55	3.79
		He = 3m vs He = 1m	7.86	7.91	7.19	7.25	8.03

Figures 4.26 (a)-(b) plot the comparison results shown in Table 4.17. The curves representing the comparison results of models with the railway embankment heights of 2 m and 1 m in different subgroups are very close. Curves representing the comparison results of models with the railway embankment heights of 3 m and 1 m also have considerable overlap. These findings indicates that an increase in the ballast pockets' depth and the rise in the water level in them have little effect on the influence of increasing the railway embankment height on the slope stability.

In addition, it can be seen from Figure 4.26 (a) that all curves rise slowly with the increase of natural slope height, indicating that the increase of natural slope height can increase the influence of railway embankment height on the models with a slope ratio of 2H:1V; but the impact is not significant. Although the curve in Figure 4.26 (b) has fluctuations when the natural slope height is 3 m or 4 m, the values on curves do not change much with the increase

of natural slope height. This outcome shows that the natural slope height hardly affects the influence of the railway embankment height increase on the models with a slope ratio of 3H:1V.

Finally, comparing Figures 4.26(a) and (b), increasing the railway embankment height of the models with slope ratios of 2H:1V and 3H:1V from 1 m to 2 m, the values of the FS change rate are similar. However, continuing to raise the railway embankment height to 3 m, the values of the FS change rate produced by models with a slope ratio of 2H:1V are significantly greater than that of models with a slope ratio of 3H:1V, which means that the railway embankment height increases from 1 m to 3 m have a more significant influence on models with the slope ratio of 2H:1V.

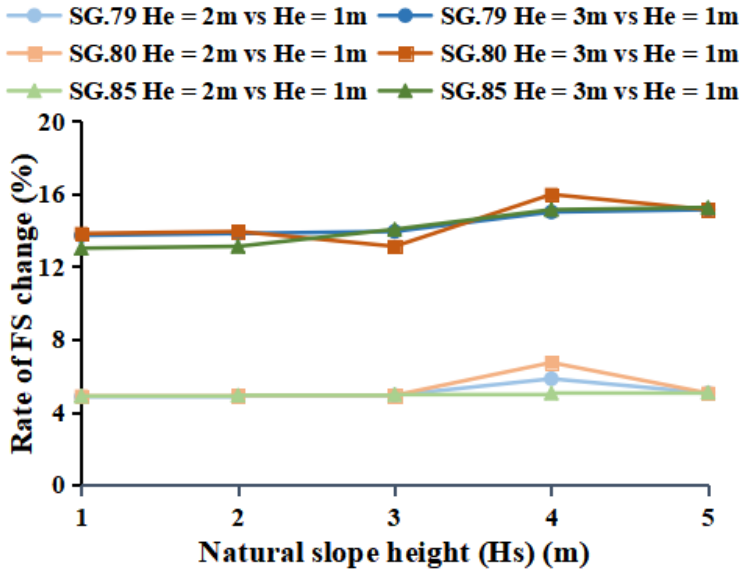

(a) Comparison results of Group 9

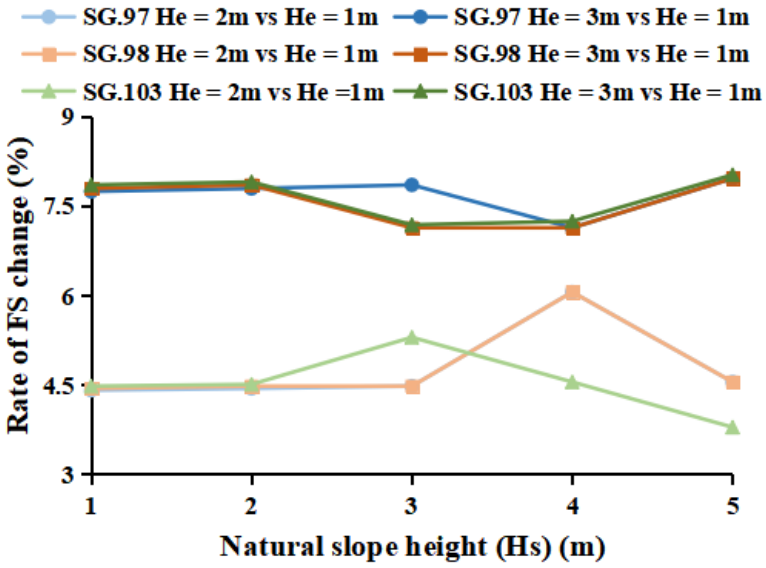

(b) Comparison results of Group 10

Fig. 4.26. Relationship between the rate of FS change of models with a stationary train in Groups 9 and 10 caused by increasing the embankment height and the natural slope height.

(c) Influence of natural slope height

In this part, Subgroups 79, 80, 85 in Group 9 and Subgroups 97, 98 103 in Group 10 are used to study the effect of natural slope height on the FS results. Table 4.18 summarizes the FS change rate due to the variations of the natural slope height. Models with a 1 m natural slope height in each subgroup are used as the reference. Figures 4.27 (a)-(d) plotted the rate of FS change caused by the natural slope height increase versus the natural slope height.

Table 4.18. Rate of FS change of models with a stationary train in Groups 9 and 10 caused by increasing the natural slope height

Groups	Subgroups	Railway embankment height (He) (m)	Rate of FS change (%)				
			Natural slope height (Hs) (m)				
			1	2	3	4	5
Group 9	Subgroup 79	1	0	-0.81	-1.61	-3.23	-4.03
		2	0	-0.77	-1.54	-2.31	-3.85
		3	0	-0.71	-1.42	-2.13	-2.84
	Subgroup 80	1	0	-0.81	-0.81	-3.25	-3.25
		2	0	-0.78	-0.78	-1.55	-3.10
		3	0	-0.71	-1.43	-1.43	-2.14
	Subgroup 85	1	0	-0.81	-1.62	-3.25	-4.07
		2	0	-0.78	-1.55	-3.10	-3.88
		3	0	-0.72	-0.72	-1.44	-2.16
Group 10	Subgroup 97	1	0	-0.74	-1.47	-2.94	-2.94
		2	0	-0.70	-1.41	-1.41	-2.81
		3	0	-0.65	-1.31	-1.96	-2.61
	Subgroup 98	1	0	-0.74	-0.74	-2.22	-2.22
		2	0	-0.71	-0.71	-0.71	-2.13
		3	0	-0.66	-1.32	-1.32	-1.97
	Subgroup 103	1	0	-0.75	-1.49	-1.49	-1.49
		2	0	-0.71	-0.71	-1.43	-2.14
		3	0	-0.66	-1.32	-1.99	-1.99

The values of the rate of FS change corresponding to all curves in Figure 4.27 are negative, and curves rise or remain unchanged with the increase of natural slope height, indicating that the increase of natural slope height can decrease the FS value of models or keep it unchanged.

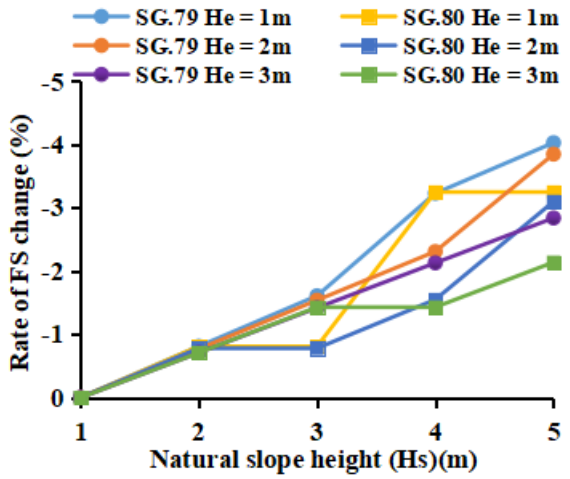

(a) Rate of FS change of Subgroups 79 and 80

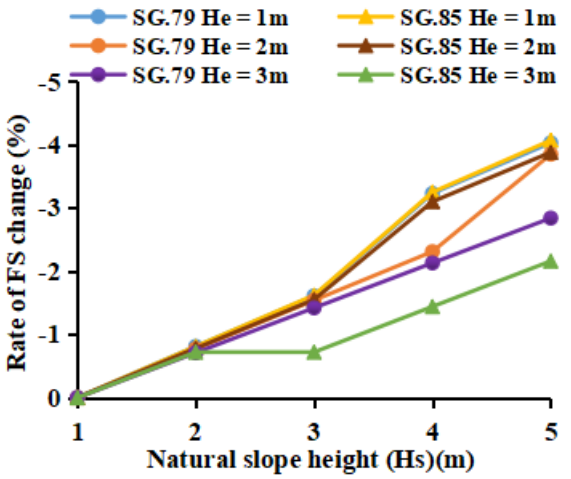

(b) Rate of FS change of Subgroups 79 and 85

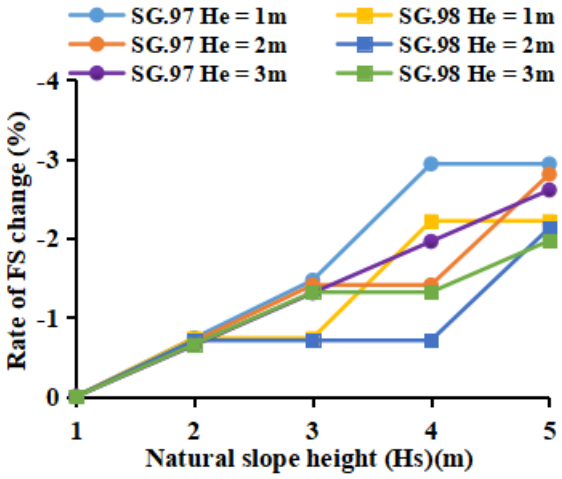

(c) Rate of FS change of Subgroups 97 and 98

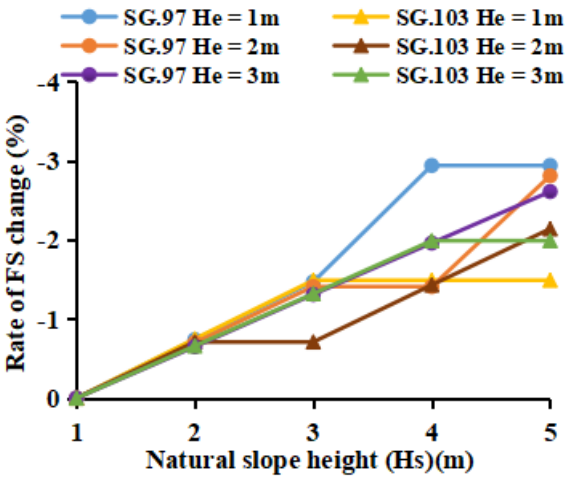

(d) Rate of FS change of Subgroups 97 and 103

Fig. 4.27. Relationship between the rate of FS change of models with a stationary train in Groups 9 and 10 caused by increasing the natural slope height and the natural slope height

An analysis of Figures 4.27 (a) and (b) show that the absolute value of the rate of FS change decreases with the increase of railway embankment height. This finding indicates that increase of the railway embankment height can reduce the impact of the natural slope height increase on slope stability. The influence of the increase of the railway embankment height on the absolute values of the rate of FS change in Figures 4.27 (c) and (d) is difficult to generalize because there are too many fluctuations.

It can be concluded by analyzing Figures 4.27 (a) and (c) that as the water level in ballast pockets increases, the absolute value of the FS change rate decreases, indicating that the increase in the water level in ballast pockets can reduce the impact of the natural slope height increase on slope stability.

It can be found from Figures 4.27 (b) and (d) that for most models, as the depth of ballast pockets increases, the change in the FS value due to the increase in the natural slope height decreases. However, in Subgroups 79 and 85, models with a 1 m railway embankment height

have similar FS change rate values.

(d) The influence of depth of ballast pockets

Subgroups 79, 85, 91 and 80, 86, 92 are involved in the study of the influence of ballast pockets' depth on slope stability. The depth of ballast pockets of models in each of three subgroups are 0.5 m, 1.0 m and 1.5 m, and the other parameters are the same. The models in the last three subgroups are obtained by increasing the water level in ballast pockets in the first three subgroups, and other parameters remain unchanged. The slope ratio of the models in these subgroups is 2H:1V. Table 4.19 lists FS change rate caused by the ballast pockets' depth variations. These results are obtained by comparing models with ballast pockets' depths of 1.0 m and 1.5 m, with models with ballast pockets' depths of 0.5m.

Table 4.19. Rate of FS change of models with a stationary train in Group 9 caused by deepening of ballast pockets

Groups	Subgroups	Railway embankment height (He) (m)	FS				
			Natural slope height (Hs) (m)				
			1	2	3	4	5
Group 9	Subgroup 79	1	1.24	1.23	1.22	1.20	1.19
	Subgroup 85	1	1.23	1.22	1.21	1.19	1.18
Rate of FS change (%)			**-0.81**	**-0.81**	**-0.82**	**-0.83**	**-0.84**
Group 9	Subgroup 79	2	1.30	1.29	1.28	1.27	1.25
	Subgroup 85	2	1.29	1.28	1.27	1.25	1.24
Rate of FS change (%)			**-0.77**	**-0.78**	**-0.78**	**-1.57**	**-0.80**
Group 9	Subgroup 79	3	1.41	1.40	1.39	1.38	1.37
	Subgroup 85	3	1.39	1.38	1.38	1.37	1.36
Rate of FS change (%)			**-1.42**	**-1.43**	**-0.72**	**-0.72**	**-0.73**
Group 9	Subgroup 91	1	1.22	1.21	1.21	1.18	1.17
Rate of FS change (%)			**-1.61**	**-1.63**	**-0.82**	**-1.67**	**-1.68**
Group 9	Subgroup 91	2	1.28	1.26	1.26	1.25	1.24
Rate of FS change (%)			**-1.54**	**-2.32**	**-1.65**	**-1.57**	**-0.80**
Group 9	Subgroup 91	3	1.38	1.37	1.37	1.36	1.36
Rate of FS change (%)			**-2.13**	**-2.14**	**-1.44**	**-1.45**	**-0.73**
Group 9	Subgroup 80	1	1.23	1.22	1.22	1.19	1.19
	Subgroup 86	1	1.22	1.21	1.21	1.19	1.18
Rate of FS change (%)			**-0.81**	**-0.82**	**-0.82**	**0**	**-0.84**
Group 9	Subgroup 80	2	1.29	1.28	1.28	1.27	1.25
	Subgroup 86	2	1.27	1.26	1.26	1.25	1.24
Rate of FS change (%)			**-1.55**	**-1.56**	**-1.56**	**-1.57**	**-0.80**
Group 9	Subgroup 80	3	1.40	1.39	1.38	1.38	1.37
	Subgroup 86	3	1.37	1.37	1.36	1.36	1.36
Rate of FS change (%)			**-2.14**	**-1.44**	**-1.45**	**-1.45**	**-0.73**

Table 4.19. Rate of FS change of models with a stationary train in Group 9 caused by deepening of ballast pockets – Continued

Groups	Subgroups	Railway embankment height (He) (m)	FS				
			Natural slope height (Hs) (m)				
			1	2	3	4	5
Group 9	Subgroup 92	1	1.21	1.20	1.20	1.18	1.17
Rate of FS change (%)			**-1.63**	**-1.64**	**-1.64**	**-0.84**	**-1.68**
Group 9	Subgroup 92	2	1.26	1.26	1.26	1.25	1.23
Rate of FS change (%)			**-2.33**	**-1.56**	**-1.56**	**-1.57**	**-1.60**
Group 9	Subgroup 92	3	1.37	1.36	1.36	1.36	1.36
Rate of FS change (%)			**-2.14**	**-2.16**	**-1.45**	**-1.45**	**-0.73**

The FS change rates summarized in Table 4.19 are not greater than zero, indicating that the deepening of ballast pockets can reduce slope stability. Figure 4.28 visualizes the rate of FS change of the subgroups analyzed above versus the natural slope height.

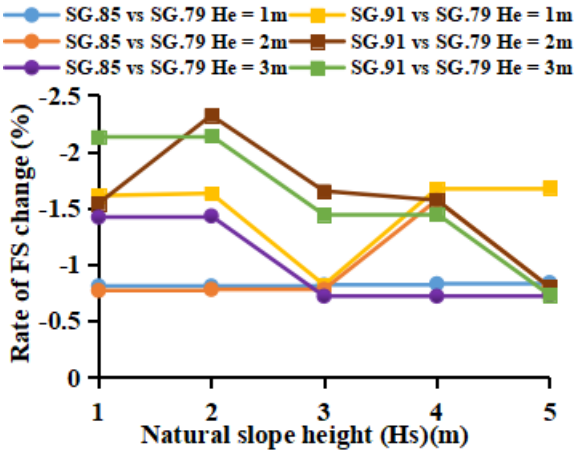

(a) Comparison results of Subgroups 79, 85 and 91

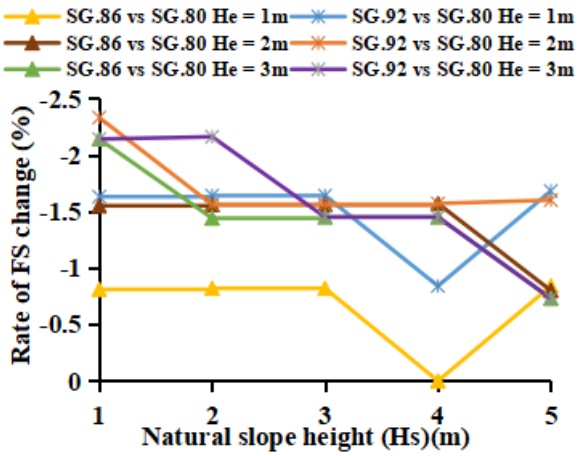

(b) Comparison results of Subgroups 80, 86 and 92

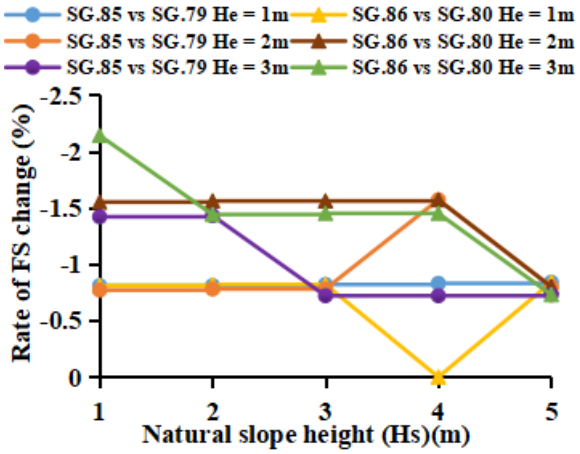

(c) Comparison results of Subgroups 79, 85 and 80, 86

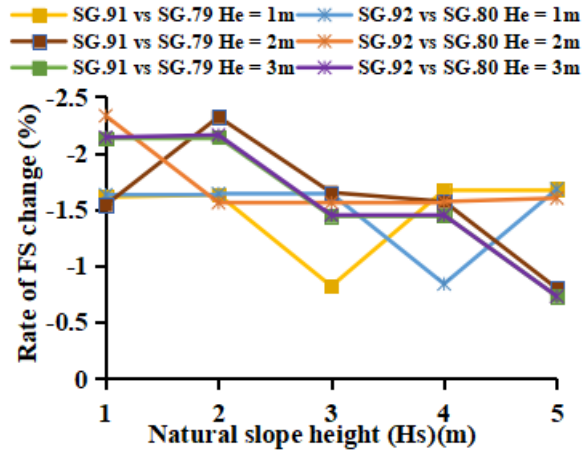

(d) Comparison results of Subgroups 79, 91 and 80, 92

Fig. 4.28. Relationship between the rate of FS change of models with a stationary train in Group 9 caused by deepening of ballast pockets versus the natural slope height.

The curves shown in Figure 4.28 have many fluctuations, but as a whole, with the increase of the natural slope height, the absolute value of the rate of FS change has two trends. One trend is very flat and almost remains level, while the other is apparent decline. These trends show that with the increase of the natural slope height, the increase of the depth of ballast pockets has a decreasing negative or almost no impact on slope stability. However, it is difficult to distinguish the effect of the increase of railway embankment height applicable to all the above subgroups on the rate of FS change.

In addition, with the increase of the water level in ballast pockets, the deepening of the ballast pockets has an increased influence on slope stability. This law is evident in Figure 4.28 (c), but the rule is not apparent in Figure 4.28 (d) since there are too many intersection points.

The slope ratio of all the models analyzed above was changed to 3H:1V for Subgroups 97, 103, 109 and Subgroups 98, 104, 110 in Group 10. The rate of FS change due to the increase in the ballast pockets' depth of these subgroups versus the natural slope height is plotted in Figure 4.29.

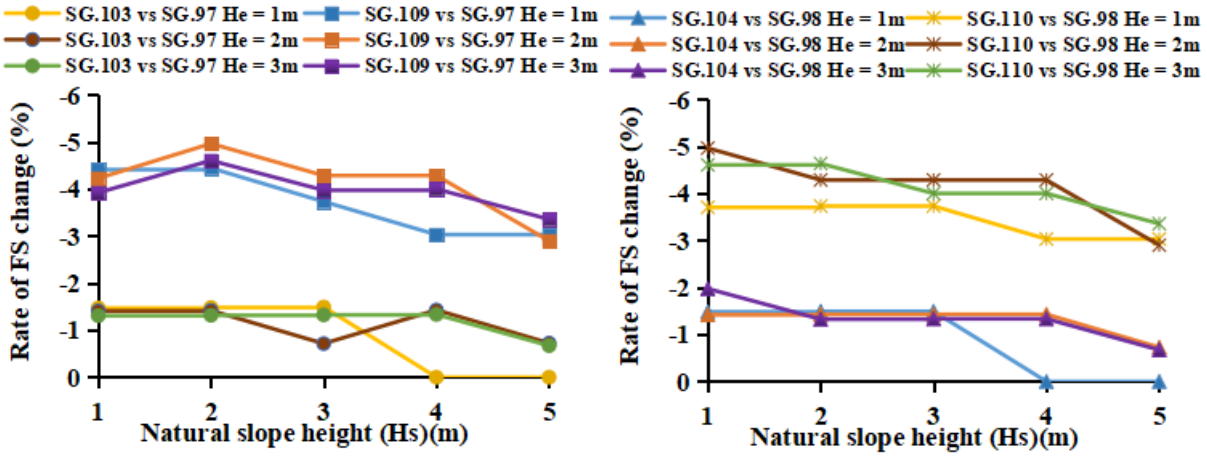

(a) Comparison results of Subgroups 97, 103 and 109

(b) Comparison results of Subgroups 98, 104 and 110

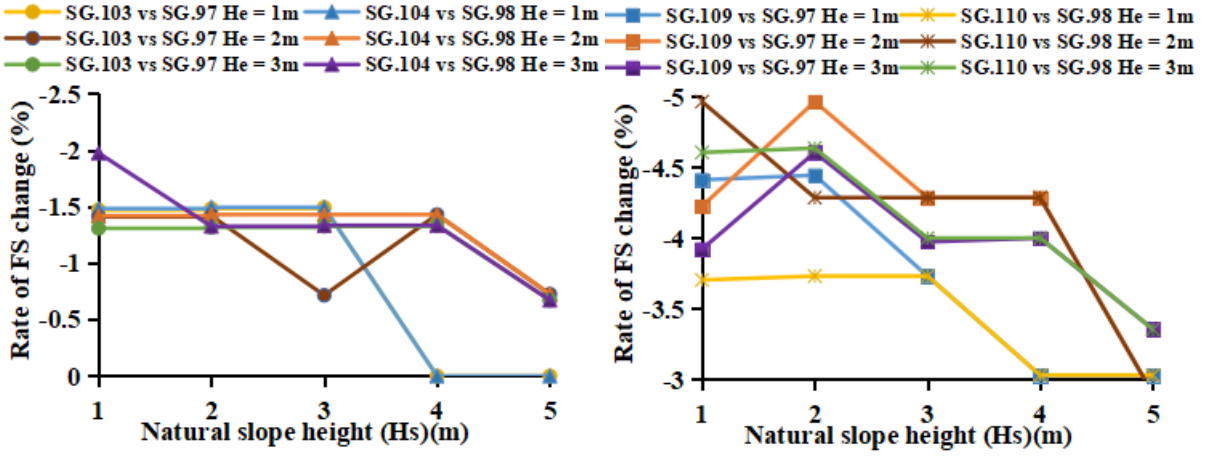

(c) Comparison results of Subgroups 97, 103 and 98, 104

(d) Comparison results of Subgroups 97, 109 and 98, 110

Fig. 4.29. Relationship between the rate of FS change of models with a stationary train in Group 10 caused by deepening of ballast pockets versus the natural slope height.

The downward trend of the curves in Figure 4.29 with the increase of the natural slope height is relatively apparent, although there are many fluctuations, which means that with the increase of natural slope height, the negative impact of deepening ballast pockets on slope stability increases. Although the impact of the enhancement of railway embankment height on the rate of FS change is challenging to generalize, the absolute value of the rate of FS change corresponding to models with a 1 m railway embankment height is often the smallest, which means that the impact of these models affected by ballast pockets deepening is small.

An analysis of Figures 4.29 (c) and (d) shows that a rise in the water level in ballast pockets has little effect on the rate of FS change value. A rise in the water level in ballast pockets has a negligible effect on the negative impact of deepening the ballast pockets on slope stability.

Comparing Figures 4.28 and 4.29, it can be seen that deepening ballast pockets from 0.5 m to 1.5 m has a more significant impact on models with a slope ratio of 3H:1V, and increasing it from 0.5 m to 1.0 m has a similar impact on models with different slope ratios.

The increase of ballast pocket depth can destroy slope stability, and it has a more substantial effect on models with a slope ratio of 3H:1V. The impact of deepening ballast pockets on slope stability decreases as the natural slope height increases. An increase in the water level of the ballast pockets has little effect on the impact of the increase in the ballast pockets' depth on the slope stability.

(e) The influence of water level in ballast pockets

Twelve subgroups used to analyze the influence of ballast pockets' depth were selected to analyze the impact of the water level of ballast pockets on FS value. They were compared in pairs. The parameters of the two subgroups compared were the same except for the water level of ballast pockets. The influence of the water level of ballast pockets on the models as the ballast pockets' depth increases could also be observed. Table 4.20 lists the comparison results of models' FS change rate caused by the water level rise in ballast pockets variations.

Values of FS change rate in Table 4.20 are not greater than zero, which means that the rise of the water level of ballast pockets can decrease the slope stability. However, the absolute value of the FS change rate shown in Table 4.20 is mostly less than 1%, indicating that the increase of the water level of ballast pockets has little effect on the FS value. In particular, the rate of FS change of models with a natural slope height of 4 m or 5 m is zero, indicating that change in water level of ballast pockets does not affect models with a natural slope height of 4 m or 5 m. For models whose natural slope height does not exceed 3 m, the absolute value of the rate of FS change produced by the increase of the water level of ballast pockets is almost unchanged with the natural slope height increasing. Since there is much sudden increase in the FS change rate and many values equal to zero, the influence of the railway embankment height increase on the rate of FS change cannot be assessed.

The comparison between the first three sets shows that the rate of FS change of some models increases slightly with the deepening of ballast pockets, but the change is almost negligible. The comparison results of the last three sets also showed this correlation.

Comparing the rate of FS change of the first three sets with that of the last three sets shows

that the difference in the slope ratio of models does not affect the rate of FS change due to the rise in water level in ballast pockets.

Table 4.20. Rate of FS change of models with a stationary train in Groups 9 and 10 caused by the water level rise in ballast pockets

Groups	Subgroups	Railway embankment height (He) (m)	Rate of FS change (%)				
			Natural slope height (Hs) (m)				
			1	2	3	4	5
Group 9	SG.80 vs SG.79	1	-0.81	-0.81	0	-0.83	0
		2	-0.77	-0.78	0	0	0
		3	-0.71	-0.71	-0.72	0	0
	SG.86 vs SG.85	1	-0.81	-0.82	0	0	0
		2	-1.55	-1.56	-0.79	0	0
		3	-1.44	-0.72	-1.45	-0.73	0
	SG.92 vs SG.91	1	-0.82	-0.83	-0.83	0	0
		2	-1.56	0	0	0	-0.81
		3	-0.72	-0.73	-0.73	0	0
	SG.98 vs SG.97	1	-0.74	-0.74	0	0	0
		2	-0.70	-0.71	0	0	0
		3	-0.65	-0.66	-0.66	0	0
Group 10	SG.104 vs SG.103	1	-0.75	-0.75	0	0	0
		2	-0.71	-0.72	-0.72	0	0
		3	-1.32	-0.67	-0.67	0	0
	SG.110 vs SG.109	1	0	0	0	0	0
		2	-1.47	0	0	0	0
		3	-1.36	-0.69	-0.69	0	0

An increase in the water level of ballast pockets can reduce slope stability, but the impact is small.

4.3.2 Influence of train speed for Set III models under a freight train with different speeds

According to the analysis of Set III models under a stationary train in Section 4.3.1, it can be seen that ballast pockets' depth is the only parameter related to ballast pockets that has a significant impact on slope stability in this study. In this section, 2 m railway embankment height models with ballast pockets under the center of the tie are selected to analyze the impact of train loads on slope stability. The width of ballast pockets is 1.0 m, and water in ballast pockets submerged half of the ballast pocket depth (m = 0.5). The moving train speed ranges from 0 km/h (0 mph) to 120 km/h (75 mph) in steps of 8 km/h (5 mph). The FS results are summarized and plotted in Figures 4.30 and 4.31. Table 4.21 shows the results of models

with a 0.5 m depth of ballast pockets. As the train moves faster, FS decreases in all subgroups. In addition, it is noticeable from the results of Table 4.21 that models with a slope ratio of 3H:1V have a greater FS value under the freight train with the same speed compared with models with a slope ratio of 2H:1V.

Table 4.21. Corresponding FS results of models in Subgroups 79 and 97 under various train speeds with the ballast pockets' depth of 0.5 m

Groups	Subgroups	Train speed		FS				
				Natural slope height (Hs) (m)				
		mph	km/h	1	2	3	4	5
Group 9	Subgroup 79	0	0	1.30	1.29	1.28	1.27	1.25
		5	8	1.28	1.27	1.26	1.25	1.23
		10	16	1.26	1.25	1.24	1.23	1.21
		15	24	1.24	1.23	1.23	1.22	1.20
		20	32	1.23	1.22	1.22	1.21	1.19
		25	40	1.22	1.21	1.21	1.20	1.18
		30	48	1.21	1.20	1.20	1.18	1.17
		35	56	1.20	1.19	1.19	1.17	1.16
		40	64	1.19	1.18	1.18	1.16	1.15
		45	72	1.18	1.17	1.17	1.16	1.14
		50	80	1.17	1.16	1.16	1.15	1.13
		55	88	1.16	1.15	1.15	1.14	1.11
		60	96	1.15	1.14	1.14	1.13	1.11
		65	104	1.14	1.13	1.13	1.12	1.10
		70	112	1.13	1.12	1.11	1.11	1.09
		75	120	1.12	1.11	1.10	1.10	1.09
Group 10	Subgroup 97	0	0	1.42	1.41	1.40	1.40	1.38
		5	8	1.40	1.39	1.38	1.38	1.36
		10	16	1.38	1.37	1.36	1.36	1.34
		15	24	1.36	1.35	1.34	1.34	1.32
		20	32	1.34	1.33	1.32	1.32	1.30
		25	40	1.32	1.31	1.30	1.30	1.28
		30	48	1.30	1.29	1.28	1.28	1.26
		35	56	1.28	1.27	1.26	1.26	1.24
		40	64	1.26	1.25	1.24	1.24	1.23
		45	72	1.24	1.23	1.22	1.22	1.22
		50	80	1.22	1.22	1.21	1.20	1.20
		55	88	1.21	1.21	1.20	1.19	1.19
		60	96	1.20	1.19	1.19	1.18	1.17
		65	104	1.19	1.18	1.18	1.17	1.16
		70	112	1.18	1.17	1.17	1.16	1.15
		75	120	1.17	1.16	1.15	1.15	1.14

Figures 4.30 and 4.31 show the FS results of Groups 9 and 10, respectively, and identify the relationship between the FS values and the natural slope and train speed. Each graph has the same color bar, ranging from 1.05 to 1.42. A more significant FS result was obtained at a smaller natural slope height and a lower train speed for each graph.

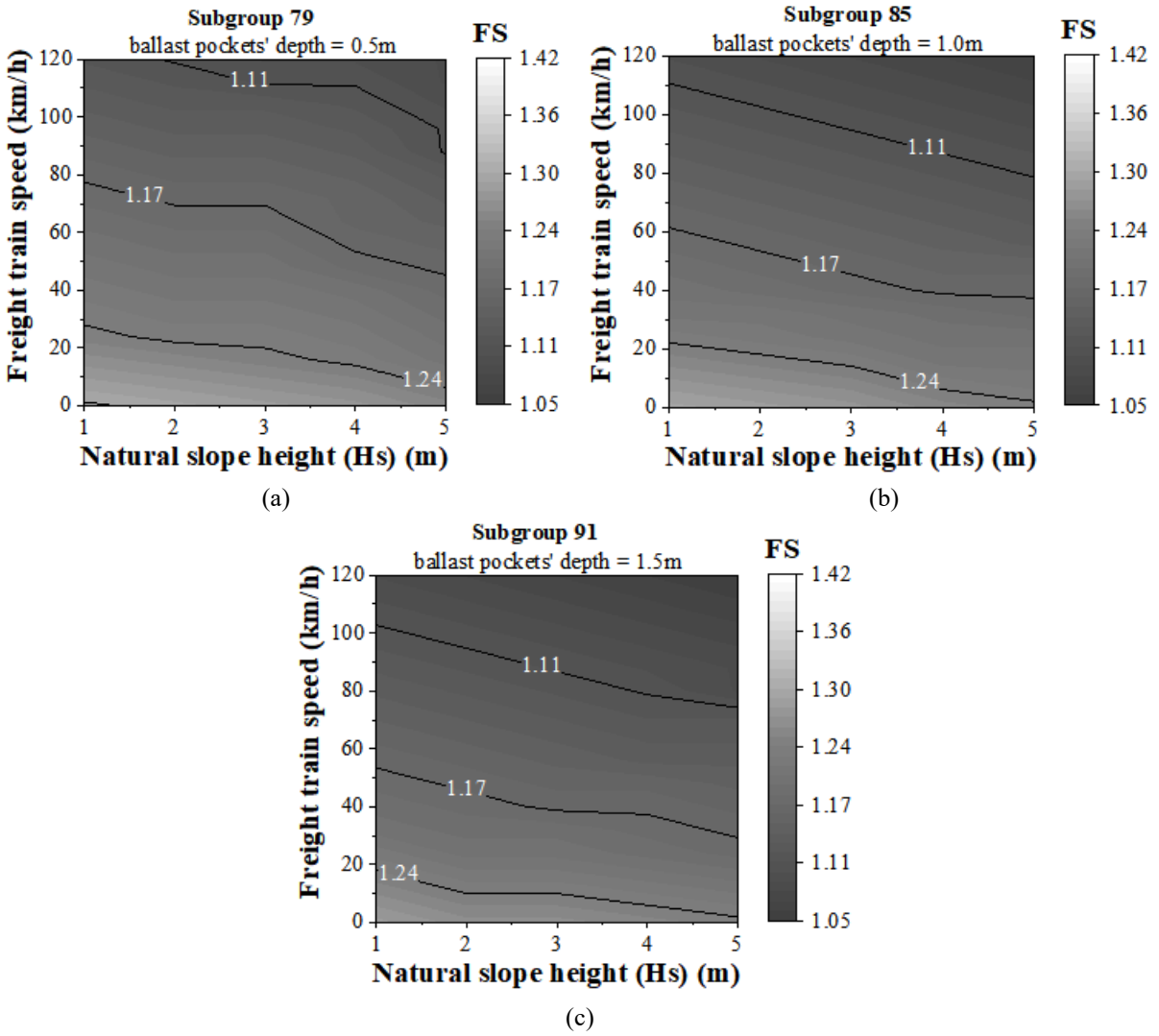

Fig. 4.30. Pseudocolor graphs of FS results for each subgroup of Group 9 (2H:1V).

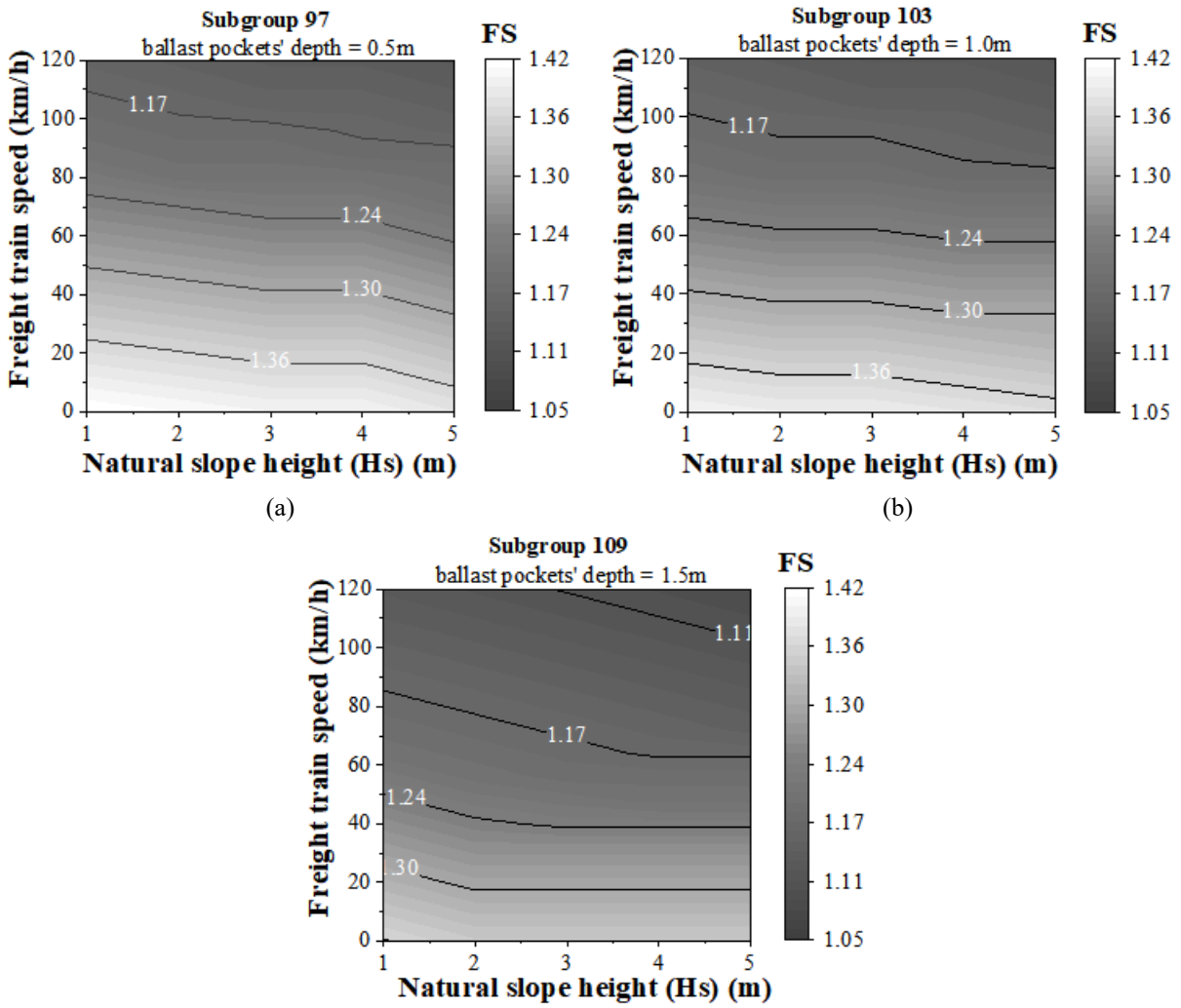

Fig. 4.31. Pseudocolor graphs of FS results for each subgroup of Group 10 (3H:1V).

4.4 General tendency existing ballast pockets and the stationary train load

This section comprehensively compares the FS values of Set I, II, and III models. Models in Set I are dry models without ballast pockets and train loads; adding groundwater flow and ballast pockets on them can obtain models in Set II, and further applying train loads on Set II models can obtain Set III models. The ballast pockets of the Set II and Set III models used for comparison are located under the center of the tie, their depth and width are both 1.0 m, and the ballast pockets are entirely submerged in water. A stationary train with a static load (ABP = 210.42 kN/m^2) is considered in Set III.

Figures 4.32 and 4.33 show the comparison results for three set models. Since Set II models are obtained by adding the groundwater flow and ballast pockets to Set I models, models obtained by only adding the groundwater flow to Set I models are also considered. The left y-axis of Figures 4.32 and 4.33 shows the FS value of models under different conditions, and the right y-axis reflects the rate of FS change between these models under different statuses. Set I models are defined as Scenario 1 in Figures 4.32 and 4.33 and Set I models adding the groundwater flow are defined as Scenario 2. Set II and Set III models are defined as Scenario

3 and Scenario 4, respectively. The scenario is abbreviated as S. in Figure 4.32; Scenario 1 is abbreviated as S.1.

Figures 4.32 and 4.33 show that adding the ballast pockets described above to models (Scenario 2) can decrease the FS value, but the decrease does not exceed 10%, and for models with a 3 m railway embankment height, the rate of FS change is close to 1%. If a stationary train load is applied to models that already have ballast pockets (Scenario 3), the FS value decreases significantly, reducing by at least 20%, indicating that the application of train load significantly decreases the slope stability. Figures 4.32 and 4.33 show that the rate of FS change caused by ballast pockets and the train load decreases with the increase of railway embankment height.

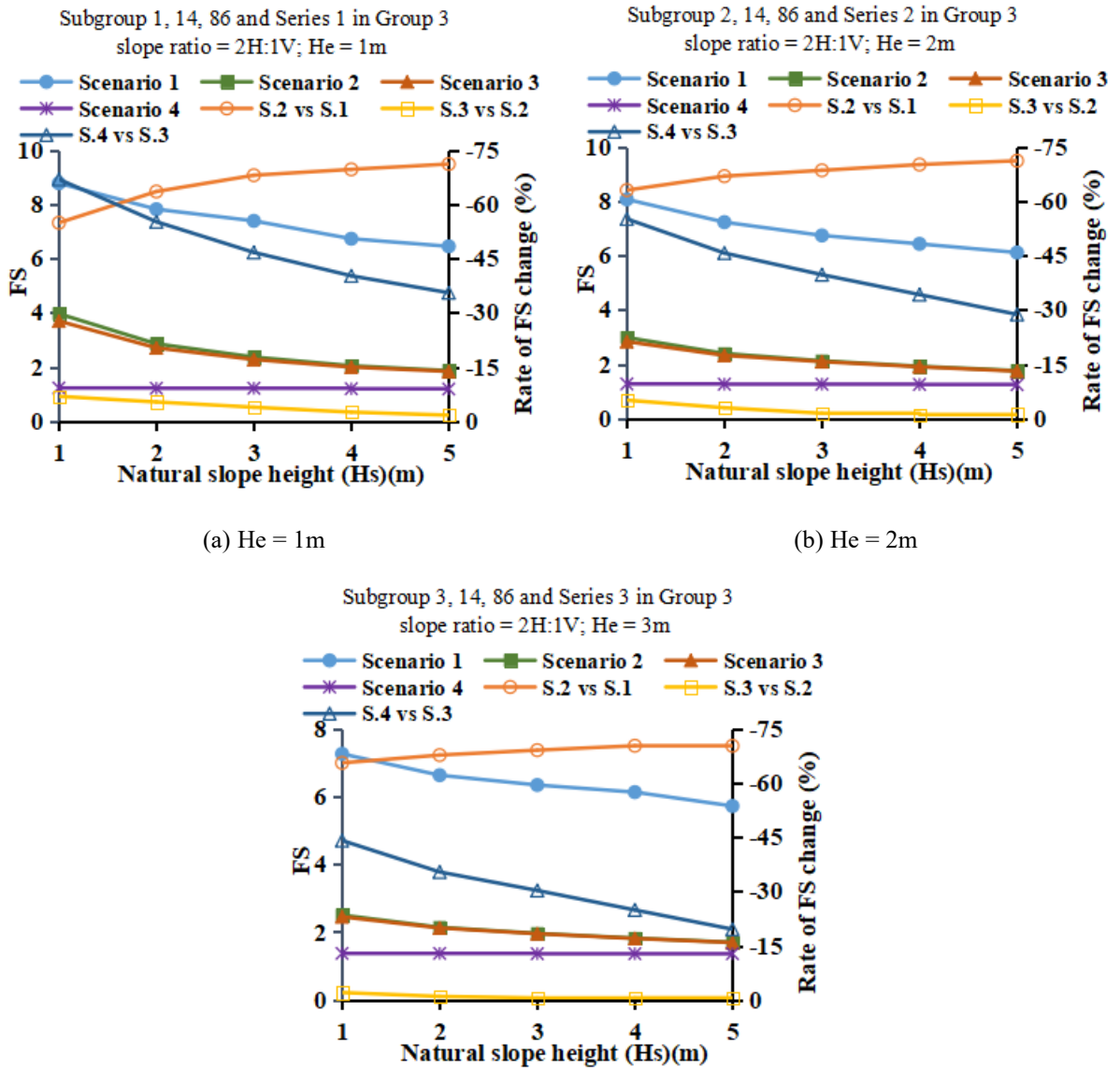

(a) He = 1m

(b) He = 2m

(c) He = 3m

Fig. 4.32. Relationships between the FS or rate of FS change under different scenarios and the natural slope height for models with a slope ratio of 2H:1V.

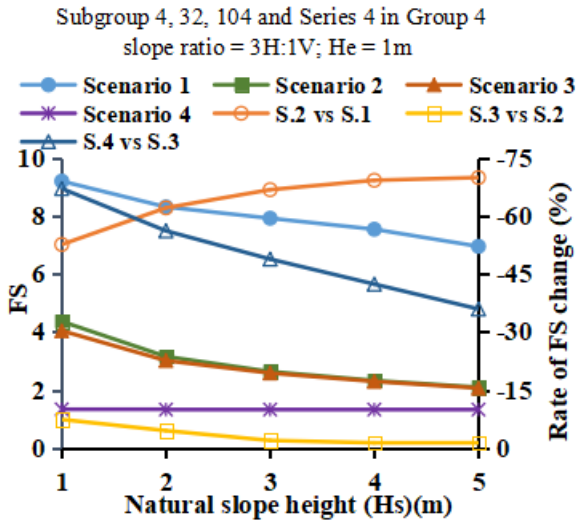

(a) He = 1m

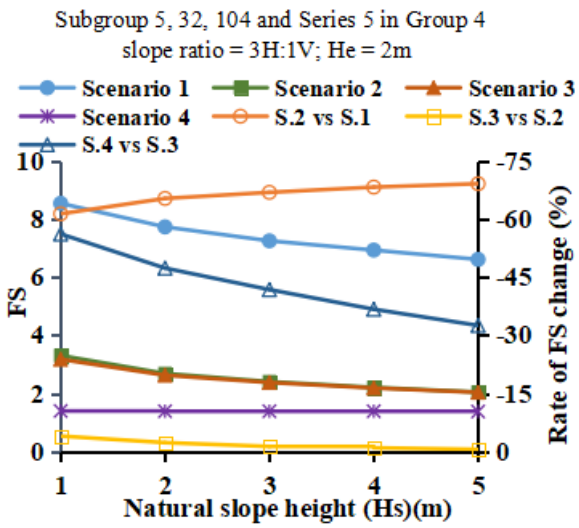

(b) He = 2m

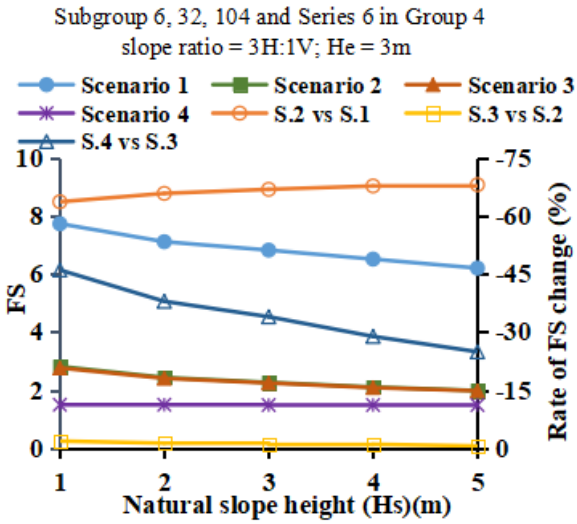

(b) He = 3m

Fig. 4.33. Relationships between the FS or rate of FS change under different scenarios and the natural slope height for models with a slope ratio of 3H:1V.

4.5 Recommendation of maximum safe train speed based on the study

Through the analysis of Set II and Set III models, it can be deduced that the depth of ballast pockets is the only parameter related to ballast pockets in this study that has a remarkable impact on slope stability. Figures 4.34 and 4.35 show the maximum safe train speeds for models with different depths of ballast pockets. In addition, some models cannot withstand the load of the freight train stopped on the track (stationary train). These models do not have a maximum safe train speed. To better represent these models in figures, the maximum safe train speed is set to a negative number and shown in black in Figures 4.34 and 4.35. Models with the same slope ratio use the same color bar.

Figures 4.34 (a) and (b) show that if ballast pockets exist under models with the 1 m or 2 m railway embankment height and the slope ratio of 2H:1V, these models cannot support the freight train to stay or pass the track. When the railway embankment height of models rises to 3 m (Figure 4.34 (c)), no matter how deep the ballast pockets are, the track can safely carry the freight train. Models with a railway embankment height of 3 m can carry a freight train with a maximum speed of 40 km/h (25 mph) when there are 0.5 m deep ballast pockets.

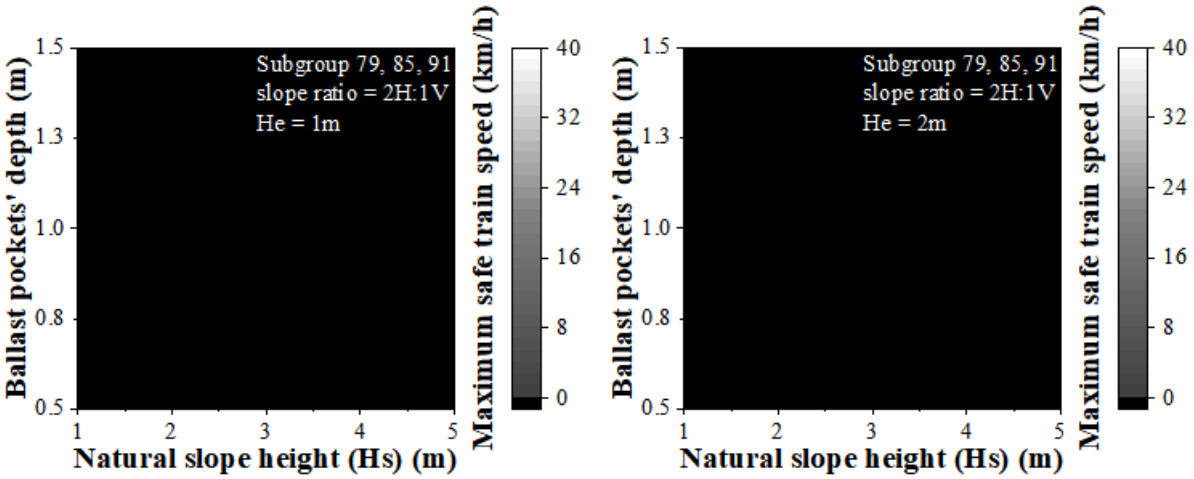

(a) He = 1m

(b) He = 2m

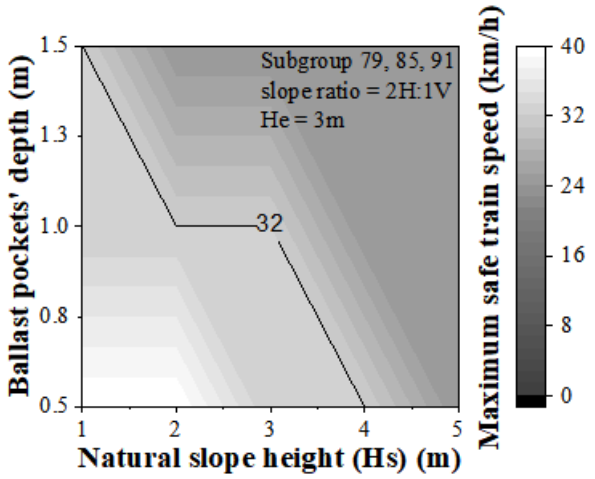

(c) He = 3m

Fig. 4.34. Pseudocolor graphs of maximum safe train speed for cases in Subgroups 79, 85 and 91.

It can be seen from Figure 4.35 that when the ballast pockets are deepened to 1.5 m, models with a 1m railway embankment height are almost unable to accept the freight train. When the railway embankment height rises to 2 m, even if the ballast pockets are deepened, the freight train can pass safely at a speed of 16 km/h (10 mph). The railway embankment height of models continues to rise to 3 m. The maximum safe speed is at least 56 km/h (35 mph), which appears on models with 1.5 m deep ballast pockets and a more than 2 m natural slope height.

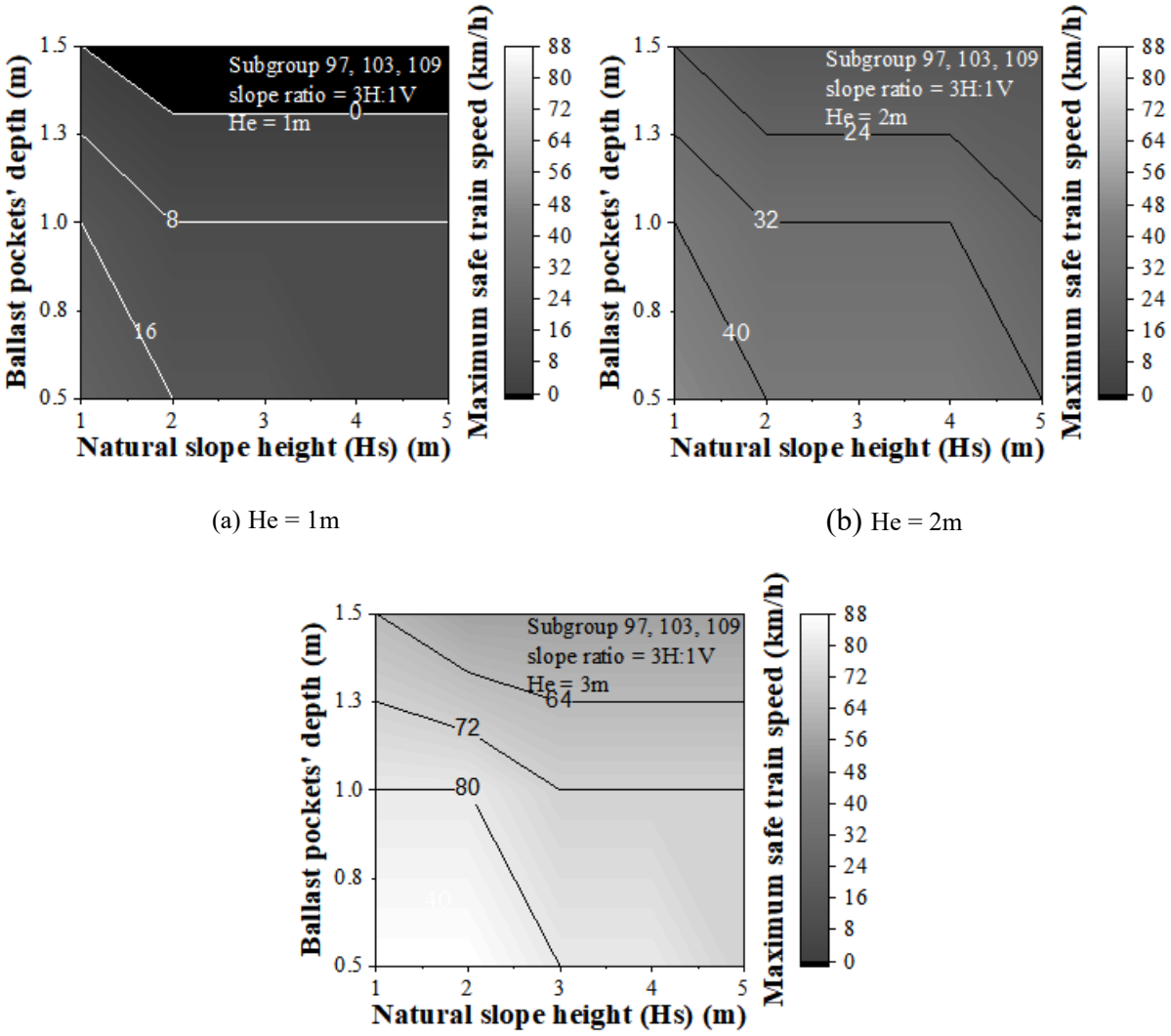

(a) He = 1m

(b) He = 2m

(c) He = 3m

Fig. 4.35. Pseudocolor graphs of maximum safe train speed for cases in Subgroups 97, 103 and 109.

It can be concluded from Figures 4.34 and 4.35 that models with a 3 m railway embankment height are an excellent choice to carry the freight train. In addition, it can be seen from each graph that a lower natural slope height can lead to a higher safe speed. When there are ballast pockets with a depth of 1.5 m, only models with a natural slope height of 1 m can stop the freight train. From Figure 4.34 (c) and Figure 4.35, it can be seen that as the ballast pockets deepen, the maximum safe speed at which models allow the freight train to pass gradually decreases. Finally, comparing graphs in Figure 4.34 with those in Figure 4.35, models with a slope ratio of 3H:1V are much safer and can pass the freight train at a higher speed.

If the train is considered to pass the track at a higher safe speed, it is more suitable to construct a 1m natural slope with a slope ratio of 3H:1V and a 3 m railway embankment height. Through the above analysis, models combining these three aspects can withstand the freight train passing safely at a speed of 88 km/h (55 mph), provided that the depth of the existing ballast pockets does not exceed 0.5 m. Through this research, the maximum safe train speed can be connected with the slope, railway embankment, and ballast pockets geometries.

4.6 Summary

At the beginning of this chapter, three sets of models were established, namely dry models (Set I), models existing ballast pockets but no train load (Set II), models existing both ballast pockets and train load (Set III). Set II models added not only ballast pockets but also the groundwater level based on the Set I models. Therefore, before the establishment of Set II models, models that were only adding the groundwater level based on Set I models eliminated the influence of the groundwater level. The establishment of three sets of models ranges from simple to complex and contrasts in pairs, reflected the influence of ballast pockets and train load on slope stability. As a particular case, a stationary train load was first applied to Set III models, and then different train loads corresponding to different train speeds were applied to the models to study the maximum safe train speed of the different models. In this research, the control variable method was used to analyze and study all model parameters.

According to the above analysis of the parameters of three sets of models, especially the analysis of Set III models, it was found that a higher railway embankment and a lower natural slope with a larger slope ratio are a safer combination for construction. In this study, the slope ratio of 3H:1V is recommended. Although ballast pockets can reduce slope stability, if the railway chooses the above combination for construction, ballast pockets in any dimension and position do not affect the capacity of the freight train to pass over the track safely.

In addition, this research could identify the maximum safe speed at which a train can pass through, given the geometric parameters of the slope, railway embankment, and ballast pockets.

Chapter 5 Conclusions and future work

5.0 Introduction

This chapter summarizes the main work and results of this research and the content that can be further studied in the future related to this research. Section 5.1 reviews the research objectives and methods of this project; Section 5.2 summarizes the research results of this project, and the limitations are briefly described in Section 5.3. Finally, the outlook and recommendations for further research related to this project are given in Section 5.4.

5.1 Thesis summary

The primary purpose of this research was to provide a guideline to identify the maximum safe train speed with respect to a railway embankment existing ballast pockets. The control variable method was used for parameter analysis to quantify the main parameters' influence on slope stability. As introduced in Chapter 1, the following method steps were used to achieve the main goal:

(a) literature review: a collection of relevant modeling methods, determination of simulation conditions, identification of the main parameters that govern slope stability and establishment of credible ranges of these parameters;

(b) verification of the RS2-based FEM to meet the requirements of models;

(c) establishment of numerical models based on the literature review;

(d) parametric study on numerical models, including the factor of safety of models and the maximum safe speed at which the train can pass under different conditions

Chapter 2 is the literature review of the study. It introduced the formation principles of ballast pockets, numerical methods in geomechanics, moving train loads analysis on the railway embankment and credible ranges of main parameters in the models. Chapter 3 used RS2 to simulate the models in the published works and compared the literature results to verify the reliability of the RS2 simulation results. This study provided a theoretical basis for the accuracy of the simulation results of the following three sets of models. Chapter 4 conducted parametric studies on three sets of models and determined the maximum safe train speed according to the factor of safety of the models in different situations. This research identifies the maximum safe speed a train can use, through given the parameters of the slope, railway embankment, and ballast pockets.

5.2 Conclusion

This thesis studied the parameters of the three sets of models and determined the slope stability based on the factor of safety of the models. Maximum safe train speeds allowed by the freight train for models of the given slope, railway embankment, and ballast pockets

geometries were determined. The dimensions of the following parameters need to be considered to stabilize the slope with ballast pockets and a moving freight train:

(a) A lower natural slope. For three sets of models, the increase of the natural slope height reduces the slope stability, so a lower natural slope needs to be selected to allow the train to pass safely at a faster speed. In this research, a 1 m natural slope is a preferred choice.

(b) A higher railway embankment height. The rise of the railway embankment of models without a train load (Sets I and II models) can reduce the slope stability; conversely, increasing the railway embankment enhances the slope stability of models with a train load (Set III models) and helps to increase the maximum safe train speed. In this research, a 3 m natural slope is preferred for allowing the train to pass safely at a faster speed.

(c) A larger slope ratio. In this study, 2H:1V and 3H:1V are two optional slope ratio values. The parametric study results show that under the same conditions, a slope with a slope ratio of 3H:1V is safer and has the more considerable maximum safe train speed.

(d) Shallow ballast pockets. Based on parametric analysis, ballast pockets' depth is the only ballast pockets parameter that has a significant impact on slope stability in this research and that causes slope instability as the ballast pockets deepen. Therefore, to improve slope stability and increase maximum safe train speed, it is necessary to prevent the formation and deepen ballast pockets.

The increase in railway embankment height has the opposite effect on the slope stability of models with a train load (Set III models) and models without a train load (Sets I and II models), while the changes in the natural slope height and slope ratio have the same effect on the slope stability of three sets of models. The deepening of ballast pockets can reduce the slope stability of Sets II and III models.

Besides, dry models have no pore pressure. For models under undrained conditions, the pore pressure above the groundwater table is negative, and its absolute value decreases with the increasing depth; conversely, the pore pressure below the groundwater table is positive, and its absolute value increases with the increase of the depth.

In conclusion, The research results show that freight trains can traverse on tracks built on a 1 m slope with a 3H:1V slope inclination and a 3 m railway embankment at a relatively higher maximum safe speed.

5.3 Limitations

Although the influence of many parameters on slope stability has been discussed, there are many premises, which are also limitations for this study.

(a) The track in this analysis is assumed as an infinitely long tangent track section. Ignoring track curves was the main limitation of the models.

(b) Rainfall, wind, and other environmental changes were not considered.

(c) The track is assumed to be smooth, and there is no friction between the train wheels and

the track.

(d) RS2 cannot combine SSR and dynamic loading. The train load is considered static, so the train speed is unchanged when passing along the track.

(e) In this study, to more conveniently measure the depth and width of ballast pockets, it was assumed that the bottom of ballast pockets are horizontal and flat. In fact, the bottom of the ballast pockets could be uneven.

(f) The fouled part in ballast pockets was strictly divided, and any potential changes in soil stratification were not considered.

5.4 Future work

Based on this research, the following areas can be improved to bring the model closer to the actual situation:

(a) consider the influence of external weather conditions, such as the influence of rainwater and temperature on the soil characteristics can be considered.

(b) the railway track was assumed to be a straight line; thus, this thesis did not consider curved tracks. The curved tracks can generate centrifugal forces on the rail, which could be studied later.

(c) classify the soil in ballast pockets into multiple levels, according to the fouling degree and not only based on clean or fouled categorization.

(d) the natural ground is set to a homogeneous soil mass in simulation. In the future study, the soil ground profile could consist of multiple layers of soil closer to actual conditions.

References

1. Ahn, T. 2019. "Excessive settlement back-analysis of railway embankment on soft soils during Service." *J. Korean Geoenviron. Soc.*, 20 (1), 13-17. https://doi.org/10.14481/jkges.2019.20.1.13.

2. Allan, J. 2012. "Soil mechanics of high speed rail tracks." *Semantic Scholar*, October 13, 2021. https://www.semanticscholar.org/paper/Soil-Mechanics-of-High-Speed-Rail-Tracks-Allan/f44fa5a2649a61409b7eacfa1ed61cf863e5a10d.

3. Alemu, A. Y. 2011. Survey of railway ballast selection and aspects of modelling techniques. M.S. thesis, KTH Royal Institute of Technology.

4. Arai, K., and K. Tagyo. 1985. "Determination of noncircular slip surface giving the minimum factor of safety in slope stability analysis." *Soils Found.*, 25 (1), 43-51. https://doi.org/10.3208/sandf1972.25.43.

5. AREMA (American Railway Engineering and Maintenance-of-Way Association). 1996. *AREMA manual for railway engineering*, Landover, MD: AREMA.

6. AREMA (American Railway Engineering and Maintenance-of-Way Association). 2000. AREMA manual for railway engineering, Landover, MD: AREMA.

7. AREMA (American Railway Engineering and Maintenance-of-Way Association). 2012. AREMA manual for railway engineering, Landover, MD: AREMA.

8. AREMA (American Railway Engineering and Maintenance-of-Way Association). 2013. AREMA manual for railway engineering, Landover, MD: AREMA.

9. AREMA (American Railway Engineering and Maintenance-of-Way Association). 2018. AREMA manual for railway engineering, Landover, MD: AREMA.

10. Ardiç, Ö. 2006. Analysis of bearing capacity using discrete element method. M.S. thesis, Middle East Technical University.

11. Australian Rail Track Corporation. 2015. "Dos and do nots of subgrade maintenance." Accessed November 11, 2019. https://extranet.artc.com.au/docs/eng/track-civil/guidelines/earthworks/subgrade_do_donts.pdf.

12. Bagińska, I. 2016. "Estimating and verifying soil unit weight determined on the basis of SCPTu tests." *Annals of Warsaw University of Life Sciences – SGGW Land Reclamation*, 48 (3), 233-242. http://doi.org/10.1515/sggw-2016-0018.

13. Basye, C., and S. Wilk. 2020. "Remediation of Ballast Pockets in a Railway Environments." *J. Perm. Way. Inst.*, April, 138, Part 2, 48-51.

14. Bathe, K. J. 1982. *Finite element procedures in engineering analysis*. New Jersey, USA:

Prentice Hall.

15. Bertram, A., and R. Glüge. 2013. *Solid mechanics: theory, modeling, and problems*. Cham, Switzerland: Springer.

16. Biot, M. A. 1941. "General theory of three-dimensional consolidation." *J. Appl. Phy.*, 12 (2), 155-164. https://doi.org/10.1063/1.1712886.

17. Bobet, A. 2010. "Numerical methods in geomechanics." *Arab. J. Sci. Eng.*, 35 (1B), 27-48.

18. Brzeziński, K., T. Rybicki, and K. Józefiak. 2018. "Analysis of stability of railway embankment including horizontal forces in light of Eurocode." *MATEC Web of Conf.*, Vol. 196. http://.doi.org/10.1051/matecconf/201819603016.

19. Budhu, M. 2008. *Soil mechanics and foudations*. New Jersey, USA: Wiley.

20. Chakeri, H., and B. Ünver. 2014. "A new equation for estimating the maximum surface settlement above tunnels excavated in soft ground." *Environ. Earth Sci.*, 71 (7), 3195-3210. http://dx.doi.org/10.1007/s12665-013-2707-2.1.

21. Cheng, Y. M., and C. K. Lau. 2008. *Slope stability analysis and stabilization: New methods and insight*. London, UK: CRC Press.

22. Chowdhury, R., P. Flentje, and G. Bhattacharya. 2010. *Geotechnical slope analysis*. London, UK: Taylor & Francis Group.

23. Clough, R. W. 1960. "The finite element method in plane stress analysis." *In Proc., 2nd American Society of Civil Engineers (ASCE) Conf. on Electronic Computation*, 345-378. Pittsburgh: ASCE.

24. Connolly, D. P., G. Kouroussis, A. Giannopoulos, O. Verlinden, P. K. Woodward, and M. C. Forde. 2014. "Assessment of railway vibrations using an efficient scoping model." *Soil Dyn. Earthq. Eng.,* 58, 37-47. https://doi.org/10.1016/j.soildyn.2013.12.003.

25. Cundall, P. A. 1974. Rational design of tunnel supports: a computer model for rock-mass behavior using interactive graphics for the input and output of geometric data. University of Minnesota.

26. Dahlberg, T. 2003. Railway track dynamics-a survey. Linköping University.

27. Dai, W., P. Jiang, J. Ding, and B. Fu. 2017. "The influence of strength reduction method on slope stability under different instability criteria." *In Proc., 2nd Int. Conf. Archit. Eng. and New Mater. (ICAENM 2017)*. Guangzhou: DEStech Publications. https://doi.org/10.12783/dtetr/icaenm2017/7839.

28. Davis, R. O., and A. P. S.Selvadurai. 2002. *Plasticity and geomechanics*. New York, USA: Cambridge University Press. https://doi.org/10.1017/CBO9780511614958.

29. Desai, C. S., and J. T. Christian. 1977. *Numerical methods in geomechanics*. New York, USA: McGraw-Hill.

30. Desai, C. S., and M. Zaman. 2013. *Advanced geotechnical engineering: Soil-structure interaction using computer and material models*. Boca Raton, USA: Taylor & Francis Group.

31. Duncan, J. M., and S. G. Wright. 2005. *Soil strength and slope stability*. Hoboken, USA: Wiley.

32. Egeli, I., and H. Usun. 2012. "Designing high-speed train railway embankments using finite element analysis." *Arab. J. Sci. Eng.*, 37 (8), 2127-2126. http://doi.org/10.1007/s13369-012-0302-6.

33. Ejezie, J. O. 2014. "Numerical modelling of rod buckling in cone penetration testing." *In Proc., 13th BGA Young Geotech. Engineers' Symp. (YGES).* Manchester: GDS Instruments.

34. Esveld, C. 2001. *Modern railway track*. Zaltbommel, Netherlands: MRT-Productions.

35. FRA (Federal Railroad Administration). 2019. *Mixed freight and higher-speed passenger trains: framework for superelevation design*. Washington, D.C., USA: FRA.

36. Greco, V. R. 1996. "Efficient Monte Carlo technique for locating critical slip surface." *J. Geotech. Eng.* 122 (7), 517-525. https://doi.org/10.1061/(ASCE)0733-9410(1996)122:7(517).

37. Griffiths, D. V. 1994. "Coupled analyses in geomechanics." *Visco-plastic behaviour of geomaterials*, Cristescu, N. D., and G. Gioda, eds., 245-317. New York, USA: Springer. https://doi.org/10.1007/978-3-7091-2710-0_5.

38. Griffiths, D. V., and P. A. Lane. 1999. "Slope stability analysis by finite elements." *Geotechnique*, 49 (3), 387-403. https://doi.org/10.1680/geot.1999.49.3.387.

39. Gupta. K. M. 2012. *Material and manufacturing technology III*. Zurich, Switzerland: Trans Tech Publications.

40. Hall, W. S., and G. Oliveto. 2004. *Boundary element methods for soil-structure interaction*. Amsterdam, USA: Kluwer Academic Publishers.

41. Hammah, R. E., T. E. Yacoub, B. C. Corkum, and J. H. Curran. 2005. "The shear strength reduction method for the generalized Hoek-Brown criterion." *In Proc., 40th U.S. Rock Mech. (USRMS) Symp*. Anchorage, Alaska: American Rock Mechanics Association.

42. Hay, W. W. 1982. *Railroad engineering*. New York, USA: Wiley.

43. Hill, J., and D. Colwell. 2018. "Rapid soil stabilisation method for high volume mainline track: An update." *Perm.Way Inst. (PWI) J. Jan. 2018*, Vol. 136, Part 1.

44. Huang, M., and C. Jia. 2009. "Strength reduction FEM in stability analysis of soil slopes subjected to transient unsaturated seepage." *Comput. Geotech*., 36 (1-2), 93-101. https://doi.org/10.1016/j.compgeo.2008.03.006.

45. Hughes, T. J. R. 1987. *The finite-element method: Linear static and dynamic finite element analysis*. New Jersey, USA: Prentice Hall.

46. Indraratna, B., D. Ionescu, and H. D. Christie. 1998. “Shear behavior of railway ballast based on large-scale triaxial tests.” *J. Geotech. Geoenviron. Eng.* 124 (5), 439-449. https://doi.org/10.1061/(ASCE)1090-0241(1998)124:5(439).

47. Indraratna, B., S. Nimbalkar, and D. Christie. 2009. “The performance of rail track incorporating the effects of ballast breakage, confining pressure and geosynthetic reinforcement.” *In Proc., 8th Int. Brg. Cap. of Rd. Ry. and A/F. (BCRRA) Conf.*, 5-24. London, UK: Taylor & Francis Group. http://dx.doi.org/10.1201/9780203865286.ch2.

48. Indraratna, B., P. K. Thakur, and J. S. Vinod. 2010. “Experimental and numerical study of railway ballast behaviour under cyclic loading.” *Int. J. Geomech.* 10 (4), 136-144. https://doi.org/10.1061/(ASCE)GM.1943-5622.0000055.

49. Indraratna, B., W. Salim, and C. Rujikiatkamjorn. 2011. *Advanced rail geotechnology–Ballasted track*. London, UK: Taylor & Francis Group.

50. Kempfert, H. G., and B. Gebreselassie. 2006. *Excavations and foundations in soft soils*. Berlin, DE: Springer.

51. Kouroussis, G., C. Caucheteur, D. Kinet, G. Alexandrou, O. Verlinden, and V. Moeyaert. 2015. “Review of trackside monitoring solutions: From strain gages to optical fibre sensors.” *Sens.*, 15 (8), 20115-20139. https://dx.doi.org/10.3390%2Fs150820115.

52. Kovacevic, M. S., M. Bacic, I. Stipanovic, and K. Gavin. 2019. “Categorization of the condition of railway embankments using a multi-attribute utility theory.” *Appl. Sci.-Basel*, 9 (23), 5089. http://dx.doi.org/10.3390/app9235089.

53. Kumara, J. J., and K. Hayano. 2016. “Deformation characteristics of fresh and fouled ballasts subjected to tamping maintenance.” *Soils Found.*, 56 (4), 652-663. https://doi.org/10.1016/j.sandf.2016.07.006.

54. Li, D., and E. T. Selig. 1995. “Evaluation of railway subgrade problems.” *Transp. Res. Rec.*, 1489, 17-25. Accessed October 16, 2021.

55. Li, D., J. Hyslip, T. Sussmann, and S. Chrismer 2016. *Railway geotechnics*. Boca Raton, USA: Taylor & Francis Group.

56. Li, D., and S. Wilk. 2021. “Recent studies on railway-track substructure at TTCI.” *Transp. Saf. and Environ.*, 3 (1), 36-49. https://doi.org/10.1093/tse/tdaa031.

57. Liu, S., Y. Wang, and C. Shen. 2018. “DEM analysis of granular crushing during simple shearing.” *Mar. Georesources Geotechnol*, 36 (5), 522-531. https://doi.org/10.1080/1064119X.2017.1349846.

58. Liu, X., Y. Wang, and D. Li. 2019. “Investigation of slope failure mode evolution during large deformation in spatially variable soils by random limit equilibrium and material point methods.” *Comput. Geotech.*, 111, 301-312. https://doi.org/10.1016/j.compgeo.2019.03.022.

59. Luan, M., Y. Wu, and T. Nian 2003. “A Criterion For Evaluating Slope Stability Based on

Development of Plastic Zone by Shear Strength Reduction FEM." *J. Disaster Prev. Mitig. Eng.*, 23 (3), 1-8.

60. Mansour, A.E.D. 2018. "Generalized finite difference approach verification on circular plates." *IOP Conf. Ser.: Mater. Sci. Eng.*, 365 (4): 042030. http://dx.doi.org/10.1088/1757-899X/365/4/042030.

61. Middleton, W. D., G. M. Smerk, and R. L. Diehl. 2007. *Encyclopedia of North American Railroads*. Bloomington, USA: Indiana University Press.

62. Nakamura, A., F. Cai, and K. Ugai. (2008). "Embankment basal stability analysis using shear strength reduction finite element method." In *Proc., 10th Int. Symp. Landslides and Engineered Slopes*. Xi'an: Joint Technical Committee on Landslides and Engineered Slopes.

63. Nikolić, M., T. R. Bonacc, and A. Ibrahimbegović. 2016. "Overview of the numerical methods for the modeling of rock mechanics problems." *Teh. Vjesn.*, 23 (2), 627-637. http://dx.doi.org/10.17559/TV-20140521084228.

64. Ortiz, J. M. R, J. S. Gesta, and C. O. Mazo. 1986. *Curso Aplicado de Cimentaciones*. Madrid, Spain :Colegio Oficial de Arquitectos.

65. Parson, B. K. 1990. Hydraulic conductivity of railroad ballast and track substructure drainage. M.S. thesis, University of Massachusetts.

66. Profillidis, V. A. 2014. *Railway management and engineering*. Farnham, UK: Ashgate Publishing.

67. Puffert, D. J. 2002. "Path dependence in spatial networks: the standardization of railway track gauge." Explor. Econ. Hist., 39 (3), 282-314. https://doi.org/10.1006/exeh.2002.0786.

68. Punmia, B. C., Ashok K. Jain, and Arun K. Jain. 2005. *Soil mechanics and foundations*. New Delhi, India: Laxmi Publications.

69. Remennikov, A. M., and S. Kaewunruen. 2008. "A review of loading conditions for railway track structures due to train and track vertical interaction." *Struct. Control Health Monit.*, 15 (2), 207-234. http://dx.doi.org/10.1002/stc.227.

70. Rocscience Inc. 2004. "A new era in slope stability analysis: shear strength reduction finite element technique." Accessed November 30, 2019. https://www.rocscience.com/documents/pdfs/library/StrengthReduction.pdf.

71. Rocscience Inc. 2018. "Convergence Criteria." Accessed December 20, 2019. https://www.rocscience.com/help/rs2/assets/docs/convergence%20criteria.pdf.

72. Rocscience Inc. 2021a. "RS2 Technical specifications." Accessed December 1, 2021. https://www.rocscience.com/help/rs2/overview/technical-specifications.

73. Rocscience Inc. 2021b. "Cam clay and modified Cam clay material models." Accessed March 29, 2022.

https://www.rocscience.com/assets/verification-and-theory/RS2/8-Cam-Clay-and-Modified-Cam-Clay-Models.pdf.

74. Rocscience Inc. 2021c. "Mohr-Coulumb material model." Accessed March 29, 2022. https://www.rocscience.com/assets/verification-and-theory/RS2/5-Mohr-Coulomb-Model.pdf.

75. Sadeghi, J. M., Zakeri, J. A. Zakeri, and M. E. M., Najar. 2016. "Developing track ballast characteristic guideline in order to evaluate its performance." *Int. J. Railw.*, 9 (2), 27-35. https://doi.org/10.7782/IJR.2016.9.2.027.

76. Saifi, I., S. Benmebarek, and L. Belounar. 2015. "Bearing capacity of ring footing on two layers soil by numerical approach." *In Proc., 13th Arab Struct. Eng. Conf.* Algeria: University of Blida 1.

77. Selig, E. T., and J. M. Waters. 1994. *Track technology and substructure management*. London, UK: Thomas Telford.

78. Shao, Y., S. Hao, Y. Luo, J. Xing, and Z. Liu. 2012. *Advanced building materials and sustainable architecture: selected, peer reviewed papers from the 2nd International Conference on Civil Engineering, Architecture and Building Materials, CEABM 2012*. Zurich, Switzerland: Trans Tech Publications.

79. Shevtsov, I. Y. 2008. Wheel/Rail interface optimisation, Ph.D. diss., Delft University of Technology.

80. Smith, I. M., D. V. Griffiths, and L. Margetts. 2013. *Programming the finite element method*. Chichester, UK: Wiley.

81. Stark, T. D., S. T. Wilk, H. B. Thompson, T. Sussmann, M. Baker, and C. L. Ho. 2016. "Evaluating Fouled Ballast Using Seismic Surface Waves." *In Proc., 2016 Joint Rail Conf.* Columbia, SC: ASME Digital Collection. http://dx.doi.org/10.1115/JRC2016-5714.

82. Statistics Canada. 2006. Overview of rail transport in 2006. Ottawa, Ontario.

83. Stephen, W., and M. Uhlig. 2013. "*RailCorp Engineering Standard-Rolling Stock 0331: Wheel and axles reference manual.*" Accessed October 16, 2020. https://www.transport.nsw.gov.au/system/files/media/asa_standards/2017/esr-0331.pdf.

84. Ti, K. S., Bujang B. K. Huat, J. Noorzaei, M. S. Jaafar, and G. S. Sew. 2009. "A review of basic soil constitutive models for geotechnical application." *Electron. J. Geotech. Eng.*, 14, 1-18.

85. Ting, J., M. Khwaja, L. R. Meachum, and J. D. Rowell. 1993. "Ellipse-based discrete element model for granular materials." *Int. J. Numer. Anal. Methods Geomech.*, 17 (9), 603-623. http://dx.doi.org/10.1002/nag.1610170902.

86. Transport Canada. 2011. Transportation in Canada 2006. Ottawa, Ontario.

87. Transport Canada. 2018. Transportation in Canada 2017. Ottawa, Ontario.

88. TRB (Transportation Research Board). 2012. *Track handbook for light rail transit, 2nd*

Ed. Washington, DC: TRB. https://doi.org/10.17226/22800.

89. TSB (Transportation Safety Board). 1998. Railway *Occurrence Report, No. R98V0100*. Nelson-Creston, British Columbia: TSB.

90. TSB (Transportation Safety Board). 1999. *Railway Occurrence Report, No. R99W0133*. Keewatin, Ontario: TSB.

91. TSB (Transportation Safety Board). 2018. *Rail transportation occurrence data*. Ottawa, Ontario: TSB.

92. Tutumluer, E., W. Dombrow, and H. Huang. 2008. "Laboratory characterization of coal dust fouled ballast behavior." *In Proc., AREMA 2008 Annu. Conf.* Salt Lake City, UT: AREMA.

93. Tzanakakis, K. 2013. *The railway track and its long term behavior: A handbook for a railway track of high quality*. Berlin, DE: Springer.

94. Wani, K. M. N. S., and R. Showkat. 2018. "Soil constitutive models and their application in geotechnical engineering: A review." *Int. J. Eng. Res. Tech.*, 7 (4), 137-145.

95. Watts, T. J. 2018. Direct measurement of crosstie-ballast interface pressures using granular material pressure cells. M.S. thesis, University of Kentucky. https://doi.org/10.13023/etd.2018.440.

96. Wei, H., W. Xu, X. Xu, Q. Meng, and C. Wei. 2018. "Mechanical properties of strongly weathered rock–soil mixtures with different rock block contents." *Int. J. Geomech.* 18 (5). https://doi.org/10.1061/(ASCE)GM.1943-5622.0001131.

97. Wu, Y., T. Yang, P. Li, and J. Lin. 2019. "Investigation of groundwater withdrawal and recharge affecting underground structures in the Shanghai Urban Area." *Sustainability*, 11 (24), 7162. http://dx.doi.org/10.3390/su11247162.

98. Xiao, L., and Zhang, Q. 2011. "铁路轨道下盾构施工所致地面沉降的数值模拟" [3D numerical modeling of ground settlements caused by shield tunneling across multi-tracks of railway]. [In Chinese.] J. Tongji Univ. Nat. Sci., 39 (9), 1286-1291. http://dx.doi.org/10.3969/j.issn.0253-374x.2011.09.006.

99. Xie, X., Y. Yang, and M. Ji. 2016. "Analysis of ground surface settlement induced by the construction of a large-diameter shield-driven tunnel in Shanghai, China." *Tunn. Undergr. Space Technol.*, 51, 120-132. https://doi.org/10.1016/j.tust.2015.10.008.

100. Xu, S. 2019. Effect of rapid drawdown on the stability of railway embankments. M.S. thesis, Concordia University.

101. Yu, J. B. Y., and J. P. Hsi. 2005. "Jet grout application for excavation in soft marine clay." *In Proc., 16th Int. Conf. Soil Mech. and Geotech. Eng.*, 1485-1488. Osaka: Rotterdam Millpress.

102. Zhang, D. 1998. "Evaluation of the slope stability with neural network." *Hydrom. Geol. Eng. Geol.*

103.Zhang, H., Z. Yin, and J. Zhu. 2005. “地铁隧道盾构法施工过程中地层变位的三维有限元模拟” [3D finite element simulation on deformation of soil mass during shield tunneling]. [In Chinese.] *Chin. J. Rock Mech. Eng.*, 24 (5), 755-760. http://dx.doi.org/10.3321/j.issn:1000-6915.2005.05.004.

104.Zhang, T. W., Y. J. Cui, , F. Lamas-Lopez, N. Calon, and S. C. D’Aguiar. 2016. “Modelling stress distribution in substructure of French conventional railway tracks.” *Constr. Build. Mater.*, 116, 326-334. https://doi.org/10.1016/j.conbuildmat.2016.04.137.

105.Zheng, H., C. Li, and C. Lee. 2002. “求解安全系数的有限元法” [Finite element method for solving the factor of Safety]. [In Chinese.] *Chin. J. Geotech. Eng.*, 24 (5), 626-628. http://dx.doi.org/10.3321/j.issn:1000-4548.2002.05.020.

106.Zhou, C., L. Gao, H. Xiao, and B. Hou. 2020. “Railway wheel flat recognition and precise positioning method based on multisensory arrays.” *Appl. Sci.*, 10 (4), 1297. http://dx.doi.org/10.3390/app10041297.

107.Zienkiewicz, O. C. 1977. *The finite element method in engineering sciences*. New York: McGraw-Hill.

Appendix I: Specific cases in Set II and Set III models

Table I-1. Cases in Set II – models existing ballast pockets

Groups	Ballast pockets' location	Slope ratio	Subgroups	Ballast pockets' depth (m)	Ballast pockets' width (m)	Value of m	He (m)	Hs (m)
Group 5	Under the center of the tie	2:1	Subgroup 7	0.5	1.0	1/2	1-3	1-5
			Subgroup 8	0.5	1.0	1	1-3	1-5
			Subgroup 9	0.5	1.5	1/2	1-3	1-5
			Subgroup 10	0.5	1.5	1	1-3	1-5
			Subgroup 11	0.5	2.0	1/2	1-3	1-5
			Subgroup 12	0.5	2.0	1	1-3	1-5
			Subgroup 13	1.0	1.0	1/2	1-3	1-5
			Subgroup 14	1.0	1.0	1	1-3	1-5
			Subgroup 15	1.0	1.5	1/2	1-3	1-5
			Subgroup 16	1.0	1.5	1	1-3	1-5
			Subgroup 17	1.0	2.0	1/2	1-3	1-5
			Subgroup 18	1.0	2.0	1	1-3	1-5
			Subgroup 19	1.5	1.0	1/2	1-3	1-5
			Subgroup 20	1.5	1.0	1	1-3	1-5
			Subgroup 21	1.5	1.5	1/2	1-3	1-5
			Subgroup 22	1.5	1.5	1	1-3	1-5
			Subgroup 23	1.5	2.0	1/2	1-3	1-5
			Subgroup 24	1.5	2.0	1	1-3	1-5
Group 6	Under the center of the tie	3:1	Subgroup 25	0.5	1.0	1/2	1-3	1-5
			Subgroup 26	0.5	1.0	1	1-3	1-5
			Subgroup 27	0.5	1.5	1/2	1-3	1-5
			Subgroup 28	0.5	1.5	1	1-3	1-5
			Subgroup 29	0.5	2.0	1/2	1-3	1-5
			Subgroup 30	0.5	2.0	1	1-3	1-5
			Subgroup 31	1.0	1.0	1/2	1-3	1-5
			Subgroup 32	1.0	1.0	1	1-3	1-5
			Subgroup 33	1.0	1.5	1/2	1-3	1-5
			Subgroup 34	1.0	1.5	1	1-3	1-5
			Subgroup 35	1.0	2.0	1/2	1-3	1-5
			Subgroup 36	1.0	2.0	1	1-3	1-5

Table I-1. Cases in Set II – models existing ballast pockets – Continued

Groups	Ballast pockets' location	Slope ratio	Subgroups	Ballast pockets' depth (m)	Ballast pockets' width (m)	Value of m	He (m)	Hs (m)
Group 6	Under the center of the tie	3:1	Subgroup 37	1.5	1.0	1/2	1-3	1-5
			Subgroup 38	1.5	1.0	1	1-3	1-5
			Subgroup 39	1.5	1.5	1/2	1-3	1-5
			Subgroup 40	1.5	1.5	1	1-3	1-5
			Subgroup 41	1.5	2.0	1/2	1-3	1-5
			Subgroup 42	1.5	2.0	1	1-3	1-5
Group 7	Under one side of the tie	2:1	Subgroup 43	0.5	1.0	1/2	1-3	1-5
			Subgroup 44	0.5	1.0	1	1-3	1-5
			Subgroup 45	0.5	1.5	1/2	1-3	1-5
			Subgroup 46	0.5	1.5	1	1-3	1-5
			Subgroup 47	0.5	2.0	1/2	1-3	1-5
			Subgroup 48	0.5	2.0	1	1-3	1-5
			Subgroup 49	1.0	1.0	1/2	1-3	1-5
			Subgroup 50	1.0	1.0	1	1-3	1-5
			Subgroup 51	1.0	1.5	1/2	1-3	1-5
			Subgroup 52	1.0	1.5	1	1-3	1-5
			Subgroup 53	1.0	2.0	1/2	1-3	1-5
			Subgroup 54	1.0	2.0	1	1-3	1-5
			Subgroup 55	1.5	1.0	1/2	1-3	1-5
			Subgroup 56	1.5	1.0	1	1-3	1-5
			Subgroup 57	1.5	1.5	1/2	1-3	1-5
			Subgroup 58	1.5	1.5	1	1-3	1-5
			Subgroup 59	1.5	2.0	1/2	1-3	1-5
			Subgroup 60	1.5	2.0	1	1-3	1-5
Group 8	Under one side of the tie	3:1	Subgroup 61	0.5	1.0	1/2	1-3	1-5
			Subgroup 62	0.5	1.0	1	1-3	1-5
			Subgroup 63	0.5	1.5	1/2	1-3	1-5
			Subgroup 64	0.5	1.5	1	1-3	1-5
			Subgroup 65	0.5	2.0	1/2	1-3	1-5
			Subgroup 66	0.5	2.0	1	1-3	1-5
			Subgroup 67	1.0	1.0	1/2	1-3	1-5

Table I-1. Cases in Set II – models existing ballast pockets – Continued

Groups	Ballast pockets' location	Slope ratio	Subgroups	Ballast pockets' depth (m)	Ballast pockets' width (m)	Value of m	He (m)	Hs (m)
Group 8	Under one side of the tie	3:1	Subgroup 68	1.0	1.0	1	1-3	1-5
			Subgroup 69	1.0	1.5	1/2	1-3	1-5
			Subgroup 70	1.0	1.5	1	1-3	1-5
			Subgroup 71	1.0	2.0	1/2	1-3	1-5
			Subgroup 72	1.0	2.0	1	1-3	1-5
			Subgroup 73	1.5	1.0	1/2	1-3	1-5
			Subgroup 74	1.5	1.0	1	1-3	1-5
			Subgroup 75	1.5	1.5	1/2	1-3	1-5
			Subgroup 76	1.5	1.5	1	1-3	1-5
			Subgroup 77	1.5	2.0	1/2	1-3	1-5
			Subgroup 78	1.5	2.0	1	1-3	1-5

Table I-2. Cases in Set III – models existing ballast pockets and a stationary train

Groups	Ballast pockets' location	Slope ratio	Subgroups	Ballast pockets' depth (m)	Ballast pockets' width (m)	Value of m	He (m)	Hs (m)	Maximum safe train speed (km/h)
Group 9	Under the center of the tie	2:1	Subgroup 79	0.5	1.0	1/2	1-3	1-5	0-120
			Subgroup 80	0.5	1.0	1	1-3	1-5	0-120
			Subgroup 81	0.5	1.5	1/2	1-3	1-5	0-120
			Subgroup 82	0.5	1.5	1	1-3	1-5	0-120
			Subgroup 83	0.5	2.0	1/2	1-3	1-5	0-120
			Subgroup 84	0.5	2.0	1	1-3	1-5	0-120
			Subgroup 85	1.0	1.0	1/2	1-3	1-5	0-120
			Subgroup 86	1.0	1.0	1	1-3	1-5	0-120
			Subgroup 87	1.0	1.5	1/2	1-3	1-5	0-120
			Subgroup 88	1.0	1.5	1	1-3	1-5	0-120
			Subgroup 89	1.0	2.0	1/2	1-3	1-5	0-120
			Subgroup 90	1.0	2.0	1	1-3	1-5	0-120
			Subgroup 91	1.5	1.0	1/2	1-3	1-5	0-120
			Subgroup 92	1.5	1.0	1	1-3	1-5	0-120
			Subgroup 93	1.5	1.5	1/2	1-3	1-5	0-120
			Subgroup 94	1.5	1.5	1	1-3	1-5	0-120
			Subgroup 95	1.5	2.0	1/2	1-3	1-5	0-120
			Subgroup 96	1.5	2.0	1	1-3	1-5	0-120
Group 10	Under the center of the tie	3:1	Subgroup 97	0.5	1.0	1/2	1-3	1-5	0-120
			Subgroup 98	0.5	1.0	1	1-3	1-5	0-120
			Subgroup 99	0.5	1.5	1/2	1-3	1-5	0-120
			Subgroup 100	0.5	1.5	1	1-3	1-5	0-120
			Subgroup 101	0.5	2.0	1/2	1-3	1-5	0-120
			Subgroup 102	0.5	2.0	1	1-3	1-5	0-120
			Subgroup 103	1.0	1.0	1/2	1-3	1-5	0-120
			Subgroup 104	1.0	1.0	1	1-3	1-5	0-120
			Subgroup 105	1.0	1.5	1/2	1-3	1-5	0-120
			Subgroup 106	1.0	1.5	1	1-3	1-5	0-120
			Subgroup 107	1.0	2.0	1/2	1-3	1-5	0-120
			Subgroup 108	1.0	2.0	1	1-3	1-5	0-120
			Subgroup 109	1.5	1.0	1/2	1-3	1-5	0-120

Table I-2. Cases in Set III – models existing ballast pockets and a stationary train – Continued

Groups	Ballast pockets' location	Slope ratio	Subgroups	Ballast pockets' depth (m)	Ballast pockets' width (m)	Value of m	He (m)	Hs (m)	Maximum safe train speed (km/h)
Group 10	Under the center of the tie	3:1	Subgroup 110	1.5	1.0	1	1-3	1-5	0-120
			Subgroup 111	1.5	1.5	1/2	1-3	1-5	0-120
			Subgroup 112	1.5	1.5	1	1-3	1-5	0-120
			Subgroup 113	1.5	2.0	1/2	1-3	1-5	0-120
			Subgroup 114	1.5	2.0	1	1-3	1-5	0-120
Group 11	Under one side of the tie	2:1	Subgroup 115	0.5	1.0	1/2	1-3	1-5	0-120
			Subgroup 116	0.5	1.0	1	1-3	1-5	0-120
			Subgroup 117	0.5	1.5	1/2	1-3	1-5	0-120
			Subgroup 118	0.5	1.5	1	1-3	1-5	0-120
			Subgroup 119	0.5	2.0	1/2	1-3	1-5	0-120
			Subgroup 120	0.5	2.0	1	1-3	1-5	0-120
			Subgroup 121	1.0	1.0	1/2	1-3	1-5	0-120
			Subgroup 122	1.0	1.0	1	1-3	1-5	0-120
			Subgroup 123	1.0	1.5	1/2	1-3	1-5	0-120
			Subgroup 124	1.0	1.5	1	1-3	1-5	0-120
			Subgroup 125	1.0	2.0	1/2	1-3	1-5	0-120
			Subgroup 126	1.0	2.0	1	1-3	1-5	0-120
			Subgroup 127	1.5	1.0	1/2	1-3	1-5	0-120
			Subgroup 128	1.5	1.0	1	1-3	1-5	0-120
			Subgroup 129	1.5	1.5	1/2	1-3	1-5	0-120
			Subgroup 130	1.5	1.5	1	1-3	1-5	0-120
			Subgroup 131	1.5	2.0	1/2	1-3	1-5	0-120
			Subgroup 132	1.5	2.0	1	1-3	1-5	0-120
Group 12	Under one side of the tie	3:1	Subgroup 133	0.5	1.0	1/2	1-3	1-5	0-120
			Subgroup 134	0.5	1.0	1	1-3	1-5	0-120
			Subgroup 135	0.5	1.5	1/2	1-3	1-5	0-120
			Subgroup 136	0.5	1.5	1	1-3	1-5	0-120
			Subgroup 137	0.5	2.0	1/2	1-3	1-5	0-120
			Subgroup 138	0.5	2.0	1	1-3	1-5	0-120
			Subgroup 139	1.0	1.0	1/2	1-3	1-5	0-120
			Subgroup 140	1.0	1.0	1	1-3	1-5	0-120

Table I-2. Cases in Set III – models existing ballast pockets and a stationary train – Continued

Groups	Ballast pockets' location	Slope ratio	Subgroups	Ballast pockets' depth (m)	Ballast pockets' width (m)	Value of m	He (m)	Hs (m)	Maximum safe train speed (km/h)
Group 12	Under one side of the tie	3:1	Subgroup 141	1.0	1.5	1/2	1-3	1-5	0-120
			Subgroup 142	1.0	1.5	1	1-3	1-5	0-120
			Subgroup 143	1.0	2.0	1/2	1-3	1-5	0-120
			Subgroup 144	1.0	2.0	1	1-3	1-5	0-120
			Subgroup 145	1.5	1.0	1/2	1-3	1-5	0-120
			Subgroup 146	1.5	1.0	1	1-3	1-5	0-120
			Subgroup 147	1.5	1.5	1/2	1-3	1-5	0-120
			Subgroup 148	1.5	1.5	1	1-3	1-5	0-120
			Subgroup 149	1.5	2.0	1/2	1-3	1-5	0-120
			Subgroup 150	1.5	2.0	1	1-3	1-5	0-120

Appendix II: FS results of models in Set II and Set III

Table II-1. FS results of models Set II

Groups	Subgroups	Railway embankment height (He) (m)	FS				
			Natural slope height (Hs) (m)				
			1	2	3	4	5
Group 5	Subgroup 7	1	3.89	2.80	2.34	2.03	1.86
		2	2.94	2.38	2.11	1.92	1.75
		3	2.48	2.14	1.96	1.82	1.70
	Subgroup 8	1	3.85	2.78	2.32	2.03	1.85
		2	2.91	2.37	2.11	1.91	1.75
		3	2.48	2.13	1.96	1.81	1.70
	Subgroup 9	1	3.88	2.79	2.33	2.03	1.86
		2	2.94	2.37	2.11	1.91	1.75
		3	2.48	2.13	1.96	1.81	1.70
	Subgroup 10	1	3.84	2.77	2.32	2.02	1.85
		2	2.91	2.37	2.11	1.91	1.75
		3	2.47	2.13	1.95	1.81	1.70
	Subgroup 11	1	3.88	2.79	2.33	2.03	1.86
		2	2.94	2.37	2.11	1.91	1.75
		3	2.48	2.13	1.96	1.81	1.70
	Subgroup 12	1	3.83	2.77	2.32	2.02	1.85
		2	2.91	2.37	2.10	1.91	1.75
		3	2.47	2.13	1.95	1.81	1.70
	Subgroup 13	1	3.77	2.74	2.30	2.01	1.84
		2	2.88	2.35	2.10	1.91	1.75
		3	2.47	2.13	1.95	1.81	1.70
	Subgroup 14	1	3.69	2.70	2.27	1.99	1.83
		2	2.83	2.32	2.09	1.90	1.74
		3	2.45	2.12	1.95	1.81	1.69
	Subgroup 15	1	3.74	2.73	2.30	2.00	1.84
		2	2.87	2.35	2.10	1.91	1.75
		3	2.46	2.12	1.95	1.81	1.69
	Subgroup 16	1	3.68	2.69	2.27	1.99	1.83
		2	2.82	2.32	2.08	1.90	1.74
		3	2.44	2.11	2.08	1.80	1.69
	Subgroup 17	1	3.73	2.73	2.30	1.99	1.84
		2	2.87	2.34	2.09	1.90	1.74
		3	2.46	2.12	1.95	1.81	1.69
	Subgroup 18	1	3.66	2.69	2.27	1.99	1.83
		2	2.82	2.32	2.08	1.90	1.74
		3	2.44	2.11	1.94	1.80	1.69

Table II-1. FS results of models Set II – Continued

Groups	Subgroups	Railway embankment height (He) (m)	FS				
			Natural slope height (Hs) (m)				
			1	2	3	4	5
Group 5	Subgroup 19	1	3.64	2.68	2.27	1.99	1.84
		2	2.83	2.32	2.08	1.90	1.74
		3	2.45	2.12	1.95	1.81	1.69
	Subgroup 20	1	3.54	2.62	2.23	1.96	1.82
		2	2.75	2.27	2.05	1.88	1.73
		3	2.40	2.09	1.94	1.80	1.69
	Subgroup 21	1	3.62	2.67	2.26	1.98	1.83
		2	2.83	2.31	2.07	1.89	1.74
		3	2.43	2.11	1.94	1.81	1.69
	Subgroup 22	1	3.53	2.61	2.22	1.96	1.82
		2	2.74	2.27	2.05	1.88	1.73
		3	2.39	2.08	1.93	1.80	1.68
	Subgroup 23	1	3.62	2.67	2.26	1.98	1.81
		2	2.82	2.31	2.07	1.89	1.74
		3	2.42	2.10	1.94	1.80	1.69
	Subgroup 24	1	3.50	2.61	2.22	1.95	1.80
		2	2.74	2.27	2.05	1.88	1.73
		3	2.39	2.08	1.93	1.79	1.68
Group 6	Subgroup 25	1	4.26	3.11	2.62	2.31	2.08
		2	3.27	2.67	2.40	2.19	2.04
		3	2.79	2.42	2.25	2.09	1.98
	Subgroup 26	1	4.21	3.09	2.61	2.30	2.07
		2	3.25	2.67	2.39	2.19	2.04
		3	2.79	2.42	2.25	2.09	1.98
	Subgroup 27	1	4.25	3.10	2.61	2.30	2.08
		2	3.26	2.66	2.39	2.19	2.04
		3	2.79	2.42	2.25	2.09	1.98
	Subgroup 28	1	4.21	3.09	2.60	2.30	2.07
		2	3.25	2.66	2.39	2.19	2.03
		3	2.78	2.42	2.25	2.09	1.98
	Subgroup 29	1	4.24	3.10	2.61	2.30	2.08
		2	3.25	2.66	2.39	2.19	2.04
		3	2.79	2.42	2.25	2.09	1.98
	Subgroup 30	1	4.20	3.08	2.60	2.30	2.07
		2	3.24	2.65	2.39	2.19	2.03
		3	2.78	2.42	2.25	2.09	1.98
	Subgroup 31	1	4.10	3.05	2.60	2.29	2.07
		2	3.22	2.65	2.38	2.19	2.03

Table II-1. FS results of models Set II – Continued

Groups	Subgroups	Railway embankment height (He) (m)	FS				
			Natural slope height (Hs) (m)				
			1	2	3	4	5
Group 6	Subgroup 31	3	2.78	2.41	2.24	2.09	1.97
	Subgroup 32	1	4.04	3.01	2.58	2.29	2.06
		2	3.17	2.62	2.37	2.18	2.03
		3	2.76	2.40	2.24	2.08	1.97
	Subgroup 33	1	4.07	3.04	2.59	2.29	2.06
		2	3.21	2.64	2.38	2.18	2.03
		3	2.77	2.41	2.24	2.09	1.97
	Subgroup 34	1	4.02	3.00	2.57	2.28	2.06
		2	3.17	2.62	2.37	2.18	2.02
		3	2.75	2.40	2.23	2.08	1.97
	Subgroup 35	1	4.04	3.04	2.59	2.29	2.06
		2	3.21	2.64	2.38	2.18	2.03
		3	2.77	2.41	2.24	2.08	1.97
	Subgroup 36	1	4.01	3.00	2.57	2.28	2.06
		2	3.16	2.62	2.37	2.17	2.02
		3	2.75	2.40	2.23	2.08	1.97
	Subgroup 37	1	3.99	2.99	2.57	2.29	2.06
		2	3.17	2.61	2.37	2.18	2.03
		3	2.76	2.40	2.24	2.08	1.97
	Subgroup 38	1	3.83	2.94	2.54	2.26	2.04
		2	3.08	2.56	2.34	2.16	2.02
		3	2.71	2.38	2.23	2.08	1.96
	Subgroup 39	1	3.96	2.98	2.56	2.28	2.05
		2	3.16	2.61	2.37	2.18	2.02
		3	2.75	2.40	2.23	2.08	1.97
	Subgroup 40	1	3.78	2.94	2.53	2.25	2.04
		2	3.08	2.56	2.34	2.16	2.01
		3	2.71	2.38	2.22	2.07	1.96
	Subgroup 41	1	3.93	2.97	2.56	2.27	2.05
		2	3.15	2.61	2.36	2.17	2.02
		3	2.74	2.39	2.23	2.08	1.97
	Subgroup 42	1	3.70	2.93	2.53	2.25	2.04
		2	3.08	2.56	2.34	2.16	2.01
		3	2.71	2.37	2.22	2.07	1.96
Group 7	Subgroup 43	1	3.82	2.80	2.34	2.03	1.86
		2	2.95	2.38	2.11	1.92	1.75
		3	2.49	2.13	1.96	1.82	1.70
	Subgroup 44	1	3.76	2.78	2.34	2.03	1.86

Table II-1. FS results of models Set II – Continued

Groups	Subgroups	Railway embankment height (He) (m)	FS				
			Natural slope height (Hs) (m)				
			1	2	3	4	5
Group 7	Subgroup 44	2	2.91	2.38	2.11	1.92	1.75
		3	2.49	2.13	1.96	1.82	1.70
	Subgroup 45	1	3.81	2.79	2.34	2.03	1.86
		2	2.93	2.37	2.11	1.92	1.75
		3	2.49	2.13	1.96	1.82	1.70
	Subgroup 46	1	3.75	2.76	2.33	2.02	1.86
		2	2.90	2.37	2.11	1.91	1.75
		3	2.48	2.13	1.96	1.81	1.70
	Subgroup 47	1	3.80	2.78	2.34	2.03	1.86
		2	2.92	2.37	2.11	1.92	1.75
		3	2.49	2.13	1.96	1.82	1.70
	Subgroup 48	1	3.74	2.75	2.32	2.02	1.86
		2	2.89	2.37	2.11	1.91	1.75
		3	2.48	2.13	1.95	1.81	1.70
	Subgroup 49	1	3.60	2.70	2.31	2.02	1.85
		2	2.86	2.36	2.10	1.91	1.75
		3	2.48	2.13	1.95	1.81	1.70
	Subgroup 50	1	3.52	2.65	2.27	2.01	1.84
		2	2.79	2.33	2.10	1.91	1.75
		3	2.45	2.13	1.95	1.81	1.69
	Subgroup 51	1	3.59	2.70	2.30	2.02	1.85
		2	2.84	2.35	2.10	1.91	1.75
		3	2.48	2.13	1.95	1.81	1.70
	Subgroup 52	1	3.50	2.64	2.26	2.00	1.85
		2	2.78	2.32	2.09	1.91	1.74
		3	2.44	2.12	1.95	1.81	1.69
	Subgroup 53	1	3.59	2.70	2.29	2.01	1.85
		2	2.83	2.34	2.10	1.91	1.75
		3	2.47	2.12	1.95	1.81	1.69
	Subgroup 54	1	3.48	2.64	2.25	1.99	1.85
		2	2.77	2.31	2.09	1.90	1.74
		3	2.44	2.12	1.95	1.81	1.69
	Subgroup 55	1	3.47	2.63	2.26	2.00	1.85
		2	2.78	2.32	2.10	1.91	1.74
		3	2.44	2.12	1.94	1.81	1.69
	Subgroup 56	1	3.32	2.56	2.20	1.96	1.84
		2	2.67	2.25	2.05	1.89	1.74
		3	2.38	2.09	1.94	1.80	1.69
	Subgroup 57	1	3.43	2.62	2.25	1.99	1.84

Table II-1. FS results of models Set II – Continued

Groups	Subgroups	Railway embankment height (He) (m)	FS				
			Natural slope height (Hs) (m)				
			1	2	3	4	5
	Subgroup 57	2	2.77	2.31	2.09	1.90	1.74
		3	2.43	2.12	1.94	1.81	1.69
	Subgroup 58	1	3.30	2.55	2.19	1.95	1.83
		2	2.67	2.25	2.05	1.89	1.74
		3	2.37	2.09	1.94	1.80	1.69
Group 7	Subgroup 59	1	3.37	2.62	2.25	1.99	1.84
		2	2.76	2.30	2.08	1.90	1.74
		3	2.43	2.12	1.94	1.81	1.69
	Subgroup 60	1	3.27	2.54	2.19	1.95	1.83
		2	2.67	2.25	2.05	1.89	1.73
		3	2.37	2.08	1.94	1.80	1.68
	Subgroup 61	1	4.23	3.12	2.63	2.31	2.08
		2	3.27	2.67	2.40	2.19	2.04
		3	2.80	2.43	2.25	2.09	1.98
	Subgroup 62	1	4.16	3.11	2.62	2.31	2.08
		2	3.26	2.66	2.39	2.19	2.03
		3	2.79	2.42	2.25	2.09	1.97
	Subgroup 63	1	4.20	3.12	2.63	2.31	2.08
		2	3.26	2.67	2.39	2.19	2.04
		3	2.80	2.42	2.25	2.09	1.98
	Subgroup 64	1	4.14	3.09	2.62	2.30	2.08
		2	3.25	2.66	2.39	2.19	2.03
		3	2.79	2.42	2.25	2.09	1.97
Group 8	Subgroup 65	1	4.19	3.11	2.63	2.31	2.08
		2	3.26	2.66	2.39	2.19	2.04
		3	2.79	2.42	2.25	2.09	1.97
	Subgroup 66	1	4..12	3.08	2.62	2.30	2.08
		2	3.24	2.66	2.39	2.19	2.03
		3	2.79	2.42	2.25	2.09	1.97
	Subgroup 67	1	3.99	3.04	2.61	2.30	2.07
		2	3.22	2.65	2.38	2.19	2.03
		3	2.78	2.42	2.24	2.09	1.97
	Subgroup 68	1	3.89	3.00	2.58	2.29	2.07
		2	3.16	2.63	2.38	2.18	2.03
		3	2.77	2.41	2.24	2.08	1.97
	Subgroup 69	1	3.97	3.03	2.61	2.30	2.07
		2	3.20	2.65	2.38	2.19	2.03
		3	2.78	2.41	2.24	2.09	1.97

Table II-1. FS results of models Set II – Continued

Groups	Subgroups	Railway embankment height (He) (m)	FS				
			Natural slope height (Hs) (m)				
			1	2	3	4	5
		1	3.88	2.98	2.58	2.29	2.06
	Subgroup 70	2	3.14	2.62	2.37	2.18	2.03
		3	2.76	2.40	2.24	2.08	1.97
		1	3.96	3.02	2.60	2.30	2.07
	Subgroup 71	2	3.19	2.64	2.38	2.18	2.03
		3	2.77	2.41	2.24	2.08	1.97
		1	3.87	2.97	2.57	2.29	2.06
	Subgroup 72	2	3.13	2.62	2.37	2.18	2.03
		3	2.76	2.40	2.23	2.08	1.97
		1	3.84	2.96	2.56	2.29	2.07
	Subgroup 73	2	3.14	2.63	2.38	2.18	2.03
		3	2.76	2.41	2.24	2.08	1.97
		1	3.69	2.89	2.52	2.27	2.05
Group 8	Subgroup 74	2	3.03	2.57	2.35	2.17	2.02
		3	2.70	2.39	2.23	2.08	1.97
		1	3.82	2.95	2.54	2.28	2.06
	Subgroup 75	2	3.12	2.62	2.38	2.17	2.03
		3	2.76	2.40	2.23	2.08	1.97
		1	3.68	2.88	2.51	2.26	2.05
	Subgroup 76	2	3.03	2.57	2.35	2.17	2.02
		3	2.70	2.38	2.22	2.07	1.96
		1	3.79	2.94	2.53	2.28	2.06
	Subgroup 77	2	3.12	2.62	2.37	2.17	2.02
		3	2.75	2.40	2.23	2.08	1.97
		1	3.58	2.87	2.51	2.26	2.05
	Subgroup 78	2	3.02	2.56	2.35	2.16	2.02
		3	2.70	2.38	2.22	2.07	1.96

Table II-2. FS results of models Set III

Groups	Subgroups	Railway embankment height (He) (m)	FS				
			Natural slope height (Hs) (m)				
			1	2	3	4	5
Group 9	Subgroup 79	1	1.24	1.23	1.22	1.20	1.19
		2	1.30	1.29	1.28	1.27	1.25
		3	1.41	1.40	1.39	1.38	1.37
	Subgroup 80	1	1.23	1.22	1.22	1.19	1.19
		2	1.29	1.28	1.28	1.27	1.25
		3	1.40	1.39	1.38	1.38	1.37
	Subgroup 81	1	1.23	1.22	1.22	1.19	1.19
		2	1.29	1.28	1.28	1.27	1.25
		3	1.39	1.38	1.38	1.38	1.37
	Subgroup 82	1	1.22	1.21	1.21	1.19	1.19
		2	1.28	1.27	1.27	1.27	1.25
		3	1.38	1.37	1.37	1.37	1.37
	Subgroup 83	1	1.23	1.22	1.21	1.19	1.19
		2	1.28	1.27	1.27	1.27	1.25
		3	1.39	1.38	1.38	1.38	1.37
	Subgroup 84	1	1.22	1.21	1.20	1.19	1.19
		2	1.27	1.26	1.26	1.27	1.25
		3	1.37	1.37	1.37	1.37	1.37
	Subgroup 85	1	1.23	1.22	1.21	1.19	1.18
		2	1.29	1.28	1.27	1.25	1.24
		3	1.39	1.38	1.38	1.37	1.36
	Subgroup 86	1	1.22	1.21	1.21	1.19	1.18
		2	1.27	1.26	1.26	1.25	1.24
		3	1.37	1.37	1.36	1.36	1.36
	Subgroup 87	1	1.22	1.21	1.21	1.19	1.18
		2	1.28	1.28	1.27	1.25	1.24
		3	1.39	1.38	1.38	1.37	1.36
	Subgroup 88	1	1.21	1.20	1.21	1.19	1.18
		2	1.27	1.27	1.26	1.25	1.24
		3	1.37	1.37	1.36	1.36	1.36
	Subgroup 89	1	1.21	1.21	1.21	1.19	1.18
		2	1.27	1.27	1.27	1.25	1.24
		3	1.38	1.37	1.38	1.37	1.36
	Subgroup 90	1	1.20	1.19	1.19	1.19	1.18
		2	1.26	1.26	1.25	1.25	1.24
		3	1.36	1.36	1.36	1.36	1.35
	Subgroup 91	1	1.22	1.21	1.21	1.18	1.17
		2	1.28	1.26	1.26	1.25	1.24
		3	1.38	1.37	1.37	1.36	1.36

Table II-2. FS results of models Set III – Continued

Groups	Subgroups	Railway embankment height (He) (m)	FS				
			Natural slope height (Hs) (m)				
			1	2	3	4	5
Group 9	Subgroup 92	1	1.21	1.20	1.20	1.18	1.17
		2	1.26	1.26	1.26	1.25	1.23
		3	1.37	1.36	1.36	1.36	1.36
	Subgroup 93	1	1.20	1.20	1.19	1.18	1.17
		2	1.26	1.25	1.26	1.25	1.24
		3	1.37	1.36	1.36	1.36	1.36
	Subgroup 94	1	1.19	1.19	1.19	1.18	1.17
		2	1.25	1.25	1.24	1.24	1.23
		3	1.36	1.35	1.35	1.35	1.34
	Subgroup 95	1	1.19	1.19	1.19	1.18	1.17
		2	1.25	1.25	1.25	1.25	1.24
		3	1.36	1.36	1.35	1.35	1.34
	Subgroup 96	1	1.18	1.18	1.17	1.18	1.17
		2	1.25	1.24	1.24	1.24	1.23
		3	1.36	1.34	1.34	1.34	1.34
Group 10	Subgroup 97	1	1.36	1.35	1.34	1.32	1.32
		2	1.42	1.41	1.40	1.40	1.38
		3	1.53	1.52	1.51	1.50	1.49
	Subgroup 98	1	1.35	1.34	1.34	1.32	1.32
		2	1.41	1.40	1.40	1.40	1.38
		3	1.52	1.51	1.50	1.50	1.49
	Subgroup 99	1	1.35	1.35	1.34	1.32	1.32
		2	1.41	1.40	1.39	1.38	1.37
		3	1.52	1.51	1.50	1.49	1.48
	Subgroup 100	1	1.34	1.34	1.33	1.32	1.32
		2	1.40	1.39	1.38	1.38	1.37
		3	1.50	1.49	1.49	1.48	1.48
	Subgroup 101	1	1.34	1.33	1.32	1.32	1.32
		2	1.40	1.39	1.39	1.38	1.37
		3	1.51	1.50	1.49	1.49	1.48
	Subgroup 102	1	1.33	1.33	1.32	1.32	1.32
		2	1.39	1.38	1.37	1.37	1.37
		3	1.50	1.49	1.48	1.48	1.48
	Subgroup 103	1	1.34	1.33	1.32	1.32	1.32
		2	1.40	1.39	1.39	1.38	1.37
		3	1.51	1.5	1.49	1.48	1.48
	Subgroup 104	1	1.33	1.32	1.32	1.32	1.32
		2	1.39	1.38	1.38	1.38	1.37

Table II-2. FS results of models Set III – Continued

Groups	Subgroups	Railway embankment height (He) (m)	FS				
			Natural slope height (Hs) (m)				
			1	2	3	4	5
	Subgroup 104	3	1.49	1.48	1.48	1.48	1.48
		1	1.33	1.33	1.32	1.32	1.32
	Subgroup 105	2	1.39	1.38	1.38	1.38	1.37
		3	1.50	1.49	1.49	1.48	1.48
		1	1.32	1.32	1.32	1.32	1.32
	Subgroup 106	2	1.38	1.37	1.37	1.37	1.37
		3	1.49	1.48	1.48	1.48	1.48
		1	1.31	1.31	1.30	1.30	1.30
	Subgroup 107	2	1.37	1.36	1.36	1.35	1.35
		3	1.48	1.47	1.47	1.47	1.46
		1	1.30	1.29	1.28	1.27	1.27
	Subgroup 108	2	1.35	1.34	1.34	1.33	1.33
		3	1.46	1.45	1.45	1.44	1.43
		1	1.30	1.29	1.29	1.28	1.28
	Subgroup 109	2	1.36	1.34	1.34	1.34	1.34
Group 10		3	1.47	1.45	1.45	1.44	1.44
		1	1.30	1.29	1.29	1.28	1.28
	Subgroup 110	2	1.34	1.34	1.34	1.34	1.34
		3	1.45	1.44	1.44	1.44	1.44
		1	1.28	1.28	1.28	1.28	1.27
	Subgroup 111	2	1.34	1.34	1.33	1.33	1.33
		3	1.45	1.45	1.44	1.44	1.43
		1	1.27	1.27	1.27	1.26	1.25
	Subgroup 112	2	1.33	1.33	1.32	1.32	1.31
		3	1.43	1.43	1.42	1.42	1.41
		1	1.27	1.27	1.27	1.27	1.27
	Subgroup 113	2	1.33	1.33	1.33	1.33	1.32
		3	1.43	1.43	1.43	1.43	1.43
		1	1.26	1.26	1.26	1.26	1.25
	Subgroup 114	2	1.32	1.32	1.32	1.32	1.31
		3	1.42	1.42	1.42	1.42	1.41
		1	1.24	1.22	1.20	1.20	1.18
	Subgroup 115	2	1.30	1.28	1.25	1.25	1.24
		3	1.40	1.40	1.39	1.39	1.38
Group 11		1	1.23	1.21	1.20	1.20	1.18
	Subgroup 116	2	1.29	1.27	1.25	1.25	1.24
		3	1.39	1.39	1.38	1.38	1.38
	Subgroup 117	1	1.23	1.21	1.20	1.20	1.18

Table II-2. FS results of models Set III – Continued

Groups	Subgroups	Railway embankment height (He) (m)	FS				
			Natural slope height (Hs) (m)				
			1	2	3	4	5
Group 11	Subgroup 117	2	1.29	1.27	1.25	1.25	1.24
		3	1.39	1.39	1.39	1.38	1.38
	Subgroup 118	1	1.22	1.20	1.20	1.20	1.18
		2	1.28	1.27	1.25	1.25	1.24
		3	1.38	1.38	1.38	1.38	1.38
	Subgroup 119	1	1.22	1.20	1.19	1.19	1.17
		2	1.28	1.27	1.24	1.24	1.23
		3	1.38	1.38	1.38	1.37	1.37
	Subgroup 120	1	1.21	1.19	1.18	1.18	1.17
		2	1.27	1.26	1.24	1.23	1.23
		3	1.37	1.37	1.37	1.36	1.36
	Subgroup 121	1	1.23	1.21	1.20	1.20	1.18
		2	1.29	1.27	1.25	1.25	1.24
		3	1.39	1.39	1.39	1.39	1.37
	Subgroup 122	1	1.22	1.20	1.19	1.19	1.18
		2	1.28	1.25	1.24	1.24	1.24
		3	1.38	1.38	1.38	1.38	1.37
	Subgroup 123	1	1.21	1.20	1.20	1.20	1.18
		2	1.27	1.25	1.25	1.25	1.24
		3	1.39	1.39	1.38	1.38	1.37
	Subgroup 124	1	1.20	1.20	1.19	1.19	1.18
		2	1.25	1.25	1.24	1.24	1.24
		3	1.38	1.38	1.38	1.38	1.37
	Subgroup 125	1	1.20	1.19	1.19	1.19	1.18
		2	1.26	1.25	1.25	1.25	1.24
		3	1.37	1.37	1.37	1.36	1.35
	Subgroup 126	1	1.2	1.19	1.19	1.19	1.18
		2	1.25	1.24	1.24	1.24	1.24
		3	1.37	1.37	1.36	1.36	1.35
	Subgroup 127	1	1.22	1.20	1.20	1.19	1.18
		2	1.28	1.26	1.25	1.25	1.24
		3	1.39	1.39	1.39	1.39	1.37
	Subgroup 128	1	1.21	1.19	1.18	1.18	1.18
		2	1.27	1.25	1.24	1.24	1.23
		3	1.37	1.37	1.37	1.37	1.36
	Subgroup 129	1	1.2	1.19	1.19	1.18	1.18
		2	1.27	1.24	1.24	1.23	1.23
		3	1.37	1.37	1.37	1.36	1.36
	Subgroup 130	1	1.19	1.19	1.18	1.18	1.18

Table II-2. FS results of models Set III – Continued

Groups	Subgroups	Railway embankment height (He) (m)	FS				
			Natural slope height (Hs) (m)				
			1	2	3	4	5
Group 11	Subgroup 130	2	1.25	1.24	1.23	1.23	1.23
		3	1.36	1.36	1.36	1.35	1.35
	Subgroup 131	1	1.19	1.19	1.19	1.18	1.18
		2	1.25	1.24	1.24	1.23	1.23
		3	1.36	1.36	1.35	1.35	1.34
	Subgroup 132	1	1.19	1.19	1.18	1.17	1.17
		2	1.24	1.24	1.23	1.23	1.23
		3	1.35	1.35	1.35	1.34	1.34
Group 12	Subgroup 133	1	1.35	1.34	1.33	1.32	1.32
		2	1.41	1.4	1.39	1.38	1.38
		3	1.53	1.51	1.50	1.49	1.49
	Subgroup 134	1	1.34	1.33	1.32	1.32	1.31
		2	1.4	1.39	1.38	1.38	1.37
		3	1.52	1.50	1.49	1.48	1.48
	Subgroup 135	1	1.34	1.33	1.32	1.32	1.32
		2	1.4	1.38	1.38	1.38	1.38
		3	1.51	1.50	1.49	1.49	1.49
	Subgroup 136	1	1.32	1.32	1.32	1.32	1.31
		2	1.38	1.37	1.37	1.37	1.37
		3	1.49	1.48	1.48	1.48	1.48
	Subgroup 137	1	1.34	1.33	1.32	1.32	1.31
		2	1.4	1.38	1.38	1.37	1.37
		3	1.51	1.50	1.49	1.48	1.48
	Subgroup 138	1	1.32	1.32	1.31	1.31	1.31
		2	1.38	1.37	1.37	1.36	1.36
		3	1.48	1.47	1.47	1.47	1.46
	Subgroup 139	1	1.33	1.32	1.32	1.31	1.31
		2	1.39	1.38	1.38	1.37	1.37
		3	1.51	1.50	1.49	1.48	1.48
	Subgroup 140	1	1.32	1.31	1.31	1.31	1.30
		2	1.38	1.38	1.37	1.37	1.36
		3	1.49	1.48	1.48	1.47	1.47
	Subgroup 141	1	1.32	1.31	1.31	1.31	1.31
		2	1.38	1.37	1.36	1.37	1.37
		3	1.49	1.48	1.48	1.48	1.48
	Subgroup 142	1	1.31	1.31	1.31	1.30	1.30
		2	1.37	1.36	1.36	1.36	1.36
		3	1.47	1.47	1.46	1.46	1.46

Table II-2. FS results of models Set III – Continued

Groups	Subgroups	Railway embankment height (He) (m)	FS				
			Natural slope height (Hs) (m)				
			1	2	3	4	5
Group 12	Subgroup 143	1	1.32	1.31	1.31	1.31	1.30
		2	1.38	1.37	1.37	1.37	1.37
		3	1.48	1.48	1.48	1.47	1.46
	Subgroup 144	1	1.31	1.31	1.30	1.30	1.29
		2	1.36	1.36	1.36	1.35	1.35
		3	1.47	1.47	1.46	1.45	1.45
	Subgroup 145	1	1.30	1.30	1.29	1.29	1.28
		2	1.36	1.36	1.35	1.35	1.34
		3	1.47	1.46	1.45	1.45	1.44
	Subgroup 146	1	1.28	1.28	1.27	1.27	1.27
		2	1.34	1.33	1.33	1.32	1.32
		3	1.45	1.44	1.44	1.44	1.43
	Subgroup 147	1	1.29	1.29	1.29	1.28	1.28
		2	1.35	1.35	1.34	1.34	1.34
		3	1.46	1.45	1.45	1.45	1.44
	Subgroup 148	1	1.28	1.27	1.27	1.27	1.26
		2	1.33	1.32	1.32	1.32	1.31
		3	1.44	1.43	1.43	1.43	1.43
	Subgroup 149	1	1.29	1.28	1.28	1.28	1.27
		2	1.35	1.34	1.34	1.34	1.34
		3	1.45	1.45	1.45	1.45	1.44
	Subgroup 150	1	1.27	1.27	1.27	1.26	1.26
		2	1.32	1.32	1.31	1.30	1.30
		3	1.43	1.43	1.43	1.43	1.42

Table II-3. Calculated maximum safe train speed for cases in Set III

Groups	Subgroups	Railway embankment height (He) (m)	Maximum safe train speed									
			mph					km/h				
			Natural slope height (Hs) (m)					Natural slope height (Hs) (m)				
			1	2	3	4	5	1	2	3	4	5
Group 9	Subgroup 79	1	\	\	\	\	\	\	\	\	\	\
		2	0	\	\	\	\	0	\	\	\	\
		3	25	25	20	20	15	40	40	32	32	24
	Subgroup 80	1	\	\	\	\	\	\	\	\	\	\
		2	\	\	\	\	\	\	\	\	\	\
		3	25	20	20	20	15	40	32	32	32	24
	Subgroup 81	1	\	\	\	\	\	\	\	\	\	\
		2	\	\	\	\	\	\	\	\	\	\
		3	20	20	20	20	15	32	32	32	32	24
	Subgroup 82	1	\	\	\	\	\	\	\	\	\	\
		2	\	\	\	\	\	\	\	\	\	\
		3	20	15	15	15	15	32	24	24	24	24
	Subgroup 83	1	\	\	\	\	\	\	\	\	\	\
		2	\	\	\	\	\	\	\	\	\	\
		3	20	20	20	20	15	32	32	32	32	24
	Subgroup 84	1	\	\	\	\	\	\	\	\	\	\
		2	\	\	\	\	\	\	\	\	\	\
		3	15	15	15	15	15	24	24	24	24	24
	Subgroup 85	1	\	\	\	\	\	\	\	\	\	\
		2	\	\	\	\	\	\	\	\	\	\
		3	20	20	20	15	15	32	32	32	24	24
	Subgroup 86	1	\	\	\	\	\	\	\	\	\	\
		2	\	\	\	\	\	\	\	\	\	\
		3	15	15	15	15	15	24	24	24	24	24
	Subgroup 87	1	\	\	\	\	\	\	\	\	\	\
		2	\	\	\	\	\	\	\	\	\	\
		3	20	20	20	15	15	32	32	32	24	24
	Subgroup 88	1	\	\	\	\	\	\	\	\	\	\
		2	\	\	\	\	\	\	\	\	\	\
		3	15	15	15	15	15	24	24	24	24	24
	Subgroup 89	1	\	\	\	\	\	\	\	\	\	\
		2	\	\	\	\	\	\	\	\	\	\
		3	20	15	15	15	15	32	24	24	24	24
	Subgroup 90	1	\	\	\	\	\	\	\	\	\	\
		2	\	\	\	\	\	\	\	\	\	\
		3	15	15	15	15	10	24	24	24	24	16
	Subgroup 91	1	\	\	\	\	\	\	\	\	\	\
		2	\	\	\	\	\	\	\	\	\	\

Table II-3. Calculated maximum safe train speed for cases in Set III – Continued

Groups	Subgroups	Railway embankment height (He) (m)	Maximum safe train speed									
			mph					km/h				
			Natural slope height (Hs) (m)					Natural slope height (Hs) (m)				
			1	2	3	4	5	1	2	3	4	5
Group 9	Subgroup 91	3	20	15	15	15	15	32	24	24	24	24
	Subgroup 92	1	\	\	\	\	\	\	\	\	\	\
		2	\	\	\	\	\	\	\	\	\	\
		3	15	15	15	15	15	24	24	24	24	24
	Subgroup 93	1	\	\	\	\	\	\	\	\	\	\
		2	\	\	\	\	\	\	\	\	\	\
		3	15	15	15	15	15	24	24	24	24	24
	Subgroup 94	1	\	\	\	\	\	\	\	\	\	\
		2	\	\	\	\	\	\	\	\	\	\
		3	15	10	10	10	10	24	16	16	16	16
	Subgroup 95	1	\	\	\	\	\	\	\	\	\	\
		2	\	\	\	\	\	\	\	\	\	\
		3	15	10	10	10	10	24	16	16	16	16
	Subgroup 96	1	\	\	\	\	\	\	\	\	\	\
		2	\	\	\	\	\	\	\	\	\	\
		3	15	10	10	10	10	24	16	16	16	16
Group 10	Subgroup 97	1	15	10	10	5	5	24	16	16	8	8
		2	30	25	25	25	20	48	40	40	40	32
		3	55	55	50	50	45	88	88	80	80	72
	Subgroup 98	1	10	10	10	5	5	16	16	16	8	8
		2	25	25	25	25	20	40	40	40	40	32
		3	55	50	50	50	45	88	80	80	80	72
	Subgroup 99	1	10	10	10	5	5	16	16	16	8	8
		2	25	25	20	20	15	40	40	32	32	24
		3	55	50	50	45	45	88	80	80	72	72
	Subgroup 100	1	10	10	5	5	5	16	16	16	8	8
		2	25	20	20	20	15	40	32	32	32	24
		3	50	45	45	45	45	80	72	72	72	72
	Subgroup 101	1	10	5	5	5	5	16	8	8	8	8
		2	25	20	20	20	15	40	32	32	32	24
		3	50	50	45	45	45	80	80	72	72	72
	Subgroup 102	1	5	5	5	5	5	8	8	8	8	8
		2	20	20	15	15	15	32	32	24	24	24
		3	50	45	45	45	45	80	72	72	72	72
	Subgroup 103	1	10	5	5	5	5	16	8	8	8	8
		2	25	20	20	20	15	40	32	32	32	24

Table II-3. Calculated maximum safe train speed for cases in Set III – Continued

Groups	Subgroups	Railway embankment height (He) (m)	Maximum safe train speed									
			mph					km/h				
			Natural slope height (Hs) (m)					Natural slope height (Hs) (m)				
			1	2	3	4	5	1	2	3	4	5
	Subgroup 103	3	50	50	45	45	45	80	80	72	72	72
	Subgroup 104	1	5	5	5	5	5	8	8	8	8	8
		2	20	20	20	20	15	32	32	32	32	24
		3	45	45	45	45	45	72	72	72	72	72
	Subgroup 105	1	5	5	5	5	5	8	8	8	8	8
		2	20	20	20	20	15	32	32	32	32	24
		3	50	45	45	45	45	80	72	72	72	72
	Subgroup 106	1	5	5	5	5	5	8	8	8	8	8
		2	20	15	15	15	15	32	24	24	24	24
		3	45	45	45	45	45	72	72	72	72	72
	Subgroup 107	1	0	0	0	0	0	0	0	0	0	0
		2	15	15	15	10	10	24	24	24	16	16
		3	45	40	40	40	40	72	64	64	64	64
	Subgroup 108	1	0	\	\	\	\	0	\	\	\	\
		2	10	10	10	5	5	16	16	16	8	8
		3	40	35	35	35	30	64	56	56	56	48
Group 10	Subgroup 109	1	0	\	\	\	\	0	\	\	\	\
		2	15	10	10	10	10	24	16	16	16	16
		3	40	35	35	35	35	64	56	56	56	56
	Subgroup 110	1	0	\	\	\	\	0	\	\	\	\
		2	10	10	10	10	10	16	16	16	16	16
		3	35	35	35	35	35	56	56	56	56	56
	Subgroup 111	1	\	\	\	\	\	\	\	\	\	\
		2	10	10	5	5	5	16	16	8	8	8
		3	35	35	35	35	30	56	56	56	56	48
	Subgroup 112	1	\	\	\	\	0	\	\	\	\	0
		2	5	5	5	5	0	8	8	8	8	0
		3	30	30	30	30	25	48	48	48	48	40
	Subgroup 113	1	\	\	\	\	\	\	\	\	\	\
		2	5	5	5	5	5	8	8	8	8	8
		3	30	30	30	30	30	48	48	48	48	48
	Subgroup 114	1	\	\	\	\	\	\	\	\	\	\
		2	5	5	5	5	0	8	8	8	8	0
		3	30	30	30	30	25	48	48	48	48	40
Group 11	Subgroup 115	1	\	\	\	\	\	\	\	\	\	\

Table II-3. Calculated maximum safe train speed for cases in Set III – Continued

Groups	Subgroups	Railway embankment height (He) (m)	Maximum safe train speed									
			mph					km/h				
			Natural slope height (Hs) (m)					Natural slope height (Hs) (m)				
			1	2	3	4	5	1	2	3	4	5
Group 11	Subgroup 115	2	\	\	\	\	\	\	\	\	\	\
		3	25	25	20	20	20	40	40	32	32	32
	Subgroup 116	1	\	\	\	\	\	\	\	\	\	\
		2	\	\	\	\	\	\	\	\	\	\
		3	20	20	20	20	20	32	32	32	32	32
	Subgroup 117	1	\	\	\	\	\	\	\	\	\	\
		2	\	\	\	\	\	\	\	\	\	\
		3	20	20	20	20	20	32	32	32	32	32
	Subgroup 118	1	\	\	\	\	\	\	\	\	\	\
		2	\	\	\	\	\	\	\	\	\	\
		3	20	20	20	20	20	32	32	32	32	32
	Subgroup 119	1	\	\	\	\	\	\	\	\	\	\
		2	\	\	\	\	\	\	\	\	\	\
		3	20	20	20	15	15	32	32	32	24	24
	Subgroup 120	1	\	\	\	\	\	\	\	\	\	\
		2	\	\	\	\	\	\	\	\	\	\
		3	15	15	15	15	15	24	24	24	24	24
	Subgroup 121	1	\	\	\	\	\	\	\	\	\	\
		2	\	\	\	\	\	\	\	\	\	\
		3	20	20	20	20	15	32	32	32	32	24
	Subgroup 122	1	\	\	\	\	\	\	\	\	\	\
		2	\	\	\	\	\	\	\	\	\	\
		3	20	20	20	20	15	32	32	32	32	24
	Subgroup 123	1	\	\	\	\	\	\	\	\	\	\
		2	\	\	\	\	\	\	\	\	\	\
		3	20	20	20	20	15	32	32	32	32	24
	Subgroup 124	1	\	\	\	\	\	\	\	\	\	\
		2	\	\	\	\	\	\	\	\	\	\
		3	20	20	20	20	15	32	32	32	32	24
	Subgroup 125	1	\	\	\	\	\	\	\	\	\	\
		2	\	\	\	\	\	\	\	\	\	\
		3	15	15	15	15	10	24	24	24	24	16
	Subgroup 126	1	\	\	\	\	\	\	\	\	\	\
		2	\	\	\	\	\	\	\	\	\	\
		3	15	15	15	15	10	24	24	24	24	16
	Subgroup 127	1	\	\	\	\	\	\	\	\	\	\
		2	\	\	\	\	\	\	\	\	\	\
		3	20	20	20	20	15	32	32	32	32	24

Table II-3. Calculated maximum safe train speed for cases in Set III – Continued

Groups	Subgroups	Railway embankment height (He) (m)	Maximum safe train speed									
			mph					km/h				
			Natural slope height (Hs) (m)					Natural slope height (Hs) (m)				
			1	2	3	4	5	1	2	3	4	5
Group 11	Subgroup 128	1	\	\	\	\	\	\	\	\	\	\
		2	\	\	\	\	\	\	\	\	\	\
		3	15	15	15	15	15	24	24	24	24	24
	Subgroup 129	1	\	\	\	\	\	\	\	\	\	\
		2	\	\	\	\	\	\	\	\	\	\
		3	15	15	15	15	15	24	24	24	24	24
	Subgroup 130	1	\	\	\	\	\	\	\	\	\	\
		2	\	\	\	\	\	\	\	\	\	\
		3	15	15	15	10	10	24	24	24	16	16
	Subgroup 131	1	\	\	\	\	\	\	\	\	\	\
		2	\	\	\	\	\	\	\	\	\	\
		3	15	15	10	10	10	24	24	16	16	16
	Subgroup 132	1	\	\	\	\	\	\	\	\	\	\
		2	\	\	\	\	\	\	\	\	\	\
		3	10	10	10	10	10	16	16	16	16	16
Group 12	Subgroup 133	1	10	10	5	5	5	16	16	16	8	8
		2	25	25	20	20	20	40	40	32	32	32
		3	55	50	50	45	45	88	80	80	72	72
	Subgroup 134	1	10	5	5	5	0	16	8	8	8	0
		2	25	20	20	20	15	40	32	32	32	24
		3	55	50	45	45	45	88	80	72	72	72
	Subgroup 135	1	10	5	5	5	5	16	8	8	8	8
		2	25	20	20	20	20	40	32	32	32	32
		3	50	50	45	45	45	80	80	72	72	72
	Subgroup 136	1	5	5	5	5	0	8	8	8	8	0
		2	20	15	15	15	15	32	24	24	24	24
		3	45	45	45	45	45	72	72	72	72	72
	Subgroup 137	1	10	5	5	5	0	16	8	8	8	0
		2	25	20	20	15	15	40	32	32	24	24
		3	50	50	45	45	45	80	80	72	72	72
	Subgroup 138	1	5	5	0	0	0	8	8	0	0	0
		2	20	15	15	15	15	32	24	24	24	24
		3	45	40	40	40	40	72	64	64	64	64
	Subgroup 139	1	5	5	5	0	0	8	8	8	0	0
		2	20	20	20	15	15	32	32	32	24	24
		3	50	50	45	45	45	80	80	72	72	72

Table II-3. Calculated maximum safe train speed for cases in Set III – Continued

Groups	Subgroups	Railway embankment height (He) (m)	Maximum safe train speed									
			mph					km/h				
			Natural slope height (Hs) (m)					Natural slope height (Hs) (m)				
			1	2	3	4	5	1	2	3	4	5
Group 12	Subgroup 140	1	5	0	0	0	0	8	0	0	0	0
		2	20	20	15	15	15	32	32	24	24	24
		3	45	45	45	40	40	72	72	72	64	64
	Subgroup 141	1	5	0	0	0	0	8	0	0	0	0
		2	20	15	15	15	15	32	24	24	24	24
		3	45	45	45	45	45	72	72	72	72	72
	Subgroup 142	1	0	0	0	0	0	0	0	0	0	0
		2	15	15	15	15	15	24	24	24	24	24
		3	40	40	40	40	40	64	64	64	64	64
	Subgroup 143	1	5	0	0	0	0	8	0	0	0	0
		2	20	15	15	15	15	32	24	24	24	24
		3	45	45	45	40	40	72	72	72	64	64
	Subgroup 144	1	0	0	0	0	\	0	0	0	0	\
		2	15	15	10	10	10	24	24	16	16	16
		3	40	40	40	35	35	64	64	64	56	56
	Subgroup 145	1	0	0	\	\	\	0	0	\	\	\
		2	15	15	10	10	10	24	24	16	16	16
		3	40	40	35	35	35	64	64	56	56	56
	Subgroup 146	1	\	\	\	\	\	\	\	\	\	\
		2	10	5	5	5	5	16	8	8	8	8
		3	35	35	35	35	30	56	56	56	56	48
	Subgroup 147	1	\	\	\	\	\	\	\	\	\	\
		2	10	10	10	10	10	16	16	16	16	16
		3	40	35	35	35	35	64	56	56	56	56
	Subgroup 148	1	\	\	\	\	\	\	\	\	\	\
		2	5	5	5	5	0	8	8	8	8	0
		3	35	30	30	30	30	56	48	48	48	48
	Subgroup 149	1	\	\	\	\	\	\	\	\	\	\
		2	10	10	10	10	10	16	16	16	16	16
		3	35	35	35	35	35	56	56	56	56	56
	Subgroup 150	1	\	\	\	\	\	\	\	\	\	\
		2	5	5	5	5	0	8	8	8	8	0
		3	35	30	30	30	30	56	48	48	48	48

Table II-4. FS results of cases with the maximum train speeds in Set III

Groups	Subgroups	Railway embankment height (He) (m)	FS				
			Natural slope height (Hs) (m)				
			1	2	3	4	5
Group 9	Subgroup 79	1	\	\	\	\	\
		2	1.30	\	\	\	\
		3	1.31	1.30	1.31	1.30	1.31
	Subgroup 80	1	\	\	\	\	\
		2	\	\	\	\	\
		3	1.30	1.31	1.30	1.30	1.31
	Subgroup 81	1	\	\	\	\	\
		2	\	\	\	\	\
		3	1.31	1.30	1.30	1.30	1.31
	Subgroup 82	1	\	\	\	\	\
		2	\	\	\	\	\
		3	1.30	1.31	1.31	1.31	1.31
	Subgroup 83	1	\	\	\	\	\
		2	\	\	\	\	\
		3	1.31	1.30	1.30	1.30	1.31
	Subgroup 84	1	\	\	\	\	\
		2	\	\	\	\	\
		3	1.31	1.31	1.31	1.31	1.31
	Subgroup 85	1	\	\	\	\	\
		2	\	\	\	\	\
		3	1.31	1.30	1.30	1.31	1.30
	Subgroup 86	1	\	\	\	\	\
		2	\	\	\	\	\
		3	1.31	1.31	1.30	1.30	1.30
	Subgroup 87	1	\	\	\	\	\
		2	\	\	\	\	\
		3	1.31	1.30	1.30	1.31	1.30
	Subgroup 88	1	\	\	\	\	\
		2	\	\	\	\	\
		3	1.31	1.31	1.30	1.30	1.30
	Subgroup 89	1	\	\	\	\	\
		2	\	\	\	\	\
		3	1.30	1.31	1.31	1.31	1.30
	Subgroup 90	1	\	\	\	\	\
		2	\	\	\	\	\
		3	1.30	1.30	1.30	1.30	1.31
	Subgroup 91	1	\	\	\	\	\
		2	\	\	\	\	\
		3	1.30	1.31	1.31	1.30	1.30

Table II-4. FS results of cases with the maximum train speeds in Set III – Continued

Groups	Subgroups	Railway embankment height (He) (m)	FS				
			Natural slope height (Hs) (m)				
			1	2	3	4	5
Group 9	Subgroup 92	1	\	\	\	\	\
		2	\	\	\	\	\
		3	1.31	1.30	1.30	1.30	1.30
	Subgroup 93	1	\	\	\	\	\
		2	\	\	\	\	\
		3	1.31	1.30	1.30	1.30	1.30
	Subgroup 94	1	\	\	\	\	\
		2	\	\	\	\	\
		3	1.30	1.31	1.31	1.31	1.30
	Subgroup 95	1	\	\	\	\	\
		2	\	\	\	\	\
		3	1.30	1.30	1.31	1.31	1.30
	Subgroup 96	1	\	\	\	\	\
		2	\	\	\	\	\
		3	1.30	1.30	1.30	1.30	1.30
Group 10	Subgroup 97	1	1.30	1.31	1.30	1.30	1.30
		2	1.30	1.31	1.30	1.30	1.30
		3	1.31	1.30	1.31	1.30	1.31
	Subgroup 98	1	1.31	1.30	1.30	1.30	1.30
		2	1.31	1.30	1.30	1.30	1.30
		3	1.30	1.31	1.30	1.30	1.31
	Subgroup 99	1	1.31	1.31	1.30	1.30	1.30
		2	1.31	1.30	1.31	1.30	1.31
		3	1.30	1.31	1.30	1.31	1.30
	Subgroup 100	1	1.30	1.30	1.31	1.30	1.30
		2	1.30	1.31	1.30	1.30	1.31
		3	1.30	1.31	1.30	1.30	1.30
	Subgroup 101	1	1.30	1.31	1.30	1.30	1.30
		2	1.30	1.31	1.31	1.30	1.31
		3	1.31	1.30	1.31	1.31	1.30
	Subgroup 102	1	1.31	1.31	1.30	1.30	1.30
		2	1.31	1.30	1.31	1.31	1.31
		3	1.30	1.31	1.30	1.30	1.30
	Subgroup 103	1	1.30	1.31	1.30	1.30	1.30
		2	1.30	1.31	1.31	1.30	1.31
		3	1.31	1.30	1.31	1.30	1.30
	Subgroup 104	1	1.31	1.30	1.30	1.30	1.30
		2	1.31	1.30	1.30	1.30	1.31

Table II-4. FS results of cases with the maximum train speeds in Set III – Continued

Groups	Subgroups	Railway embankment height (He) (m)	FS				
			Natural slope height (Hs) (m)				
			1	2	3	4	5
	Subgroup 104	3	1.31	1.31	1.30	1.30	1.30
		1	1.31	1.31	1.30	1.30	1.30
	Subgroup 105	2	1.31	1.30	1.30	1.30	1.31
		3	1.30	1.31	1.31	1.30	1.30
		1	1.30	1.30	1.30	1.30	1.30
	Subgroup 106	2	1.30	1.31	1.31	1.31	1.31
		3	1.31	1.30	1.30	1.30	1.30
		1	1.31	1.31	1.30	1.30	1.30
	Subgroup 107	2	1.31	1.30	1.30	1.31	1.31
		3	1.30	1.31	1.31	1.31	1.30
		1	1.30	\	\	\	\
	Subgroup 108	2	1.31	1.30	1.30	1.31	1.31
		3	1.30	1.31	1.31	1.30	1.31
		1	1.30	\	\	\	\
	Subgroup 109	2	1.30	1.30	1.30	1.30	1.30
Group 10		3	1.31	1.31	1.31	1.30	1.30
		1	1.30	\	\	\	\
	Subgroup 110	2	1.30	1.30	1.30	1.30	1.30
		3	1.31	1.30	1.30	1.30	1.30
		1	\	\	\	\	\
	Subgroup 111	2	1.30	1.30	1.31	1.31	1.31
		3	1.31	1.31	1.30	1.30	1.31
		1	\	\	\	\	\
	Subgroup 112	2	1.31	1.31	1.30	1.30	1.31
		3	1.31	1.31	1.30	1.30	1.31
		1	\	\	\	\	\
	Subgroup 113	2	1.31	1.31	1.31	1.31	1.30
		3	1.31	1.31	1.31	1.31	1.31
		1	\	\	\	\	\
	Subgroup 114	2	1.30	1.30	1.30	1.30	1.31
		3	1.30	1.30	1.30	1.30	1.31
		1	\	\	\	\	\
	Subgroup 115	2	\	\	\	\	\
		3	1.30	1.30	1.31	1.31	1.30
Group 11		1	\	\	\	\	\
	Subgroup 116	2	\	\	\	\	\
		3	1.31	1.31	1.30	1.30	1.30
	Subgroup 117	1	\	\	\	\	\

Table II-4. FS results of cases with the maximum train speeds in Set III – Continued

Groups	Subgroups	Railway embankment height (He) (m)	FS				
			Natural slope height (Hs) (m)				
			1	2	3	4	5
Group 11	Subgroup 117	2	\	\	\	\	\
		3	1.31	1.31	1.31	1.30	1.30
	Subgroup 118	1	\	\	\	\	\
		2	\	\	\	\	\
		3	1.30	1.30	1.30	1.30	1.30
	Subgroup 119	1	\	\	\	\	\
		2	\	\	\	\	\
		3	1.30	1.30	1.30	1.31	1.31
	Subgroup 120	1	\	\	\	\	\
		2	\	\	\	\	\
		3	1.31	1.31	1.31	1.30	1.30
	Subgroup 121	1	\	\	\	\	\
		2	\	\	\	\	\
		3	1.31	1.31	1.31	1.31	1.31
	Subgroup 122	1	\	\	\	\	\
		2	\	\	\	\	\
		3	1.30	1.30	1.30	1.30	1.31
	Subgroup 123	1	\	\	\	\	\
		2	\	\	\	\	\
		3	1.31	1.31	1.30	1.30	1.31
	Subgroup 124	1	\	\	\	\	\
		2	\	\	\	\	\
		3	1.30	1.30	1.30	1.30	1.31
	Subgroup 125	1	\	\	\	\	\
		2	\	\	\	\	\
		3	1.31	1.31	1.31	1.30	1.313
	Subgroup 126	1	\	\	\	\	\
		2	\	\	\	\	\
		3	1.31	1.31	1.30	1.30	1.31
	Subgroup 127	1	\	\	\	\	\
		2	\	\	\	\	\
		3	1.31	1.31	1.31	1.31	1.31
	Subgroup 128	1	\	\	\	\	\
		2	\	\	\	\	\
		3	1.31	1.31	1.31	1.31	1.30
	Subgroup 129	1	\	\	\	\	\
		2	\	\	\	\	\
		3	1.31	1.31	1.31	1.30	1.30
	Subgroup 130	1	\	\	\	\	\

Table II-4. FS results of cases with the maximum train speeds in Set III – Continued

Groups	Subgroups	Railway embankment height (He) (m)	FS				
			Natural slope height (Hs) (m)				
			1	2	3	4	5
Group 11	Subgroup 130	2	\	\	\	\	\
		3	1.30	1.30	1.30	1.31	1.31
	Subgroup 131	1	\	\	\	\	\
		2	\	\	\	\	\
		3	1.30	1.30	1.31	1.31	1.30
	Subgroup 132	1	\	\	\	\	\
		2	\	\	\	\	\
		3	1.31	1.31	1.31	1.30	1.30
Group 12	Subgroup 133	1	1.30	1.30	1.31	1.30	1.30
		2	1.31	1.30	1.31	1.30	1.30
		3	1.31	1.31	1.30	1.31	1.31
	Subgroup 134	1	1.30	1.31	1.30	1.30	1.31
		2	1.30	1.31	1.30	1.30	1.31
		3	1.30	1.30	1.31	1.30	1.30
	Subgroup 135	1	1.30	1.31	1.30	1.30	1.30
		2	1.30	1.30	1.30	1.30	1.30
		3	1.31	1.30	1.31	1.31	1.31
	Subgroup 136	1	1.30	1.30	1.30	1.30	1.31
		2	1.30	1.31	1.31	1.31	1.31
		3	1.31	1.30	1.30	1.30	1.30
	Subgroup 137	1	1.30	1.31	1.30	1.30	1.31
		2	1.30	1.30	1.30	1.31	1.31
		3	1.31	1.30	1.31	1.30	1.30
	Subgroup 138	1	1.30	1.30	1.31	1.31	1.31
		2	1.30	1.31	1.31	1.30	1.30
		3	1.30	1.31	1.31	1.31	1.30
	Subgroup 139	1	1.31	1.30	1.30	1.31	1.31
		2	1.31	1.30	1.303	1.31	1.31
		3	1.31	1.30	1.31	1.30	1.30
	Subgroup 140	1	1.30	1.31	1.31	1.31	1.30
		2	1.30	1.30	1.31	1.31	1.30
		3	1.31	1.30	1.30	1.31	1.31
	Subgroup 141	1	1.30	1.31	1.31	1.31	1.31
		2	1.30	1.31	1.30	1.31	1.31
		3	1.31	1.31	1.30	1.30	1.30
	Subgroup 142	1	1.31	1.31	1.31	1.30	1.30
		2	1.31	1.31	1.31	1.30	1.30
		3	1.31	1.31	1.30	1.30	1.30

Table II-4. FS results of cases with the maximum train speeds in Set III – Continued

Groups	Subgroups	Railway embankment height (He) (m)	FS				
			Natural slope height (Hs) (m)				
			1	2	3	4	5
Group 12	Subgroup 143	1	1.30	1.31	1.31	1.31	1.30
		2	1.30	1.31	1.31	1.31	1.31
		3	1.30	1.30	1.30	1.31	1.30
	Subgroup 144	1	1.31	1.31	1.30	1.30	\
		2	1.30	1.30	1.30	1.31	1.31
		3	1.31	1.31	1.30	1.31	1.31
	Subgroup 145	1	1.30	1.30	\	\	\
		2	1.30	1.30	1.31	1.31	1.30
		3	1.31	1.30	1.31	1.31	1.30
	Subgroup 146	1	\	\	\	\	\
		2	1.30	1.31	1.31	1.30	1.30
		3	1.31	1.30	1.30	1.30	1.31
	Subgroup 147	1	\	\	\	\	\
		2	1.31	1.31	1.30	1.30	1.30
		3	1.30	1.31	1.31	1.31	1.30
	Subgroup 148	1	\	\	\	\	\
		2	1.31	1.30	1.30	1.30	1.31
		3	1.30	1.31	1.31	1.31	1.31
	Subgroup 149	1	\	\	\	\	\
		2	1.31	1.30	1.30	1.30	1.30
		3	1.31	1.31	1.31	1.31	1.30
	Subgroup 150	1	\	\	\	\	\
		2	1.31	1.30	1.30	1.30	1.31
		3	1.30	1.31	1.31	1.31	1.30